

Aus der Abt. Cardiovascular Genomics and Epigenomics
der Medizinischen Fakultät Mannheim der Universität Heidelberg
(Direktor: Prof. Dr. Gergana Dobрева)

Epigenetic priming and GATA4 activation upon lamin A/C loss-of-
function results in aberrant cardiovascular cell fate and function

Inauguraldissertation
zur Erlangung des Doctor scientiarum humanarum (Dr. sc. hum.)
der
Medizinischen Fakultät Mannheim
der Ruprecht-Karls-Universität
zu
Heidelberg

vorgelegt von
Wang, YINUO

aus
Henan, China
2023

Dekan: Prof. Dr. med. Sergij Goerd
Referent in: Frau Prof. Dr. rer. nat. Gergana Dobrev

CONTENT

	Page
LIST OF ABBREVIATIONS	1
1 INTRODUCTION.....	3
1.1 Epigenetics and laminopathies	3
1.1.1 Structure, expression and post modifications of lamins.....	3
1.1.2 Function of lamins: from nuclear structure to spatial chromatin organization	5
1.1.3 Laminopathies.....	10
1.2 <i>LMNA</i> -related cardiomyopathy.....	13
1.2.1 Dilated cardiomyopathy.....	13
1.2.2 Left ventricle non-compaction cardiomyopathy	21
1.2.3 Arrhythmogenic right ventricular cardiomyopathy	22
1.2.4 Restrictive cardiomyopathy	24
1.3 Changes of chromosome architecture and gene expression in <i>LMNA</i> -associated cardiomyopathies	24
1.3.1 Lamina-associated domains reorganization in cardiomyopathy.....	24
1.3.2 Role of lamin A/C in chromatin organization and transcription in <i>LMNA</i> -related cardiomyopathy	25
1.3.3 The role of polycomb group proteins in <i>LMNA</i> -related cardiomyopathy	26
1.4 Mechano-protective role of lamin A/C in heart	28
1.5 Heart development.....	31
1.5.1 Mouse heart development.....	31
1.5.2 Early cardiac precursor within the primitive streak	33
1.5.3 First heart field and second heart field	33
1.5.4 Different cardiac cell types during heart development.....	34
1.5.5 Cardiac cushions and valve formation	36
1.5.6 Myocardial compaction and trabeculation	37
1.6 Objective	39
2 MATERIALS AND METHODS.....	40
2.1 Materials	40
2.1.1 Equipment.....	40
2.1.2 Chemicals	41
2.1.3 Cell culture medium and supplements	42

2.1.4 Buffers and solutions.....	44
2.1.5 kits.....	45
2.1.6 Consumables	46
2.1.7 Antibodies	46
2.1.8 Primers and oligonucleotides	47
2.1.9 Programs and algorithms	50
2.1.10 Transgenic mouse lines	51
2.2 Methods	52
2.2.1 Cell lines and cell culture.....	52
2.2.2 DNA extraction, RNA Isolation, RT-PCR, and Real-Time PCR.....	52
2.2.3 Western blotting	52
2.2.4 Mouse mESC lines generation and differentiation	52
2.2.5 Knockdown of <i>Lmna</i> at the cardiac progenitor and cardiomyocyte stages	54
2.2.6 siRNA mediated gene knockdown	54
2.2.7 Primed hiPSC cell culture, differentiation, and conversion to naïve hiPSC.....	54
2.2.8 Neonatal cardiomyocytes isolation and culture	55
2.2.9 Measurements of calcium transients in ventricular CMs	56
2.2.10 Histology	56
2.2.11 Immunofluorescence staining.....	56
2.2.12 Wheat germ agglutinin (WGA) and isolectin B4 (IB4) co-staining	57
2.2.13 Immunofluorescence imaging and quantifications.....	58
2.2.14 DNA Fluorescence In Situ Hybridization (FISH).....	58
2.2.15 Chromosome painting	59
2.2.16 Flow cytometry	59
2.2.17 Echocardiographic assessment of cardiac dimensions and function ...	60
2.2.18 Contraction analysis	60
2.2.19 RNA-Sequencing and data analysis.....	60
2.2.20 ATAC-Sequencing and data analysis.....	61
2.2.21 Hi-C and data analysis	62
2.2.22 Statistics and reproducibility.....	64
3 RESULTS.....	65
3.1 <i>Lmna</i> deficiency leads to aberrant cardiovascular cell fate choices	65
3.1.1 <i>Lmna</i> knockout mESC generation by CRISPR/Cas9 gene editing.....	65
3.1.2 <i>Lmna</i> deficiency leads to aberrant cardiovascular cell fate choices	65

3.1.3	<i>Lmna</i> deficiency promotes cardiac differentiation by using direct CMs differentiation method.....	66
3.1.4	Loss of <i>Lmna</i> doesn't affect early cardiac mesoderm commitment.....	67
3.1.5	<i>Lmna</i> regulates cardiovascular progenitor cell fate choices.....	67
3.1.6	RNA-seq analysis of Nkx2-5 sorted <i>Lmna</i> ^{-/-} cardiac progenitors.....	68
3.1.7	RNA-seq analysis of <i>Lmna</i> ^{-/-} embryonic bodies at day10.....	69
3.1.8	RNA-seq analysis of Nkx2-5 sorted <i>Lmna</i> ^{-/-} cardiomyocytes.....	69
3.1.9	Impact of lamin B1 on CMs differentiation.....	70
3.2	Lamin A/C loss induces 3D chromatin reorganization in mESCs.....	71
3.2.1	Lamin A/C expresses in mESCs and CMs.....	71
3.2.2	Chromosome 14 decompaction in <i>Lmna</i> ^{-/-} by Hi-C analysis.....	72
3.2.3	Loss of <i>Lmna</i> leads to B/A compartments transitions.....	73
3.2.4	A-B compartments transition correlates with lamin A/C LADs.....	74
3.2.5	Dissociation of cardiac-specific genes from the repressive nuclear periphery already in <i>Lmna</i> ^{-/-} mESCs.....	75
3.3	Lamin A/C deficiency in ESCs primes cardiac specific gene expression.....	76
3.3.1	Ectopic cardiac gene activation in <i>Lmna</i> ^{-/-} mESC.....	76
3.3.2	Activation of primed cardiac gene in subsequent differentiation steps...	77
3.3.3	Increased chromatin accessibility in <i>Lmna</i> ^{-/-} mESCs.....	78
3.3.4	Loss of <i>Lmna</i> primes cardiac genes for later activation.....	79
3.3.5	Lamin A rather than lamin C plays an important role in cardiac lineage restriction.....	80
3.4	Cell-type specific role of lamin A/C in shaping chromatin accessibility.....	81
3.4.1	Increased chromatin accessibility in <i>Lmna</i> ^{-/-} CMs.....	81
3.4.2	Up-regulated genes in <i>Lmna</i> ^{-/-} CMs show a mESC and CM specific increased chromatin accessibility.....	83
3.4.3	LADs genes in <i>Lmna</i> ^{-/-} mESCs show a mESC and CMs specific increased chromatin accessibility.....	84
3.4.4	Lamin A/C rather than lamin B1 plays a dominant function of in cardiogenesis.....	84
3.5	Lamin A/C is crucial for naïve pluripotency.....	85
3.5.1	Lamin A/C expression during mouse and human development.....	85
3.5.2	Lamin A/C is expressed in naïve mESCs and hiPSCs.....	86
3.5.3	Lamin A/C maintains naïve hiPSC pluripotency.....	87
3.6	Distinct roles of lamin A/C in naïve PSC and CMs for cardiac laminopathies.....	88
3.6.1	Functional changes in cardiovascular cells following stage-specific loss of lamin A/C.....	88
3.6.2	RNA-seq analysis of CMs with CM-specific depletion of lamin A/C.....	89

3.6.3 Comparison the transcriptome of <i>Lmna</i> KO mESC-CMs with the expression data from <i>LMNA</i> -associated DCM patients.....	90
3.6.4 Comparison the transcriptome of <i>Lmna</i> KD CMs with the expression data from <i>LMNA</i> -associated DCM patients	91
3.7 <i>Lmna</i> deficiency results in non-compaction cardiomyopathy	92
3.7.1 Ectopic cardiac gene activation in vivo upon <i>Lmna</i> ablation	92
3.7.2 Lamin A/C tethers CM specific genes to the nuclear periphery in non-CMs	93
3.7.3 Increased ejection fraction and fractional shortening in <i>Lmna</i> ^{+/-} and <i>Lmna</i> ^{-/-} right ventricle	94
3.7.4 Non-compaction hearts in both <i>Lmna</i> ^{+/-} and <i>Lmna</i> ^{-/-} embryos	95
3.7.5 Decreased CM proliferation in E18.5 <i>Lmna</i> ^{+/-} and <i>Lmna</i> ^{-/-} hearts	96
3.7.6 Increased CMs binucleation in E18.5 <i>Lmna</i> ^{+/-} and <i>Lmna</i> ^{-/-} hearts	97
3.7.7 Decreased capillary density in E18.5 <i>Lmna</i> ^{+/-} and <i>Lmna</i> ^{-/-} hearts.....	97
3.7.8 Echocardiographic analysis of P1 heart function.....	98
3.7.9 Echocardiographic analysis of P14 heart function.....	99
3.7.10 Decreased capillary density in postnatal hearts	100
3.7.11 Decreased CM proliferation in P1 and P4 <i>Lmna</i> ^{+/-} and <i>Lmna</i> ^{-/-} hearts.....	101
3.8 Premature binucleation, altered contractility and increased cell death of <i>Lmna</i> ^{-/-} CMs.....	102
3.8.1 Precocious of <i>Lmna</i> ^{+/-} and <i>Lmna</i> ^{-/-} CMs binucleation.....	102
3.8.2 DNA damage in <i>Lmna</i> ^{+/-} and <i>Lmna</i> ^{-/-} CMs	102
3.8.3 Proarrhythmic beating in <i>Lmna</i> ^{-/-} CMs.....	103
3.8.4 Loss of <i>Lmna</i> leads to CMs specific cell death.....	104
3.9 <i>Gata4</i> activation upon <i>Lmna</i> loss leads to aberrant cardiac development	105
3.9.1 Transient knockdown of <i>Gata4</i> in <i>Lmna</i> ^{-/-} mESC rescues <i>Lmna</i> ^{-/-} phenotype	105
3.9.2 Rescue <i>Lmna</i> ^{-/-} phenotype by stable knockdown of <i>Gata4</i> in <i>Lmna</i> ^{-/-} mESC.....	106
3.9.3 Rescue <i>Lmna</i> ^{-/-} phenotype by ablation of one <i>Gata4</i> allele in <i>Lmna</i> ^{-/-} mESC.....	107
3.9.4 Ablation of one <i>Gata4</i> allele rescues <i>Lmna</i> ^{+/-} and <i>Lmna</i> ^{-/-} mice capillary density.....	107
3.9.5 Ablation of one <i>Gata4</i> allele rescues <i>Lmna</i> ^{+/-} and <i>Lmna</i> ^{-/-} CMs proliferation in vivo	108
3.10 Working Model: key function of lamin A/C in naïve pluripotent stem cells for cardiac development and disease.....	109
4 DISCUSSION.....	111

4.1 LaminA/C plays a key role in alternative cardiovascular cell fate choices.....	111
4.2 3D chromatin reorganization upon <i>Lmna</i> loss.....	112
4.3 Role of pioneer transcription factors during cardiac development.....	114
4.4 Cardiac defects in lamin A/C loss of function cardiomyopathy.....	115
4.5 Endothelial cell dysfunction in lamin A/C LOF cardiomyopathy	116
4.6 Distinct role of lamin A/C in pluripotent stem cells and committed CMs.....	117
5 SUMMARY	119
6 REFERENCES.....	121
7 CURRICULUM VITAE	142
8 ACKNOWLEDGEMENT	143

LIST OF ABBREVIATIONS

ACs	Astrocytes
AHA	American Heart Association
ANOVA	Analysis of variance
ARVC	Arrhythmogenic right ventricular cardiomyopathy
ATAC-seq	Assay for Transposase-Accessible Chromatin using sequencing
cDNA	Complementary DNA
Chip-seq	Chromatin Immunoprecipitation Sequencing
CMs	Cardiomyocytes
CP	Cardiac progenitor
CRISPR	Clustered regularly interspaced short palindromic repeats
cTnT	TroponinT
DamID	DNA adenine methyltransferase identification
DCM	Dilated cardiomyopathy
DNA	Deoxyribonucleic acid
ECL	Chemiluminescence
ECs	Endothelial cells
EDMD	Emery-Dreifuss muscular dystrophy
EDTA	Ethylenediaminetetraacetic acid
FBS	Fetal bovine serum
FISH	Fluorescence in situ hybridization
HCM	Hypertrophic cardiomyopathy
HGPS	Hutchinson Gilford Progeria Syndrome
Hi-C	High-throughput chromosome conformation capture
hiPSCs	Human Induced pluripotent stem cells
IF	Immunofluorescence
INM	Inner nuclear membrane
LADs	Lamin-associated domains
LIF	Leukemia inhibitory factor
LVNC	Left ventricle noncompaction cardiomyopathy

MEFs	Mouse embryonic fibroblasts
MES	Mesoderm
mESCs	Mouse embryonic stem cells
NSCs	Neural stem/progenitor cells
ONM	Outer nuclear membrane
PCA	Principal component analysis
qPCR	Quantitative polymerase chain reaction
RNA	Ribonucleic acid
ROS	Reactive oxygen species
SMCs	Smooth muscle cells
SUN1	SUN-domain containing protein 1
TAD	Topologically associating domain
TF	Transcription factor
μl	Microliter
μm	Micrometre
μM	Micromolar
%	Percent
°C	Degree celsius

1 INTRODUCTION

1.1 Epigenetics and laminopathies

1.1.1 Structure, expression and post modifications of lamins

Nuclear lamins are type V intermediate filament proteins which line below the inner nuclear membrane. There are two type of lamins in metazoan cell nuclei: A-type of lamin and B-type of lamin (Peter, Kitten et al. 1989, Vorburger, Lehner et al. 1989). A-type lamins consist of lamin A and lamin C which are encoded by the *LMNA* gene through alternative splicing within exon 10 (Fisher, Chaudhary et al. 1986, McKeon, Kirschner et al. 1986). In addition to A-type of lamin, mammals such as mice also have lamin B1 and lamin B2 (B-type lamins), which are encoded *LMNB1* and *LMNB2* gene respectively (Peter, Kitten et al. 1989, Vorburger, Lehner et al. 1989, Lin and Worman 1995, Gruenbaum and Foisner 2015). *LMNB2* also encodes the germ-line-specific lamin B3, produced by alternative splicing (Höger, Zatloukal et al. 1990). A- and B-type lamins have a common structural organization: a short “head” domain at the N-terminus followed by a central helical rod domain and a C-terminal “tail” domain. The central rod domain is composed of four coiled-coil regions that allow lamins to form parallel coiled-coil dimers and higher-order meshworks (Burke and Stewart 2013, Turgay, Eibauer et al. 2017, Walling and Murphy 2021). The “tail” consists of a globular region, which adopts an immunoglobulin (Ig)-like β -fold involved in protein–protein interactions. Pre-lamin A- and B-type lamins also have a CaaX motif at the C-terminus which guides protein farnesylation and carboxyl methylation, important for targeting to the nuclear envelope (Burke and Stewart 2013, Turgay, Eibauer et al. 2017, Walling and Murphy 2021) (Fig. 1).

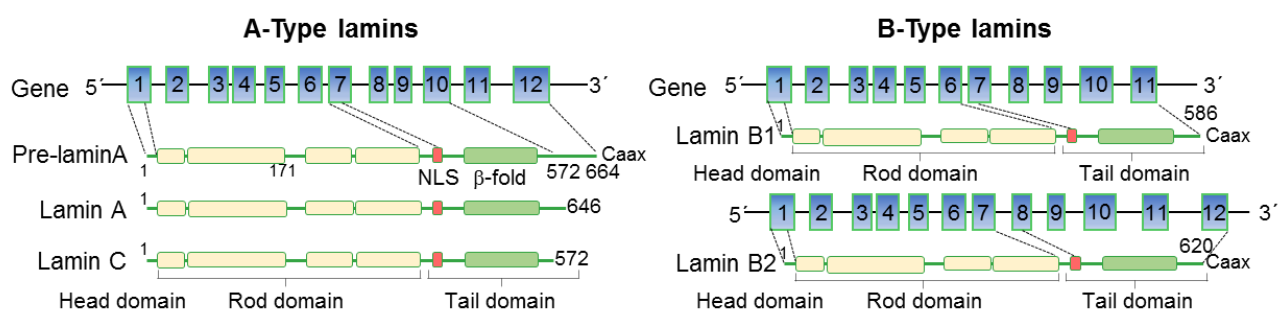


Figure 1. Structure of nuclear lamins. A- and B-type lamins have a conserved domain structure, consisting of a short N-terminal “head” domain, central helical coiled-coil rod domain, and a C-terminal immunoglobulin (Ig)-like β -fold domain. The nuclear localization signal (NLS) is located at the beginning of the tail domain. Pre-lamin A- and B-type lamins also have a CaaX motif at the C-terminus guiding their targeting to the inner nuclear membrane.

A-type lamins and B-type lamins form interconnected but separated networks with differential localization, membrane association, and network organization. These meshworks not only provide structural support to the nuclear envelope (Shimi, Kittisopikul et al. 2015, Nmezi, Xu et al.

2019), but also play important roles in chromatin organization, gene positioning, DNA replication and repair, as well as cell proliferation, differentiation and stress responses (Dittmer and Misteli 2011, Burke and Stewart 2013). Lamins are also key components of the LINC complex, which physically couples the nucleoskeleton with the cytoskeleton (Stroud, Banerjee et al. 2014, Jahed and Mofrad 2019, Lityagina and Dobrova 2021). Decoupling this connection via abnormal lamin A/C expression or mutation increases sensitivity to mechanical stress and impairs mechanosensing, which is particularly important for tissues that experience high levels of mechanical stress (Stroud, Banerjee et al. 2014, Jahed and Mofrad 2019, Lityagina and Dobrova 2021).

Tissues with higher mechanical stress and are stiff, like heart, lung and diaphragm muscle, express high lamin A/C levels. Whereas, soft tissues like brain, which bears little stress, have a higher B-type lamins (Fig. 2). Unlike A-type lamins, B-type lamins are expressed in all mammalian cells. For example, lamin B2 is constitutively expressed at relatively stable levels, whereas lamin B1 shows different expression during development and in adult (Kim, Sharov et al. 2011). The expression of A-type lamins is developmentally regulated and it has been long thought that A-type lamins are only expressed in committed cells such as cardiomyocytes and absent in mouse embryonic stem cells (mESCs) (Stewart and Burke 1987, Schirmer and Gerace 2004, Constantinescu, Gray et al. 2006, Kim, Sharov et al. 2011). However, recent studies show lamin A/C is detectable in both mRNA level and protein level in mESC (Constantinescu, Gray et al. 2006, Guo, Kim et al. 2014, Amendola and van Steensel 2015). This discrepancy could be due to the sensitivity of the antibodies and the mESC culture methods used. Moreover, the expression of A-type lamins also scales with matrix stiffness (Swift, Ivanovska et al. 2013, Majkut, Dingal et al. 2014).

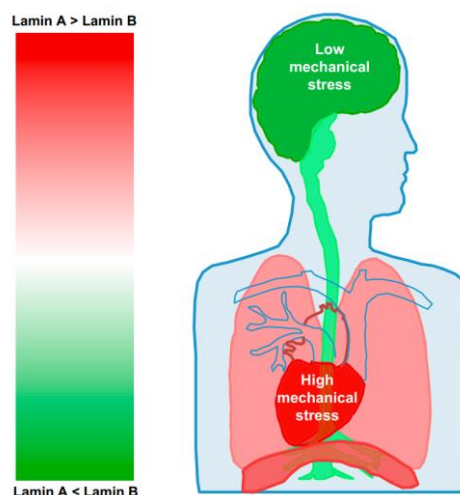


Figure 2. Expression pattern of A-type and B-type lamins. Tissues with higher mechanical stress and are stiff, like heart, lung and diaphragm muscle, express high lamin A/C levels. Whereas, soft tissues like brain, which bears little stress, have a higher B-type lamins. Reprint from (Majkut, Dingal et al. 2014). Permission is conveyed through Copyright Clearance Center, Inc.

1.1.2 Function of lamins: from nuclear structure to spatial chromatin organization

The nuclear lamina, together with the inner nuclear membrane (INM), the outer nuclear membrane (ONM) and the nuclear pore complex are the major components of the nuclear envelope. The nuclear lamina plays a key role in maintaining nuclear envelope structural integrity and genome stability. Nuclear lamina deficiency or mutation leads to nuclear abnormalities such as irregular nuclear shape (Lammerding, Hsiao et al. 2005), uneven distribution and mislocalization of nuclear pore complexes (Guo, Kim et al. 2014), nuclear rupture (Earle, Kirby et al. 2020), nuclear blebs (Funkhouser, Sknepnek et al. 2013) and micronuclei (Cho, Vashisth et al. 2019). Nuclear rupture causes DNA damage and this could be due to exposure of genomic DNA to cytoplasmic nucleases, nuclear exclusion and cytoplasmic mislocalization of DNA repair factors (Cho, Vashisth et al. 2019, Maynard, Keijzers et al. 2019). The nuclear lamina also regulates telomere length and positioning by interacting with shelterin protein TRF2 (Gonzalez-Suarez, Redwood et al. 2009, Wood, Danielsen et al. 2014, Pennarun, Picotto et al. 2021) thus affecting genome instability. A study from Wood et al. shows that lamin A/C interacts with TRF2 and stabilizes the t-loop formation between TRF2 and interstitial telomeric sequences. Mutation of *LMNA* that causes an autosomal dominant premature ageing disorder—Hutchinson Gilford Progeria Syndrome (HGPS)—leads to reduced interstitial t-loop formation and telomere attrition (Wood, Danielsen et al. 2014). Furthermore, another recent study shows that lamin B1 also interacts with TRF2 and RAP1 and protects telomere from being recognized as damage and inappropriately repaired by DNA repair machinery (Pennarun, Picotto et al. 2021).

In addition, nuclear lamina also tethers chromatin to the nuclear periphery, thereby shaping higher order chromatin structures (Fig. 3) (Van Steensel and Belmont 2017). In metazoan cell nuclei, nuclear lamins interact with chromatin by several distinct classes of transmembrane proteins including LEM domain proteins (Emerin, LAP2a/b and MAN1), lamin B receptor (LBR) and SUN domain proteins. Chromatin regions that are in close contact with the nuclear lamina are termed lamina-associated domains (LADs). During the past decade, genome-wide mapping methods, such as DNA adenine methyltransferase identification (DamID) and chromatin immunoprecipitation sequencing (ChIP-seq), have been used to identify LADs (Guelen, Pagie et al. 2008, Shimi, Pflieger et al. 2008, Peric-Hupkes, Meuleman et al. 2010, Berman, Weisenberger et al. 2012). DamID is a method to detect protein-DNA interactions in which bacterial DNA adenine methyltransferase (Dam) is tethered to a nuclear lamina protein leading to adenine methylation of DNA regions that contact the nuclear lamina protein (Steensel and Henikoff 2000, van Steensel, Delrow et al. 2001). LADs can also be mapped by chromatin immunoprecipitation, but this has been technically challenging because of the solubility and immunoprecipitation efficiency of nuclear lamins (Lund, Duband-Goulet et al. 2015, Gesson, Rescheneder et al. 2016).

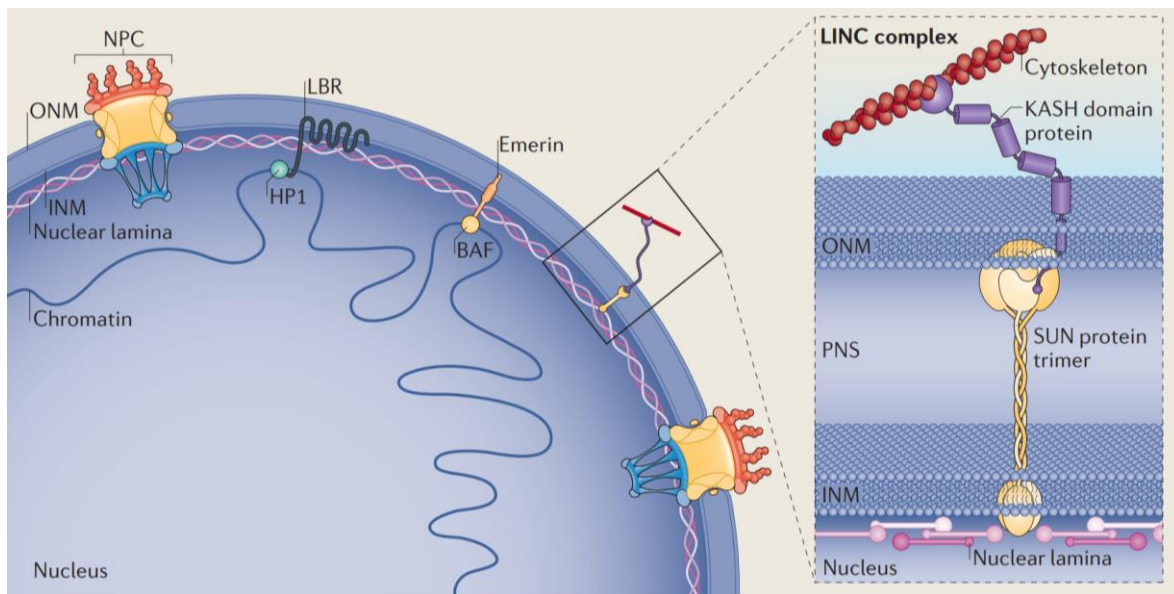


Figure 3. The nuclear lamina supports nuclear envelop and shapes chromatin organization. The nuclear lamins line below the inner nuclear membrane not only supporting nuclear envelope structural integrity. The nuclear lamins also interact with chromatin by several distinct classes of transmembrane proteins including LEM domain proteins (Emerin, LAP2a/b and MAN1), lamin B receptor (LBR) and SUN do-main proteins. The nuclear lamina is also coupled to components of the cytoskeleton by linker of the nucleoskeleton and cytoskeleton (LINC) complexes. Reprint from (Burke and Stewart 2013). Permission is conveyed through Copyright Clearance Center, Inc.

In mammalian cells, about 30%-40% of the genome is covered by LADs with the size ranging from 10 kb to 10 Mb. LADs exhibit a low overall gene density and include most “gene deserts”, defined as gene-free genomic regions >1 Mb (Guelen, Pagie et al. 2008, Peric-Hupkes, Meuleman et al. 2010, Leemans, van der Zwalm et al. 2019). Mapping of genome nuclear lamina interactions by DamID in various mouse and human cell types characterized two types of LADs: constitutive LADs (cLADs) and facultative LADs (fLADs) (Meuleman, Peric-Hupkes et al. 2013). cLADs are universally characterized by long stretches of DNA of high A/T content, long interspersed nuclear element (LINE) and poor in short interspersed nuclear element (SINE) repetitive elements, as well as forming the most gene-poor subset of LADs (Meuleman, Peric-Hupkes et al. 2013). In addition, cLAD genomic positions and sizes, rather than their actual DNA sequences, are strongly conserved between mouse and human suggesting cLADs may contribute to a basal chromosome architecture (Meuleman, Peric-Hupkes et al. 2013). Compared with cLADs, fLADs make up over half of all LADs and are more gene-dense than cLADs, and their positions are less conserved between mouse and human (Meuleman, Peric-Hupkes et al. 2013). During differentiation of mouse cells, hundreds of genes change position relative to the nuclear lamina, demonstrating the flexibility and dynamics of genome intranuclear spatial organization (Peric-Hupkes, Meuleman et al. 2010).

Electron microscopy and DNA fluorescence in situ hybridization (FISH) revealed that LADs are condensed and genomic loci within LADs exhibit low transcriptional activity (Poleshko, Shah et al. 2017, Van Steensel and Belmont 2017). Compacted LADs are enriched in repressive histone markers such as H3K9me2 and H3K9me3, and in some cases H3K27me3, which are

typical features of heterochromatin (Guelen, Pagie et al. 2008, Peric-Hupkes, Meuleman et al. 2010). Initial studies showed that genes within LADs are expressed at very low levels, suggesting that LADs may form a repressive chromatin state (Guelen, Pagie et al. 2008, Peric-Hupkes, Meuleman et al. 2010, Leemans, van der Zwalm et al. 2019). However, studies from different groups also show that LADs are heterogeneous and nuclear lamins do not generally repress their bound genes (Finlan, Sproul et al. 2008, Kumaran and Spector 2008, Leemans, van der Zwalm et al. 2019). In addition to nuclear lamina, heterochromatin also accumulates in the perinucleolar region and pericentromeric bodies (Fig. 4). Chromatin regions that are in close contact with nucleoli and centromeres are termed nucleolus associated domains (NADs) and pericentric heterochromatin domains (PADs) respectively (van Koningsbruggen, Gierliński et al. 2010). Similar to LADs, NADs also have a high density of AT-rich sequence elements, low gene density and a statistically significant enrichment in transcriptionally repressed genes (van Koningsbruggen, Gierliński et al. 2010). Although PADs and non-PADs have similar chromatin states in embryonic stem cells, but during lineage commitment, chromocenters progressively associate with constitutively inactive genomic regions at the nuclear periphery (Wijchers, Geeven et al. 2015). Moreover, experimentally induced proximity of an active locus to chromocenters was sufficient to cause gene repression (Wijchers, Geeven et al. 2015). A number of studies have shown that there is a redundancy and overlap between LADs, NADs and PADs. (Kind, Pagie et al. 2013, Kind and van Steensel 2014, Ragoczy, Telling et al. 2014, Politz, Scalzo et al. 2016). Multicolor FISH analysis revealed that late replicating loci, particularly on the smaller chromosomes, may associate with any of these 3 repressive subcompartments, including more than one at the same time (Ragoczy, Telling et al. 2014). Disruption of nucleoli resulted in an increased association of late replicating loci with peripheral heterochromatin, while deletion of the regions that conferred nuclear lamina association of the HBB transgenes resulted in a shift toward the pericentromeric compartment (Bian, Khanna et al. 2013, Ragoczy, Telling et al. 2014).

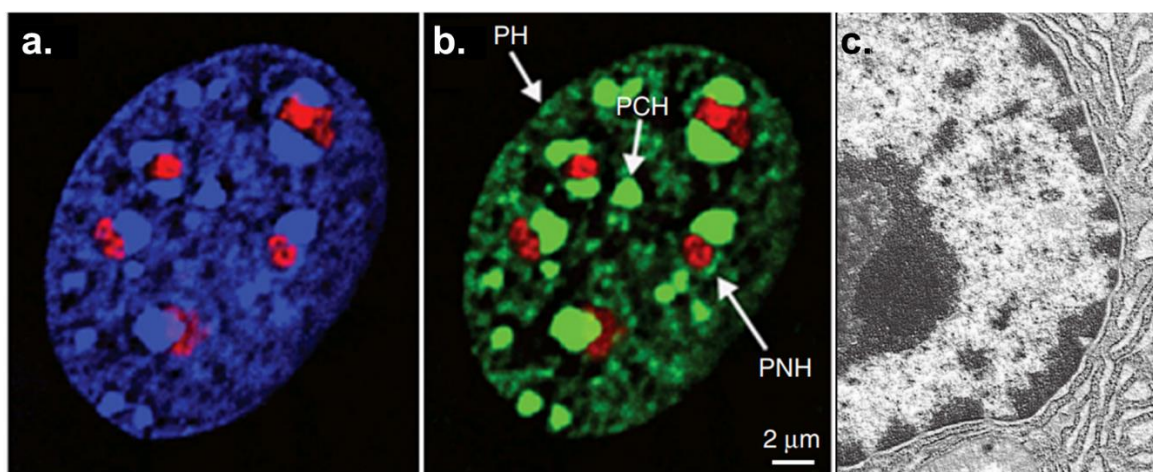


Figure 4. Heterochromatin distribution in mammalian cell. **a** and **b** Murine embryonic fibroblast stained with **(a)** DAPI (blue) plus antibodies to fibrillarin (red) to mark nucleoli and **(b)** antibodies to H3K9me3 (green) and fibrillarin

(red). **c** Electron micrograph of part of a mouse cell nucleus. Densely stained chromatin is closely associated with the NL, but is also present around nucleoli and in patches elsewhere in the nucleus. PH, peripheral heterochromatin; PNH, perinucleolar heterochromatin; PCH, pericentromeric heterochromatin. Reprint from (Politz, Scalzo et al. 2016, Van Steensel and Belmont 2017). Permission is conveyed through Copyright Clearance Center, Inc.

On a larger scale, chromosomes display a nonrandom nuclear organization highly influenced by their gene density and transcriptional status (Lieberman-Aiden, Van Berkum et al. 2009, Bickmore and van Steensel 2013, Gibcus and Dekker 2013). By chromosome conformation capture (3C) and its derivatives (e.g., 4C, Hi-C), the genome has been shown to be organized into higher order structural domains referred to as topologically associated domains (TADs). TADs tend to interact based on their epigenetic status and transcriptional activity, thus dividing chromosomes into two types of large-scale compartments generally called A compartments (active) and B compartments (inactive) (Rao, Huntley et al. 2014). An emerging body of work has shown that TAD boundaries are conserved between cell types (Dixon, Selvaraj et al. 2012, Nora, Lajoie et al. 2012, Dixon, Jung et al. 2015) and during differentiation (Fraser, Ferrai et al. 2015, Rubin, Barajas et al. 2017, Siersbæk, Madsen et al. 2017). Nevertheless, the strength of TAD boundaries can also decrease during differentiation (Bonev, Cohen et al. 2017), suggesting that TAD–TAD interactions and therefore large-scale genome conformation can be modulated in response to external stimuli. 3D organization of chromatin brings pairs of genomic sites that lie far apart along the linear genome into proximity. This ‘looping’ is part of the overall chromosomal folding process but also involves protein-mediated contacts between enhancers and gene promoters (Palstra, Tolhuis et al. 2003). Such contact can result in the assembly of RNA polymerase II at the core promoter and the consecutive cell type-specific activation of transcription. A nuclear lamina contact frequency map in human cells showed B, A compartment correlates with LADs inter-LADs domains respectively (Fig. 5) (Kind, Pagie et al. 2015). Considering the strong overlap of LADs, NADs, and PADs, compartment B may also correspond to the union of all heterochromatin compartments, including at the nuclear lamina, nucleoli, and centromeres.

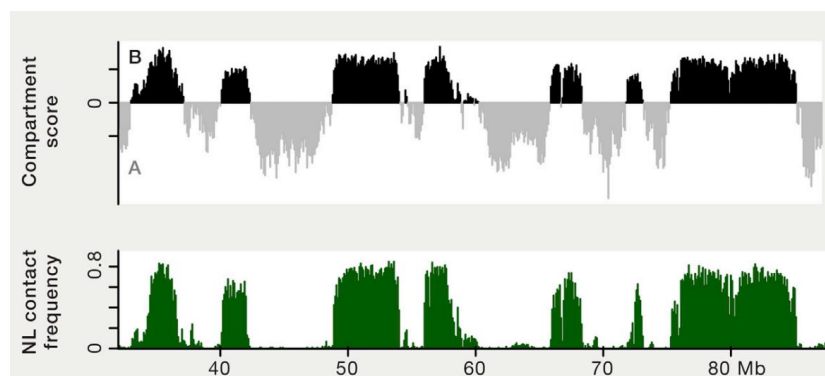


Figure 5. Overlaps between LADs and B compartment. Comparison of a NL contact frequency profile and Hi-C data in human KBM7 cells revealing remarkably strong similarity of NL contact frequencies to the compartment A/B profile. Reprint from (Van Steensel and Belmont 2017). Permission is conveyed through Copyright Clearance Center, Inc.

Chromatin-nuclear lamina dynamics play a key role in cell fate decisions by “locking” or “unlocking” genes conferring cell identity at the nuclear periphery (Fig. 6). For example, during mouse embryonic stem cell (ESC) differentiation into astrocytes (ACs), LADs are reorganized. This reorganization, on one hand, facilitates the detachment of the ACs genes from the ESCs LADs and involves ACs gene activation. On the other, a substantial number of genes are not immediately activated upon detachment from the nuclear lamina but rather become unlocked for activation at a later stage (Peric-Hupkes, Meuleman et al. 2010). Intriguingly, similar mechanism also occurs during cardiomyocytes differentiation. *Hdac3* directly represses cardiac differentiation through tethering of cardiomyocyte genes to the nuclear lamina. And loss of *Hdac3* in cardiac progenitor cells releases genomic regions from the nuclear periphery, leading to precocious cardiac gene expression and differentiation (Poleshko, Shah et al. 2017). Expanding these works further will likely impact our understanding of cardiac laminopathy involving defects in the nuclear lamina: dysregulated gene expression causing by genomic reorganization of LADs in cardiomyocytes has emerged as a plausible mechanism.

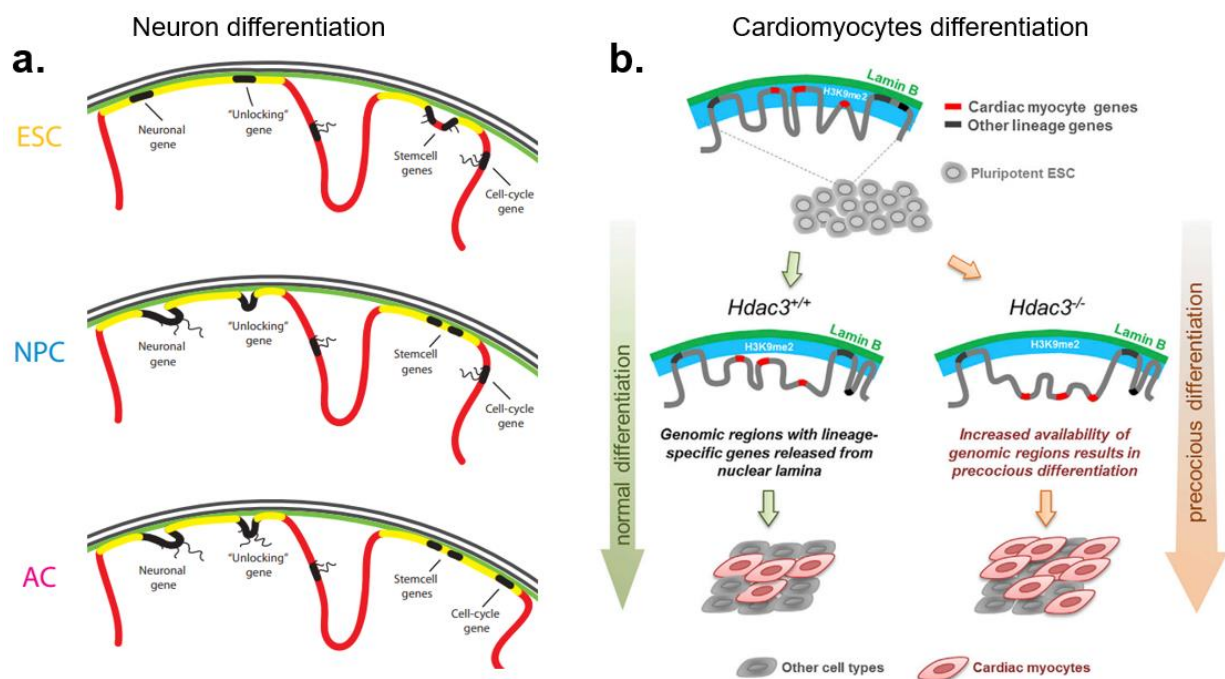


Figure 6. Chromatin-nuclear lamina dynamic changes during neuron and cardiomyocytes differentiation. Reprint from (Peric-Hupkes, Meuleman et al. 2010, Poleshko, Shah et al. 2017). Permission is conveyed through Copyright Clearance Center, Inc.

Previously studies revealed that nuclear lamina also affect TADs architecture of the genome. Hi-C chromosome conformation capture analysis showed that lamina-bound and lamina-unbound regions show a tendency to self-aggregate (Yaffe and Tanay 2011), indicating that nuclear lamina may affect gene expression by preventing long-range interactions of promoters within LADs with their distant enhancers outside of LADs. Furthermore, a recent study, which mapped genome wide chromatin interactions in lamin null mESCs using an insitu ligation-

based Hi-C method, showed that depletion of all lamins doesn't disrupt the overall TAD structure, but it leads to alterations in TAD-TAD interactions. Transcriptional changes upon lamin loss are correlated with alteration of 3D chromatin interactions. Interestingly, TAD pairs which show strong lamin B1 associations in both TADs exhibit increased inter-TAD interactions; whereas TAD pairs which show strong lamin B1 associations in one TAD or no lamin B1 associations have a decreased inter-TAD interactions (Zheng, Hu et al. 2018). The dynamic association of nuclear lamina with the 3D genome organization has also been implicated in hematopoiesis and immune activation. During T-cell activation, a sequestering of enhancers in LADs are, like genes, released from the nuclear periphery, enabling to interact with their promoters and to be activated (Robson, Jose et al. 2017).

On the other hand, lamin A/C also exists in the nuclear interior and interacts with euchromatin, which plays a role in gene regulation and cell differentiation (Naetar, Korbei et al. 2008, Kolb, Maaß et al. 2011, Gesson, Rescheneder et al. 2016). Loss of *LMNA* cause strikingly alters genome dynamics in the nuclear interior, inducing a dramatic transition from slow anomalous diffusion to fast and normal diffusion (Bronstein, Kepten et al. 2015). Thus, a dynamic association of *LMNA* with the 3D genome organization would constitute a mode of regulation of transcriptional activity.

1.1.3 Laminopathies

Mutations in nuclear lamins result in multisystem disease phenotypes collectively referred to as laminopathies (Schreiber and Kennedy 2013), including striated muscle disease, lipodystrophy syndrome, accelerated aging disorders and bone disease (Table 1).

Table 1. Diseases caused by mutations in nuclear lamins and lamin-associated proteins (Schreiber and Kennedy 2013)

Diseases	Genes Mutated
Striated Muscle Diseases	
Emery-Dreifuss muscular dystrophy	<i>LMNA</i> , <i>EDMD</i> , <i>SYNE1</i> , <i>SYNE2</i> , <i>TMEM43</i> , <i>TMPO</i>
Limb-girdle muscular dystrophy	<i>LMNA</i>
Dilated cardiomyopathy	<i>LMNA</i> , <i>EDMD</i> , <i>SYNE1</i> , <i>SYNE2</i> , <i>TMEM43</i> , <i>TMPO</i>
Congenital muscular dystrophy	<i>LMNA</i>
Heart-hand syndrome	<i>LMNA</i>
Lipodystrophy Syndromes	
Dunnigan-type familial partial lipodystrophy	<i>LMNA</i>
Mandibuloacral dysplasia	<i>LMNA</i> , <i>ZMPSTE24</i>
Lipoatrophy	<i>LMNA</i>
Partial lipodystrophy	<i>LMNB2</i>
Accelerated Aging Disorders	
Atypical Werner syndrome	<i>LMNA</i>

Hutchinson-Gilford progeria syndrome	<i>LMNA</i>
Restrictive dermopathy	<i>LMNA, ZMPSTE24</i>
Atypical progeria syndrome	<i>BANF1</i>
Peripheral Nerve Disorders	
Charcot-Marie-Tooth disease	<i>LMNA</i>
Adult-onset leukodystrophy	<i>LMNB1</i>
Spinocerebellar ataxia type 8	<i>SYNE1</i>
Bone Diseases	
Buschke-Ollendorff syndrome	<i>LEMD3</i>
Melorheostosis	<i>LEMD3</i>
Osteopoikilosis	<i>LEMD3</i>
Greenberg skeletal dysplasia	<i>LBR</i>
Others	
Pelger-Huet anomaly	<i>LBR</i>
Arthrogryposis	<i>SYNE2</i>

Diseases associated with *LMNA* mutation include Emery-Dreifuss muscular dystrophy (EDMD) (Bonne, Di Barletta et al. 1999), dilated cardiomyopathy (DCM) (Quarta, Syrris et al. 2012, Roncarati, Anselmi et al. 2013), lipodystrophy syndromes (Shackleton, Lloyd et al. 2000) and accelerated aging disorders (Cao and Hegele 2003). EDMD is characterized by early contractures, slowly progressive muscle wasting and cardiomyopathy (Bione, Maestrini et al. 1994, Bonne, Barletta et al. 1999). Striated muscle is selectively affected in EDMD with perturbations of the nuclear envelope, mislocalization of emerin and activation of MAPK pathways (Manilal, Man et al. 1996, Ostlund, Ellenberg et al. 1999, Muchir, Pavlidis et al. 2007). Dilated cardiomyopathy caused by *LMNA* mutation (Quarta, Syrris et al. 2012, Roncarati, Anselmi et al. 2013) is a common inherited cardiomyopathy that is associated with atrial arrhythmias, atrioventricular conduction block, and ventricular tachycardia, which often precede the development of systolic dysfunction (Marsman, Bardai et al. 2011, Quarta, Syrris et al. 2012, Van Rijsingen, Arbustini et al. 2012, Haugaa, Hasselberg et al. 2015). Defects in nuclear structures and alteration of calcium handling proteins are observed in *LMNA* mutant myocytes (Nikolova, Leimena et al. 2004, Cho, Vashisth et al. 2019, Lee, Termglinchan et al. 2019).

LMNA-linked lipodystrophy syndromes and premature ageing share several clinical similarities, such as hypertriglyceridemia, insulin resistance, type 2 diabetes, atherosclerosis and early cardiovascular complications (Cao and Hegele 2000, Caux, Dubosclard et al. 2003, Chen, Lee et al. 2003, Bidault, Garcia et al. 2013, Hamczyk, Villa-Bellosta et al. 2018, Patni, Li et al. 2019). HGPS is most frequently caused by a mutation in exon 11 of *LMNA* gene. This mutation leads to an aberrant mRNA splicing and a removal of 150 nucleotides from exon 11. The resulting lamin A Δ 150 mRNA gives rise to a truncated lamin A protein, referred to as progerin which

lacks 50 amino acids where a proteolytic cleavage site is located. As a consequence, progerin cannot undergo the C-terminal cleavage like wild type pre-lamin A and is permanently farnesylated. Accumulation of farnesylated progerin in cells induces genomic instability, DNA damage, vascular smooth muscle cell loss and triggers atherosclerosis and premature death in HGPS (Liu, Wang et al. 2005, Varga, Eriksson et al. 2006, Osorio, Navarro et al. 2011, Hamczyk, Villa-Bellosta et al. 2018). Interestingly, accumulation of pre-lamin A is also observed in *LMNA*-linked lipodystrophy syndromes and this could be due to the altered recognition of the mutated pre-lamin A by the Zmpste24 protease (Capanni, Mattioli et al. 2005, Caron, Auclair et al. 2007). Although accumulated progerin has been linked to DNA damage in HGPS, the function of accumulated pre-lamin A in lipodystrophy mutant cells still need to be further studied.

Besides *LMNA*, B-type lamins are shown to be linked with aging as well. Dermal fibroblasts from an E145K progeria patient show a remarkable reduced lamin B1 and lamin B2 expression (Taimen, Pflieger et al. 2009). And lamin B1 decline is also found in primary human and mouse fibroblasts when induced to senesce by DNA damage, replicative exhaustion, or oncogene expression, which is independent of p38 MAPK, NF- κ B, ataxia telangiectasia mutated kinase, and ROS signaling (Freund, Laberge et al. 2012). Conversely, silencing lamin B1 in human fibroblasts leads to cell proliferation defects and induces cell senescence. The proliferation defects induced by silencing lamin B1 is through a reactive oxygen species (ROS) signaling pathway (Shimi, Butin-Israeli et al. 2011). Whereas, another study from Barascu, Aurelia, et al. shows a lamin B1 accumulation and p38 MAPK activation in fibroblasts from patients with ataxia telangiectasia. And lamin B1 overexpression is sufficient to induce senescence in primary human fibroblasts (Barascu, Le Chalony et al. 2012). Although these two studies are discrepancy, both of the authors do agree that increased ROS generation is associated with increased lamin B1 levels.

Links between lamin B1 decline and age-related loss of adult hippocampal neurogenesis have also been reported (Bedrosian, Houtman et al. 2021, Bin Imtiaz, Jaeger et al. 2021). *LMNB1* and *LMNB2* are essential to the maintenance of nervous system development (Vergnes, Péterfy et al. 2004, Coffinier, Chang et al. 2010, Chen, Yang et al. 2019). *Lmnb1*^{-/-} and *Lmnb2*^{-/-} mice survived embryonic development but died after birth immediately with defects in brain, lung, diaphragms (Vergnes, Péterfy et al. 2004, Kim, Sharov et al. 2011). Defects in spindle orientation in neural progenitor cells and migration of neurons have been shown to cause brain disorganizations found in lamin B null mice (Kim, Sharov et al. 2011). Indeed, recent studies further showed that lamin B1 is highly expressed in adult neural stem/progenitor cells and plays a key role in maintenance of adult neural stem/progenitor cells proliferation and differentiation (Alcalá-Vida, Garcia-Forn et al. 2021, Bedrosian, Houtman et al. 2021, Bin Imtiaz, Jaeger et al. 2021). During aging, lamin B1 expression in neural progenitors is sharply decreased, whereas protein levels of SUN-domain containing protein 1 (SUN1), previously

implicated in HGPS, increase. Balancing the levels of lamin B1 and SUN1 in aged NSCs restores the strength of the endoplasmic reticulum diffusion barrier that is associated with segregation of aging factors in proliferating NSCs (Bedrosian, Houtman et al. 2021, Bin Imtiaz, Jaeger et al. 2021).

1.2 LMNA-related cardiomyopathy

As mentioned above (Table 1), patients harbouring mutations in *LMNA* can develop a number of different tissue-specific syndromes collectively termed laminopathies. Cardiomyopathy is one of the common phenotypes frequently caused by *LMNA* mutations. The American Heart Association (AHA) defines cardiomyopathies as a heterogeneous group of diseases of the myocardium associated with mechanical and/or electrical dysfunction that usually (but not invariably) exhibit inappropriate ventricular hypertrophy or dilatation (Maron, Towbin et al. 2006). Types of (primary) cardiomyopathies include hypertrophic cardiomyopathy (HCM), dilated cardiomyopathy (DCM), left ventricle noncompaction cardiomyopathy (LVNC), arrhythmogenic right ventricular cardiomyopathy (ARVC) and restrictive cardiomyopathy (Maron, Towbin et al. 2006). *LMNA* mutation has been shown to be associated with dilated cardiomyopathy, left ventricle noncompaction cardiomyopathy, arrhythmogenic right ventricular cardiomyopathy.

1.2.1 Dilated cardiomyopathy

Dilated cardiomyopathy (DCM) is characterized by enlargement and dilatation of one or both ventricles of the heart, which occurs together with impaired contractility and heart function (Gerull, Klaassen et al. 2020). The *LMNA* gene is the second most commonly mutated gene in familial dilated cardiomyopathy (DCM), accounting for 5% to 8% of cases (McNally and Mestroni 2017). Patients carrying pathogenic *LMNA* mutations have a poor prognosis due to the high rate of sudden cardiac death resulting from malignant arrhythmias. Atrial fibrillation (AF), atrioventricular (AV) conduction block, ventricular tachycardia, and sudden cardiac death often precede the development of systolic dysfunction (Fatkin, MacRae et al. 1999, Quarta, Syrris et al. 2012, Van Rijsingen, Arbustini et al. 2012). Although *LMNA*-related DCM is an adult-onset disease, it cannot be excluded that structural changes and arrhythmias may be present in early asymptomatic individuals (Kumar, Baldinger et al. 2016).

To date, around 500 mutations and 300 protein variants have been reported for *LMNA*; detailed information on the different mutations is available through the UMD-*LMNA* mutation database (www.umd.be/LMNA, accessed on 1 January 2023) (Table 2). Most of the mutations associated with cardiomyopathies are located in the head and rod domains and are mostly truncation or missense mutations (Nishiuchi, Makiyama et al. 2017). Heterozygous truncation mutations often result in lamin A/C haploinsufficiency due to a premature termination codon generated by insertions or deletions resulting in a frameshift, aberrant splice site, or nonsense mutations.

A homozygous *LMNA* nonsense mutation (Y259X) has also been reported, resulting in a lethal phenotype (van Engelen, Muchir et al. 2005). *LMNA* missense mutations, on the other hand, are thought to mostly act through a dominant negative mechanism (Nishiuchi, Makiyama et al. 2017). Patients carrying heterozygous mutations in *LMNA* in combination with mutations within other genes such as *TTN*, *DES*, *SUN1/2*, etc., display a particularly severe clinical cardiac phenotype (Roncarati, Viviani Anselmi et al. 2013, Meinke, Mattioli et al. 2014, Galata, Kloukina et al. 2018, Maggi, Mavroidis et al. 2021, Vincenzo, Michelangelo et al. 2022).

Table 2. Cardiomyopathies caused by the most well studied pathogenic *LMNA* mutations in patients.

LMNA mutation	Expression pattern of mutant LaminA/C	Disease	Clinical phenotypes	References
p. N195K	Reduced lamin A/C	DCM	Heart dilation, interstitial fibrosis, arrhythmia, sarcomere disorganization, mislocalization of emerin	(Mounkes, Kozlov et al. 2005, Ho, Jaalouk et al. 2013, Markandeya, Tsoubouchi et al. 2016)
p. R225X	Haploinsufficiency, a nonsense mutation causing premature truncation	DCM	Atrial fibrillation, complete atrioventricular block, ventricular tachyarrhythmia and heart failure	(Lee, Lau et al. 2017, Cai, Lee et al. 2020)
p. K117fs	NMD-mediated degradation of mutant <i>LMNA</i> mRNA induces lamin A/C haploinsufficiency	DCM	Atrioventricular block, ventricular tachycardia, atrial fibrillation, arrhythmias at the single-cell level	(Lee, Termglinchan et al. 2019)
p.c.908_909 delCT	Reduced and truncated lamin A/C expression causing by frameshift	DCM	Atrial fibrillation, sick sinus syndrome, dilated cardiomyopathy	(MacLeod, Culley et al. 2003)
p.28insA	Reduced, insertion mutation leads to an aberrant truncated protein of 38 amino acids	DCM	Dilated cardiomyopathy with conduction defects	(Sebillon, Bouchier et al. 2003)
p. T101	Reduced lamin A/C expression	DCM, lipodystrophy, APS	Hypertriglyceridemia, diabetes mellitus, insulin resistance, left ventricular myocyte hypertrophy, interstitial fibrosis	(Mory, Crispim et al. 2008, Hussain, Patni et al. 2018, Sahinoz, Khairi et al. 2018, Shah, Lv et al. 2021)
p. R541S	Reduced lamin A/C expression	DCM	LV systolic dysfunction, left ventricular dilation	(Gupta, Bilinska et al. 2010)
p. R377H	Reduced lamin A/C expression	EDMD, DCM	Atrial fibrillation or flutter, cardiac conduction disease	(Muchir, Bonne et al. 2000, Charniot, Pascal et al. 2003, Yang, Argenziano et al. 2021)
p. S143p	No change, loss of function phenotype, p. S143P lamin A/C is more nucleoplasmic and soluble	DCM	Atrioventricular conduction defect, left ventricular systolic dysfunction and dilatation	(West, Gullmets et al. 2016, West, Turunen et al. 2022)
p.H222P	No change, gain of function phenotype	DCM, EDMD	Atria and ventricles dilation, fibrosis, atrio-ventricular conduction abnormality, prenatal heart abnormalities	(Arimura, Helbling-Leclerc et al. 2005, Wada, Kato et al. 2019, Guevantin, Jebeniani et al. 2021)
p. K219T	No change Gain of function phenotype	DCM	Heart dilation, arrhythmogenic conduction disorders such as atrial fibrillation, atrioventricular block	(Perrot, Hussein et al. 2009, Salvarani, Crasto et al. 2019)
p. R541C	No change, gain of function phenotype, increased H3K9me2/3	DCM	Reduced heart contractility, left ventricle dilatation, polymor-	(Shah, Lv et al. 2021, Yang, Sun et al. 2022)

			phic ventricular premature contractions and diffuse ST-T change	
p.R190W	-----	DCM, LVNC, ARVC	Left ventricular noncompaction, conduction system defect, abnormal activation of ERK1/2 signaling and sarcomeric disorganization	(Hermida-Prieto, Monserrat et al. 2004, Liu, Shan et al. 2016, Chatzifrangkeskou, Yadin et al. 2018)
p. R190Q	-----	DCM	Heart dilation, AV block, atrial fibrillation, muscular involvement	(Perrot, Hussein et al. 2009, Gerbino, Forleo et al. 2021)
p. R644C	-----	DCM, LVNC, ARVC, lipodystrophy, APS	Phenotypic diversity and low penetrance associated with the R644C mutation	(Rankin, Auer-Grumbach et al. 2008, Parent, Towbin et al. 2015)
p. V445e	-----	LVNC	Ventricular tachycardia/fibrillation,	(Liu, Shan et al. 2016)
p. R60G	-----	FLPD, cardiomyopathy	Hypertriglyceridemia, diabetes, ventricular dysfunction, conduction defect, and arrhythmia, left-ventricular systolic dysfunction	(Van der Kooi, Bonne et al. 2002, Subramanyam, Simha et al. 2010)
p. R62G	-----	FLPD, DCM	Diabetes, hyperlipidemia, atrioventricular conduction defects and atrial fibrillation, dilated cardiomyopathy	(Garg, Speckman et al. 2002, Subramanyam, Simha et al. 2010)
p. E203K	-----	DCM	Ventricular dysrhythmias, left ventricular enlargement, and systolic dysfunction	(Jakobs, Hanson et al. 2001)
p. E203G	-----	DCM	Ventricular dysrhythmias, left ventricular enlargement, and systolic dysfunction	(Fatkin, MacRae et al. 1999)
p. E161K	Seems laminA/C normally expressed in CMs	DCM	Dilation, atrial fibrillation, conduction system disease, chromosome positioning changes	(Sebillon, Bouchier et al. 2003, Mewborn, Puckelwartz et al. 2010)
p. L85R	-----	DCM	Progressive conduction-system disease such as sinus bradycardia, atrioventricular conduction block, or atrial arrhythmias and dilated cardiomyopathy, Mislocalization of emerin	(Fatkin, MacRae et al. 1999, Raharjo, Enarson et al. 2001)
p.c.835 delG:p.Glu279Ar-gfsX201	Reduced and truncated lamin A/C expression	RCM	Diastolic dysfunction, biatrial enlargement, atrial fibrillation, skeletal muscle weakness	(Paller, Martin et al. 2018)

Dilated cardiomyopathy (DCM); left ventricular noncompaction cardiomyopathy (LVNC); arrhythmogenic right ventricular cardiomyopathy (ARVC); restrictive cardiomyopathy (RCM); Emery–Dreifuss muscular dystrophy (EDMD); limb–girdle muscular dystrophy (LGMD); APS, atypical progeroid syndrome.

Since a number of *LMNA* mutations result in a loss of function, lamin A/C haploinsufficient (*Lmna*^{+/-}) and *Lmna* knockout mice (*Lmna*^{-/-}) have been extensively used to study the molecular mechanisms underlying *LMNA* loss-of-function (LOF) cardiomyopathy (Table 3). *Lmna*^{-/-} mice develop DCM two weeks after birth and died within one month (Kim and Zheng 2013). Although *Lmna*^{+/-} mice are viable and fertile, the conduction system defects and heart dilation are also observed in heterozygous *Lmna*^{+/-} mice by longitudinal evaluations (Wolf, Wang et al. 2008). Myocytes isolated from *Lmna*^{-/-} mice show defects in proliferation, precocious

nucleation, nuclear structures deformation, chromatin rearrangement and alteration of calcium handling (Nikolova, Leimena et al. 2004).

Table 3. Mouse models of laminopathies.

Mouse Model	Gene Targeting Strategy	Disease	Homozygous Phenotype	Heterozygous Phenotype	References
<i>Lmna</i> ^{-/-} *	Deletion of exons 8-11; a truncated lamin A protein of 54 kDa is still expressed	DCM, EDMD	Retarded postnatal growth, conduction disorders, DCM, EDMD, death by 8 weeks of age	AV conduction defects, both atrial and ventricular arrhythmias; develop DCM by 50 weeks	(Nikolova, Leimena et al. 2004, Wolf, Wang et al. 2008)
<i>Lmna</i> ^{-/-}	Deletion of exon 2	DCM LVNC	Retarded postnatal growth, conduction disorders, DCM, noncompaction, death within 1 month, developmental defects	RV dilatation, RV noncompaction, developmental defects	(Kim and Zheng 2013)
<i>Lmna</i> GT ^{-/-}	A gene trap cassette inserted upstream of exon 2 of <i>Lmna</i>	N/A	Growth retardation at 2 weeks, impaired postnatal cardiac hypertrophy, skeletal muscle hypotrophy, defects in lipid metabolism	No apparent abnormalities	(Kubben, Voncken et al. 2011)
<i>Myh6</i> cre - <i>Lmna</i> f/f	Conditional deletion of <i>Lmna</i> gene in cardiomyocytes	DCM	DCM, cardiac dysfunction, conduction defects, ventricular arrhythmias, fibrosis, apoptosis, and premature death within 4 weeks	Develop cardiac dilatation and dysfunction, cardiac arrhythmias, fibrosis in older mice	(Auguste, Rouhi et al. 2020)
Lamin C only	Deletion of the last 150 nucleotides of exon 11 and the complete intron 11	N/A	No obvious phenotype	No obvious phenotype	(Fong, Ng et al. 2006)
Lamin A only	Deletion of introns 10 and 11, the last 30 bp of exon 11, and the first 24 bp of exon 12	N/A	No apparent abnormalities	N/A	(Coffinier, Jung et al. 2010)
Pre-lamin A only	Deletion of intron 10	N/A	No apparent abnormalities	N/A	(Coffinier, Jung et al. 2010)
<i>Lmna</i> N195K	Missense mutation in exon 3	DCM	DCM, conduction defects, fibrosis, minor growth retardation, increased heart weight, death at 12–14 weeks	No obvious phenotype	(Mounkes, Kozlov et al. 2005)
<i>Lmna</i> R225X	Nonsense mutation at exon 4 causing premature truncation of both lamin A and lamin C	DCM	Retarded postnatal growth, conduction disorders, dilated cardiomyopathy, AV node fibrosis, death within postnatal 2 weeks	No apparent abnormalities	(Cai, Lee et al. 2020)
<i>Lmna</i> E82K	Transgenic mice expressing <i>Lmna</i> E82K under the control of α -MHC promoter	DCM	N/A	DCM, conduction defects, fibrosis, increased heart weight	(Dan, Lian et al. 2010)
<i>Lmna</i> Δ K32	Deletion of lysine 32 of lamin A/C in exon 1	DCM	Retarded postnatal growth, striated muscle maturation delay, metabolic defects including	Develop a progressive cardiac dysfunction and DCM	(Bertrand, Renou et al. 2012, Cattin, Bertrand et

			reduced adipose tissue and hypoglycemia, death within 3 weeks		al. 2013, Cattin, Ferry et al. 2016)
<i>Lmna</i> R541C	Missense mutation in exon 10	DCM	Ventricular dilatation and reduced systolic function	N/A	(Yang, Sun et al. 2022)
<i>Lmna</i> H222P	Missense mutation in exon 4	EDMD DCM	Heart dilatation, conduction defects, increased fibrosis, hypertrophy defects, death by 9 months of age, developmental defects	No apparent abnormalities	(Arimura, Helbling-Leclerc et al. 2005, Wada, Kato et al. 2019, Guenantin, Jebeniani et al. 2021)
<i>Lmna</i> M317K	Transgenic mice expressing <i>Lmna</i> M317K missense mutation under the control of α -MHC promoter	EDMD	N/A	Increased eosinophilia and fragmentation of cardiomyofibrils, nuclear pyknosis and edema without fibrosis or significant inflammation, death at 2–7 weeks of age	(Wang, Herron et al. 2006)
<i>Lmna</i> D300N	Transgenic mice expressing <i>Lmna</i> D300N; Myh6-tTA mice	DCM	N/A	Heart dilatation, increased heart-to-body-weight ratio, fibrosis, death within two months	(Chen, Lombardi et al. 2019)
<i>Lmna</i> L530P	Missense mutation in exon 9	HGPS	Loss of subcutaneous fat, reduction in growth rate, and death by 4 weeks of age	No apparent abnormalities	(Mounkes, Kozlov et al. 2003)
<i>Lmna</i> G609G	Point mutation in exon 11	HGPS	Shortened life span, reduced body weight, bone and cardiovascular abnormalities, death at an average of 100 days	Develop a similar phenotype to homozygotes but at an older age, average death at 242 days	(Osorio, Navarro et al. 2011)
<i>Lmna</i> HG	Deletion of introns 10–11 and last 150 nucleotides of exon 11	HGPS	Growth retardation osteoporosis, micrognathia, loss of adipose tissue, death by 3–4 weeks of age	Similar phenotype to homozygotes but less severe, death by 21 weeks	(Yang, Meta et al. 2006)
<i>Lmna</i> nHG	Deletion of introns 10 and 11 and the last 150 bp of exon 11 together with an exchange of cysteine to serine in the CaaX motif	HGPS	Weight loss, reduced subcutaneous and abdominal fat by 4–8 weeks of age, death at 17 weeks of age	Similar spectrum of disease phenotypes as <i>Lmna</i> HG/+ mice but less severe, death by 36 weeks of age	(Yang, Andres et al. 2008)
csmHG	Deletion of introns 10 and 11 and the last 150 bp of exon 11, three-nucleotide deletion (the isoleucine in progerin's CaaX motif)	HGPS	No bone phenotype, normal body weight and survival	No bone disease, normal body weight and survival	(Yang, Chang et al. 2011)
G608G BAC	164-kb BAC carrying mutated G608G human <i>LMNA</i>	HGPS	N/A	Progressive loss of vascular smooth muscle cells	(Varga, Eriksson et al. 2006)

te-top_LAG608G	Targeted expression of the lamin A G608G minigene using the keratin 5 transactivator	HGPS	N/A	Growth retardation, skin and teeth abnormalities, fibrosis, loss of hypodermal adipocytes	(Sagelius, Rosengardt et al. 2008)
Keratin14-progerin	Vector expressing progerin in epidermis under the control of the keratin 14 promoter	HGPS	N/A	Severe abnormalities in skin keratinocyte nuclei, including nuclear envelope lobulation and decreased nuclear circularity	(Wang, Panteleyev et al. 2008)

*: Although initially this mouse model has been used as a *Lmna* knockout mouse model, later studies revealed that a truncated lamin A protein of 54 kDa is still expressed.

Another mutation often used for modeling the *LMNA* LOF mutation is the p.R225X mutation, a nonsense mutation causing premature truncation of both lamin A and lamin C splice isoforms. Patients carrying this pathogenic mutation show early onset of AF, secondary AV block, and DCM (Lee, Jiang et al. 2016). Like *Lmna*^{-/-} mice, homozygote *Lmna* R225X mice also exhibit retarded postnatal growth, conduction disorders, and DCM (Cai, Lee et al. 2020). Other LOF mutations, e.g., K117fs and 28insA, also lead to a DCM phenotype. *LMNA* p. K117fs mutation is a frameshift mutation that leads to a premature translation-termination codon (Lee, Termglinchan et al. 2019), whereas 28insA is an adenosine insertion mutation in exon 1 resulting similarly in a premature stop codon (Sebillon, Bouchier et al. 2003). Messenger RNAs (mRNAs) that contain a premature stop codon often undergo degradation through the nonsense-mediated mRNA decay (NMD) surveillance mechanism and thus can cause haploinsufficiency. Consistent with this, a significant decrease in lamin A/C protein levels is observed in K117fs iPSC-CMs as a result of NMD-mediated degradation of *LMNA* mRNA (Lee, Termglinchan et al. 2019). In addition to truncation mutations, which can result in *LMNA* haploinsufficiency, mutations such as N195K, T10I, R541S, and R337H also show reduced lamin A/C protein levels (Mounkes, Kozlov et al. 2005, Shah, Lv et al. 2021). Patients carrying these pathogenic mutations also develop DCM (Fatkin, MacRae et al. 1999, Bonne, Mercuri et al. 2000, Gupta, Bilinska et al. 2010). It is still unclear why these mutations lead to decreased lamin A/C levels. Possible reasons could be that protein translation or the stability of lamin A/C are affected in mutant CMs. For example, although *Lmna* mRNA does not change, both lamin A and lamin C levels are decreased in CMs and MEFs derived from *Lmna* N195K/N195K mutant mice (Mounkes, Kozlov et al. 2005). Studies from the Discher lab shows that *LMNA* levels are tightly linked to the changing stiffness of the heart during development. Soft matrix favors lamin A/C phosphorylation at Ser22, localization to nucleoplasm and its subsequent proteolytic degradation. Intriguingly, this proteolytic degradation can be rescued by a cyclin-dependent kinase (CDK) inhibitor that was found significantly decreased in heart disease (Burton, Yacoub et al. 1999, Buxboim, Swift et al. 2014, Cho, Vashisth et al. 2019). Interestingly, patients carrying different *LMNA* missense mutations resulting in DCM also exhibit lower protein levels

(Cheedipudi, Matkovich et al. 2019). To what extent the decrease in lamin A/C levels or changes in protein function result in disease pathogenesis is still largely unknown and needs further investigation.

Although it seems DCM is predominantly caused by *LMNA* haploinsufficiency, mutations of *LMNA* which don't lead to changes of lamin A/C protein level also result in DCM. *LMNA* H222P missense mutation has been shown to cause emery-dreifuss muscular dystrophy and DCM. Compared with *Lmna* H222P/+ mice which are indistinguishable from wild type mice with regard to phenotype and life expectancy, homozygous mice display muscular dystrophy, left ventricular dilatation, and conduction defects in adulthood and die by 9 months of age (Arimura, Helbling-Leclerc et al. 2005). Interestingly, western blot analysis of cardiac and skeletal muscle samples shows no obvious difference of lamin A/C protein levels between WT and *Lmna* H222P/H222P mice (Wada, Kato et al. 2019). Similarly, patients with *LMNA* K219T mutation are characterized by severe DCM and heart failure with conduction system disease (Perrot, Hussein et al. 2009). And immunofluorescence of lamin A/C in iPSC-CMs with *LMNA* K219T mutation also doesn't show a decrease of lamin A/C expression (Salvarani, Crasto et al. 2019).

Among laminopathy-associated missense mutations, the addition of proline is the most common. Proline addition can significantly alter protein structure. For example, *LMNA* S143P missense mutation causes DCM and disturbs the coiled-coil domain, thus affecting lamin A/C assembly into the nuclear lamina. This results in nuclear fragility and reduced cellular stress tolerance (West, Gullmets et al. 2016). The addition of proline might also affect protein phosphorylation through proline-directed kinases, such as the mitogen-activated protein (MAP) kinases, cyclin-dependent protein kinase 5 (CDK5), glycogen synthase 3, etc. Mutations resulting in the addition of proline often result in striated muscle disease, suggesting a common underlying mechanism (Lin, Brady et al. 2020).

Since *LMNA* related DCM arises from distinct point mutations and is characterized by a diversity heart phenotype such as LV dilation, cardiac arrhythmias and fibrosis. Thus, the precise molecular mechanisms resulting in DCM also show a complexity. Taking into account the variety of different functions of the nuclear lamina, three central mechanisms have been suggested to drive disease pathogenesis.

The "mechanical hypothesis" proposes that disruption of the nuclear lamina causes increased nuclear fragility and increased susceptibility to mechanical stress (Brayson and Shanahan 2017). This hypothesis is supported by observations that CMs from patients or mouse models with lamin A/C mutations exhibit nuclear rupture, DNA damage, and cell cycle arrest (Nikolova, Leimena et al. 2004, Gupta, Bilinska et al. 2010, Cho, Vashisth et al. 2019). Importantly, a recent study revealed that disrupting the LINC complex and thereby decoupling the nucleus/nucleoskeleton from the mechanical forces transduced by the cytoskeleton increases

more than fivefold the lifespan of *LMNA*-deficient mice (Chai, Werner et al. 2021), pointing to therapeutic opportunities for patients carrying mutations resulting in nuclear fragility.

Myriad studies have demonstrated a role of lamins in regulating MAPK, TGF- β , Wnt- β -catenin, and Notch signaling cascades (Andres and Gonzalez 2009, Bernasconi, Carboni et al. 2018) and suggested that altered signaling is a key driver of *LMNA*-related dilated cardiomyopathy. For instance, *LMNA*-related cardiomyopathy shows a significant increase in myocardial fibrosis which contributes to left ventricular dysfunction and heart failure (Mounkes, Kozlov et al. 2005, Wu, Muchir et al. 2011, Quarta, Syrris et al. 2012, Chatzifrangkeskou, Le Dour et al. 2016). Profibrotic signaling, such as TGF- β , MAPK, and ERK signaling, is activated in *Lmna* H222P/H222P mice, and the partial inhibition of ERK and JNK signaling before the onset of cardiomyopathy in *Lmna* H222P/H222P mice significantly reduces cardiac fibrosis and prevents the development of left ventricle dilatation and decreased cardiac ejection fraction (Muchir, Pavlidis et al. 2007, Wu, Shan et al. 2010, Wu, Muchir et al. 2011, Umbarkar, Tousif et al. 2022). Therapies targeting intracellular signaling alterations are being developed in a pre-clinical setting (Cattin, Muchir et al. 2013).

Although the “mechanical hypothesis” explains the heart dilation phenotype, the molecular mechanisms linking the *LMNA* mutations to the increased arrhythmogenicity is still not known. The “gene expression hypothesis” implies that mutation in *LMNA* disrupts chromatin organization and leads to gene dysregulation in cardiomyopathies (Worman and Courvalin 2004, Brayson and Shanahan 2017). Recently, several groups using iPSC-CMs uncovered an epigenetic regulation of transcriptional changes of different channels such as *SCN5A*, *CACNA1A* and *Pdgf*. This might explain the arrhythmogenic conduction defects in *LMNA* patients (Bertero, Fields et al. 2019, Lee, Termglinchan et al. 2019, Salvarani, Crasto et al. 2019). Since iPSCs don't express detectable lamin A/C protein levels and all these studies are performed in CMs, the possible developmental defects may not be able to see by using iPSC. Indeed, a more recent study showed a developmental defects origin of *LMNA* associated cardiomyopathy. Guenantin et al. discovered that *Lmna* H222P/H222P embryonic hearts showed hypertrabeculation, interventricular septum defect and enlarged atria during development, as early as embryonic day 13.5. *Lmna* H222P/H222P embryos also display higher rates of lethality compared with normal or heterozygous controls. Using *Lmna* H222P/+ mouse ESCs, the author shows that cardiac mesoderm marker *Mesp1* as well as *Snai1* and *Twist* which are involved in epithelial-to-mesenchymal transition of epiblast cells was decreased and cardiac mesoderm specification and cardiomyocytes differentiation were impaired (Guenantin, Jebeniani et al. 2021). Guenantin et al. discovered a cardiac developmental defect as a prenatal feature and ascertaining whether other *LMNA* mutations have an impaired heart development and act through the same pathways will be a critical next step. Links between alternative fate choices and tissue-specific

phenotypes caused by pathogenic *LMNA* mutations would also be interesting for further studies.

1.2.2 Left ventricle non-compaction cardiomyopathy

Left ventricular non-compaction (LVNC) cardiomyopathy is a rare congenital heart disease caused by the arrest of normal embryogenesis of the endocardium and myocardium (Fig.7). Patients with LVNC exhibit a thin compacted myocardium and an excessive endocardium trabeculations and can eventually develop progressive cardiac dysfunction and heart failure.

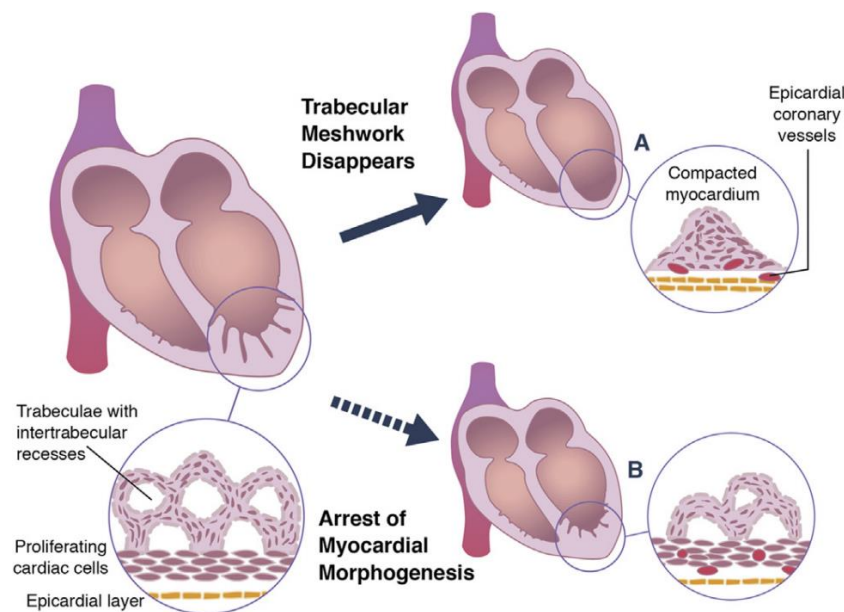


Figure 7. Embryonic development of LVNC. Reprint from (Gati, Rajani et al. 2014). Permission is conveyed through Copyright Clearance Center, Inc.

LVNC can be associated with other cardiomyopathies and congenital heart disease and classified into different types: (1) the isolated or benign form of LVNC characterized by normal LV size and wall thickness with preserved systolic and diastolic function and no arrhythmias (2) the arrhythmogenic form of LVNC, (3) the dilated form of LVNC, (4) the hypertrophic form of LVNC, (5) the “mixed” form (hypertrophic and dilated) of LVNC, (6) the restrictive form of LVNC, (7) the biventricular form of LVNC, (8) the right ventricular hypertrabeculation with normal LV form, and (9) the congenital heart disease form of LVNC (Towbin, Lorts et al. 2015).

Studies have identified various genes associated with LVNC, such as *TTN*, *MYH7*, *TNNT2*, *LDB3*, *MYBPC3*, *ACTC1*, *DSP*, *CASQ2*, *RBM20*, and the intermediate filaments *DES* (Kulikova, Brodehl et al. 2021) and *LMNA* (Probst, Oechslin et al. 2011, Sedaghat-Hamedani, Haas et al. 2017), with the two most affected genes being *TTN* and *LMNA* (Sedaghat-Hamedani, Haas et al. 2017). The first reported *LMNA* mutant variant causing LVNC is R190W which has also been reported to be associated with familial DCM (Hermida-Prieto, Monserrat

et al. 2004). Hermida-Prieto et al. showed that patients with R190W mutation exhibit a thin compact epicardial and a prominent trabeculations with deep recesses in a thickened left ventricular wall. Since the ejection fraction was persevered and the left ventricular end-diastolic diameter was normal, the patients were diagnosed as isolated left ventricular noncompaction cardiomyopathy (Hermida-Prieto, Monserrat et al. 2004). Another pathogenic *LMNA* variant causing LVNC is *LMNA* R644C. R644C mutation shows an extreme phenotypic diversity and can result in DCM, lipodystrophy, atypical progeria as well as LVNC (Rankin, Auer-Grumbach et al. 2008). Parent and his colleagues described a cases of 4 family members with *LMNA* R644C mutation, 3 of whom developed left ventricular noncompaction cardiomyopathy with normal LV dimensions and function, and absent evidence of dysrhythmias (Parent, Towbin et al. 2015). Other mutations such as *LMNA* V74fs, R572C and V445E have also been identified associated with LVNC. Patients with the V445E missense mutation are characterized by an arrhythmogenic form of LVNC, suggested to be due to dysfunctional *SCN5A* (Liu, Shan et al. 2016, Sedaghat-Hamedani, Haas et al. 2017). Although it is believed that an arrest in embryonic endomyocardial morphogenesis contributes to LVNC, the precise mechanisms of LVNC upon *LMNA* mutations haven't been reported yet.

1.2.3 Arrhythmogenic right ventricular cardiomyopathy

Arrhythmogenic right ventricular cardiomyopathy (ARVC) is an inherited heart-muscle disorder that predominantly affects the right ventricle. Progressive loss of myocytes and fibrofatty replacement associated with arrhythmias in right ventricular myocardium is the pathological hallmark of the disease (Fig. 8) (Marcus, McKenna et al. 2010). Diffuse RV involvement and LV abnormalities progressively develop with age (Corrado, Basso et al. 1997). Desmosomal mutations such as *PKP2*, *DSP*, *DSG2* and *JUP*, are the main cause of ARVC (Awad, Dalal et al. 2006, Awad, Dalal et al. 2006, Corrado and Thiene 2006, Yang, Bowles et al. 2006, Joshi-Mukherjee, Coombs et al. 2008). In addition, mutations of the calcium-handling protein *RYR2* (Tiso, Stephan et al. 2001), the structural sarcomeric protein Titin (Taylor, Graw et al. 2011), the cytokine signalling proteins *TGFB3* (Beffagna, Occhi et al. 2005) and the cytoskeletal protein *TMEM43* as well as lamin A/C have also been reported in ARVC (Merner, Hodgkinson et al. 2008, Quarta, Syrris et al. 2012, Hodgkinson, Connors et al. 2013, Kato, Takahashi et al. 2016).

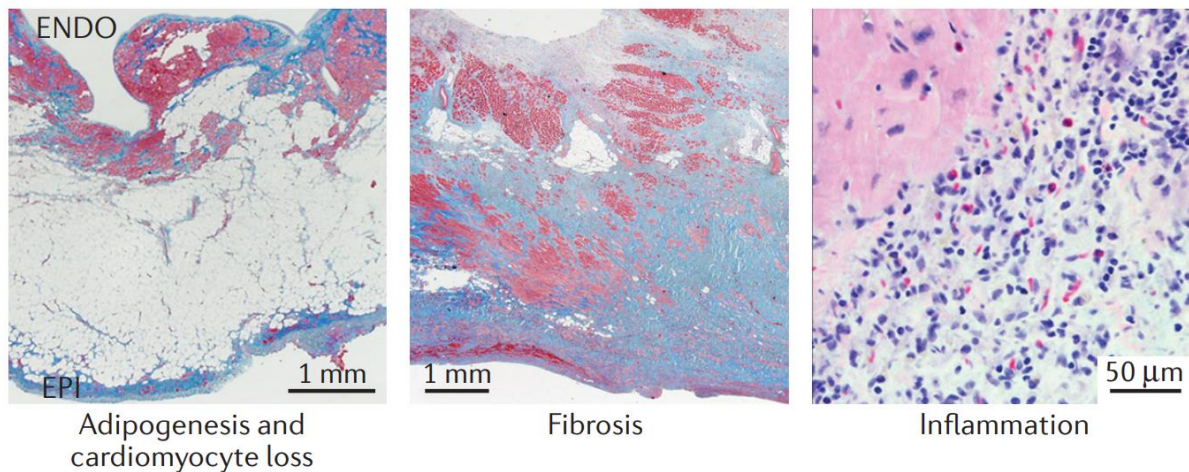


Figure 8. Histological features of ARVC. Reprint from (Austin, Trembley et al. 2019). Permission is conveyed through Copyright Clearance Center, Inc.

In 2011, Quarta et al. firstly reported ARVC caused by mutations in *LMNA*. Four *LMNA* variants were identified: R190W, R644C, R72C and G382V (Quarta, Syrris et al. 2012). R190W and R644C variants have been shown to cause DCM and LVNC. In addition, R644C can also lead to lipodystrophy and atypical progeria, thus showing an extreme phenotypic diversity. ARVC patients with these 4 mutations all exhibit RV dilation and systolic dysfunction. Histology of the right ventricular myocardium from R190 and G382W patients showed >50% myocytes loss and extensive interstitial fibrosis and fatty replacement. Interestingly, immunohistochemical staining showed a significantly reduced plakoglobin expression at the intercalated discs in the myocardium. Moreover, M1K, W514X and M384I mutations in *LMNA* have also been identified in ARVC. Patients with M1K and W514X mutations show RV dilatation, non-sustained ventricular tachycardia, and complete atrioventricular block (Kato, Takahashi et al. 2016). Whereas, patient with M384I variant not only shows ARVC, but also exhibits peripheral neuropathy and peroneal muscular atrophy (Liang, Goodsell et al. 2016).

So far, it remains unknown how *LMNA* mutations result in ARVC. Since *LMNA* is a ubiquitously expressed protein, its mechanoprotective function in cardiomyocytes, which can limit the progressive loss of myocytes, its role in the regulation of genes involved in cardiac contractility, and its important role in regulating cell fate choices, which may result in an excess of fibroblasts and adipocytes, might be involved. Tracing back the origins of fat tissue in a mouse model of ARVC, Lombardi et al. suggested that second heart field (SHF)-derived progenitor cells switch to an adipogenic fate through nuclear plakoglobin (JUP)-mediated Wnt signaling inhibition (Lombardi, Dong et al. 2009). A subset of resident cardiac fibro-adipocyte progenitor cells characterized by $PDGFRA^{pos}Lin^{neg}THY1^{neg}DDR2^{neg}$ expression signatures have been shown to be a major source of adipocytes in ARVC caused by Desmoplakin (*DSP*) haploinsufficiency (Lombardi, Chen et al. 2016). Furthermore, the endocardium, epicardium, and cardiac mesenchymal stromal cells also serve as a source of adipocytes in the heart (Matthes, Taffet et al.

2011, Sommariva, Brambilla et al. 2016, Zhang, Pu et al. 2016). Because the endocardium and epicardium give rise to diverse cardiac cell lineages, including mesenchyme and adipocytes (Zhang, Lui et al. 2018), via endothelial-to-mesenchymal transition (EndMT) and epithelial-to-mesenchymal transition (EMT), lamin A/C function in regulating EMT (Guenantin, Jebeniani et al. 2021) might also be a key mechanism driving ARVC pathogenesis.

1.2.4 Restrictive cardiomyopathy

Restrictive cardiomyopathy (RCM) is a rare cardiac disease characterized by increased myocardial stiffness resulting in impaired ventricular filling. Patients with RCM show enlarged atria and diastolic dysfunction, while systolic function and ventricular wall thicknesses are often normal until the later stages of the disease (Mogensen and Arbustini 2009, Nihoyannopoulos and Dawson 2009, Muchtar, Blauwet et al. 2017). Although most causes of RCM are acquired, several gene mutations have also been identified in patients with RCM (Mogensen and Arbustini 2009, Nihoyannopoulos and Dawson 2009, Muchtar, Blauwet et al. 2017, Brodehl and Gerull 2022). The most common mutated genes found in RCM are sarcomere-related genes such as *TTN* (Peled, Gramlich et al. 2014), *TNNI3* (Kostareva, Gudkova et al. 2009), *MYH7* (Greenway, Wilson et al. 2012), *ACTC1* (Kaski, Syrris et al. 2008), etc. Mutations in non-sarcomere genes such as *DES* (Brodehl, Pour Hakimi et al. 2019), *TMEM87B* (Yu, Coughlin et al. 2016), *FLNC* (Brodehl, Ferrier et al. 2016), etc., have also been reported. Recently, Paller et al. reported a truncation mutation of *LMNA* (c.835 delG:p.Glu279ArgfsX201) in an RCM patient who had a significant biatrial enlargement, atrial fibrillation, and skeletal muscle weakness. Both right and left ventricular size and function were normal, and histological analysis revealed cardiac hypertrophy and focal interstitial fibrosis in the endomyocardial tissue (Paller, Martin et al. 2018). How *Lmna* mutations cause RCM is not known; a plausible mechanism could be the activation of profibrotic signaling, as discussed above.

1.3 Changes of chromosome architecture and gene expression in *LMNA*-associated cardiomyopathies

1.3.1 Lamina-associated domains reorganization in cardiomyopathy

Cardiomyocytes differentiated from iPSCs have been used to understand the mechanisms and pathophysiology of many cardiac diseases and provide a reliable tool for drug screening applications. Indeed, recent investigations using induced pluripotent stem cells (iPSCs) gave a further insight into the role of LADs in cardiomyopathy. Several iPSC models of lamin-dependent DCM have been reported so far such as R225X (Siu, Lee et al. 2012, Lee, Lau et al. 2017, Bertero, Fields et al. 2019), K117fs (Lee, Termglinchan et al. 2019), T101 (Shah, Lv et al. 2021), R541C (Shah, Lv et al. 2021), K219T and R190W (Salvarani, Crasto et al. 2019). For

instance, Lee et al. showed that iPSCs derived cardiomyocytes which carry a frameshift mutation in *LMNA* that leads to the early termination of translation exhibit proarrhythmic activity in both atrial- and ventricular-like cardiomyocytes compared to healthy controls. By using lamin A/C Chip-seq and ATAC-seq, the authors showed that lamin A/C haploinsufficiency results in reduced lamin A/C enrichment at LADs. Most of the gene promoters that resided in LADs showed increased open chromatin in mutant iPSC derived cardiomyocytes. The repressive chromatin marker H3K9me2 were less enriched in LADs and were not equally distributed throughout the nuclear periphery in mutant iPSC-CMs. Consequently, genes associated with LADs were more actively expressed in mutant cardiomyocytes compared to control and were functionally enriched in terms associated with PDGF pathway. Inhibition PDGF pathway rescued the arrhythmic phenotype, suggesting that PDGF inhibitors could be beneficial in preventing fatal arrhythmias often manifested in patients with *LMNA*-related cardiomyopathy (Lee, Termglinchan et al. 2019).

In addition, chromatin and expression analysis of CMs from patients with different *LMNA*-related DCM mutations revealed extensive rearrangement of *LMNA*-chromatin interactions in DCM patients (Cheedipudi, Matkovich et al. 2019). The reorganization of lamin A/C LADs is associated with altered CpG methylation and dysregulated expression of a large number of genes involved in cell metabolism, the cell cycle, and cell death. Most of the *LMNA*-related DCM patients' samples used in this study showed a decrease in lamin A/C protein levels, suggesting that *LMNA* LOF might account for the observed DNA, chromatin, and expression changes (Cheedipudi, Matkovich et al. 2019).

As discussed above, different mutations may result in either a loss or a gain of function. Another study performed using iPSCs model showed a dominant negative truncation of the K219T mutation (Salvarani, Crasto et al. 2019). In this study, the authors showed that the *SCN5A* genomic region is localized in the nuclear interior and actively transcribed in healthy CMs and the Nav1.5 sodium channel density at the plasma membrane is sufficient to assure proper impulse propagation. However, in K219T mutant CMs, the lamin A/C binds PRC2 with high affinity at the *SCN5A* promoter region. This leads to H3K27me3 and H3K9me3 repressive histone mark deposition and *SCN5A* silencing.

1.3.2 Role of lamin A/C in chromatin organization and transcription in *LMNA*-related cardiomyopathy

3D chromatin architecture remodeling also plays a role during cardiogenesis (Choy, Javierre et al. 2018, Montefiori, Sobreira et al. 2018, Zhang, Li et al. 2019) and heart disease (Montefiori, Sobreira et al. 2018). During human embryonic stem cell differentiation into cardiomyocytes, stage specific promotor-enhancer loops form interaction networks around both cardiac progenitors genes, such as *GATA6*, *TBX5*, *NKX2-5* and *MEF2A* (Zhang, Li et al. 2019), as well

as cardiomyocytes genes such as *MYH6* and *MYH7* (Choy, Javierre et al. 2018). The majority of genome maintains the same compartment state throughout cardiomyocyte differentiation (Bertero, Fields et al. 2019, Zhang, Li et al. 2019). However, a portion of genome changes compartment. These changes correlate with an increased or decreased chromatin accessibility (Bertero, Fields et al. 2019). In a recent study, Bertero et al. reported an association of *LMNA* mutation with chromatin compartment dynamics in cardiomyocytes (Bertero, Fields et al. 2019). By using human iPSC cells carrying the haploinsufficient *LMNA* mutation R225X and two gene-edited, isogenic control lines, the authors showed that mutant hiPSC-CMs have marked electrophysiological defects such as prolonged action potentials and enhanced calcium fluxes, consistent with the disease phenotype. RNA-seq and Hi-C data showed that lamin A/C haploinsufficiency strengthens the separation between chromosome territories and between chromatin compartments. In addition, the authors identified *CACNA1A* as a disease-associated gene that is dysregulated both on the gene expression level and its chromatin compartment localization. *CACNA1A* transitioned from the inactive B chromatin compartment to the active A chromatin compartment correlating with the ectopic expression of this calcium channel in the mutant cells. Furthermore, the authors showed that inhibition of *CACNA1A* rescued the electrophysiological defects in mutant cells (Fig. 9) (Bertero, Fields et al. 2019).

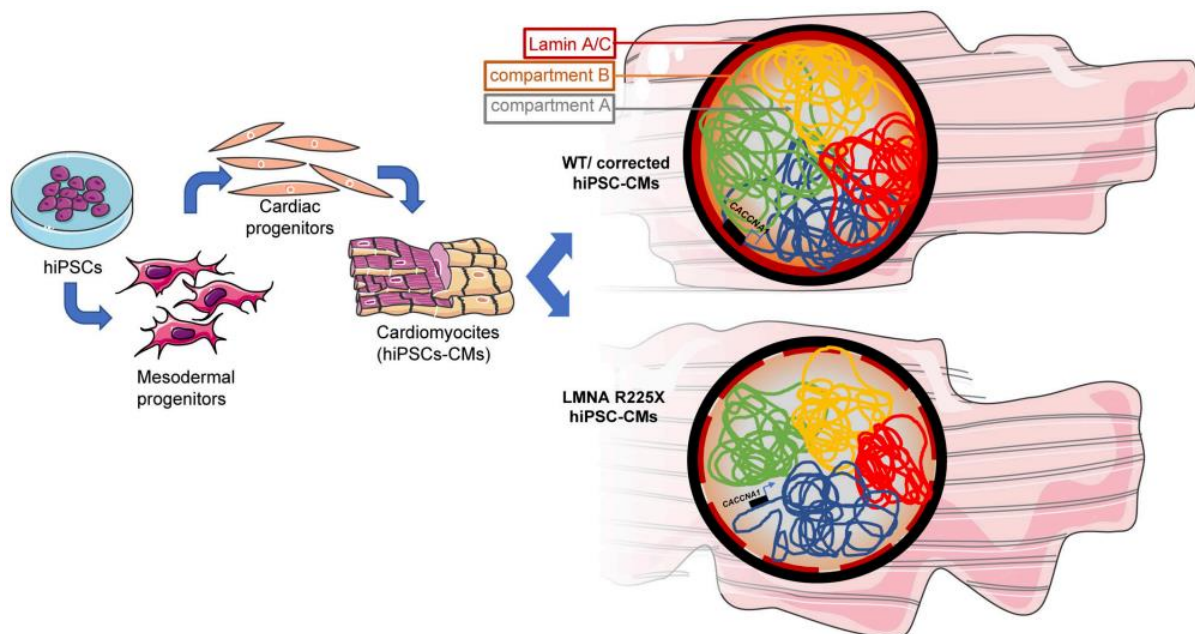


Figure 9. Chromatin compartmentalization dynamics in control and *LMNA* haploinsufficient CMs derived from hiPSC. Reprint from (Mozzetta and Tedesco 2019). Permission is conveyed through Copyright Clearance Center, Inc.

1.3.3 The role of polycomb group proteins in *LMNA*-related cardiomyopathy

Polycomb group (PcG) proteins are key epigenetic repressors during development and differentiation (Dobrev and Braun 2012). In mammals, two major PcG complexes exist: Polycomb repressive complex 1 (PRC1) and 2 (PRC2). PRC1 contains the E3 ligases Ring1A/B, which

monoubiquitinate lysine 119 at histone H2A (H2A119Ub1) (Luis, Morey et al. 2012). PRC2 catalyzes di- and tri- methylates the Lys 27 of histone H3 (H3K27me_{2/3}). The core of PRC2 is formed by a complex between the proteins EED and SUZ12 with either EZH2 or EZH1 (Schuettengruber, Chourrout et al. 2007, Margueron and Reinberg 2011). To date, both PRC1 and PRC2 have been described to be important for in vivo or in vitro cardiac development and differentiation (Dobrova and Braun 2012). *Ezh2* mediated gene silencing in cardiac progenitors has been shown to be essential for cardiomyocytes proliferation, survival, and postnatal cardiac homeostasis. Inactivation of *Ezh2* specifically in cardiac progenitors results in ectopic transcriptional programs, which leads to lethal heart defects (Delgado-Olguín, Huang et al. 2012, He, Ma et al. 2012). PRC2 function is also required in cardiomyocytes to ensure proper cardiac growth, because *Eed* deficiency by TnT-Cre leads to embryonic lethality and heart defects, including compact myocardial hypoplasia (He, Ma et al. 2012). Compared with the function of *Ezh2* as a gene repressor in cardiac progenitors, *Mel18*, one of the PRC1 subunits, functions as both a repressor and an activator during early cardiac mesoderm cell differentiation (Morey, Santanach et al. 2015). *Mel18* directly controls the activity of genes encoding transcription factors essential for early cardiac mesoderm cell specification yet also directly controls the expression of the negative regulators of the BMP pathway and genes involved in late cardiac differentiation, pluripotency, and ectoderm and endoderm cell fate to ensure their transcriptional repression in the early steps of cardiac differentiation (Morey, Santanach et al. 2015).

Downregulation of lamin A/C leads to dissociation of lamin A/C from promoters and remodels repressive H3K27me₃ and permissive H3K4me₃ histone modifications by enhancing transcriptional permissiveness (Lund, Oldenburg et al. 2013). This evidence suggests that the lamin A/C might alter PcG protein activity and function. Indeed, several investigations have shown that lamin A/C interacts with PRC in murine muscular cells (Cesarini, Mozzetta et al. 2015) and human 293 cells (Marullo, Cesarini et al. 2016). Downregulation of lamin A in myoblasts redistributes PRC2 complexes and leads to ectopic expression of polycomb targets and premature activation of myogenic differentiation (Cesarini, Mozzetta et al. 2015). Since lamin A/C also exists in nucleoplasmic (Naetar, Korbei et al. 2008), it is not surprising that lamin A/C and PcG complexes may interact either at nuclear interior or nuclear periphery. By using different combinations of antibodies against lamin A/C and PRC components, F. Marullo et al. showed that lamin A/C interacts with PcG at nuclear interior in 293 cells (Marullo, Cesarini et al. 2016). Lamin B1 also recruits the PRC2 to alter the H3K27me₃ landscape and repress genes involved in cell migration and signaling (Jia, Vong et al. 2019).

Interestingly, the lipodystrophy-associated *LMNA* p.R482W mutation is linked to epigenetic alterations at the MIR335 promoter and enhancers after adipogenic induction. These include decreased H3K27me₃ deposition and increased H3K27 acetylation, suggesting a defective

PRC2 recruitment or stabilization by the lamin A/C R482W mutant at the MIR335 locus (Oldenburg, Briand et al. 2017). In a murine model of Emery-Dreifuss Muscular Dystrophy, loss of lamin A/C deregulates PcG positioning in muscle satellite stem cells leading to de-repression of non-muscle specific genes and *p16INK4a*, a senescence driver encoded in the *Cdkn2a* locus. This aberrant transcriptional program causes impairment in self-renewal, loss of cell identity and premature exhaustion of quiescent satellite cell pool (Bianchi, Mozzetta et al. 2020). In a recent study using iPSC-CMs carrying the cardiac laminopathy associated K219T mutation, it was shown that the binding of lamin A/C together with PRC2 at the *SCN5A* promoter represses its expression, resulting in decreased conduction velocity (Salvarani, Crasto et al. 2019). Together, aberrant PRC activity upon *LMNA* mutation might play an important role in *LMNA*-related cardiomyopathies (Fig. 10).

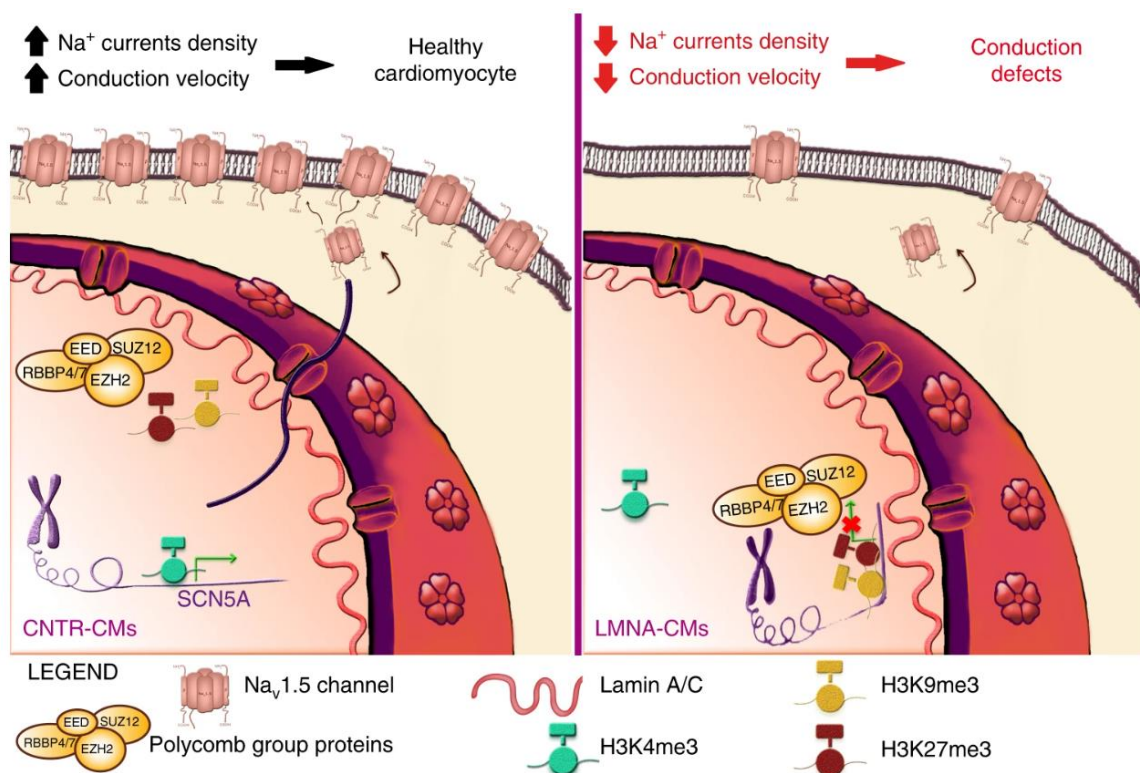


Figure 10. Mutant lamin A/C and PRC2 bind each other with high affinity and repress cardiac gene expression. Reprint from (Salvarani, Crasto et al. 2019). Permission is conveyed through Copyright Clearance Center, Inc.

1.4 Mechano-protective role of lamin A/C in heart

It has been recognized that mechanical forces act as an important regulator during development and differentiation (Hahn and Schwartz 2009, Lemke and Schnorrer 2017, Vining and Mooney 2017). Tissues and organs, like the heart which sustains high stress due to the regular cyclic contraction and hemodynamic pressure are more sensitive to mechanical stimuli. Previous studies revealed that contraction of the heart primordium starts well before convective transport is necessary (Fujii, Hirota et al. 1981, Wiens, Mann et al. 1992, Hogers, DeRuiter et al. 1995) and the hemodynamic forces generated from early cardiac contraction influence heart

morphogenesis. Experimental alteration of the hemodynamics during cardiogenesis can in turn, induce cardiac defects (Hogers, DeRuiter et al. 1999, Sedmera, Pexieder et al. 1999). In addition, the blood flow generated by embryonic cardiac contraction imposes a cyclic force on the endocardium or over the entire wall of the developing heart. The frictional force applied to the apical surface of the endothelial cells by blood flow activate Notch signaling which is essential for epithelial-mesenchymal transition in the endocardial cushions and for trabeculae formation in the developing common ventricle (Timmerman, Grego-Bessa et al. 2004, Grego-Bessa, Luna-Zurita et al. 2007, Niessen and Karsan 2008).

The biomechanical forces can be sensed by mechanosensors and activate mechano-responsive signaling, such as RhoA, MAPK, JAK/STAT, PKC, YAP, TAZ, SFR, calcineurin and intracellular calcium regulation. Until now, a large number of mechanosensor proteins related to the cytoskeleton (e.g. intermediate filaments, Microtubules), cell–substrate (e.g. integrins) and cell–cell adhesions (e.g. cadherins, Ca²⁺ dependent transmembrane adhesion molecules) have been identified (Ward and Iskratsch 2019). The nuclear lamin A/C which lies below the inner nuclear membrane tethers the nucleus to the cytoskeleton via the linker of the nucleoskeleton and cytoskeleton (LINC) complexes. The LINC complexes consist of SUN domain proteins in the inner nuclear membrane and Klarsicht–ANC-1–SYNE homology (KASH) domain proteins in the outer nuclear membrane (Sosa, Rothballer et al. 2012). As SUN proteins bind lamins while KASH proteins bind the contractile cytoskeleton interacting with the extracellular matrix or neighboring cells via adhesion complexes, thus, the LINC complexes form a direct physical link between the nucleoskeleton and the cytoskeleton and play a key role in mechanotransduction (Méjat 2010, Rothballer, Schwartz et al. 2013, Tapley and Starr 2013).

Lamin A/C deficient fibroblasts revealed increased numbers of misshapen nuclei, severely reduced nuclear stiffness, decreased cell viability and reduced mechanosensitive genes expression in response to mechanical distortion (Lammerding, Schulze et al. 2004, Lammerding, Fong et al. 2006). When cardiomyocytes are stretched excessively, detectable physical changes occur in a stretch-length dependent manner, including increases in cardiomyocytes length or width, increases in nuclear length, and reduced wrinkling of the nuclear envelope, which can be accompanied by pathological cardiomyocyte dysfunction, cardiac hypertrophy and fibrosis (Bloom and Cancilla 1969).

In a recent study, lamin A/C levels were reported to be regulated in response to mechanical stimuli. The authors showed that lamin A/C plays a key role in stiffening the nucleus, preventing the nucleus from rupture, and keeping DNA repair factors in the nucleus. Knockdown of *LMNA* in embryonic hearts leads to mis-localization of fluorescently tagged DNA repair factors outside of the nucleus, cell-cycle arrest and aberrant beating. When hiPSC-CMs were cultured on stiff matrices, DNA repair factors were again mis-localized due to nuclear envelope rupture, which was aggravated by *LMNA* knockdown. Importantly, treatment of *LMNA* knocked down

cells with blebbistatin on rigid plastic rescued nuclear rupture as well as DNA damage. Moreover, cyclic (passive) stretching of cardiomyocytes and U2OS cells also led to DNA damage and mis-localization of DNA repair factors especially after *LMNA* knockdown, confirming the link between mechanical forces, *LMNA* levels, and nuclear damage (Fig. 11) (Cho, Vashisth et al. 2019).

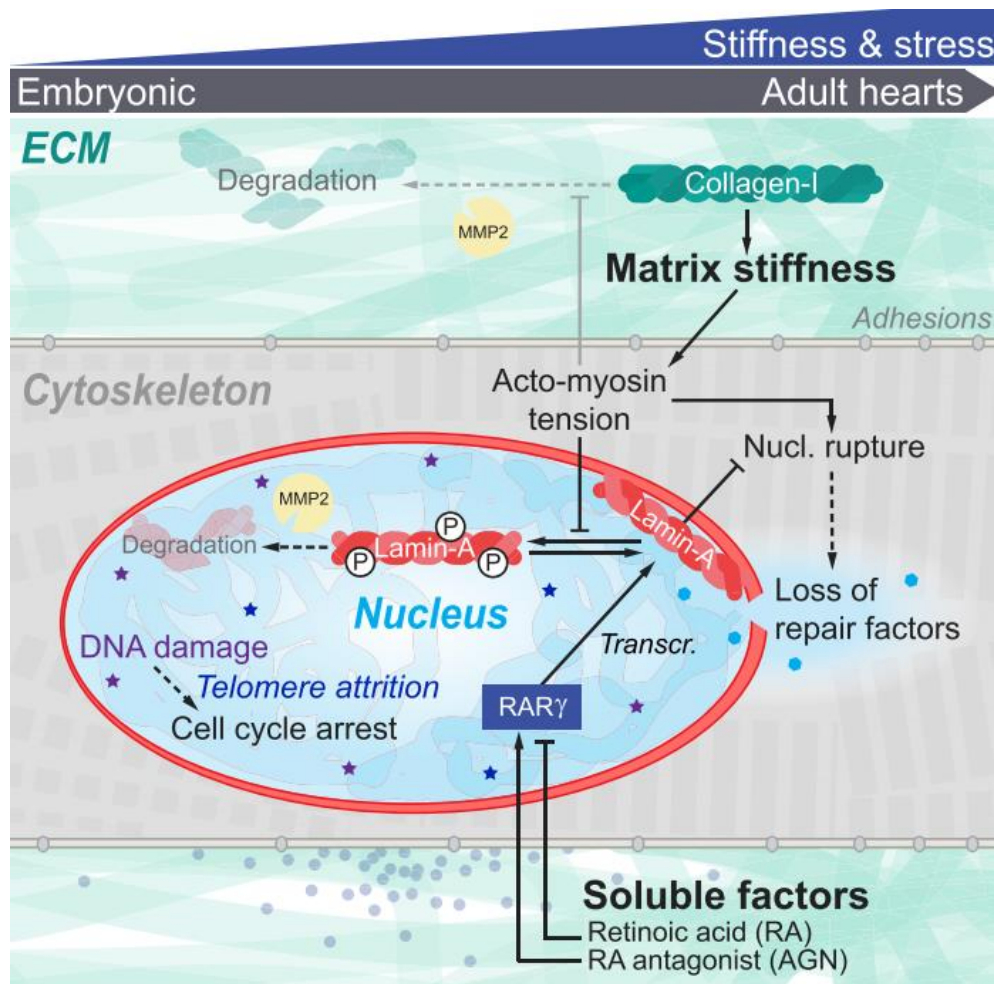


Figure 11. Mechanosensing by the lamina protects against nuclear rupture, DNA Damage, and Cell-Cycle arrest. Reprint from (Cho, Vashisth et al. 2019). Permission is conveyed through Copyright Clearance Center, Inc.

Recent work has also shown that lamin A/C connects the LINC complex and directly translates mechanical cues and changes in extracellular matrix mechanics into alterations in chromatin structure and transcriptional activity (Lityagina and Dobrova 2021). When rat cardiomyocytes are stretched, there are changes in the spatial arrangement of both the desmin lamin intermediate filament network and the nuclear envelope-associated chromatin, which indicates that stretch induced changes in chromatin can lead to activation of hypertrophy-associated genes (Bloom, Lockard et al. 1996). In nucleus, chromosome maintains its own discrete territory during interphase and genes tend to be nonrandomly positioned and preferentially near the surface of chromosome territories (Volpi, Chevret et al. 2000, Cremer, Küpper et al. 2004). The 3D organization of genes in chromosomal territories may allow regulation of their expression

through physical interaction with force-transmitting structures within the nucleus. A recent work has shown that local stresses applied to integrins propagate from the tensed actin cytoskeleton to the LINC complex and then through lamina-chromatin interactions to directly stretch chromatin and upregulate transcription (Tajik, Zhang et al. 2016). Interestingly, nuclear elongation and chromatin dispersion are evident in *LMNA* deficient cardiomyocytes (Nikolova, Leimena et al. 2004). Chromatin decondensation is shown to correlate with nuclear stiffness and extrinsic forces may directly upregulate transcription by deforming the nucleus (Pagliara, Franze et al. 2014), which indicates that loss of lamin A/C may lead to chromatin stretched at mechano-sensitive genes.

1.5 Heart development

1.5.1 Mouse heart development

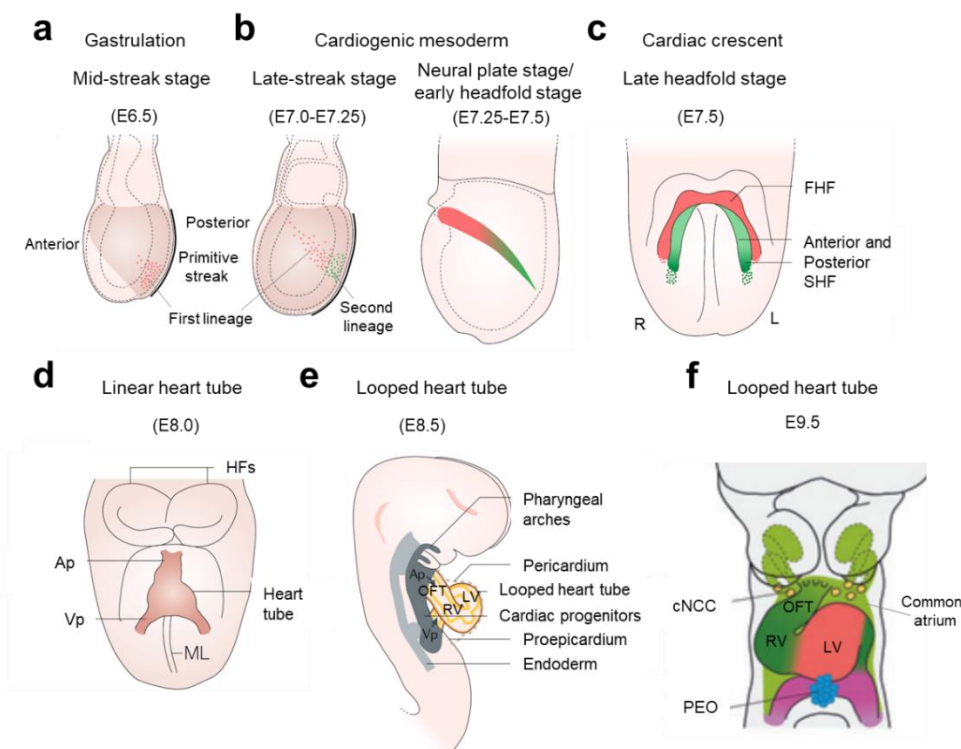
During vertebrate embryogenesis, the heart is the initial vital organ to form, enabling the efficient circulation of nutrients and removal of metabolic waste. Once the embryo grows to a size at which passive diffusion is no longer effective, the heart becomes essential. Fate mapping research has revealed that the lateral epiblast is the major source of embryonic mesoderm, with the heart mesoderm being localized to the posterior areas of the lateral epiblast (Parameswaran and Tam 1995, Tam, Parameswaran et al. 1997). At the early primitive streak stage, cells in the anterior and posterior epiblast are not yet to commit to a cardiac fate, and their ultimate fate is determined by their location (Tam, Parameswaran et al. 1997). During the mid-streak stage, the first cardiac progenitors ingress and position themselves within the anterior area of the primitive streak, in close proximity to the cranial mesoderm progenitors (Fig. 12a). *Mesp1* is transiently expressed during the primitive streak stage, and is subsequently turned off as cardiac precursors migrate away from the primitive streak. Moreover, descendants of *Mesp1*⁺ cells colonize the entire myocardium enabling *Mesp1* to be reliably used as an early cardiac precursor marker (Saga, Hata et al. 1996).

At embryonic day 7.5 (E7.5), cells extend across the midline and form the cardiac crescent, an epithelial structure where differentiated myocardial cells can be observed (Fig. 12c). In this stage, cardiac precursors irreversibly commit to cardiovascular lineages and begin to express transcription factors such as *Nkx2-5*, *Gata4* and *Isl1*. These cardiogenic cells are multipotent and give rise to cardiomyocytes, endothelial cells, and vascular smooth muscle cells in the developing heart (Kattman, Huber et al. 2006).

Subsequently, the cardiac crescent goes on to fuse at the midline to form the early heart tube (Fig. 12d). Clonal analyses in the mouse embryo revealed the existence of two lineages that segregate early from a common precursor and contribute to the myocardium of the heart (Meilhac, Esner et al. 2004). The first lineage gives rise to left ventricular myocardium, while

the second lineage forms the outflow tract and most of the right ventricular myocardium, with both lineages contributing to the atria and other parts of the heart (Meilhac, Esner et al. 2004). By embryonic day 7.5, the first lineage has already begun differentiating into cardiomyocytes in the cardiac crescent, while the second lineage remains as progenitor cells, located medially to the crescent and more posteriorly in the splanchnic mesoderm. These cells contribute to different regions of the developing heart. Based on the contributions of the first and second myocardial cell lineages, the sources of these cardiac cells are referred to as the first heart field (FHF, shown in red in Fig. 12c) and second heart field (SHF, shown in green in Fig. 12c) respectively.

The early cardiac tube forms through fusion of the cardiac crescent at the midline with FHF cells forming the primary heart tube and SHF cells being added to the poles of the primary heart tube (E8.0). By E8.5, the heart tube, which is composed of an inner layer of endocardium and an outer layer of myocardium, elongates from both the arterial and venous poles (Fig. 12e). Subsequently, the myocardial layer expands and proepicardial progenitor cells migrate over the surface of the heart, contribute fibroblasts that invade the myocardial layer, and form the outermost epicardial layer. Complex asymmetric morphogenetic movements coupled with uneven growth rates contribute to heart tube looping and chamber formation. A series of septation events results in a fully functional four chambered heart integrated with systemic and pulmonary circulation. Neural crest cells, which migrate from the dorsal neural tube and invade the cardiac outflow tract, also contribute to the smooth muscle of the great vessels and the innervation of the heart.



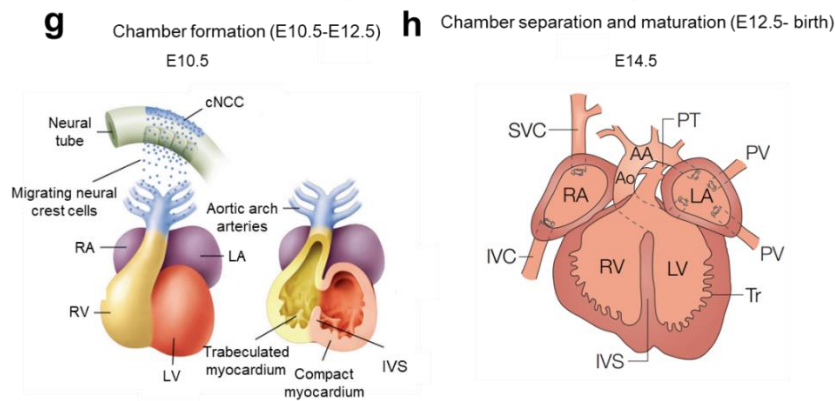


Figure 12. Overview of the mouse heart development. **a** Myocardial progenitor cells originate from the primitive streak (PS), from where they migrate to the anterior of the embryo at about embryonic day E6.5. Red: first cell lineages. **b** and **c** After gastrulation, cardiac progenitors migrate laterally towards the head folds at E7.25 (**b**), where the cardiac crescent forms at E7.5 (**c**). red, first cell lineages; green, second cell lineages. **d** The early cardiac tube forms through fusion of the cardiac crescent at the midline (ML) at E8.0. **e** At E8.5, the heart tube, which is composed of an inner layer of endocardium (yellow) and an outer layer of myocardium (orange), elongates from both the arterial (Ap) and venous (Vp) poles (arrows). **f** Front view of the looped heart tube at E9.5, at which cardiac neural crest cells (cNCC) migrate from the pharyngeal arches (PA) to the arterial pole (Ap) and the proepicardial organ (PEO) forms in the vicinity of the venous pole (Vp). **g** By E10.5, the heart has acquired well defined chambers, but is still a tube. Cardiac neural crest cells (cNCC) from the dorsal neural tube migrate via the pharyngeal arches to the cardiac outflow tract (OFT). **h** By E14.5, the chambers are now separated and connected to the pulmonary trunk (PT) and aorta (Ao). R, right; L, left; AA, aortic arch; IVC, inferior vena cava; IVS, interventricular septum; OFT, outflow tract; PV, pulmonary vein; PT, pulmonary trunk; SVC, superior vena cava; Tr, trabeculae; RA, right atrium; RV, right ventricle; LA, left atrium; LV, left ventricle; cNCC, cardiac neural crest cells; PEO, proepicardial organ, FHF, first heart field; SHF, second heart field; Ap, arterial pole; Vp, venous pole. Reprint from (Buckingham, Meilhac et al. 2005, Vincent and Buckingham 2010, Epstein, Aghajanian et al. 2015, Meilhac and Buckingham 2018). Permission is conveyed through Copyright Clearance Center, Inc.

1.5.2 Early cardiac precursor within the primitive streak

Mesp1, a transcription factor of the b-HLH family, is expressed the earliest, at E6.5 along the primitive streak, and marks the nascent cardiac mesodermal population, and is then rapidly downregulated after E7.5 (Saga, Hata et al. 1996). Genetic tracing showed *Mesp1* marks of most (70%) cells in the heart (Ragni, Diguët et al. 2017). *Mesp1* deficiency leads to severe cardiac defects and lethality by E10.5 (Saga, Miyagawa-Tomita et al. 1999). Furthermore, ablation of *Mesp1* and its homolog *Mesp2* results in mesodermal layer defect and lethality at E9.5 (Kitajima, Takagi et al. 2000). Transient *Mesp1* expression in embryonic stem cell (ESC) promotes changes associated with epithelial-mesenchymal transition (EMT) and is sufficient to induce cardiovascular mesoderm, including endothelial cells, smooth muscle cells, and cardiomyocytes, while the development of other mesodermal lineages were inhibited (David, Brenner et al. 2008, Lindsley, Gill et al. 2008). These observations showed that *Mesp1* is responsible for specifying a cardiovascular fate within the mesoderm by acting as a master regulator at the apex of a hierarchy of cardiac transcription factors.

1.5.3 First heart field and second heart field

The first and second heart field progenitors are derived from a common progenitor that segregates into distinct heart field precursors early at the onset of gastrulation (Meilhac, Esner et al. 2004). Reliable molecular markers of the first heart field are lacking because myocardial cells

express *Hand1* and *Tbx5* which are regarded as the first heart field markers are also detected in a subpopulation of cells of SHF (Barnes, Firulli et al. 2010, Rana, Théveniau-Ruissy et al. 2014). Markers for second heart progenitors include *Isl1*, *Fgf10* and *Tbx1*. *Isl1* is a LIM-homeodomain transcription factor previously studies showed that most of the early second heart field myocardial, smooth muscle, and endothelial cells are derived from multipotent *Isl1*⁺ cardiovascular progenitors (Moretti, Caron et al. 2006, Bu, Jiang et al. 2009). *Isl1* mutant mice show defects at the venous pole and arterial pole development, including major defect in right ventricular and outflow tract development (Cai, Liang et al. 2003). In the anterior SHF, *Isl1* directly activates the enhancers of *Mef2c* and is regulated by *Gata4* and *Foxc2*. *Fgf10* is expressed in the anterior SHF and is required for the development of the right ventricle and outflow region of the heart (Watanabe, Miyagawa-Tomita et al. 2010). Whereas, *Tbx1* marks cells that contribute to the inferior part of the outflow tract (Baldini, Fulcoli et al. 2017). Transcription factors *Gata4* and *Nkx2-5* are widely expressed in both FHF and SHF in the early cardiac crescent at E7.5. Homozygotes *Gata4* deficient embryos show developmental defects, including lack of primitive heart tube and foregut and developed partially outside the yolk sac. These mutant embryos arrest in development between E7.0 and E9.5 die between 8.5 and 10.5 (Kuo, Morrisey et al. 1997, Molkentin, Lin et al. 1997).

1.5.4 Different cardiac cell types during heart development

The heart is predominantly made up of epicardium, myocardium, endocardium and cardiac fibroblasts (Doetschman and Azhar 2012). All the components of the heart originate from mesoderm except for neural crest cells which derive from neurectoderm. The myocardium is the thickest layer which lies between the innermost endocardium layer, and the outermost epicardium layer and is composed of multiple highly specialized myocardial lineages, including those of the ventricular and atrial myocardium, and the specialized conduction system (Evans, Yelon et al. 2010). As discussed above, two major lineages contribute to the myocardium of the heart. The first lineage contributes left ventricular myocardium, whereas the second lineage is the source of outflow tract and most right ventricular myocardium, with both lineages contributing to the atria and other parts of the heart (Meilhac and Buckingham 2018).

Endocardium constitutes the inner endothelial layer of the heart. During heart development, *Nfatc1*⁺ endocardium gives rise to endothelial cells of the coronary vasculature, most mesenchymal cells that constitute the cardiac cushions and subsequently contribute to the heart valves (Fig. 13). A subpopulation of *Nkx2-5*⁺ endocardial cells present mainly in the outflow tract and dorsal atria from E8.0 also gives rise to haematopoietic cells (Meilhac and Buckingham 2018). Epicardium is the outermost layer of the heart and originates from proepi-

cardium, a transitory cluster of mesothelial cells protruding from septum transversum mesenchyme near the venous pole of the heart (Quijada, Trembley et al. 2020). Epicardial cells contribute a number of cell types to the heart, including smooth muscle cells of the coronary vessels, cardiac fibroblasts, and potentially a subset of cardiomyocytes. Grafting experiments have shown that myocardium, endocardium and epicardium share a common origin marked by *Isl1* and *Nkx2-5*. Markers of epicardial include *Tbx18* and *Wt1* (Meilhac and Buckingham 2018, Quijada, Trembley et al. 2020).

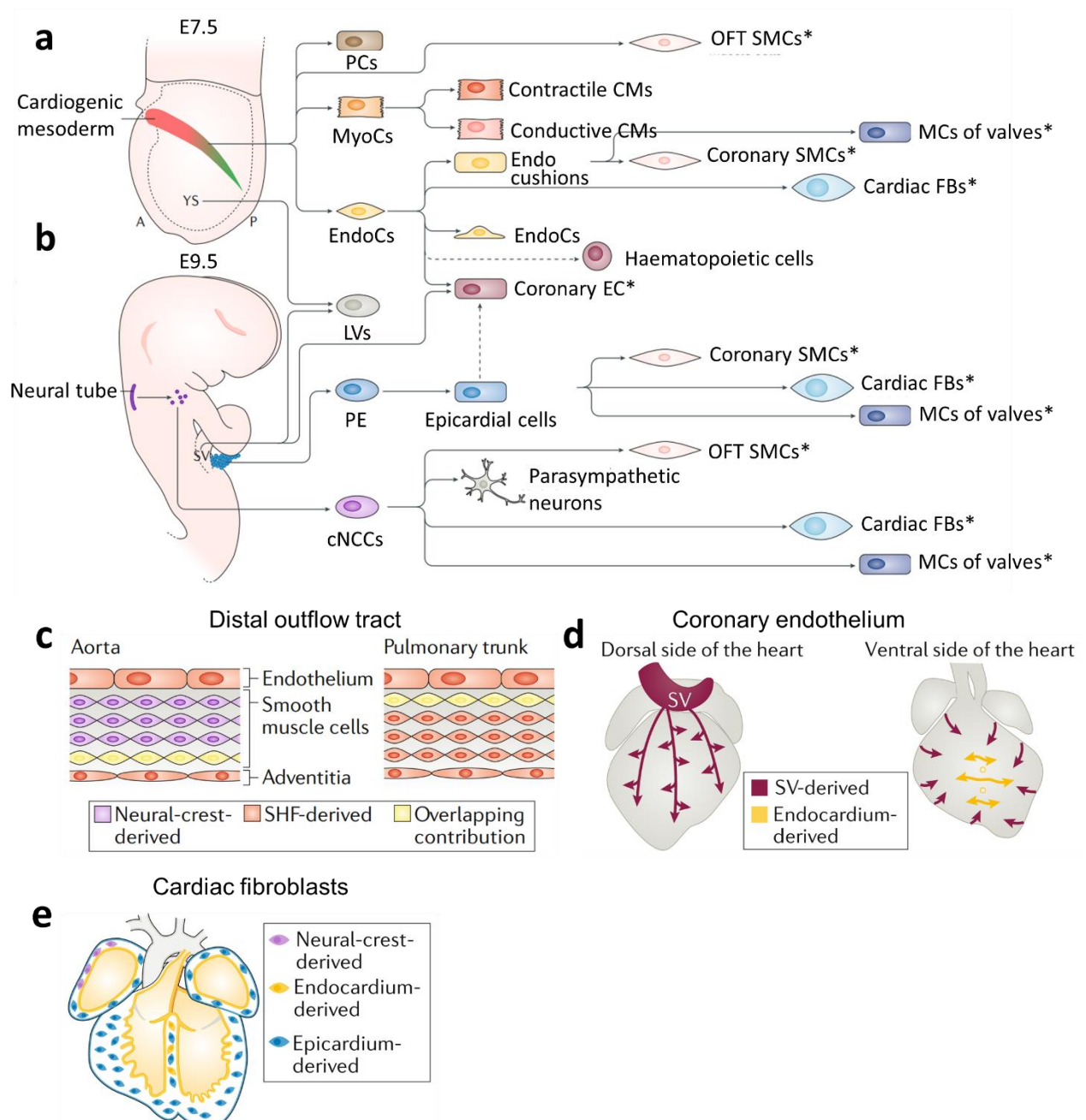


Figure 13. Sources of the different cardiac cell types. **a** Cardiogenic mesoderm contributes to most cardiac cells. **b** Cardiac cells derived from sinus venosus (SV), proepicardium (PE) and cardiac neural crest cells (cNCCs). Overlapping lineages are marked with an asterisk. Minor contributions are indicated with a dotted line. **c-e** Regionalization of the distinct cell sources colonizing the distal outflow tract (OFT) or coronary endothelium, or giving rise to the interstitial cardiac fibroblasts. A, anterior; E, embryonic day; P, posterior; SHF, second heart field; YS, yolk sac; PCs, pericardial cells; MyoCs, myocardial cells; EndoCs, endocardial cells; LVs, lymphatic vessels; PE, proepicardium; cNCCs, cardiac neural crest cells; OTF, outflow tract; CMs, cardiomyocytes; ECs, endothelial cells; SMCs,

smooth muscle cells; FBs, fibroblasts; MCs, Mesenchymal cells. Reprint from (Meilhac and Buckingham 2018). Permission is conveyed through Copyright Clearance Center, Inc.

1.5.5 Cardiac cushions and valve formation

As already mentioned above, at E8.5, the heart tube is composed of an outer layer of myocardium and an inner lining of endocardial cells, separated by an extensive extracellular matrix (ECM) referred to as the cardiac jelly. After rightward looping of the heart (E9.5), the cardiac jelly overlying the future atrioventricular canal (AVC) and outflow tract (OT) expands into swellings known as cardiac cushions (Fig. 14) (O'Donnell and Yutzey 2020). These cardiac cushions then become populated with mesenchymal cells that are derived from a subpopulation of endocardial endothelial cells that undergo endothelial-to-mesenchymal transition (EndoMT), referred to as valve primordia. The valve primordia elongate and stratify into mature valve leaflets through a combination of cell proliferation and ECM synthesis (O'Donnell and Yutzey 2020). The remodeling process continues until birth when the endocardial cushions eventually become the mature heart valves with thin leaflets (Wang, Fang et al. 2021). A number of signaling pathways are involved in valve formation. For example, *Tbx2* and *Tbx3* stimulate cardiac jelly formation in endocardial swellings in the atrioventricular canal (AVC). Myocardial BMP signaling and endocardial Notch1, Wnt/ β -catenin, TGF β and Hippo/Yap1 signaling promote EndoMT and the expression of the mesenchymal markers *Twist*, *Msx1/2* and *Snail* (O'Donnell and Yutzey 2020).

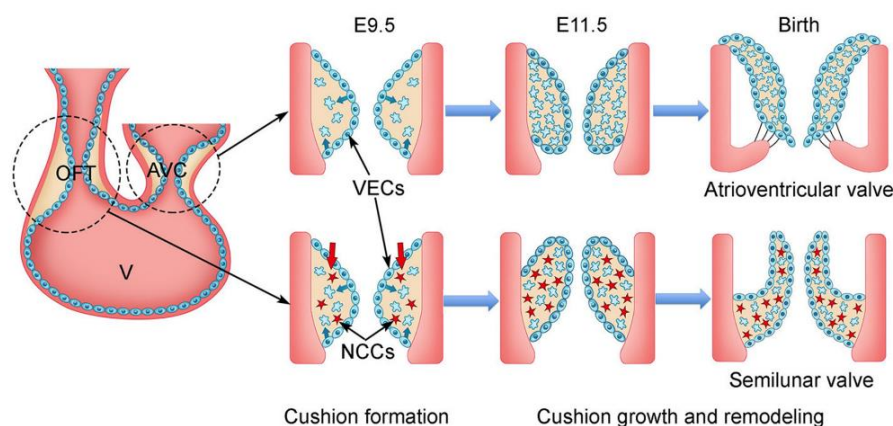


Figure 14. Valves and valve development in the mammalian heart. **a** The adult mammalian heart consists of four chambers: the left and right atria, and the left and right ventricles, which are separated by four valves. The atrioventricular (AV) valves, which include the mitral valve and the tricuspid valve, lie between the atria and the ventricles; the semilunar (SL) valves, which include the pulmonary valve and the aortic valve, lie between the ventricles and the outflow tracts. **b** After rightward looping of the heart (E9.5), the cardiac jelly overlying the future atrioventricular canal (AVC) and outflow tract (OT) expands into swellings known as cardiac cushions. These cardiac cushions then become populated with mesenchymal cells that are derived from a subpopulation of endocardial endothelial cells that undergo endothelial-to-mesenchymal transition and migrate internally, referred to as valve primordia. The valve primordia elongate and stratify into mature valve leaflets through a combination of cell proliferation and ECM synthesis. Reprint from (Wang, Fang et al. 2021). Permission is conveyed through Copyright Clearance Center, Inc.

1.5.6 Myocardial compaction and trabeculation

Ventricular trabeculation and compaction are essential for creating a functionally competent ventricular wall. The trabeculation starts from embryonic day 8.5 (E8.5) when the heart tube is composed of a slowly proliferative epithelial myocardium and an inner endocardium lining the lumen with extracellular matrix (cardiac jelly) in between (Fig. 15) (Bartman and Hove 2005, Zhang, Chen et al. 2013). As the myocardium thickens, endocardial cells invaginate and cardiomyocytes in specific regions along the inner wall of the heart form sheet-like protrusions into the lumen to give rise to trabecular myocardium, while the outside layer of myocardium becomes the base for forming the compact myocardium later in development (MacGrogan, Münch et al. 2018). A rapidly dividing outer layer of compact myocardium and a slowly dividing inner trabecular myocardium are defined at this stage. Various cellular mechanisms, including oriented cell division, cardiomyocyte migration, epithelial-to-mesenchymal transition (EMT)-like process, as well as proliferation are involved in formation of these protrusions (MacGrogan, Münch et al. 2018). Ventricular trabeculation has been suggested to facilitate oxygen and nutrient exchange by increasing surface area in early embryonic hearts which does not have a coronary circulatory system (Sedmera, Pexieder et al. 2000). At around E13.5, the trabecular myocardium collapses towards the myocardial wall in a process termed compaction, which contributes to forming a thicker, compact ventricular wall. In parallel, coronary vessels begin to form to nourish the thickening compact myocardium. Compaction continues postnatally and concludes approximately at postnatal day 28 (P28) in mice (Sedmera, Pexieder et al. 2000, MacGrogan, Münch et al. 2018).

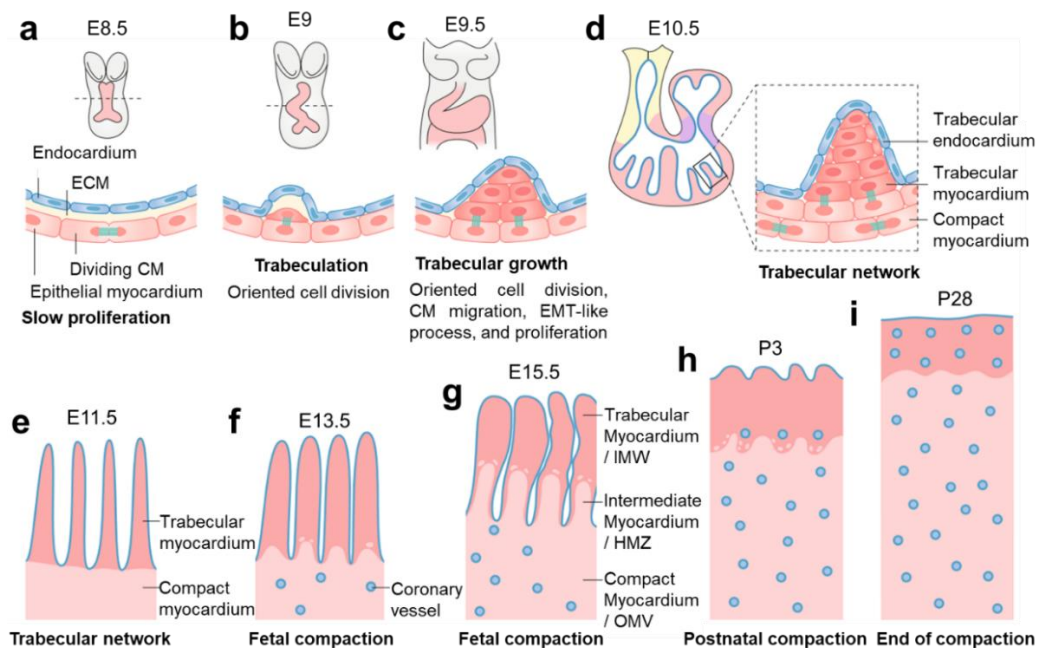


Figure 15. Ventricular chamber development: trabeculation and compaction. **a** The initial stages of trabeculation starts from embryonic day 8.5 (E8.5) when the heart tube is composed of an inner endocardium and a slowly proliferative epithelial myocardium. **b** At E9, the trabeculae myocardial protrusions covered by endocardium appear bulging towards the ventricular lumen. Various cellular mechanisms, including oriented cell division are involved in

formation of these protrusions. **c** and **d** By E9.5–E10.5, a growing trabecular network is formed by oriented cell division, cardiomyocyte migration, epithelial-to-mesenchymal transition (EMT)-like process, and proliferation. A rapidly dividing outer layer of compact myocardium and a slowly dividing inner trabecular myocardium are defined at this stage. **e** and **f** By E11.5, trabeculae form a complex network, and at around E13.5, compaction begins and trabeculae integrate into the compact myocardium. In parallel, coronary vessels begin to form to nourish the thickening compact myocardium. **g** At E15.5, the trabecular myocardium or inner myocardial wall (IMW), the intermediate myocardium or hybrid myocardial zone (HMZ), and the compact myocardium or outer myocardial wall (OMW) can be distinguished. **h** and **i** Compaction continues postnatally and concludes approximately at postnatal day 28 (P28) in mice. ECM, extracellular matrix. Reprint from (MacGrogan, Münch et al. 2018). Permission is conveyed through Copyright Clearance Center, Inc.

1.6 Objective

LMNA mutations lead to broad range of *LMNA*-related cardiomyopathies, however, the precise mechanism is still largely unexplored. Modeling of *LMNA* cardiomyopathies in vitro using induced pluripotent stem cell (iPSCs)-derived CMs revealed increased chromatin accessibility at LADs upon *LMNA* haploinsufficiency, resulting in PDGF pathway activation contributing to an arrhythmic phenotype (Lee, Termglinchan et al. 2019). However, analysis of the 3D genome organization in CMs of another *LMNA* haploinsufficient model, which also showed contractile alterations (Bertero, Fields et al. 2019), did not detect pronounced changes in chromatin compartmentalization into open and closed states that could explain the altered transcriptional activity. This leaves the question open to whether lamin A/C-mediated 3D chromatin architecture plays a role in *LMNA* cardiomyopathies. Furthermore, these studies were conducted in CMs as it has been long thought, that A-type lamins play an important function after commitment of cells to a particular differentiation pathway, such as CMs. However, a developmental origin of cardiac laminopathies have been suggested using mouse embryonic stem cells (mESCs) and a mouse model harboring *Lmna* p.H222P mutation, causing Emery-Dreifuss muscular dystrophy and cardiomyopathy. *Lmna* p.H222P mutation resulted in impaired epithelial-to-mesenchymal transition of epiblast cells, which in turn caused CM differentiation defects. The aim of this study is:

- (1) Does lamin A/C loss of function results in defects in heart development?
- (2) How does lamin A/C loss of function affect chromatin organization and gene expression during cardiac development?
- (3) How does lamin A/C affect cardiomyocyte function and the function of the heart?

2 MATERIALS AND METHODS

2.1 Materials

2.1.1 Equipment

Equipment	Source of supply
Agilent 2100 Bioanalyzer System	Agilent
Bacterial incubator 37°C	Thermo Scientific
Balance LC 4800 P	Sartorius
BD FACSCanto II	BD Biosciences
Binocular microscope M165FC	Leica
Binocular microscope MZ16FA	Leica
Cell culture incubator	Thermo Scientific
Cell culture safety cabinet	Thermo Scientific
Centrifuge HERAEUS Fresco 17	Thermo Electron Corporation
Centrifuge HERAEUS Multifuge 1S-R	Thermo Electron Corporation
Centrifuge HERAEUS Pico 17	Thermo Electron Corporation
Cold light source KL2500 LCD	Zeiss
Confocal microscope LSM 700	Zeiss
Developing machine	GE Healthcare
Diagenode Bioruptor Homogenizer	Diagenode
Fluorescence microscope DM6000B	Leica
GentleMACS™ Dissociators	Miltenyi Biotec
Heating block TH 21	HLC BioTech
Light microscope Wilovert S	Hund Wetzlar
MyoPacer	IonOptix
Qubit™ Fluorometer	Thermo Scientific
Real-Time StepOne Plus Real-Time PCR System	Applied Biosystems
Rocking platform 444-0142	VWR
Rotator SB3	Stuart
SDS-PAGE apparatus	Bio-Rad
Sonifier Sonopuls GM 2070	Bandelin electronic
Thermal cycler C1000 Touch	BIO-RAD
Thermo block 5436	Eppendorf
Thermo block MHR 23	HLC BioTech
Vevo 3100 imaging system	Visualsonics
Vortexer VF2	IKA®-Labortechnik Staufen
Water bath cell culture WMB 22	Memmert
Water bath Julabo U3	Julabo Labortechnik GMBH
Western Blotting Transfer apparatus	Bio-Rad

2.1.2 Chemicals

Chemicals	Source of supply	Reference number
1 kb Plus DNA ladder (0.1-10.0 kb)	NEB	N3200L
Agarose NEEO Ultra	Roth	2267.3
Albumin fraction V (BSA)	Roth	8076.2
Ammonium persulfate (APS)	Sigma	A3678-25G
Ampicillin sodium salt	Sigma	A99518-25G
Aqueous 30 % acrylamide and bisacrylamide stock solution (37.5:1)	Carl Roth	3029.1
Bromophenol Blue	Sigma	B0126
BSA (for ChIP)	NEB	B9000s
Chloroform (CHCl ₃)	Roth	3313.4
Dimethyl sulfoxide (DMSO)	Sigma	D2438
Dithiothreitol (DTT)	Roth	6908.3
Dry-milk, non fat milk	Cell Signling	9999
dNTP (Nucleoside triphosphate) Set 1	Roth	178.1
Ethanol	Roth	K928.3
Ethanol	Sigma	459844
Ethidium bromide solution	Sigma	E1510-10ML
Ethylene glycol tetraacetic acid (EGTA)	Roth	3054.2
Ethylenediaminetetraacetic acid (EDTA)	Sigma	E5134-250G
Formaldehyde	Sigma	F8775
FuGENE® HD Transfection Reagent	Roche	4709705/100
Formamide (CH ₃ NO)	Fluka	47670
Gelatin from bovine skin, Type B	Sigma	G9391-100g
Glycerol	Roth	3783,1
Glycine	Sigma	15527
Halt Protease Inhibitor Cocktail (100X) 5 mL	Thermo Fischer	78429
Hexadimethrine bromide (polybrene)	Sigma-Aldrich	H9268
Isopropanol (C ₃ H ₈ O)	Roth	6752,4
Kanamycinsulfate	Roth	T832,1
LB-agar	Roth	X965,2
LB-medium	Roth	X964,2
Magnesium chloride (MgCl ₂)	Sigma	M2393-500G
Methanol (CH ₃ OH)	Roth	4627.5
Nonidet P-40 (NP-40)	Fluka	74385
PageRuler Plus Prestained Protein Ladder, 10 to 250 kDA	Thermo Fischer	26620
Paraformaldehyde (PFA)	Thermo Fischer	12587010
Phosphatase inhibitor cocktail set	Millipore	524632-1SET
Poly(2-hydroxyethylmethacrylate) (PolyHEMA)	Sigma	P3932-10G

Potassium chloride (KCl)	Roth	6781.3
Puromycin Dihydrochloride 10x1 mL	Thermo Fischer	A1113803
Sodium dodecyl sulfate (SDS)	Sigma	L4390-100G
Sodium phosphate monobasic monohydrate (NaH ₂ PO ₄ · H ₂ O)	Sigma-Aldrich	53522-1KG
Sodium phosphate dibasic dodecahydrate (Na ₂ HPO ₄ · 12H ₂ O)	Sigma-Aldrich	04273
Salmon sperm DNA	Upstate	16-157
Tetramethylethylenediamine (TEMED)	Roth	2367,1
Tris(hydroxymethyl)aminomethane (TRIS)	Roth	4855.2
Triton X-100	Sigma	X100-500ML
TRIzol LS Reagent 200 mL	Thermo	10296028
TRIzol® reagent	Invitrogen	15596026
Tween 20	Sigma	T2700-500ML
β-mercaptoethanol (C ₂ H ₆ SO)	Sigma	60-24-2

2.1.3 Cell culture medium and supplements

Medium/supplements	Source	Catalogue number
DMEM (1x) high glucose. no glutamine	Gibco	10938-025
DMEM. high glucose. GutaMAX supplement	Gibco	61965-026
DMEM/F-12 Medium no glutamine	Gibco	21331020
Ham's F 12 Nutrient Mix	Gibco	11765054
IMDM	Gibco	12440053
KnockOut DMEM medium	Gibco	10829-018
Neurobasal medium	Gibco	1103049
StemPro™-34 SFM	Gibco	10639011
Essential 8 (E8) medium	Gibco	A1517001
Fetal Bovine Serum	Gibco	16000044
Opti-MEM	Gibco	31985062
Polybrane	Sigma-Aldrich	H9268
Horse serum, heat inactivated	Gibco	26050088
KnockOut Serum Replacement	Gibco	10828-028
L-Glutamine	Gibco	25030-024
Non-essential amino acids	Gibco	11140-035
Penicillin-Streptomycin	Gibco	15140-122
Sodium pyruvate	Gibco	11360-039
B27 supplement	Gibco	17504-044
B27 Supplement (50X) minus vitamin A 10 mL	Gibco	12587-010
N2 supplement	Gibco	17502-048

Activin A	R&D systems	338-AC
VEGF	R&D systems	293-VE-010
bFGF	R&D systems	233-FB
BMP4	R&D systems	314-BP
FGF10	R&D systems	345-FG
IGF	STEMCELL	78022.1
Recombinant human insulin	Sigma	91077C
PD0325901(Merk inhibitor)	Selleckchem	S1036
CHIR99021(GSK3 inhibitor)	Selleckchem	S1263
SP600125(JNK inhibitor)	Selleckchem	S1460
BIRB796(p38 inhibitor)	Selleckchem	S1574
Y-27632(Rock inhibitor)	STEMCELL	72302
IWP2(WNT inhibitor)	STEMCELL	72122
L-Ascorbic Acid	Sigma	A4403
Leukemia inhibitory factor	Millipore	ESG1107
Recombinant human LIF	Miltenyibiotec	130-108-156
StemPro Accutase	Thermo Fisher	A1110501
Trypsin-EDTA (1x) 0.05%	Gibco	25300-054
1-Thioglycerol	Sigma	M6145
7.5% BSA	Gibco	15260037
AlbuMAX™ I Lipidreiches BSA	Thermo	11020021
DMSO	Sigma	D2650
DPBS	Gibco	14190-094
FBS	Gibco	10270-106
Gelatin	Sigma	G9391
Corning Matrigel Growth Factor Reduced (GFR) Basement Membrane Matrix	Corning	354230
Laminin	Corning	354232
Poly-L-lysine solution	Sigma	P4832
Lipofectamine 2000	Invitrogen	11668019
Lipofectamine 3000	Invitrogen	L3000008
Lipofectamine™ RNAiMAX Transfection Reagent	Invitrogen	13778075
Mitomycin	Sigma	M4287
Poly (2-hydroxyethyl methacrylate)	Sigma	P3932
Puromycin	Gibco	A11138-03
X-tremeGENE HP DNA Transfection Reagent	Roche	6366236001
β-mercaptoethanol	Sigma	M3148

2.1.4 Buffers and solutions

Medium/buffer	Recipe	Usage
ESC medium	DMEM + High glucose, 15% FBS, 2 mM L-Glutamine, 0.1 mM β -mercaptoethanol, 0.1 mM nonessential amino acids, 0.1 mM sodium pyruvate, 1% Penicillin-Streptomycin 1000 U/ml leukemia inhibitory factor	mESC
MEF medium	DMEM +High glucose 10% FBS, 2 mM L-Glutamine, 0.1 mM β -mercaptoethanol, 0.1 mM nonessential amino acids, 0.1 mM sodium pyruvate, 1% Penicillin-Streptomycin	MEF, NIH3T3, feeder cells
HEK293T medium	DMEM. high glucose. Guta-MAX supplement 10% FBS, 0.1 mM nonessential amino acids, 0.1 mM sodium pyruvate, 1% Penicillin-Streptomycin	HEK293T
Neurobasal, DMEM/F12 medium	50% Neurobasal, 50% DMEM-F12, 1 \times N2 supplement, 1 \times B27 supplement, 1% Penicillin-Streptomycin, 2 mL-Glutamine, 0.05% BSA, 0.01% 1.5 \times 10 ⁴ M monothio-glycerol, 10 ng/ml BMP4, 2000 U/ml LIF	Direct cardiac differentiation
Differentiation medium	75% IMDM, 25% F12, 1 \times N2, 1 \times B27 supplement without VA, 1% Penicillin-Streptomycin, 1% 50 μ g/ml L-Ascorbic acid, 0.04% 4.5 \times 10 ⁻⁴ M monothio-glycerol	Direct cardiac differentiation

Stempro-34 medium	Stempro-34 medium, 2.6% StemPro supplement, 100U/ml Penicillin-Streptomycin	Direct cardiac differentiation
Co-IP buffer	50mM TRIS-HCl pH=7.5 15mM EGTA 100mM NaCl 0.1% (v/v) Triton X-100	immunoprecipitation

2.1.5 kits

Kit	Source of supply	Reference number
2x SYBR Green master mix	Applied Biosystems	4367659
Amersham ECL Prime Western Blotting Detection Reagent	GE Healthcare	RPN2232
Bioanalyzer High Sensitivity DNA Analysis	Agilent	5067-4626
Chip DNAb Clean&Concentrator	Zymo	D5205
GenElute™ gel extraction kit	Sigma	NA1111
GenElute™ HP plasmid midiprep kit	Sigma	NA0200
GenElute™ HP plasmid miniprep kit	Sigma	NA0160
GenElute™ PCR clean-up kit	Sigma	NA1020
High-Capacity cDNA Reverse Transcription Kit	Applied Biosystems	4368813
NEBNext High-Fidelity 2X PCR Master Mix	NEB	M0541S
NEBNext Ultra II DNA Library Prep Kit with Purification Beads 96 reactions	NEB	E7103L
NEBNext® Multiplex Oligos for Illumina® (96 Index Primers)	NEB	E6609S
NEBNext® Multiplex Oligos for Illumina® (Index Primers Set 1)	NEB	E7335S
Pierce™ BCA Protein Assay Kit	Thermo Scientific	23225
Qubit dsDNA HS Assay Kit-100 assays	Thermo Fisher S	Q32851
RNeasy Plus Universal Mini Kit 50	Qiagen	73404
SuperSignal™ West Femto Maximum Sensitivity Substrate	Thermo Fisher	34094
Nick Translation Kit	Roche	10976776001

2.1.6 Consumables

Cell culture materials	Source of supply	Reference number
15ml Centrifuge Tubes	Greiner Bio-One	188271
50ml Centrifuge Tubes	Greiner Bio-One	227261
5ml Plastic pipet	Greiner Bio-One	606180
10ml Plastic pipet	Greiner Bio-One	607180
25ml Plastic pipet	Greiner Bio-One	760180
6-cm dish (cell culture)	Greiner Bio-One	628160
10-cm dish (cell culture)	Greiner Bio-One	664160
15-cm dish (cell culture)	Greiner Bio-One	639160
10-cm petri-dish	Greiner Bio-One	633180
6-well plates (cell culture)	Greiner Bio-One	657160
12-well plates (cell culture)	Greiner Bio-One	665180
24-well plates (cell culture)	Greiner Bio-One	662160
48-well plates (cell culture)	Greiner Bio-One	677180
96-well plate F bottom with lid	Greiner Bio-One	655180
96-well plate V bottom with lid	Greiner Bio-One	651180
Reservior	VWR	89094-664

2.1.7 Antibodies

Antibody	Source	Catalogue number
Mouse monoclonal anti-LaminA/C (E-1)	Santa Cruz	Cat# sc-376248, RRID: AB_10991536
Mouse monoclonal anti-LaminA/C (131C3)	Abcam	Cat# ab8984, RRID: AB_306913
Rabbit polyclonal anti-LaminB1	Abcam	Cat# ab16048, RRID: AB_10107828
Rabbit polyclonal anti-LaminB1	Sigma	Cat# HPA050524, RRID: AB_2681156
Mouse monoclonal anti-LaminB1 (B10)	Santa Cruz	Cat# sc-374015
Goat polyclonal anti- <i>Gata4</i> (C-20)	Santa Cruz	Cat# sc-1237, RRID: AB_2108747

Mouse monoclonal anti-OCT3/4 (C-10)	Santa Cruz	Cat# sc-5279, RRID: AB_628051
Rabbit polyclonal anti-MYL4	Sigma	Cat# HPA051884, RRID: AB_2681651
Goat polyclonal anti-Cardiac Troponin I	Abcam	Cat# ab56357, RRID: AB_880622
Monoclonal Anti- α -Actinin	Thermo	A7811
Goat polyclonal anti-Pecam1	R&D Systems	AF3628
PECAM 1 CD31 (clone390)	eBioscience	553370
Mouse monoclonal Anti-phospho-Histone H2A.X (Ser139)	Millipore	Cat# 05-636-I, RRID: AB_2755003
CD31 (PECAM-1) Monoclonal Antibody (390), APC, eBioscience™	Thermo Fisher Scientific	Cat# 17-0311-82, RRID: AB_657735
Alexa Fluor® 647 Mouse Anti-Cardiac Troponin T Clone 13-11	BD Biosciences	Cat# 565744, RRID: AB_2739341
Wheat germ agglutinin, Alexa Fluor®488 conjugate	Thermo Fisher Scientific	Cat# W11261
Isolectin GS-IB4 from Griffonia simplicifolia, Alexa Fluor® 568 conjugate	Thermo Fisher Scientific	Cat# 121412
CD309 (FLK1) Monoclonal Antibody (Avas12a1), APC, eBioscience™	Thermo Fisher Scientific	Cat# 17-5821-81, RRID: AB_657866
CD140a (PDGFRA) Monoclonal Antibody (APA5), PE, eBioscience™	Thermo Fisher Scientific	Cat# 12-1401-81, RRID: AB_657615
Rabbit polyclonal anti-phospho-Histone H3 (Ser10)	Millipore	Cat# 06-570, RRID: AB_310177
Rabbit polyclonal anti-Ryr2	Sigma	Cat# HPA020028, RRID: AB_1856528
Mouse monoclonal anti-alpha-Tubulin clone 2-28-33	Sigma	Cat# T5168, RRID: AB_477579
Sheep polyclonal anti-Digoxigenin-Rhodamine, Fab fragments	Roche	Cat# 11207750910, RRID: AB_514501
Rabbit polyclonal anti-Aurora B	Abcam	Cat# ab2254, RRID: AB_302923
Donkey anti-Mouse IgG (H+L) Ready-Probes™ Secondary Antibody, Alexa Fluor 488	Thermo Fisher Scientific	Cat# R37114, RRID: AB_2556542
Donkey anti-Mouse IgG (H+L) Highly Cross-Adsorbed Secondary Antibody, Alexa Fluor 555	Thermo Fisher Scientific	Cat# A-31570, RRID: AB_2536180
Donkey anti-Goat IgG (H+L) Cross-Adsorbed Secondary Antibody, Alexa Fluor 555	Thermo Fisher Scientific	Cat# A-21432, RRID: AB_2535853
Donkey anti-Rabbit IgG (H+L) Highly Cross-Adsorbed Secondary Antibody, Alexa Fluor 488	Thermo Fisher Scientific	Cat# A-21206, RRID: AB_2535792
Donkey anti-Goat IgG (H+L) Cross-Adsorbed Secondary Antibody, Alexa Fluor 488	Thermo Fisher Scientific	Cat# A-11055, RRID: AB_2534102

2.1.8 Primers and oligonucleotides

Genes	Sequence of oligos
<i>Lmna</i> shRNA	gcttgactccagaagaacat
<i>Lmna</i> siRNA	gagagcaggccugaagccaaagaaa
<i>Lmnc</i> siRNA	tctcccactccatgccaaag
<i>Gata4</i> shRNA	catctcctgtcactcagacat

<i>Gata4</i> siRNA	Dharmacon/GE, L-040759-01-0005
<i>Lmna</i> mouse geno_for	aaccagcctcagaaactggtggatg
<i>Lmna</i> mouse geno_rev	gacagctctcctctgaagtgccttga
<i>Gata4</i> mouse Geno_for1	tgcaattactaggaccacgaga
<i>Gata4</i> mouse Geno_for2	cccagtaaagaagtcagcacaaggaac
<i>Gata4</i> mouse Geno_rev	agactattgatcccggagtgacatt
<i>Lmna</i> ^{-/-} mESC genotype1	ttggtttgcagaactccacg
<i>Lmna</i> ^{-/-} mESC genotype2	aggccataacagagttgggt
<i>Lmna</i> ^{-/-} mESC genotype3	ctgaagtgcctgctggggt
<i>Lmna</i> ^{-/-} mESC genotype4	gggattaggggtggaaggact
<i>Lmna</i> ^{-/-} mESC genotype5	gagtgcctggaatcaaaggca
<i>Lmna</i> ^{-/-} mESC genotype6	gcaagttgtcccctggtctt
<i>Lmna</i> ^{-/-} mESC gRNA1_for	caccgcactgctcacgtccaccac
<i>Lmna</i> ^{-/-} mESC gRNA1_rev	aaacgtggtggaacgtgagcagtc
<i>Lmna</i> ^{-/-} mESC gRNA2_for	caccgtccctcccctagatgcatcc
<i>Lmna</i> ^{-/-} mESC gRNA2_rev	aaacggatgcatctaggggagggac
<i>Lmna</i> ^{-/-} mESC gRNA3_for	caccgagctatcagcactctgttat
<i>Lmna</i> ^{-/-} mESC gRNA3_rev	aaacataacagagtgctgatagctc
<i>Lmna</i> ^{-/-} mESC gRNA4_for	caccgcagcactctgttatgggggc
<i>Lmna</i> ^{-/-} mESC gRNA4_rev	aaacgccccataacagagtgctgc
<i>Lmnb1</i> ^{-/-} mESC gRNA1_for	caccgaaactctaaggatgcggcgc
<i>Lmnb1</i> ^{-/-} mESC gRNA1_rev	aaacgcgccgcatccttagagtttc
<i>Lmnb1</i> ^{-/-} mESC gRNA2_for	caccgatgaggatcgagagcctct
<i>Lmnb1</i> ^{-/-} mESC gRNA2_rev	aaacagaggctctcgatcctcatc
<i>Lmnb1</i> ^{-/-} mESC genotype_for1	caccggctacctgttataaaa
<i>Lmnb1</i> ^{-/-} mESC genotype_for2	cttggtgaattacgcttctca
<i>Lmnb1</i> ^{-/-} mESC genotype_rev	tggacaacaacaacaaccaca
<i>Gata4</i> ^{-/-} mESC gRNA1_for	caccgtgcagctccaccggctcgt
<i>Gata4</i> ^{-/-} mESC gRNA1_rev	aaacacgagccggtggagactgcac
<i>Gata4</i> ^{-/-} mESC gRNA2_for	caccgctgtcaggagcacggtaat
<i>Gata4</i> ^{-/-} mESC gRNA2_rev	aaacattagccgtgctcctgacagc
<i>Gata4</i> ^{-/-} mESC_genotype_for	ccccacttcaccttttgattg
<i>Gata4</i> ^{-/-} mESC_genotype_for1	cggtaatagggccctgtgat
<i>Gata4</i> ^{-/-} mESC_genotype_for2	gaaaccctatgacgactgcc
<i>Gata4</i> ^{-/-} mESC_genotype_rev	tcttgagctacatagagactgtg
<i>Gata4</i> ^{-/-} mESC_genotype_rev1	tcctactctcagtggtcca
<i>Gata4</i> ^{-/-} mESC_genotype_rev2	tggtagtctgtctgtctgc
qhACTN2_for	agaacgaggtggagaagggtg
qhACTN2_rev	gcttcacctgtcccacttg
qhAURKA_for	gcccgtaatcccagcatttt
qhAURKA_rev	tcggtccatgatgcctgtaa
qhGATA4_for	tgtcaactgtggggctatgt
qhGATA4_rev	tcacttgtggttagaggccg
qhLMNA(A)_for	ccatcaccaccacggctc
qhLMNA(A)_rev	gtgaccagattgtccccgaa
qhLMNA(C)_for	caactccactggggaagaagtg
qhLMNA(C)_rev	cggcggctaccactcac
qhMYOM1_for	tgggagagaggggagagacaa
qhMYOM1_rev	cactggatctctggctggaa
qhNKX2-5_for	gagccgaaaagaaagcctgaa
qhNKX2-5_rev	caccgacacgtctcactcag
qhSCN3B_for	gccccaggtttaagcaatcc
qhSCN3B_rev	agcccaggagttcaagatca
qmAngpt2_for	cagccacggtaacaactc

qmAngpt2_rev	cttctttacggatagcaaccgag
qmAtp2a3_for	tgggtaagggtgatccggct
qmAtp2a3_rev	gtacctgttctcccactgcc
qmBAF60c_for	aggggaagctcttgatgat
qmBAF60c_rev	ttgtctgggccataaaggct
qmBeta-Actin_for	cactgtcagatcgctcc
qmBeta-Actin_rev	tcatccatggcgaactggtg
qmBmp4_for	ttcctggaaccgaatgctga
qmBmp4_rev	cctgaatctcggcgactttt
qmBrachyury_for	agggagaccccaccgaacgc
qmBrachyury_rev	ccgggaacatcctcctgccgtt
qmCalca_for	tcttggtgtcagcatctg
qmCalca_rev	gcatatagtctgcaccagt
qmEomes_for	cagggcaggcgcatgttct
qmEomes_rev	tccgcttgccgaggcac
qmFlk1_for	gggttggtttggaaggtt
qmFlk1_rev	aggagcaagctgcatcatt
qmGapdh_for	aactttggcattgtggaagg
qmGapdh_rev	ggatgcagggatgatgttct
qmGata4_for	tctcactatgggcacagcag
qmGata4_rev	gcatgtctgagtgacagga
qmGata6_for	caaaagctgtccggtaac
qmGata6_rev	tgagggtgctgctgtgtag
qmHand1_for	gcggaaaagggagttgcctcagc
qmHand1_rev	gctccagcgcccagactgc
qmHand2_for	cggagaggcggaggcctca
qmHand2_rev	cagggcccagacgtgctgtg
qmHopx_for	ttaagcagacaggcaccag
qmHopx_rev	gaagttgtactccaggatctcc
qmIsl1_for	acgtgcttgttagggatgg
qmIsl1_rev	caagaagtcttctgtgta
qmKlf4_for	ggcgagtctgacatggctg
qmKlf4_rev	gctggacgcagtgtcttctc
qmKlf5_for	caccggatctagacatgcc
qmKlf5_rev	acgtctgtggaacagcagag
qmLmnb1_for	agatcagggaccagatgcag
qmLmnb1_rev	gaagggcttgagagagctt
qmMef2c_rev	tccatcagccattcaacaa
qmMef2c_rev	agttacagagccgaggtgga
qmMesp1_for	gtttaagcccggcgtctgca
qmMesp1_rev	atgtcgctgctgaagagcggaga
qmMesp2_for	tagaaagagccgctgactcc
qmMesp2_rev	ctaggctctggggacatctg
qmMlc2a_for	cccatcaacttcaccgtctt
qmMlc2a_rev	cggtgggtgatgatgtagcag
qmMlc2v_for	ctgccctaggacgagtgaac
qmMlc2v_rev	cctctctgctgtgtgtgca
qmMyl4_for	cccaatcagccatcctaactg
qmMyl4_rev	ttcttaggctcgggttcttg
qmMyom1_for	catggactgacgactgctca
qmMyom1_rev	agacactcctccccgatag
qmPecam1_for	aacagaaacccgtggagatg
qmPecam1_rev	ggctccacactaggctcag
qmSM-22a_for	aacgaccaagccttctctgcc

qmSM-22a_rev	tcgctcctccagctcctcgt
qmSM-actin_for	ctgacagaggcaccactgaa
qmSM-actin_rev	agaggcatagaggacagca
qmTnnt2_for	atccccgatggagagagagt
qmTnnt2_rev	ctgttctcctcctcctcagc
qmTtn_for	accaccaacttcagtcagc
qmTtn_rev	tcccggtagaacttcaccac
qmTuba1a_for	ccgcaagcagcaacccat
qmTuba1a_rev	ccaggtctacgaacactgcc

2.1.9 Programs and algorithms

Programs and algorithms	Source	Website
IGV2.8.13	Integrative Genomics Viewer	https://software.broadinstitute.org/software/igv/download
Image J 1.47v	Image J	https://imagej.nih.gov/ij/download.html
Vevo LAB Software Package V3.2.6	FUJIFILM VisualSonics	https://www.visualsonics.com/resource/vevo-lab-software
IonWizard 7.4	IonOptix	https://www.ionoptix.com/
MUSCLEMOTION V1.0	(Sala, van Meer et al. 2018)	https://github.com/l-sala/MUSCLEMOTION
BD FACSDiva Software (version 8.0.1, firmware version 1.49 BD FACSCanto II).	BD Biosciences	https://www.bdbiosciences.com/en-eu/products/software/instrument-software/bd-facs-diva-software
Zen 2.3	ZEISS	https://www.zeiss.de/mikroskopie/produkte/mikroskopsoftware/zen-lite/zen-lite-download.html
DAVID 6.8	(Huang da, Sherman et al. 2009)	https://david.ncifcrf.gov/summary.jsp
Heatmapper	(Babicki, Arndt et al. 2016)	http://www.heatmapper.ca/expression/
GraphPad Prism 8.0.2	GraphPad	https://www.graphpad.com/
WashU Epigenome Browser	(Zhou, Maricque et al. 2011)	http://epigenomegateway.wustl.edu/
Calculate and draw custom Venn diagrams	Bioinformatics & Evolutionary Genomics	http://bioinformatics.psb.ugent.be/web-tools/Venn/
STAR version 2.7.3a	(Dobin, Davis et al. 2013)	https://github.com/alexdobin/STAR/blob/master/doc/STARmanual.pdf
Trimmomatic version 0.39	(Bolger, Lohse et al. 2014)	http://www.usadellab.org/cms/?page=trimmomatic
BamTools version 2.5.1	(Barnett, Garrison et al. 2011)	https://github.com/pezmaster31/bamtools
MultiQC version 1.6	(Ewels, Magnusson et al. 2016)	https://multiqc.info/

DESeq2 version 1.28.0	(Love, Huber et al. 2014)	http://bioconductor.org/packages/release/bioc/vignettes/DESeq2/inst/doc/DESeq2.html
NgsploT version 2.41.4	(Shen, Shao et al. 2014)	https://github.com/shenlab-sinai/ngsploT
Homer version 4.11	(Heinz, Benner et al. 2010)	http://homer.ucsd.edu/homer/motif/
Bowtie2 version 2.3.4.1	(Langmead and Salzberg 2012)	https://github.com/BenLangmead/bowtie2
SAMtools version 1.7	(Li, Handsaker et al. 2009)	http://www.htslib.org/
Picard-tools version 1.119		https://broadinstitute.github.io/picard/
deepTools version 3.3.0	(Ramirez, Ryan et al. 2016)	https://deeptools.readthedocs.io/en/develop/
MACS2 version 2.1.1.20160309	Gaspar, 2018	https://pypi.org/project/MACS2/
Bedtools version 2.28.0	(Quinlan and Hall 2010)	https://bedtools.readthedocs.io/en/latest/
R package DiffBind version 2.16.0	(Ross-Innes, Stark et al. 2012)	http://bioconductor.org/packages/release/bioc/vignettes/DiffBind/inst/doc/DiffBind.pdf
R package ChIPseeker version 1.24.0	(Yu, Wang et al. 2015)	https://guangchuangyu.github.io/software/ChIPseeker/
R package rtracklayer version 1.48.0	(Lawrence, Gentleman et al. 2009)	https://bioconductor.org/packages/release/bioc/html/rtracklayer.html
R package EnhancedVolcano version 1.6.0	Blighe K et al, 2020	https://github.com/kevinblighe/EnhancedVolcano
HiC-Pro 2.1.1.4	Github, Servant N et al., 2015	https://github.com/nservant/HiC-Pro
FitHiChIP 8.1	(Bhattacharyya, Chandra et al. 2019)	https://ay-lab.github.io/FitHiChIP/
HiCExplorer 3.6	(Ramirez, Bhardwaj et al. 2018)	https://hicexplorer.readthedocs.io/en/latest/

2.1.10 Tansgenic mouse lines

The *Lmna*^{tm1.1Yxz/J} line (Kim and Zheng 2013) and the *Gata4*^{tm1.1Sad} were obtained from Jackson Laboratory. All mouse lines were maintained on a C57BL/6 J background. Both male and female mice at the indicated in the figure legends age were used within the study. Mice were housed in a pathogen-free animal facility under standard conditions with a 12 hour light/dark cycle, temperature of 20-25 degrees and humidity range of 30-70%. All animal experiments were performed according to the regulations issued by the Committee for Animal Rights Protection of the State of Baden-Württemberg (Regierungspraesidium Karlsruhe, permit number: G-194/18).

2.2 Methods

2.2.1 Cell lines and cell culture

HEK293T cells were purchased from ATCC (CRL-3216) and cultured in DMEM supplemented with 10% FCS, 1% penicillin-streptomycin (Thermo Fisher Scientific, 15140122) and 2 mM L-glutamine (Thermo Fisher Scientific, 25030123).

Murine E14-NKX2-5-EmGFP mESCs generated by Hsiao et al (Hsiao, Yoshinaga et al. 2008) were maintained on mitomycin (Sigma, M4287) treated mouse embryonic fibroblasts (MEF) in DMEM high glucose (Thermo Fisher Scientific, 10938025) supplemented with 15% fetal bovine serum (FBS, Thermo Fisher Scientific, 10270106), 2 mM L-glutamine (Thermo Fisher Scientific, 25030123), 0.1 mM 2-mercaptoethanol (Sigma, M3148), 0.1 mM non-essential amino acids (Thermo Fisher Scientific, 11140035), 1 mM sodium pyruvate (Gibico, 11360070), 4.5 mg/ml D-glucose, 1% penicillin-streptomycin (Thermo Fisher Scientific, 15140122) and 1000 U/ml leukemia inhibitory factor (LIF ESGRO, Millipore, ESG1107).

2.2.2 DNA extraction, RNA Isolation, RT-PCR, and Real-Time PCR

RNA was isolated using the TRIzol RNA Isolation Reagent (Invitrogen, 15596018). For real-time PCR analysis cDNA was synthesized with the High Capacity cDNA Reverse Transcription Kit (Applied Biosystems, 4368813) and real-time PCR was performed using the SYBR GREEN PCR master mix (Applied Biosystems, A25742). Cycle numbers were normalized to those of α -Tubulin (Tuba1a).

2.2.3 Western blotting

Cells were collected and lysed in RIPA buffer supplemented with protease inhibitor cocktail (Millipore, 535142). Protein concentration was quantified using Pierce BCA protein assay kit (Pierce Biotechnology, 23225). After separation via SDS-PAGE, proteins were transferred to nitrocellulose membranes (GE, 10600002), blocked in 5% skimmed milk/PBST and incubated with appropriate primary antibodies: Lamin A/C (Abcam, ab8984; 1:1000), Lamin A/C (Santa Cruz, sc-376248; 1:1000), Lamin B1 (Abcam, ab16048; 1:1000), H3K9me3 (Abcam, ab8898; 1:5,000), H3 (Abcam, ab1791; 1:5000), Ryr2 (Sigma, HPA020028, 1:1000), α -tubulin (Sigma, T5168, 1:1000) followed by incubation with corresponding secondary antibody. The images were acquired on Amersham Imager 600.

2.2.4 Mouse mESC lines generation and differentiation

For generation of *Lmna*^{-/-}, *Lmna*^{+/-}, *Lmnb1*^{-/-} and *Gata4*^{+/-} murine mESCs by CRISPR/Cas9-mediated gene targeting, a single guide RNA or a combination of two guide

RNAs (gRNAs) and mutation donor templates were used as follows: *Lmna* gRNA-1: 5'-CACCGCACTGCTCACGTTCCACCAC-3' and *Lmna* gRNA-2: 5'-CACCGAGCTATCAGCACTCTGTTAT-3'; *Lmnb1* gRNA-1: 5'-CACCGAAACTCTAAGGATGCGGCGC-3' and *Lmnb1* gRNA-2: 5'-CACCGAGAGGCTCTCGATCCTCATC-3'; *Gata4* gRNA-1: 5'-CACCGTGCAGTCTCCACCGGCTCGT-3' and *Gata4* gRNA-2: 5'-CACCGCTGTCAGGAGCACGGCTAAT-3. Annealed gRNAs were ligated in pSpCas9(BB)-2a-Puro (PX459) V2.0 plasmid, a kind gift from Feng Zhang (Addgene, 62988). Recombinant plasmids or mutation donors were transfected into WT mESCs using Lipofectamine 2000 (Thermo Fisher Scientific, 11668019) according to the manufacturer's protocol. Positive cells were selected after 24 h of transfection for 48 h using puromycin (Thermo Fisher Scientific, A1113803, 4 µg/ml) and 5 000 cells were further plated on a 6-cm dish with feeders. After 7 days of culture, single clones were picked and screened by PCR, followed by Sanger sequencing.

For stable knockdown mESC lines generation, HEK293T cells were seeded on a 6-well plate and cultured in DMEM, high glucose, GlutaMAX (Gibco, 61965059) supplemented with 10% fetal bovine serum and 1% penicillin-streptomycin. Cells were transfected at 70% confluence with 1.5 µg *Lmna* (GCTTGACTTCCAGAAGAACAT), *Gata4* (CATCTCCTGTCACTCAGACAT) or control (pLKO) shRNA obtained from the RNAi consortium (TRC) shRNA library along with 0.975 µg CMV Δ R8.74 packaging plasmid and 0.525 µg VGV.G envelope plasmids using the X-tremeGENE DNA transfection reagent (Roche, 6366236001). 48 h after transfection the viral supernatant was collected and 2 ml virus were used to transduce 100 000 mouse mESCs in the presence of 8 µg/ml polybrene (Sigma, TR-1003-G) on 5% poly-HEMA (Sigma, P3932) treated 6-well plates for 12 h. The following day, the transduced mESCs were plated on feeders. 24 h after transduction, the transduced mESCs were selected with 10 ng/mL puromycin for 48 h.

mESCs were differentiated into CMs using either undirected differentiation in hanging droplets or by a directed differentiation method, as described before (Gao, Liang et al. 2019). Briefly, differentiation through the hanging drop method was initiated following ESCs dissociation by 0.05% trypsin-EDTA (Thermo Fisher Scientific, 25300054) and suspension at 3.3×10^4 cells/ml in ESC growth medium without LIF in 15 µl drops. After two days, the resulting embryoid bodies (EBs) were transferred to low attachment culture dishes (Greiner Bio-One, 633180). At day 6 (d6) and d10, EBs were dissociated and CPCs and CMs, respectively, were FACS sorted for Nkx2-5-GFP expression. For directed cardiomyocyte differentiation, ESCs were maintained on mouse feeders in Knockout DMEM medium (Thermo Fisher Scientific, 10829018) containing 4.5 mg/ml D-glucose, supplemented with 10% serum replacement (Thermo Fisher Scientific, 10828028), 2 mM L-glutamine, 0.1 mM 2-mercaptoethanol, 1 mM sodium pyruvate, 1% penicillin-streptomycin and 1000 U/ml leukemia inhibitory factor. Before differentiation, ESCs were dissociated and grown on 0.1% gelatin (Sigma, G9391) coated 10-cm dishes in Neurobasal

medium: DMEM/F12 (1:1; Thermo Fisher Scientific, 21103049 and 21331020) supplemented with 2000 U/ml LIF and 10 ng/ml BMP4 (R&D, 314-BP) for 2 days. Differentiation was initiated by aggregation in low attachment bacterial dishes at a cell density of 75 000 cells/ml in IMDM: F12 medium (3:1; Thermo Fisher Scientific, 12440053 and 11765054). After 48 h aggregates were dissociated and re-aggregated in the presence of Activin A (R&D, 338-AC, 5 ng/ml), VEGF (R&D, 293-VE-010, 5 ng/ml) and BMP4 (R&D, 314-BP, 0.1-0.8 ng/ml, BMP4 concentration was optimized for each lot). 40 h following the second aggregation, aggregates were dissociated and plated as a monolayer in Stempro-34 medium (Thermo Fisher Scientific, 10639011), supplemented with 2 mM L-glutamine, L-ascorbic acid (Sigma, A4403, 50 µg/ml), VEGF (R&D, 293-VE-010, 5 ng/ml), bFGF (R&D, 233-FB, 10 ng/ml), and FGF10 (R&D, 345-FG, 25 ng/ml) growth factors. Analysis were done at day 5 (cardiac progenitor stage) and at day 10 (cardiomyocyte stage).

2.2.5 Knockdown of *Lmna* at the cardiac progenitor and cardiomyocyte stages

For *Lmna* knockdown at the cardiac progenitor (CP) stage, virus particles in Stempro-34 medium supplemented with growth factors were used to transduce cells on 0.1% gelatin-coated 24-well plates 7 hours after the second aggregation of the direct cardiac differentiation protocol in the presence of 8 µg/ml polybrene. 24 hours after transduction, the medium was replaced with normal differentiation medium. CMs at d10 were harvested for analysis. For *Lmna* knockdown at the cardiomyocyte (CM) stage, d8 monolayer CMs were trypsinized and 50% of the cells were re-seeded on 0.1% gelatin-coated 24-well plates in the presence of 8 µg/ml polybrene together with virus produced in Stempro-34 medium. The medium was changed to normal Stempro-34 medium 24 hours after virus transduction and CMs were harvested at d10.

2.2.6 siRNA mediated gene knockdown

siRNA-mediated knockdown experiments were performed as follows: 30 000 mESCs were seeded in 6-well plates with feeders. 24 hours later, cells were transfected with either 50 nM scrambled siRNA or 50 nM siRNA against *Gata4* (Dharmacon/GE, L-040759-01-0005), *Lmna* (5'-GAGAGCAGGCCUGAAGCCAAAGAAA-3'), *Lmnc* (5'-TCTCCCACCTCCATGCCAAAG-3') using Lipofectamine RNAiMax (Thermo Fisher Scientific, 13778-075). 48 h after transfection, the cells were subjected to hanging drop differentiation or further analysis.

2.2.7 Primed hiPSC cell culture, differentiation, and conversion to naïve hiPSC

The use of hiPSC within this study has been approved by the Ethics Committee of the Medical Faculty Mannheim, University of Heidelberg (approval number: 2022-539). Human iPSC line was cultured in a primed state on Matrigel coated plates in Essential 8 (E8) medium (Thermo Fisher Scientific). Cells were passaged as small clumps with EDTA, and 5 µM ROCK inhibitor Y-27632 (Miltenyi Biotec) was added for the first 24 h. For hiPSCs differentiation, cells were

seeded into 24-well plate precoated with Matrigel and allowed to reach 85-95% confluence (day 0). On day 0, medium was changed to cardiac differentiation medium (RPMI-1640 with glutamine supplemented with 500 µg/ml BSA and 200 µg/ml ascorbic acid) and supplemented with 6 µM CHIR99021. At day 2, medium was substituted with cardiac differentiation medium supplemented with 5 µM IWP2, followed by a change to cardiac differentiation medium on day 4. From day 6 on, cells were cultured in RPMI-B27 media (RPMI with 1× B-27 supplement).

For naïve hiPSCs differentiation, cells were dissociated by 0.05% trypsin-EDTA and cultured in hanging drops, with a density of 500 cells per drop in medium (DMEM medium with 15% FCS, 1% nonessential amino acids, 0.1 mM β-mercaptoethanol, 1% Penicillin-Streptomycin), in the absence of LIF. After two days, the resulting embryoid bodies were transferred to low attachment culture dishes and cultured in differentiation medium. Day10 EBs were harvested for analysis. For transfection, hiPSCs were cultured feeder free with 5 µM ROCK inhibitor for 24 h before virus infection. After infection, cells were subsequently plated on Matrigel coated plate or MEF feeder layers.

Conversion of primed human iPSC line to naïve state was performed as described before (Gafni, Weinberger et al. 2013). Briefly, primed human iPSCs were seeded on feeder cells as small clumps in E8 medium supplemented with 5 µM ROCK inhibitor. 24 hours later, medium was switched to 4i medium (knockout DMEM, 1% AlbuMAXI, 1 X N2 supplement, 12.5 µg/ml recombinant human insulin, 20 ng/ml of recombinant human LIF, 8 ng/ml recombinant bFGF and 5 ng/ml recombinant IGF, 1 mM glutamine, 1% nonessential amino acids, 0.1 mM β-mercaptoethanol, 1% Penicillin-Streptomycin and small molecule inhibitors: 1 µM PD0325901; 3 µM CHIR99021; 10 µM SP600125 and 2 µM BIRB796). Following an initial wave of widespread cell death, dome-shaped naïve colonies appeared about 6 to 8 days and were passaged by accutase treatment for 3–5 min.

Toggling of naïve mESCs to primed state was performed as described before (Sperber, Mathieu et al. 2015). Briefly, naïve mESC were preplated and seeded on 0.1% gelatin coated plate in DMEM/F12 supplemented with 20% knock-out serum replacement, 1mM sodium pyruvate, 0.1mM nonessential amino acids, 0.1mM β-mercaptoethanol, 1% Penicillin-Streptomycin, 10ng/ml Activin A, and 10ng/ml bFGF.

2.2.8 Neonatal cardiomyocytes isolation and culture

Neonatal CMs were isolated from 1-day-old (P1) mice using a neonatal heart dissociation kit (Miltenyi Biotec, 130-098-373) and neonatal mouse CM isolation kit (Miltenyi Biotec, 130-100-825), according to the manufacturer's instructions. The cells were then cultured on coverslips in 24-well plates or glass bottom microwell dishes pre-coated with 10 µg/ml Laminin (Corning, 354232) in DMEM/F12 medium supplemented with 1% L-glutamine, 1% Na-pyruvate, 1% non-essential amino acids, 1% penicillin/streptomycin, 5% horse serum and 10% FBS.

2.2.9 Measurements of calcium transients in ventricular CMs

50 000 freshly isolated neonatal CMs from *Lmna*^{+/+}, *Lmna*^{+/-} and *Lmna*^{-/-} mice were seeded on glass bottom microwell dishes (MatTeK, P35g-1.5-20-C) pre-coated with 10 µg/ml laminin (Corning, 354232). After 2 days, CMs were washed twice with Tyrode's solution (140 mM NaCl, 5.4 mM KCl, 1 mM MgCl₂, 25 mM HEPES, 1 mM CaCl₂, 10 mM glucose, pH7.4) and then loaded with 2 µM Fura-2, AM (Thermo Fisher Scientific Fisher, F1221) in Tyrode's solution at 37 °C for 20 min. The cells were then washed three times for 5 min with Tyrode's solution at 37 °C. Calcium transients were measured at 10 V and 1 Hz stimulation on MyoPacer (IonOptix) and data were analyzed with IonWizard 7.4. Fura-2, AM-loaded cells were excited at both 340 and 380 nm, and the fluorescence emission signal was collected at 510 nm. Intracellular calcium changes were expressed as changes in the ratio $R = F_{340}/F_{380}$. For measuring neonatal CMs calcium transients after knockdown of *Lmna*, lentiviruses carrying shRNA for lamin A/C were produced as above and 1 ml supernatant containing viral particles was used to transduce 50 000 neonatal CMs. Calcium transients were measured as above 48 h after transduction.

2.2.10 Histology

Embryos were sacrificed by cervical dislocation, hearts were dissected and fixed with 4% paraformaldehyde overnight at 4 °C. The hearts were then dehydrated, embedded and sectioned. H&E staining was performed according to the manufacturer's instruction (GHS116, HT-110216; Sigma-Aldrich). Representative images of histological analysis of mice with the same genotype are presented. Heart sections were imaged by Zeiss Axio Scan (Zeiss).

2.2.11 Immunofluorescence staining

For immunofluorescence staining on heart sections, 7µm cryosections were fixed in 4% paraformaldehyde (Arcos, 416780010) for 20 minutes, washed 3 times with PBS, and permeabilized with 0.3% Triton X-100/PBS for 30 minutes. Slides were then blocked in 3% BSA (Roth,8076.2) for 30 minutes and then incubated with Anti-phospho-Histone H3 (Ser10) (Millipore,06-570,1:100); Anti-Cardiac Troponin I (Abcam, ab56357, 1:100); Anti-Aurora B (Abcam, ab2254, 1:100) in 1% BSA overnight at 4°C. On the following day, the sections were washed 3 times with PBS and incubated with a corresponding secondary antibody, conjugated to Alexa 555 or Alexa 488 (Thermo Fisher Scientific,1:500) for 2 hours. Then slides were washed 3 times with PBS, each time 5 min and stained with DAPI in PBS 15 min at room temperature. Slides were washed with PBS 3 times and mounted with Mowiol 4-88 (Millipore, 475904) mounting medium.

For immunofluorescence staining of mESCs, 60,000 mESCs were spotted on 0.1% Poly-L-lysine (Sigma, P8920) coated coverslips in 24 well plate. mESCs were allowed to adhere for 10min at 37°C followed by brief washing with PBS and then fixed in 4% formaldehyde (Sigma,

F1635) for 10 min at room temperature. mESCs were then permeabilized for 10 min with 0.5% Triton X-100/PBS. After blocking in 3%BSA in PBS for 30 min, mESCs were incubated with Anti-Lamin A/C (E-1) (Santa cruz, sc376248,1:100), Anti-Lamin A/C (131C3) (Abcam, ab8984,1:100), Anti-Lamin B1 (Abcam, ab16048, 1:100), Anti-Lamin B1 (Sigma, HPA050524, 1:100) antibodies in 0.3% Triton X-100/ 1% BSA overnight in a humidified chamber at 4°C. After three consecutive 5 min washing in PBS, mESCs were incubated for a further 1 hours with a corresponding secondary antibody, conjugated to Alexa 555 or Alexa 488 in PBS. mESCs were then washed with PBS and stained with DAPI in PBS for 15 min at room temperature. After washing 3 times with PBS, mESCs were mounted with Mowiol 4-88 mounting medium. For immunofluorescence staining of CMs, 30,000 of isolated cardiomyocytes or differentiated cardiomyocytes were seeded on 10 µg/ml laminin coated coverslips in 24-well plate. 24 hours later, CMs were subjected to staining procedures as described above.

For immunofluorescence staining of mESC colonies, 50,000 of mESCs were seeded on coverslips with feeders in 12-well plate and cultured for 2 days. After washing with PBS, mESC colonies were fixed in 4% formaldehyde for 20 min at room temperature and permeabilized for 20 min by 0.5% Triton X-100/PBS. After blocking in 3%BSA/PBS 30 min, mESC colonies were incubated with Anti-*Gata4* (C-20) (Santa cruz, sc1237, 1:100), Anti-Myl4 (Sigma, HPA051884, 1:100) and Anti-Oct3/4 (Santa cruz, sc5279, 1:100) antibodies in 0.3% Triton X-100 / 1%BSA overnight in a humidified chamber at 4°C. After three consecutive 5-min washing in PBS, mESC colonies were incubated for a further 3 hours with secondary antibody in 0.3% Triton X-100/1%BSA. mESC colonies were washed with PBS three times and stained with DAPI in PBS for 30 min at room temperature. After washing with PBS, mESC colonies were then mounted with Mowiol 4-88 mounting medium.

2.2.12 Wheat germ agglutinin (WGA) and isolectin B4 (IB4) co-staining

For isolectin B4 (IB4) and wheat germ agglutinin (WGA), staining, 7 µm heart sections were fixed in 4% paraformaldehyde for 20 minutes, washed 3 times with PBS, blocked in 3% BSA for 30 minutes and then incubated with WGA Alexa 488 Conjugate (Thermo Fisher Scientific, W11261, 1 mg/ml, 1:100) antibody diluted in 1%BSA for 1 hour at room temperature in a humidified dark chamber. Slides were then washed with PBS 3 times, each time 5min, permeabilized with 0.3% Triton in PBS for 30 minutes and then incubated with IB4 Alexa 568 conjugate (Thermo Fisher Scientific, I21412, 1 mg/ml,1:100) antibody diluted in 1% BSA for 2 hours at room temperature in a humidified dark chamber. Then slides were washed with PBS 3 times for 5min and stained with DAPI in PBS for 15 min at room temperature. After DAPI staining, slides were washed with PBS 3 times and mounted with Mowiol 4-88 mounting medium.

2.2.13 Immunofluorescence imaging and quantifications

WGA and IB4 immunostaining images were acquired using Leica DMI8 microscope with 63X objective. The rest of the fluorescence images were acquired using a Zeiss LSM 710 confocal microscope with a 25x or 63x objective. To quantify the cross-sectional cell size, capillary density and cardiomyocytes proliferation, a minimum three independent hearts per group from three different views and positions, each from left and right ventricles, and septum were captured at 63x magnification. ImageJ was used to quantify the size of CMs that were round and contained a nucleus. About 200 cells per sample were quantified. Capillary density was expressed as the ratio of number of capillaries to CMs.

2.2.14 DNA Fluorescence In Situ Hybridization (FISH)

DNA FISH probes for *Mef2c*, *Actc1*, *Ttn* and *Kcnq1* were labeled with digoxigenin by Nick Translation kit (Roche, 10976776001) according to manufacturer's protocol using BAC DNA clones: *Mef2c* (Thermo Fisher Scientific, RP23-187H18), *Actc1* (Thermo Fisher Scientific, RP23-196J13), *Ttn* (Thermo Fisher Scientific, RP23-310F9), *Kcnq1* (Thermo Fisher Scientific, RP23-207G7). 60,000 mESCs were attached on Poly-L-lysine coated coverslips for 30 min at 37°C and air-dried. The mESCs were allowed to adhere for 10 min at 37°C. Cells were washed with PBS 3 times and fixed in 4% paraformaldehyde (Electron Microscopy Sciences, 15710) at room temperature for 10 min. Afterwards, cells were rinsed in PBS, permeabilized with 0.5% Triton X-100/PBS for 10 min at room temperature and rinsed briefly in PBS. Then cells were incubated in 20% glycerol (Roth, 3783.1) in PBS for a minimum of 60 min at room temperature and were left at 4°C overnight. Next day, coverslips were removed from the glycerol solution, dipped into liquid nitrogen about 15s until the coverslips were completely frozen and thawed at room temperature. The freeze/thaw treatment was repeated 6 times. The cells were then washed with 0.05% Triton X-100/PBS 3 times for 5 min. After a brief wash with 0.1N HCl the cells were incubated in a fresh 0.1N HCl for 10 min followed by three time washes with 0.05% Triton X-100/PBS, 5 min each, one wash in 2x SSC (0.3M NaCl, 30 mM sodium citrate) and prehybridized in 50% formamide (Sigma, F9037)/2XSSC for 4h at 37°C. 5 µl labeled DNA probes in hybridization buffer were added to the slides and sealed with rubber cement. Slides were then incubated at 75°C for 3min and hybridized for 2 days, at 37°C. Hybridization was followed by three washes with 2xSSC, 3x 10min at 37°C and two washes with 0.1xSSC at 60°C. Afterwards, cells were incubated with anti-digoxigenin-rhodamine, Fab fragments (Roche, 11207750910, 1:200) in 4%BSA/4xSSCT 1hour at room temperature followed by two washes with 4xSSCT at 37°C, a brief wash in PBS followed by post-fixation in 2% formaldehyde/PBS for 10min. Cell nuclei were counterstained with DAPI/PBS (1:500) for 10min and after a brief wash in PBS were mounted with ProLong Diamond Antifade Mountant (Life Technologies, P36930).

2.2.15 Chromosome painting

Cells were prepared as described for FISH until the permeabilization step. 10 µl of whole chromosome painting probes (MetaSystems, D-1414-050-FI) were applied on the coverslip of a slide followed by sealing with rubber cement for 30 min at room temperature. Slides were then denatured at 75°C for 2 min and hybridized at 37°C overnight. Cells were washed with 0.4xSSC (pH7.0) at 72°C for 2 min and 2xSSC, 0.05% Tween-20 (pH7.0) at room temperature for 30 seconds. Cells were rinsed briefly in distilled water to avoid crystal formation and counterstained with DAPI/PBS (1:500) for 10 min followed by a wash with PBS prior to mounting in ProLong Diamond Antifade Mountant.

2.2.16 Flow cytometry

For FACS staining of extracellular markers, EBs were washed with HBSS twice and dissociated into single cells by incubation with 1 mg/ml collagenase I (Cell Systems, LS004196) at 37°C for 30 min. Cells were then washed with 5% FCS/PBS and blocked in 10% FCS/PBS buffer for 30 min at room temperature. 200 000 cells were used for staining with 2.5 µl APC-conjugated anti-Flk1 (e-Bioscience, 17-5821-81,1:40), PE-conjugated anti-PDGFR α (e-Bioscience, 12-1401-81,1:40), APC-conjugated anti-Pecam1 (Thermo Fisher Scientific, 17-0311-82,1:40) antibody in 100 µl FACS buffer (0.4% BSA) for 1 hour at room temperature in a dark place. After washing with FACS buffer twice, cells were resuspended in 300 µl FACS buffer and subjected to analysis by BD FACSDiva Software (version 8.0.1, firmware version 1.49 BD FACSCanto II).

For FACS staining of intracellular cardiac Troponin T, single cells were prepared as above. After washing with 5% FCS/PBS, 400 000 cells were fixed in 500 µl 3.7% PFA for 30 min at RT. Cells were then washed with 5% FCS/PBS buffer and incubated in permeabilization buffer (0.5% saponin/5% FCS/PBS) for 15 minutes on ice. Cells were further stained with 2.5 µl APC-conjugated anti-troponin T antibody (BD, 1:40) in 100 µl permeabilization buffer for 2 hours at RT in a dark place, followed by washes with permeabilization buffer, PBS and FACS buffer and resuspended in 300 µl FACS buffer for FACS analysis.

For apoptosis assay by FACS, one million cells were used for staining with 5 µl of APC Annexin V and 5 µl of 7-AAD in 100 µl Annexin V binding buffer for 15 min at room temperature according to the APC Annexin V Apoptosis Detection Kit with 7-AAD (Biolegend, 640930) instructions. Cells were then resuspended in 400 µl of Annexin V Binding Buffer and subjected to FACS analysis. CMs and non-CMs were distinguished by Nkx2-5 GFP expression.

To assess CM binucleation by FACS, E14.5 and E18.5 hearts were freshly harvested, washed with cold HBSS and dissociated into single cells by incubation with digestion buffer (1 mg/ml collagenase I and 1 mg/ml DNase I in HBSS) at 37°C 30 min. Cell suspension was then applied

to a 70 μ m cell strainer to remove cell debris. Single cells were stained with APC-conjugated anti-Pecam1 antibody for 30 min at 4 °C followed by washing with cold HBSS/10%FCS three times. Cells were then stained with Vybrant™ DyeCycle™ Green (Thermo Fisher Scientific, 1:500 dilutions by HBSS/10%FCS) at 37 °C for 30 min and were subjected to FACS analysis.

2.2.17 Echocardiographic assessment of cardiac dimensions and function

Transthoracic echocardiography was performed using a Vevo 3100 high-resolution system (Visualsonics, Toronto, ON, Canada) and a 50-MHz MX-700 transducer. Two-dimensional B-mode tracings were recorded in both parasternal long and short axis views at the level of the papillary muscles, followed by one-dimensional M-mode tracings in both axes, wherein at least three consecutive cardiac cycles were used for analysis. Left- and right-ventricular area at end-diastole (LVEDA; d and RVEDA; d, respectively) as well as left-ventricular posterior wall thickness at end-diastole (LVPW; d), were used to characterize cardiac microanatomy while the change of left-ventricular diameter length from end-diastole to end-systole was used to judge cardiac contractility and calculate left-ventricular fractional shortening (FS) and ejection fraction (EF) with Vevo LAB Software Package V3.2.6.

For fetal echocardiography, pregnant mice were anesthetized and one-dimensional AM-mode tracings of E16.5 mouse embryonic hearts were recorded with a 50MHz MX700 transducer. Right and left ventricular diameter at end-systole, right ventricular diameter at end-diastole, right and left ventricular ejection fraction and fractional shortening (RV diameter; s and LV diameter; s, RV diameter; d, RVEF, LVEF, RVFS and LVFS, respectively) were calculated with the integrated cardiac measurement package, where at least three consecutive cardiac cycles were used for analysis.

2.2.18 Contraction analysis

EBs at d6 were seeded on 0.1% gelatin-coated 24-well plates. Movies of spontaneous beating at day 8 and day 10 were acquired for at least 30s with a Leica DMI8 microscope at 100 frames/sec and a 20 \times objective. Contractility parameters were obtained by analyzing movies with MUSCLEMOTION V1.0 (Sala, van Meer et al. 2018).

2.2.19 RNA-Sequencing and data analysis

Control and *Lmna* KO Nkx2-5-GFP ES cell lines were differentiated using the hanging drop method. Cardiac progenitors at d6 and CMs at d10 were sorted by Nkx2-5-GFP from three different control and three different *Lmna*^{-/-} clones. Day10 EBs containing CMs, endothelial and other types of cells were also harvested for RNA-Seq. For RNA-Seq of control, *Lmna* knockdown CMs, wild type Nkx2-5-GFP ES cell lines were differentiated by the directed car-

diac differentiation method and CMs were transduced with pLKO control or *Lmna* shRNA lentivirus at d8 and harvested at d10. RNA was isolated using the RNeasy Plus Universal Mini kit (Qiagen #73404). The integrity of the RNA was assessed on a Bioanalyzer 2100 (Agilent). Library preparation and sequencing were performed on a BGISEQ-500 platform. RNA-Seq reads were trimmed of adapters using Trimmomatic-0.39 and mapped to the mm10 reference genome using STAR (-alignIntronMin 20 -alignIntronMax 500000). Read quality was controlled by the MultiQC tool. Reads were counted using the analyzeRepeats.pl function (rna mm10 -count exons -strand both -oadj) from HOMER after creating the tag directories with makeTagDirectory. For visualization of RNA-seq reads in the genome browser IGV, bam files of the three individual replicates were first merged by BamTools, then the BamCoverage function of deepTools with normalization to RPKM was used to generate the bigwig files (-bs 20 --smoothLength 40 --normalizeUsing RPKM -e 150). Differential expression was quantified and normalized using DESeq2. Reads per kilobase per millions mapped (RPKM) was determined using rpkm.default from EdgeR. Excel was used to filter differentially regulated genes (fold change ≥ 1.5 ; log2 fold change ≤ -0.58 , ≥ 0.58 ; p-value < 0.05). Gene ontology pathway analysis was performed using DAVID Bioinformatics Resources 6.8. Clustering analysis displayed as heatmap was performed using heatmapper.ca. All Heatmaps represent the row-based Z-scores calculated from trimmed mean of M-values (TMM). The PCA plots were obtained using prcomp into a custom R-script and volcano plots were obtained using a custom R-script. Boxplots were performed with the function boxplot from library Graphic from R using RPKM normalized values. All data, including publicly available data, were normalized with the same parameters.

2.2.20 ATAC-Sequencing and data analysis

Both *Lmna*^{+/+} and *Lmna*^{-/-} ESC and *Nkx2.5*-GFP sorted CM were processed using a modified protocol from Corces, Trevino et al. (2017). In brief, 50,000 cells were centrifuged at 500g for 5 min at 4°C and washed with PBS. The cell pellet was resuspended in 50 μ l cold lysis buffer (10 mM Tris-HCl pH 7.4, 10 mM NaCl, 3 mM MgCl₂, 0.1% Igepal CA-630) and incubated for 3 min on ice, followed by stopping the reaction by diluting with 1 ml ATAC resuspension buffer (10 mM Tris-HCl pH 7.4, 10 mM NaCl, 3 mM MgCl₂) and 10 min centrifugation (500g, 4°C). Isolated nuclei were incubated in 50 μ l transposase mixture with 2.5 μ l Nextera Tagment DNA Enzyme TDE (Illumina, 15027916) in 47.5 μ l transposition buffer (20 mM Tris-HCl pH 7.6, 10 mM MgCl₂, 20% Dimethylformamide) for 30 min at 37 °C. Following the transposition reaction, the DNA was purified using CHIP DNA Clean and Concentrator Kit (Zymo, D5205). Library amplification together with indexing was performed by a 5-cycle pre-amplification step, a SYBR green qPCR side reaction with 1/10 of the pre-amplified material to determine the cycle numbers required for amplification, followed by PCR with individually adapted cycle numbers. PCR was done using the NEBNext High-Fidelity 2x PCR Master Mix (New England Biolabs, M0541S)

and Nextera Index Kit (Illumina, 15055290). Magnetic bead purification with two-sided size selection using undiluted Agencourt AMPure XP Beads (Beckman Coulter, A63881) ensured library sizes between 150 and 1000 bp, detected by Bioanalyzer High Sensitivity DNA analysis (Agilent, 5067-4626). Libraries were mixed in equimolar ratios and prepared according to the *Denature and Dilute Libraries Guide* (15048776v02). 1.8 pM concentrated libraries including PhiX sequencing control were sequenced on NextSeq550 platform using v2.5 chemistry (Illumina Nextseq 500/550, 20024907).

ATAC-seq reads were trimmed of adapters using Trimmomatic-0.39 and then mapped to mm10 mouse genome with Bowtie2 (Langmead and Salzberg 2012). Following removal of unmapped reads by SAMtools (-F 1804 -f 2) (Li, Handsaker et al. 2009), PCR artefacts were excluded by the MarkDuplicates.jar from Picard-tools-1.119 (Tools 2015). BamCoverage function of deepTools (Ramírez, Dündar et al. 2014) with normalization to RPKM was used to generate the bigwig files for visualization of ATAC-seq reads in the genome browser IGV (-bs 20 --smoothLength 40 --normalizeUsing RPGC --effectiveGenomeSize 2150570000 -e). Afterwards, fastq.gz files of each 3 replicates were merged and processing was performed like described. Peak calling was applied from merged bam-files with MACS2 (-q 0.01 --nomodel -shift -75 --extsize150) (Gaspar 2018), whereas peaks overlapping blacklist defined by ENCODE were discarded by the help of Bedtools v2.28.0 (intersect -wa) (Quinlan and Hall 2010). Called peaks from merged files and individual bam files were further used to quantify and normalize counts as well as to calculate differentially accessible chromatin regions upon *Lmna* deletion using the R package DiffBind (Stark and Brown) with normalizing to RPKM and using DESeq2 method to perform differential analysis. Peaks were annotated by a custom R script combining ChIPseeker (Yu, Wang et al. 2015) and rtracklayer packages (Lawrence, Gentleman et al. 2009). Promoter regions were defined as ± 3 kb around the mm10 gene transcription start site unless otherwise stated.

Principle component analysis (PCA), correlation heatmap, heatmap of 10000 most significant peaks and annotation pie chart were generated by the help of the DiffBind package. Volcano plots are based on the EnhancedVolcano package (Blighe K 2020). Homer motif enrichment analysis was performed with the findMotifsGenome.pl (-size 200 -len 8 -mask) function.

2.2.21 Hi-C and data analysis

Hi-C libraries were generated according to (Rao, Huntley et al. 2014) with modifications. Five million mESC were crosslinked with 1% formaldehyde for 10 min at RT and quenched with 120 μ M Glycine for 5 min at RT on a rotator. Cells were pelleted at 4 °C for 5 min at 2,500 relative centrifugal force (RCF) and washed twice with ice cold PBS. Cells were lysed in 500 μ l of ice-cold Hi-C lysis buffer (10 mM Tris-HCl pH 7.5, 10 mM NaCl, 0.2% NP-40, 1 \times protease inhibitors) with rotation at 4 °C for 30 min. Nuclei were then pelleted and resuspended in 100 μ l of 0.5% SDS and incubated at 62 °C for 10 min. The SDS reaction was stopped by adding

285 μ l of water and 50 μ l of 10% Triton X-100 to each sample at 37 °C for 15 min. 200 U of MboI restriction enzyme (NEB, R0147) and 50 μ l of NEB Buffer 2 were used to digest the chromatin. Samples were then incubated at 37 °C for 3 h with rotation. The restriction enzyme was then heat inactivated at 62 °C for 20 min. To fill-in the MboI overhang and mark the ends, 52 μ l of incorporation master mix (37.5 μ l of 0.4 mM biotin-dATP (Thermo Fisher, 19524016); 4.5 μ l of a dCTP, dGTP, and dTTP mix at 10 mM each; and 10 μ l of 5 U/ μ l DNA Polymerase I, Large (Klenow) Fragment (NEB, M0210)) were added to the nuclei and incubated at 37 °C for 1 h with rotation. 948 μ l of ligation master mix (150 μ l of 10 \times NEB T4 DNA ligase buffer with 10 mM ATP (NEB, B0202), 125 μ l of 10% Triton X-100, 3 μ l of 50 mg/mL BSA (Thermo Fisher, AM2616), 10 μ l of 400 U/ μ l T4 DNA Ligase (NEB, M0202), and 660 μ l of water) were then added to each sample and incubated overnight at 16 °C. After proximity ligation, the nuclei were pelleted at 2,500 RCF for 5 min at room temperature and the supernatant was used further. Reverse crosslinking was done by overnight incubation at 65°C. DNA was purified using ChIP DNA Clean & Concentrator Kit (Zymo Research, D5205) and then sheared to a length of \sim 400 bp. 50 ng of the sheared DNA was used for pull down of biotinylated proteins with 5 μ l of Streptavidin C-1 beads (Thermo Fisher, 65001) in biotin binding buffer (10 mM Tris-HCl pH 7.5, 1 mM EDTA, 2 M NaCl) at room temperature for 15 min while shaking. Beads were then captured on the magnet, washed twice with 500 μ l of Tween Wash Buffer at 55 °C for 2 min with shaking followed by one washing step using 100 μ l of 1 \times TD Buffer (10 mM Tris-HCl pH 7.5, 5 mM magnesium chloride, 10% dimethylformamide). The beads were then re-suspended in 25 μ l of 2 \times TD Buffer, 2.5 μ l Tn5 and water to 50 μ l and incubated at 55 °C for 10 min while shaking. The beads were captured with a magnet and incubated in 50 mM EDTA at 50 °C for 30 min while shaking. Beads were further washed two times with 50 mM EDTA followed by a wash with Tween Wash Buffer at 55 °C for 2 min and with 10 mM Tris before PCR amplification. Beads were then resuspended in 25 μ l of Phusion HF 2 \times (New England Biosciences), 1.25 μ l of illumine Index 1 (i7) adapters and Index 2 (i5) Adapters from Nextera kit (Illumina, 15055290) and 22.5 μ l of water and amplification was carried out using the following PCR program: 72 °C for 5 min, 98 °C for 1 min, then cycle at 98 °C for 15 s, 63 °C for 30 s, and 72 °C for 1 min. Cycle numbers needed for amplification (beginning of exponential amplification) was determined for each sample. Afterwards, Ampure beads were used for double size selection to purify DNA with size range of 300- 700 bp. After size selection, libraries were quantified on Bioanalyzer and sequenced paired end with read length of 75.

Hi-C paired-end reads were aligned to the mm10 genome, duplicate reads were removed, reads were assigned to MboI restriction fragments, filtered into valid interactions, and the interaction matrices were generated using the HiC-Pro pipeline default settings (Servant, Varoquaux et al. 2015). HiC-Pro valid interaction reads were then used to detect significant loops and generate Washu epigenome browser file using FitHiChIP. Significant loops were

detected using the following settings: FDR 0.01, All to All loop detection without providing peak file (Hi-C mode), binsize 10 kb, LowDistThre 20000 and UppDistThr 2000000. The PE alignment output of HiC-Pro was used to build a .h5 matrix of 100Kb using hicBuildMatrix command with default settings from HiCExplorer. The .h5 matrixes were normalized (hiNormalize command), corrected (HicCorrectMatrix command) and matrix bins were merged (hicMergeMatrixbins -nb 50). The merged bins matrix was then used to generate heatmaps. Validpairs HiC-Pro output were used to generate HOMER TagDirectories (Heinz, Benner et al. 2010) which were used to do the principal component analysis with a resolution of 25 kb. DNA segments with a positive principal component 1 (PC1) value in at least two biological replicates were defined as compartment A, while those with a negative value were defined as compartment B. DNA compartment switches from A to B or B to A was considered if changes were observed in at least two biological replicates in both control and knockout. A DNA segment was defined as static if it stayed in compartment A or B in at least two biological replicates from the control and *Lmna* knockout mESCs.

2.2.22 Statistics and reproducibility

All experiments were performed at least three independent times and the respective data were used for statistical analyses. Values for n represent always biologically independent samples. Data are presented as mean \pm SD. Differences between groups were assessed using an unpaired two-tailed Student's t-test or ANOVA multiple comparisons, as indicated in the figure legends. For small size samples (n=3) which cannot meet the normal distribution, differences between groups were assessed using the nonparametric Mann-Whitney U Test or Kruskal-Wallis Test for multiple comparisons. P values represent significance *P<0.05, **P<0.01, ***P<0.001. GraphPad Prism v8.0.2 was used to perform the statistical analysis and prepare figures.

3 RESULTS

3.1 *Lmna* deficiency leads to aberrant cardiovascular cell fate choices

3.1.1 *Lmna* knockout mESC generation by CRISPR/Cas9 gene editing

Chromatin tethering to the nuclear lamina have been proposed to control cardiac lineage restriction (Poleshko, Shah et al. 2017), however, to what extent nuclear lamins are involved in this process remains unknown. To determine whether lamin A/C plays a role in cardiac differentiation, I generated lamin A/C knockout E14-NKX2-5-EmGFP mESCs cell line by deleting the first two exons of the *Lmna* genome with CRISPR/Cas9. After initial prescreening, 3 independent clones were used further for the study (Fig. 16a). Western blot analysis confirmed a complete loss of lamin A/C protein level in mESC (Fig. 16b).

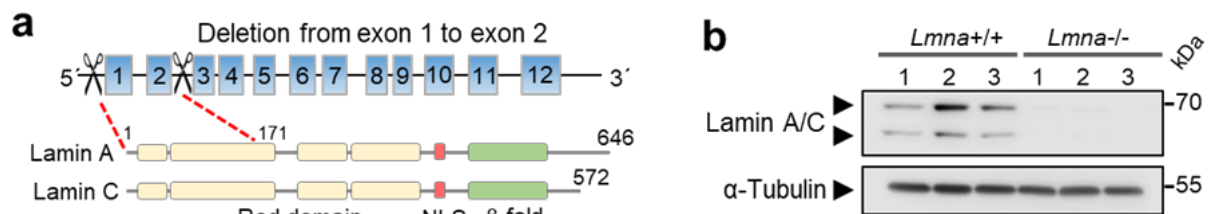


Figure 16. *Lmna* knockout mESC generation. **a** Schematic diagram of *Lmna* knockout ESC generation by CRISPR/Cas9 gene editing. **b** Western blot analysis of lamin A/C in control and *Lmna*^{-/-} ESCs.

3.1.2 *Lmna* deficiency leads to aberrant cardiovascular cell fate choices

I therefore studied the role of lamin A/C in cardiovascular differentiation using undirected mESC differentiation to generate different cardiovascular cell types (Fig. 17a). Interestingly, *Lmna*^{-/-} mESC differentiated embryoid bodies (EBs) started beating already at day 7 (d7), and I observed a significantly higher number of beating EBs at later days of differentiation (Fig. 17b). Consistent with this, I detected a significant increase in the CM marker genes *Tnnt2*, *Mlc2v*, *Mlc2a* in *Lmna*^{-/-}, while the endothelial cell (EC) marker genes *Pecam1* and *Flk1* were downregulated (Fig. 17c). Similar changes were detected in *Lmna*^{+/-} EBs, suggesting loss of one allele results in *Lmna* haploinsufficiency and aberrant cardiovascular cell fate choices (Fig. 17d).

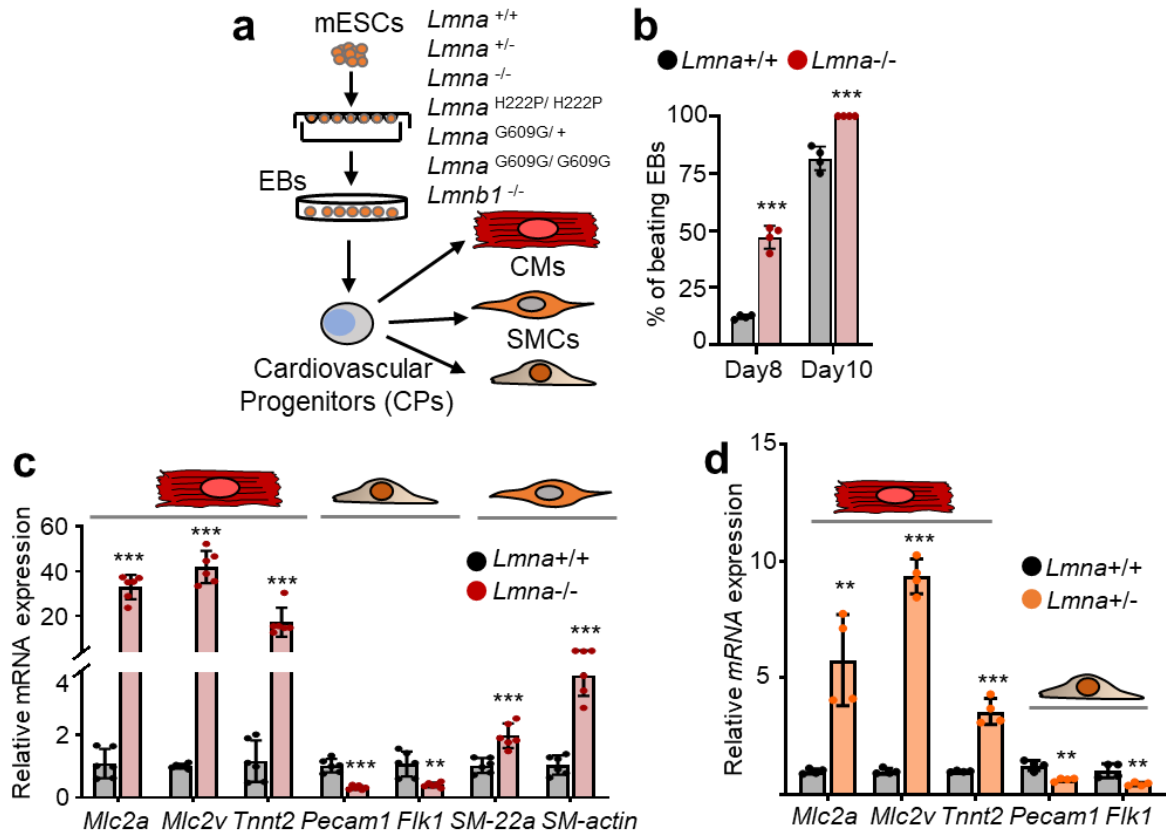


Figure 17. *Lmna* deficiency leads to aberrant cardiovascular cell fate choices. **a** Schematic diagram of the experimental setup. CMs, cardiomyocytes; SMCs, smooth muscle cells; ECs, endothelial cells. **b** Percentage of beating EBs derived from *Lmna*^{+/+} and *Lmna*^{-/-} mESCs at day 8 and day 10. n=4 biologically independent samples. **c, d** qPCR analysis of CM (*Mlc2a*, *Mlc2v*, *Tnnt2*), endothelial (*CD31*, *Flk1*) and smooth muscle (*SM-22a*, *SM-actin*) genes in day 10 (d10) EBs differentiated from *Lmna*^{+/+} and *Lmna*^{-/-} mESCs (**c**, n=6 biologically independent samples) or *Lmna*^{+/+} and *Lmna*^{+/-} mESCs (**d**, n=4 biologically independent samples).

3.1.3 *Lmna* deficiency promotes cardiac differentiation by using direct CMs differentiation method

To further study how lamin A/C regulates CMs differentiation, I used a protocol for directed CMs differentiation from mESC (Fig. 18a) (Kattman, Witty et al. 2011). I observed a similar significant increase in the expression of CM marker genes upon lamin A/C depletion (Fig. 18b). Taken together, these results suggest that lamin A/C depletion results in a premature cardiomyocytes differentiation.

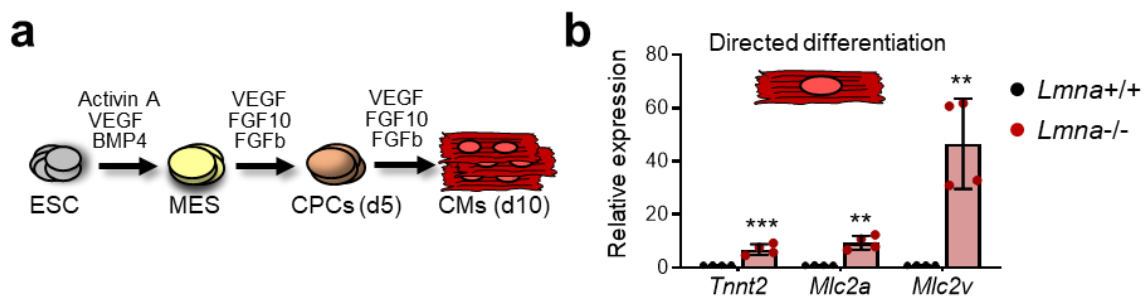


Figure 18. *Lmna* deficiency promotes CMs differentiation by direct CMs differentiation method. **a** Schematic diagram of directed differentiation of ESCs into CMs. **b** Relative mRNA expression of CM genes at day 10 of directed cardiac differentiation.

3.1.4 Loss of *Lmna* doesn't affect early cardiac mesoderm commitment

To gain a better understanding of the mechanisms underlying lamin A/C function in cardiogenesis, I collected day2, day3 as well as day4 EBs and analyzed cardiac mesoderm commitment and cardiovascular in more detail. Real-time PCR analysis for mesoderm (*Eomes*) and cardiac mesoderm markers (*Mesp1*) showed no significant difference in expression levels between control and lamin A/C-deficient EBs (Fig. 19a, b). Similarly, FACS analysis for FLK-1 and PdgfR- α , found no differences in early cardiovascular progenitor cell numbers (Fig. 19c, d).

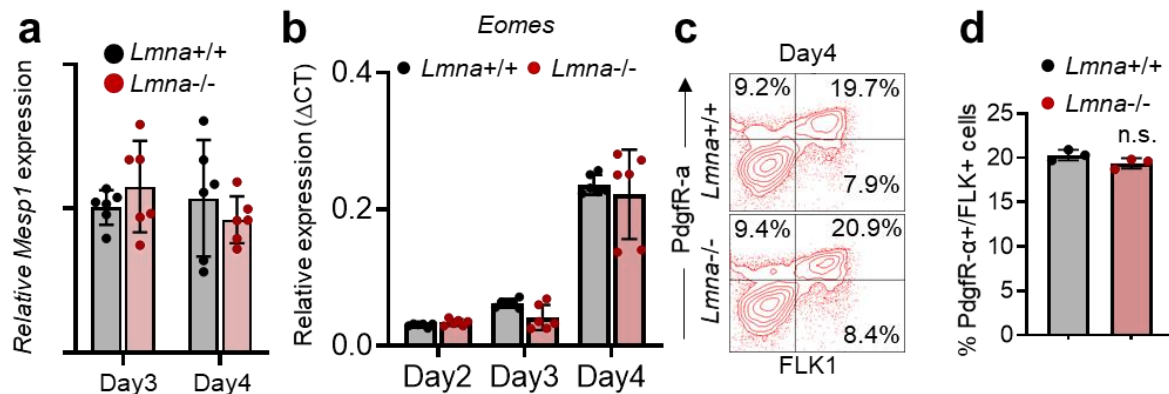
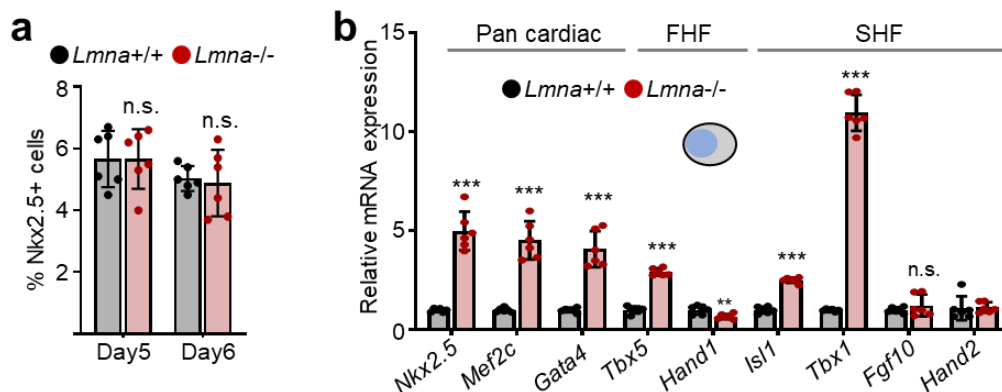


Figure 19. Loss of *Lmna* doesn't affect early cardiac mesoderm commitment. **a** Relative mRNA expression of the cardiac mesoderm marker *Mesp1* in EBs differentiated from control and *Lmna*^{-/-} mESCs at different days. n=6 biologically independent samples. **b** Relative mRNA expression of the mesodermal marker *Eomes* in EBs differentiated from control and *Lmna*^{-/-} mESCs at different days (n=6). **c** Representative FACS analyses of early PdgfR- α /FLK1+ cardiovascular precursors in d4 EBs differentiated from control and *Lmna*^{-/-} mESCs. **d** Percentage of early PdgfR- α /FLK+ cardiovascular precursors in d4 EBs differentiated from control and *Lmna*^{-/-} ESCs determined by FACS analysis (n=3).

3.1.5 *Lmna* regulates cardiovascular progenitor cell fate choices

Next, I investigated whether lamin A/C depletion affects cardiac progenitor cells diversification. FACS analysis of day5 and day6 EBs shows no differences in early cardiac progenitor numbers (Fig. 20a). However, at the cardiac progenitor stage (d6) I detected significant upregulation of core cardiac transcription factors (TFs) such as *Gata4*, *Isl1*, *Mef2C* and *Nkx2-5* ect. (Fig. 20b), followed by increase in CM and decrease of EC numbers at later stages (Fig. 20c and 20d), suggesting a role for lamin A/C in regulating cardiovascular progenitor cell fate choices.



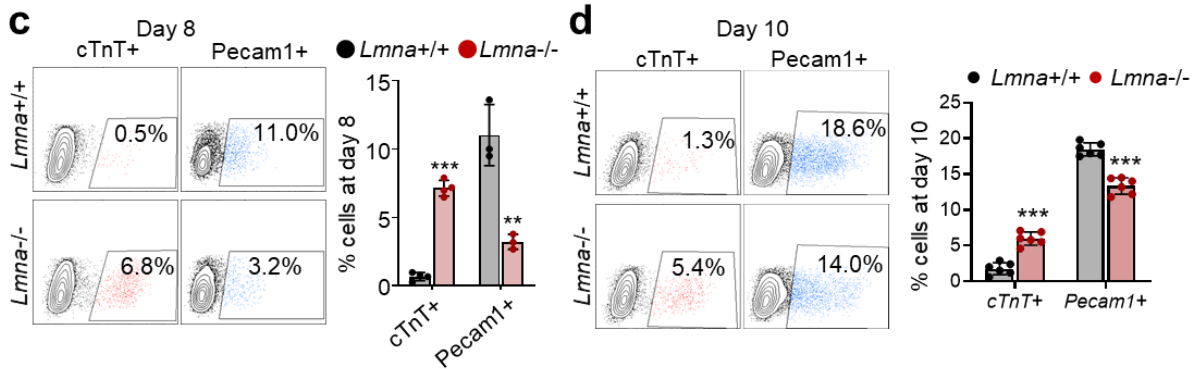


Figure 20. *Lmna* plays a role in regulating cardiovascular progenitor cell fate choices. **a** Percentage of Nkx2-5+ cardiac precursors in d5 and d6 control and *Lmna*^{-/-} EBs determined by FACS analysis. n=6 biologically independent samples. **b** Relative mRNA expression of cardiac progenitor marker genes in d6 EBs. FHF, first heart field markers; SHF, second heart field markers, n=6 biologically independent samples. **c-d** Representative FACS analyses of cardiac troponin (TnT)+ CMs and Pecam1+ ECs (left) and percentage of cTnT+ CMs and Pecam1+ ECs determined by FACS (right) at day 8 (n=4 biologically independent samples for CMs and n=3 biologically independent samples for ECs) and day10 of mESC differentiation (n=6 biologically independent samples).

3.1.6 RNA-seq analysis of Nkx2-5 sorted *Lmna*^{-/-} cardiac progenitors

To further study the mechanisms underlying cardiac cell fate choices upon lamin A/C loss, I performed RNA-sequencing (RNA-Seq) of sorted cardiac progenitors from day 6 EBs using Nkx2.5 GFP reporter that allows for selectively sorting of cardiac cells (Fig. 21a). Next I performed Gene Ontology (GO) analysis using DAVID 6.7 and found the genes upregulated in *Lmna*^{-/-} cardiac progenitor cells (CPs) revealed over-representation of GO terms linked to heart and cardiac muscle tissue development, including many key cardiac TFs such as *Gata4*, *Isl1*, *Mef2C*, *Smarcd3* ect., as well as genes involved in cardiac contraction and regulation of biosynthetic processes (Fig. 21b). In contrast, genes downregulated upon lamin A/C loss were enriched in GO terms linked to anterior/posterior patterning, alternative cell fates including vasculature development (Fig. 21b), consistent with the decreased number of ECs.

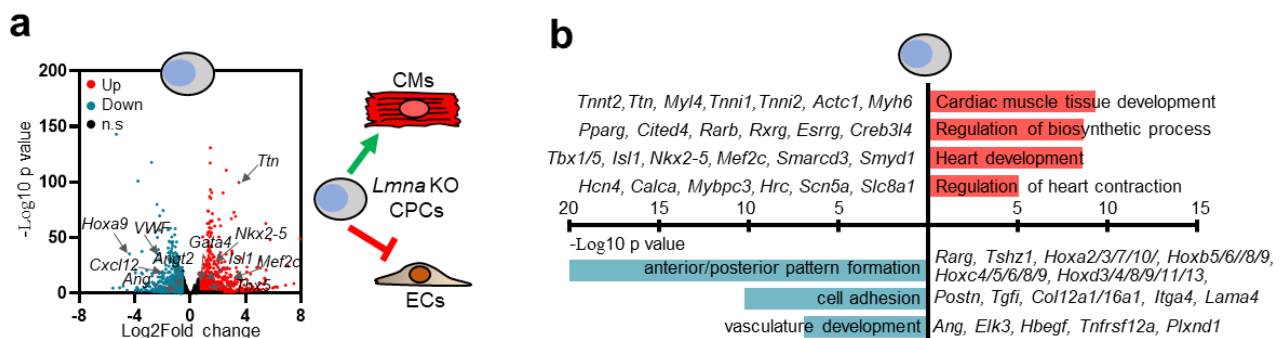


Figure 21. RNA-seq analysis of Nkx2-5 sorted *Lmna*^{-/-} cardiac progenitors. **a** Volcano plot showing the distribution of differentially expressed genes (DEG) between *Lmna*^{+/+} and *Lmna*^{-/-} FACS-sorted Nkx2-5+ CPs from d6 EBs. n = 3 biologically independent samples; log₂ fold change ≤ -0.58, ≥ 0.58; p-value < 0.05. P-value was calculated by DESeq2. **b** Representative genes and enriched GO terms in upregulated (red) and downregulated (blue) genes are presented. Significance is presented as p-values from pathway analysis using DAVID Bioinformatics Resources 6.8.

3.1.7 RNA-seq analysis of *Lmna*^{-/-} embryonic bodies at day10

To further study the function of lamin A/C on CMs and ECs cell fate choices, I collected day10 EBs which contain all embryonic cell types and performed RNA-seq. Similarly, RNA-Seq analysis of d10 EBs revealed that genes involved in heart contraction and calcium ion transport showed elevated expression (Fig. 22a and 22b), further confirming the results obtained from the transcriptome analysis of sorted cardiac progenitors. In addition, we observed upregulated genes involved in carbohydrate metabolic process such as *Pdk4*, *Hk1*, *Pfkf* and *Pgm2*. Lipid transport related apolipoproteins and transcription factors *Ppar-γ* and *Ppar-δ* were also upregulated. In contrast, large numbers of *Hox* family genes involved in anterior/posterior patterning and *Wnt* signaling related genes which are crucial for cell fate commitment during development were decreased. Similar to cardiac progenitors, genes involved in vascular development such as *Kdr*, *Nrp1*, and *Angptl4* were decreased as well (Fig. 22b). Moreover, I also observed an increased apoptotic process and decreased meiotic cell cycle process in day10 EBs (Fig. 22b).

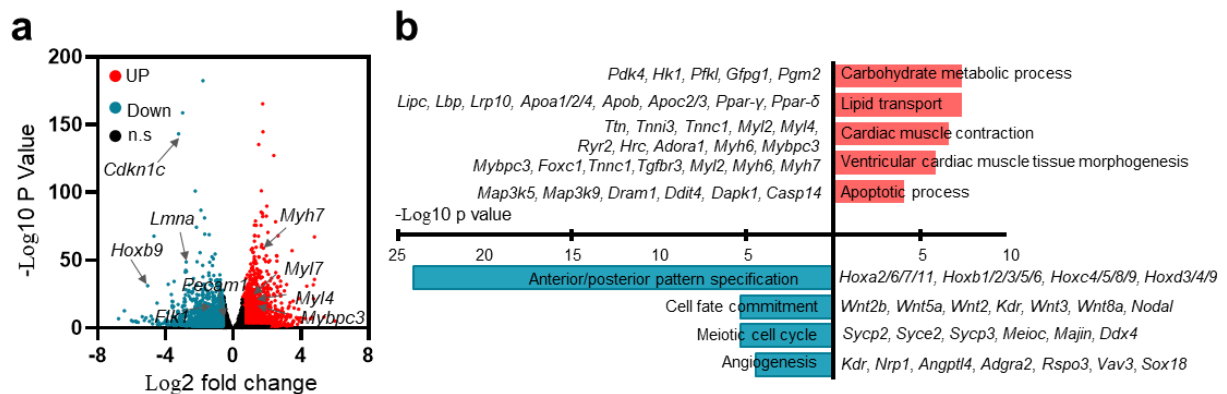


Figure 22. RNA-seq analysis of d10 EBs. **a** Volcano plot showing the distribution of differentially expressed genes (DEG) in *Lmna*^{+/+} and *Lmna*^{-/-} d10 EBs. n = 3 biologically independent samples; log₂ fold change ≤ -0.58, ≥ 0.58; p-value < 0.05. P-value was calculated by DESeq2. **b** Representative genes and enriched GO terms in up-regulated (red) and downregulated (blue) genes are presented. Significance is presented as p-values from pathway analysis using DAVID Bioinformatics Resources 6.8.

3.1.8 RNA-seq analysis of Nkx2-5 sorted *Lmna*^{-/-} cardiomyocytes

To study whether the increased expression of cardiac structural and contraction genes is simply due to the increased number of CMs or if *Lmna*^{-/-} CMs express these genes in higher level compared to control cells, I performed RNA-Sequencing of sorted Nkx2-5⁺ CMs. GO analysis revealed that upregulated genes in CMs were similarly enriched in GO terms linked to cardiac muscle contraction, regulation of heart rate as well as calcium ion transport, while downregulated genes were linked to nervous system development, anterior/posterior patterning and cell cycle (Fig. 23a and 23b).

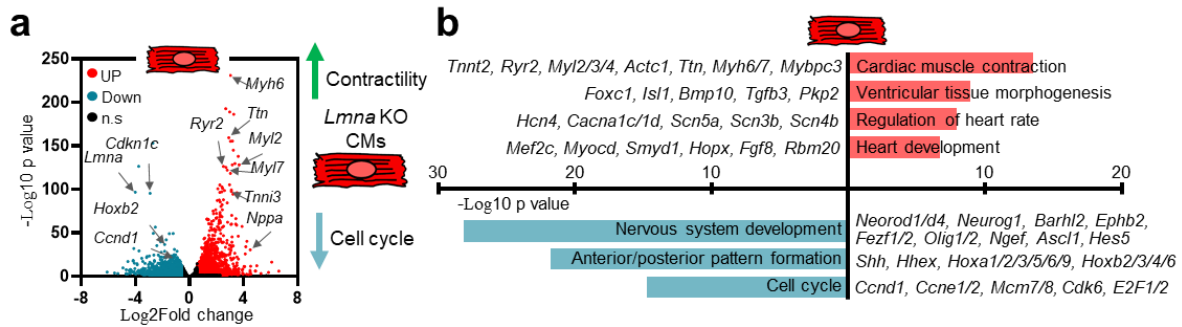


Figure 23. RNA-seq analysis of Nkx2.5 sorted *Lmna*^{-/-} CMs. **a** Volcano plot showing the distribution of differentially expressed genes (DEG) between *Lmna*^{+/+} and *Lmna*^{-/-} FACS-sorted Nkx2-5+ CMs from d10 EBs. *n* = 3 biologically independent samples; log₂ fold change ≤ -0.58, ≥ 0.58; *p*-value < 0.05. *P*-value was calculated by DESeq2. **b** Representative genes and enriched GO terms in upregulated (red) and downregulated (blue) genes are presented. Significance is presented as *p*-values from pathway analysis using DAVID Bioinformatics Resources 6.8.

3.1.9 Impact of lamin B1 on CMs differentiation

To determine whether lamin B1 plays a similar role as lamin A/C in cardiac differentiation, I generated lamin B1 knockout mESC cell line by deleting from exon 2 to exon 5 of the *Lmnb1* genome with CRISPR/Cas9 (Fig. 24a). After initial prescreening, 3 independent clones were used further for the study. Western blot analysis confirmed a complete loss of lamin B1 protein level in mESC (Fig. 24b). Similarly, I differentiated *Lmnb1*^{-/-} mESCs into cardiomyocytes by using hanging drop method and collected EBs from different stages for RNA isolation. Quantitative PCR (qPCR) analysis of early cardiac mesoderm markers, cardiac progenitors and CMs markers showed that ablation of lamin B1 in mESCs did not largely affect cardiomyocyte differentiation (Fig. 24c-24e), suggesting that lamin A/C rather than lamin B1 plays a key role in cardiac lineage restriction.

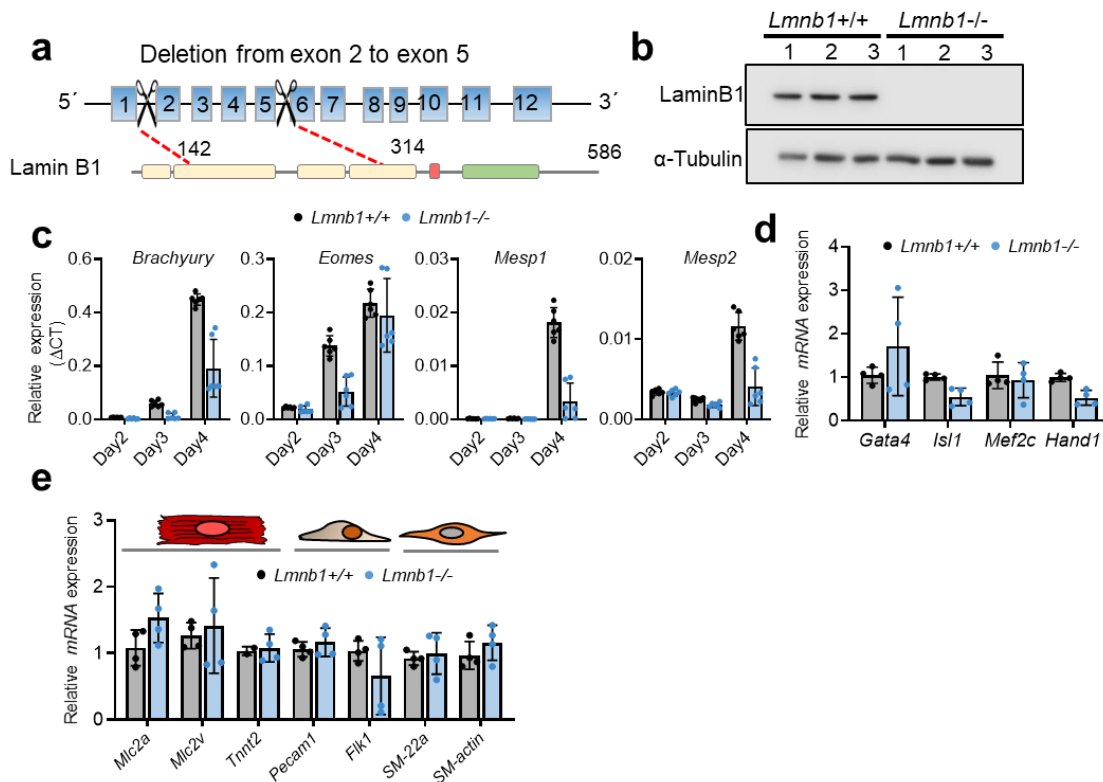


Figure 24. Impact of lamin B1 on cardiomyocyte differentiation. **a** Schematic representation of the strategy used to generate *Lmnb1*^{-/-} ESCs using CRISPR/Cas9 gene editing. **b** Western blot analysis of lamin B1 in control and *Lmnb1*^{-/-} ESC. **c** Relative mRNA expression of mesodermal markers in EBs at different days (n=6). **d** Relative mRNA expression of cardiac progenitor marker genes in d6 EBs (n=4). **e** Relative mRNA expression of CM (*Mlc2a*, *Mlc2v* and *Tnni2*), EC (*Flk1* and *Pecam1*), and smooth muscle (*SM-22a*, *SM-actin*) genes in d10 EBs (n=4). **a-e**: Data are represented as mean \pm SD, unpaired two-tailed Student's t-test (top panel) were used. P-values are as follows: ***p < 0.001, **p < 0.01, *p < 0.05. Source data are provided as a Source Data file.

3.2 Lamin A/C loss induces 3D chromatin reorganization in mESCs

3.2.1 Lamin A/C expresses in mESCs and CMs

Since I detected major changes in gene expression in *Lmna*^{-/-} versus *Lmna*^{+/+} cardiac precursors, which have very low lamin A/C levels, I analyzed lamin A/C levels in more detail. Lamin A/C was expressed in mESC cells (Kim, Zheng et al. 2013), absent after exit of pluripotency and during early differentiation, and showed high levels in cardiomyocytes (Fig. 25a). To further confirm the expression of lamin A/C in mESC, I performed immunofluorescence by using two different antibodies of lamin A/C. Consistent with lamin A/C expression in mESCs, I observed dramatic changes in nuclear structure in mESCs lacking lamin A/C. *Lmna*^{-/-} nuclei were bigger, showed irregular shape and enlarged nucleoli (Fig. 25b and 25c). In addition to irregular nuclear shape, lamin A/C-deficient mESCs formed flatter and more irregular colonies with varying levels of the pluripotency marker Oct4, in comparison to the compact and round control and lamin B1-deficient mESCs colonies which highly expressed Oct4 (Fig. 25d and 25e).

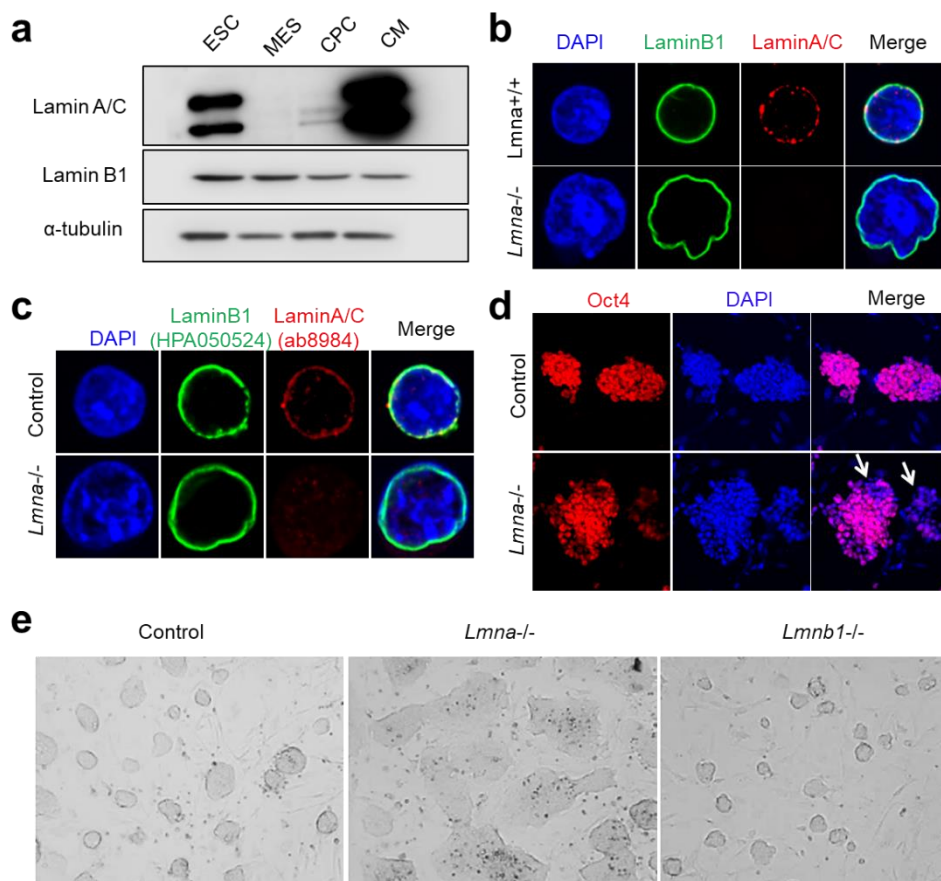


Figure 25. LaminA/C expression in mESC and CMs. **a** Western blot analysis of lamin A/C and lamin B1 during directed CM differentiation. **b-c** Confocal images of immunostaining for lamin A/C (red), lamin B1 (green) and nucleus (DAPI, blue) of *Lmna*^{+/+} and *Lmna*^{-/-} mESCs by two different antibodies. Scale bars, 4 μ m. **c** Confocal images of immunostaining for Oct4 (red) and nucleus (DAPI, blue) in *Lmna*^{+/+} and *Lmna*^{-/-} ESCs. Scale bars, 20 μ m. **d** Phase contrast images showing colony morphology of control, *Lmna*^{-/-} and *Lmnb*^{-/-} ESC colonies. Scale bars, 120 μ m.

3.2.2 Chromosome 14 decompaction in *Lmna*^{-/-} by Hi-C analysis

Since I observed major nuclear enlargement in *Lmna*^{-/-} mESCs, I next studied the effect of lamin A/C loss on the three-dimensional (3D) chromatin organization of mESCs using Hi-C. Hi-C data analysis was performed with the help of Adel Elsherbiny. Interestingly, the Hi-C contact matrices of Chr. 14 were markedly different (Fig. 26a, 26c), whereas I did not observe major changes in other chromosomes (Fig. 26d). To further confirm this observation, I next performed Chr.14 painting by using a fluorescence labeled probe for Chr. 14. FISH analysis showed a significantly enlarged Chr. 14 territory, supporting the Hi-C analysis and pointing to an important role of lamin A/C in Chr. 14 compaction (Fig. 26b).

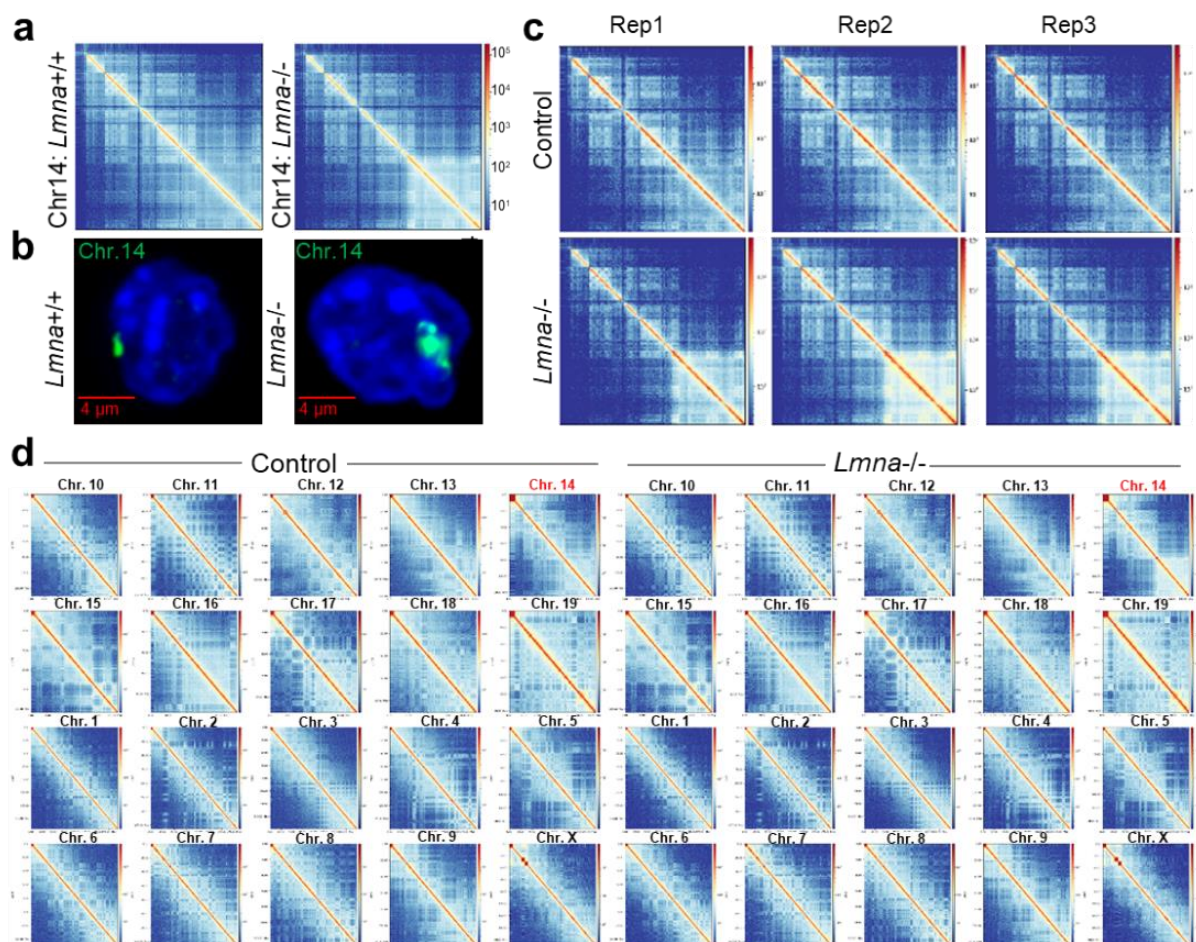


Figure 26. Hi-C analysis of the three-dimensional (3D) chromatin organization of *Lmna*^{-/-} mESCs. **a** Representative log transformed contact matrices of Chr. 14 at 100 kb resolution in *Lmna*^{+/+} (n=3) and *Lmna*^{-/-} mESCs (n=3). **b** FISH chromosome painting of Chr. 14 (green) in control and *Lmna*^{-/-} mESCs. **c** Log-transformed contact matrices of Chr. 14 at 100 kb resolution in *Lmna*^{+/+} and *Lmna*^{-/-} biological triplicates. **d** Log transformed contact matrices of all chromosomes at 100 kb resolution in *Lmna*^{+/+} and *Lmna*^{-/-} ESCs.

3.2.3 Loss of *Lmna* leads to B/A compartments transitions

More detailed analysis revealed a decrease in trans-interactions (involving different chromosomes) and an increase of long distance cis-interactions in *Lmna*^{-/-} mESCs (Fig. 27a). Previous studies demonstrated that the genome is organized into relatively active and inactive regions, referred to as A and B compartments, respectively (Lieberman-Aiden, van Berkum et al. 2009). Interestingly, around 8% of the chromatin compartments switched from A to B and vice versa as a result of lamin A/C depletion (Fig. 27b). GO analysis of genes located in inactive B compartments that transitioned to active A compartments in *Lmna*^{-/-} mESCs were enriched for GO terms linked to calcium ion transmembrane transport, chromatin organization, muscle cell differentiation and relaxation of cardiac muscle, including genes such as *Myl4*, *Atp2a3*, *Ryr2*, *Camk2d*, etc. (Fig. 27c). Active chromatin compartments that transitioned to an inactive state were enriched for genes linked to protein phosphorylation, nervous system development, cell migration and adhesion (Fig. 27d). Chr. 14 showed the most changes with around 13% active to inactive or vice versa transitions, consistent with the large-scale chromatin decompaction at this chromosome (Fig. 27e).

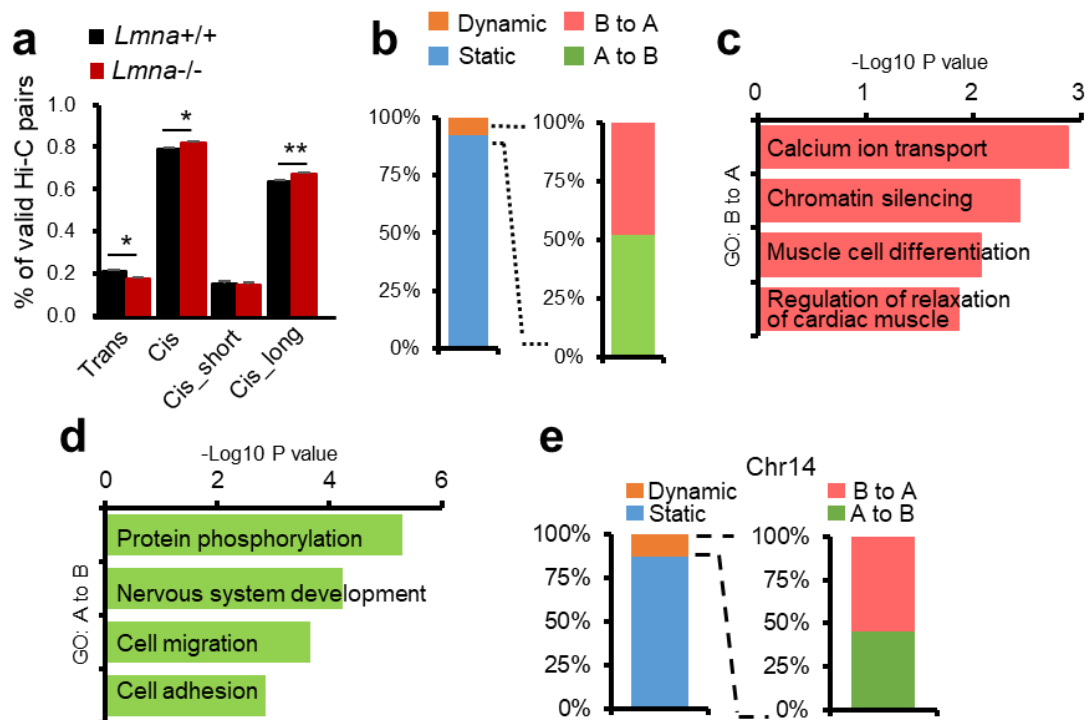


Figure 27. Loss of *Lmna* leads to an inactive B and active A compartments transitions. **a** Percentage of trans or cis interactions as well as cis interactions with distances less than 20 kb (cis_short) and distances more than 20 kb (cis_long). **b** Genomic regions divided into static, i.e. without compartment transitions (blue) and dynamic – with A/B compartment transitions (orange, left graph). Dynamic regions are subdivided into A to B (green) and B to A (pink) transitions (right graph). **c-d** GO analysis of genes showing B to A and A to B transitions. **e** Static (blue) and dynamic (orange) compartments at Chr. 14. Regions with A/B compartment switch are subdivided into A to B (green) and B to A (pink) transitions.

3.2.4 A-B compartments transition correlates with lamin A/C LADs

Using lamin A/C-DamID and lamin B1-DamID data from murine mESC (Peric-Hupkes, Meuleman et al. 2010, Amendola and van Steensel 2015), which map chromatin domains associated with lamin A/C and lamin B1, also referred to as lamin A/C LADs and lamin B1 LADs, I found a strong overlap of lamin A/C LADs as well as common lamin A/C and B1 LADs with the compartments changes observed in *Lmna*^{-/-} mESCs (Fig. 28a, 28b). Intersection of the genes found within lamin A/C-DamID and lamin B1-DamID data, revealed that 92% of the genes found in lamin B1 LADs were in lamin A/C LADs, whereas 6524 genes were uniquely found in lamin A/C LADs (Fig. 28c). Within genes localized specifically in lamin A/C LADs were key cardiac TFs, such as *Gata4/6*, *Isl1* as well as cardiac structural proteins, such as *Actc1*, *Myh4*, *Myh7*, etc, whereas *Ryr2*, *Mef2c*, *Hcn1*, *Calca*, *Camk2d*, etc. were found in close proximity to both lamin A/C and B1 LADs.

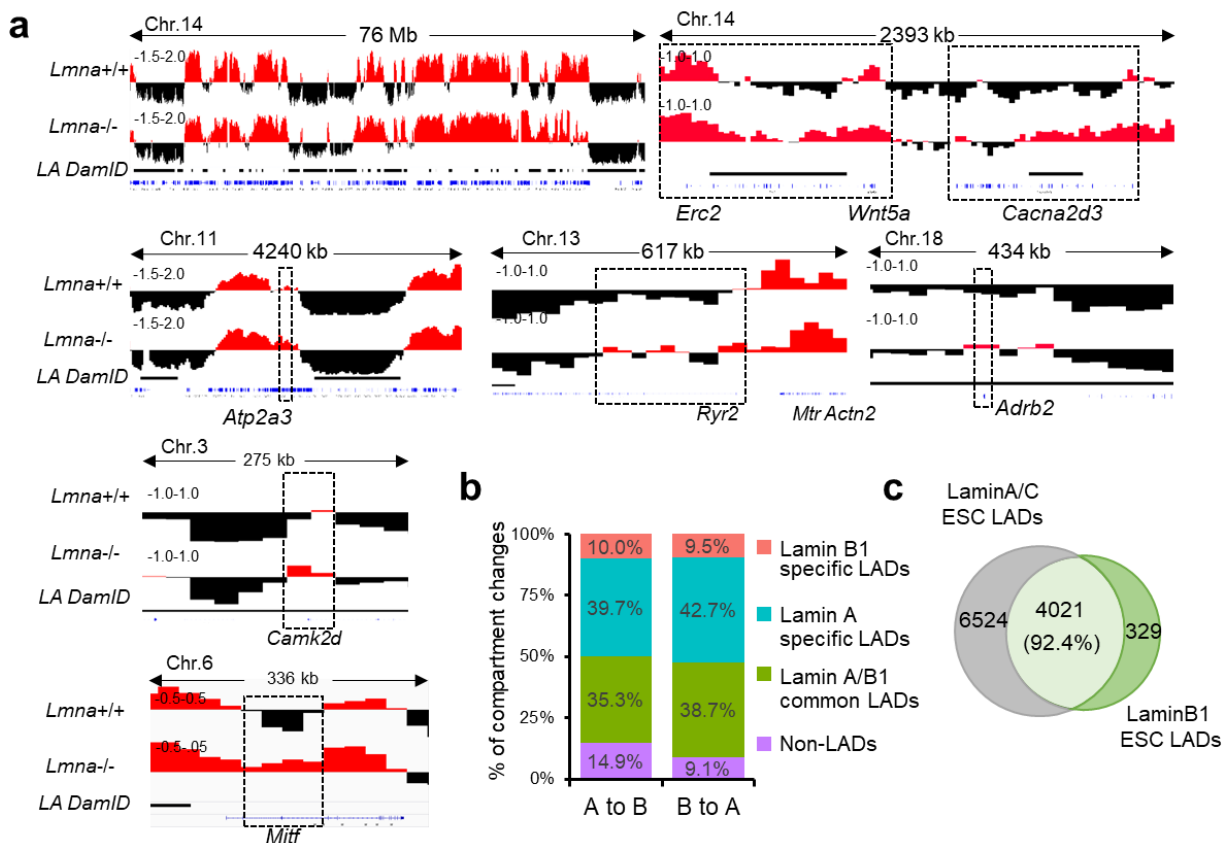


Figure 28. A-B compartments transition correlates with lamin A/C LADs. **a** Genome tracks of Hi-C PC1 at 25 kb resolution and lamin A/C DamID regions at cardiac genes upregulated in *Lmna*^{-/-} mESCs showing A (red) and B (black) compartments in *Lmna*^{+/+} and *Lmna*^{-/-} mESC. Lamin A/C DamID regions are presented as black boxes below the tracks. **b** Percentage of compartment changes showing overlap with lamin A/C specific LADs, lamin B1 specific LADs and lamin A/C/lamin B1 common LADs as well as non-LADs. **c** Overlap of genes within lamin A/C and lamin B1 LADs.

3.2.5 Dissociation of cardiac-specific genes from the repressive nuclear periphery already in *Lmna*^{-/-} mESCs

Nuclear lamins tether chromatin at the nuclear periphery, which is characterized by low transcriptional activity. To analyze whether lamin A/C loss leads to dissociation of cardiac-specific genes from the repressive nuclear periphery already in mESCs, I performed 3D FISH with probes for *Gata4*, *Mef2c*, *Actc1*, *Ttn* and *Kcnq1*. Interestingly, I observed a shift of CM-specific genes from the nuclear periphery to the active nuclear interior for genes found specifically in lamin A LADs as well as for genes found in lamin A/B1 LADs, whereas *Kcnq1*, which is not found in LADs, was not affected (Fig. 29a). Quantification of the percentage of cells showing zero (grey), one (orange) or two (blue) alleles at the nuclear periphery for the indicated genes revealed more than 60% of the cells with a shift of cardiac locus from the nuclear periphery to the active nuclear interior (Fig. 29b). And the distance of *Gata4*, *Mef2c*, *Actc1*, *Ttn* locus to nuclear periphery in individual nuclei of *Lmna*^{-/-} mESCs was increased compared with *Lmna*^{+/+} suggesting a role of lamin A/C in tethering cardiac genes to the repressive nuclear periphery in mESCs (Fig. 29c).

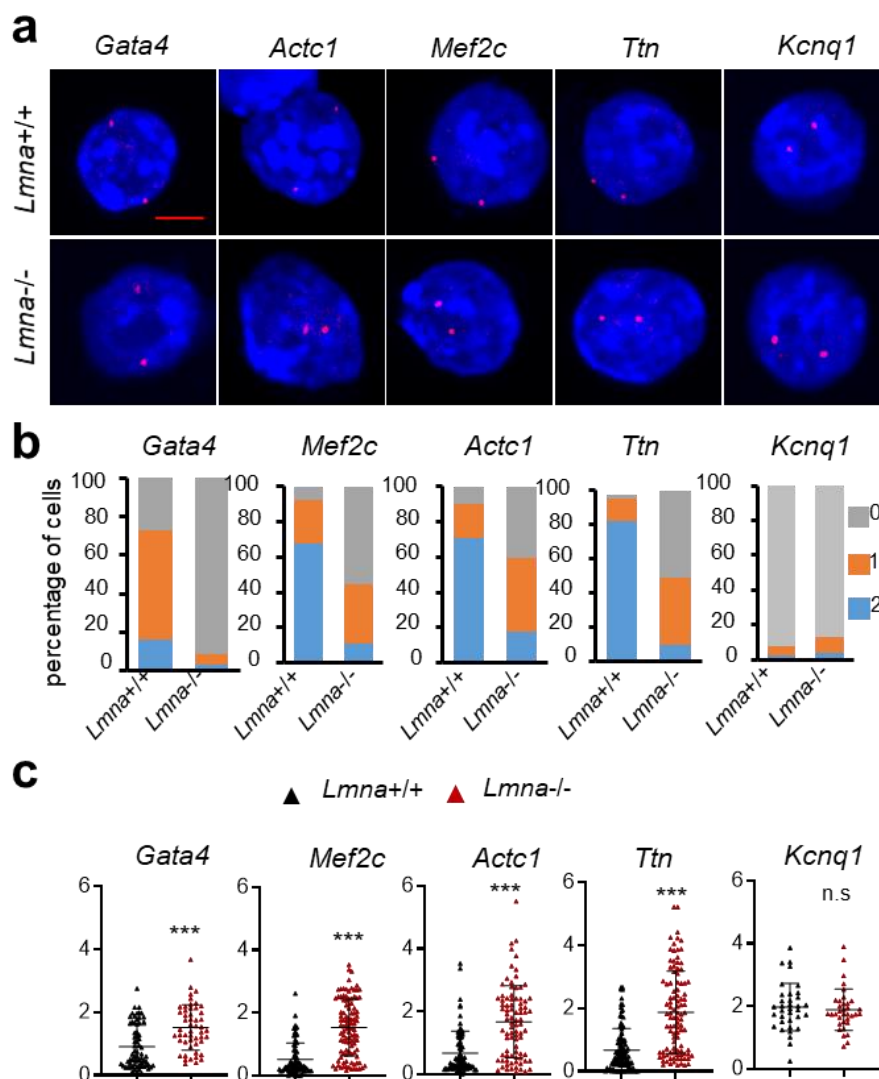


Figure 29. Loss of *Lmna* leads to a dissociation of cardiac-specific genes from the repressive nuclear periphery to nuclear interior. **a** Representative DNA FISH images of cardiac-specific genes within LADs showing re-localization from the nuclear periphery to the nuclear interior in *Lmna*^{+/+} or *Lmna*^{-/-} mESCs. *Kcnq1*, a gene not found in LADs, did not show any change in localization. **b** Quantification of the percentage of cells showing zero (grey), one (orange) or two (blue) alleles at the nuclear periphery for the indicated genes. **c** Quantification of the distance of *Gata4*, *Mef2c*, *Actc1*, *Ttn* and *Kcnq1* to nuclear periphery in individual nuclei of *Lmna*^{+/+} and *Lmna*^{-/-} mESCs. Data are represented as mean \pm SD, n=30-50, unpaired two-tailed Student's t-test was used.

3.3 Lamin A/C deficiency in ESCs primes cardiac specific gene expression

3.3.1 Ectopic cardiac gene activation in *Lmna*^{-/-} mESC

Since I observed large scale of chromatin changes in *Lmna* depleted mESC, I next performed RNA-seq of *Lmna*^{+/+} and *Lmna*^{-/-} mESCs (n=3). Further transcriptome analysis revealed a significant upregulation of genes associated with the nuclear lamina and encoding for major TFs and signaling molecules involved in stem cell differentiation, consistent with the primed state of *Lmna*^{-/-} mESCs (Fig. 30a-30c). Intriguingly, heart contractile proteins and Ca²⁺ transporters such as *Myl4*, *Myl7*, *Calca*, *Atp2a3* ect. were also already transcriptionally upregulated in mESCs upon lamin A/C loss, consistent with the chromatin organization changes observed at these genes. To further confirm the protein levels of the upregulated genes in mESCs, I performed the immunofluorescence. In line with the transcriptional up-regulation of cardiac structural components such as *Myl4* and core cardiac TFs such as *Gata4*, I observed greatly increased MYL4 and GATA4 protein expression in lamin A/C-deficient mESCs further supporting a role a lamin A/C in gene expression in mESCs. (Fig. 30c).

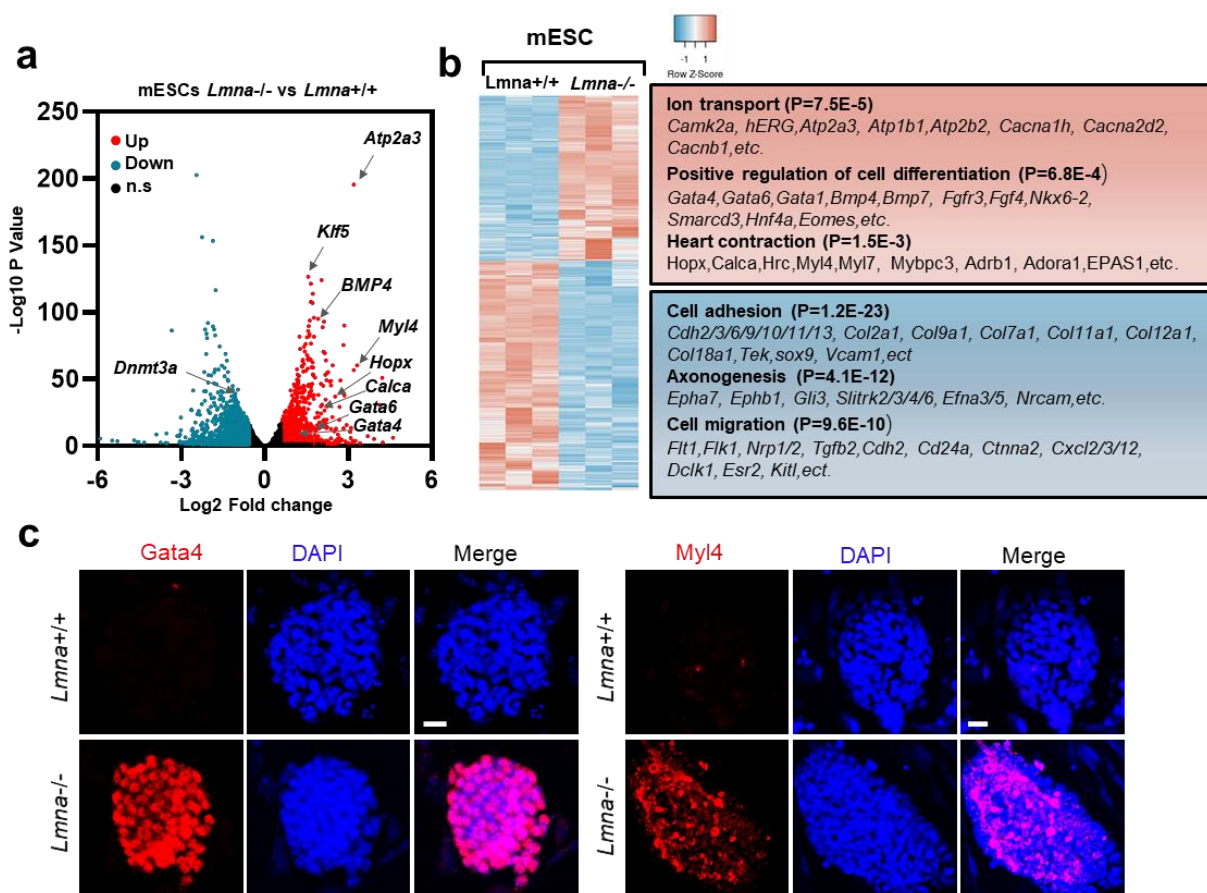


Figure 30. Ectopic cardiac gene activation in *Lmna*^{-/-} mESC. **a** Volcano plot showing the distribution of differentially expressed genes between *Lmna*^{+/+} and *Lmna*^{-/-} mESCs (n=3; log₂ fold change ≤ -0.58, ≥0.58; p-value < 0.05). Representative genes in upregulated (red) and downregulated (blue) genes are indicated. **b** Heat-map representation of RNA-Seq analysis of control and *Lmna*^{-/-} mESCs. Representative genes and enriched GO terms in upregulated (red) and downregulated (blue) genes are presented. **c** Confocal images of immunostaining for *Gata4* (red), *Myl4* (red), and nucleus (DAPI, blue) of *Lmna*^{+/+} and *Lmna*^{-/-} mESCs. Scale bars, 20 μm.

3.3.2 Activation of primed cardiac gene in subsequent differentiation steps

Intersection of the genes found upregulated in *Lmna*^{-/-} mESC with lamin A-DamID and lamin B1-DamID data, revealed that 28.8% of the up-regulated genes found in *Lmna*^{-/-} mESC were within lamin A LADs, whereas only 5.1% of the up-regulated genes were uniquely found in lamin B1 LADs (Fig. 31a). Within genes localized specifically in lamin A LADs were key cardiac TFs, such as *Gata4/6*, *Isl1* as well as cardiac structural proteins, such as *Actc1*, *Myl4*, *Myhk*, etc, whereas *Ryr2*, *Mef2c*, *Hcn1*, *Calca*, *Camk2d*, etc. were found in close proximity to both lamin A and B1 LADs (Fig. 31a). Cluster analysis revealed that a large set of genes associated with lamin A LADs in mESCs were either upregulated in all stages of cardiac differentiation (Fig. 31b, 31c, cluster A) or specifically in mESCs, CPs or CMs (Fig. 31b,31c, clusters B to G). These genes were linked to stem cell differentiation, heart development, calcium ion transport, as well as Wnt signaling (Fig. 31b, 31c). Interestingly, I found a high overlap of genes associated to lamin A LADs in mESCs and genes that are upregulated in *Lmna*^{-/-} CPs and CMs linked to heart morphogenesis and stem cell differentiation (Fig. 31b, 31c), suggesting that lamin A/C deficiency and LADs reorganization in mESCs prime cardiac specific genes for expression in later stages during development.

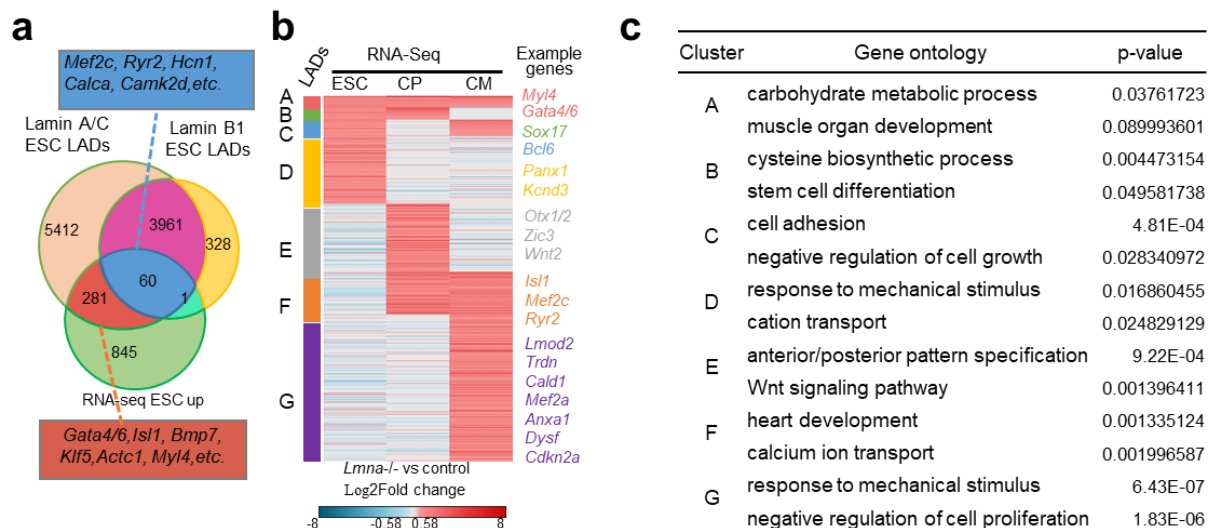


Figure 31. Activation of primed cardiac genes in subsequent differentiation steps. **a** Overlap of genes within lamin A/C LADs, lamin B1 LADs and genes upregulated in *Lmna*^{-/-} mESCs. Representative genes are indicated in the boxes on the side in colors corresponding to the respective overlaps. **b** Hierarchical cluster analysis of genes within lamin A/C LADs and upregulated either in *Lmna*^{-/-} mESCs, *Lmna*^{-/-} CPs or *Lmna*^{-/-} CMs. **c** Representative GO terms in the different clusters presented in Fig. 3b.

3.3.3 Increased chromatin accessibility in *Lmna*^{-/-} mESCs

Since I observed 3D chromatin organization changes upon *Lmna* loss, I next analyzed chromatin accessibility in wild-type and *Lmna*^{-/-} ESCs using ATAC-Seq. ATAC-seq and data analysis were performed with the help of Linda Kessler. I observed a widespread increase in chromatin accessibility across the genome, as well as at genes upregulated upon lamin A/C LOF such as *Hopx*, *Gata4*, *Atp2a3*, *Bmp4* ect. (Fig.27a-c). In contrast, there was little change in chromatin accessibility for genes that were downregulated in *Lmna*^{-/-} ESCs (Fig. 27b, right panel). Consistent with the wide-spread chromosome 14 (Chr. 14) decompaction, I observed substantial accumulation of ATAC sequence peaks in Chr. 14 (Fig. 27a), where *Gata4*, *Bmp4*, *Wnt5a*, *Myh6* and *Myh7* are located. The increased chromatin accessibility was accompanied by an upregulation of a large number of genes within this chromosome region not only in *Lmna*^{-/-} ESCs, but also in *Lmna*^{-/-} CPs and *Lmna*^{-/-} CMs (Fig. 27a).

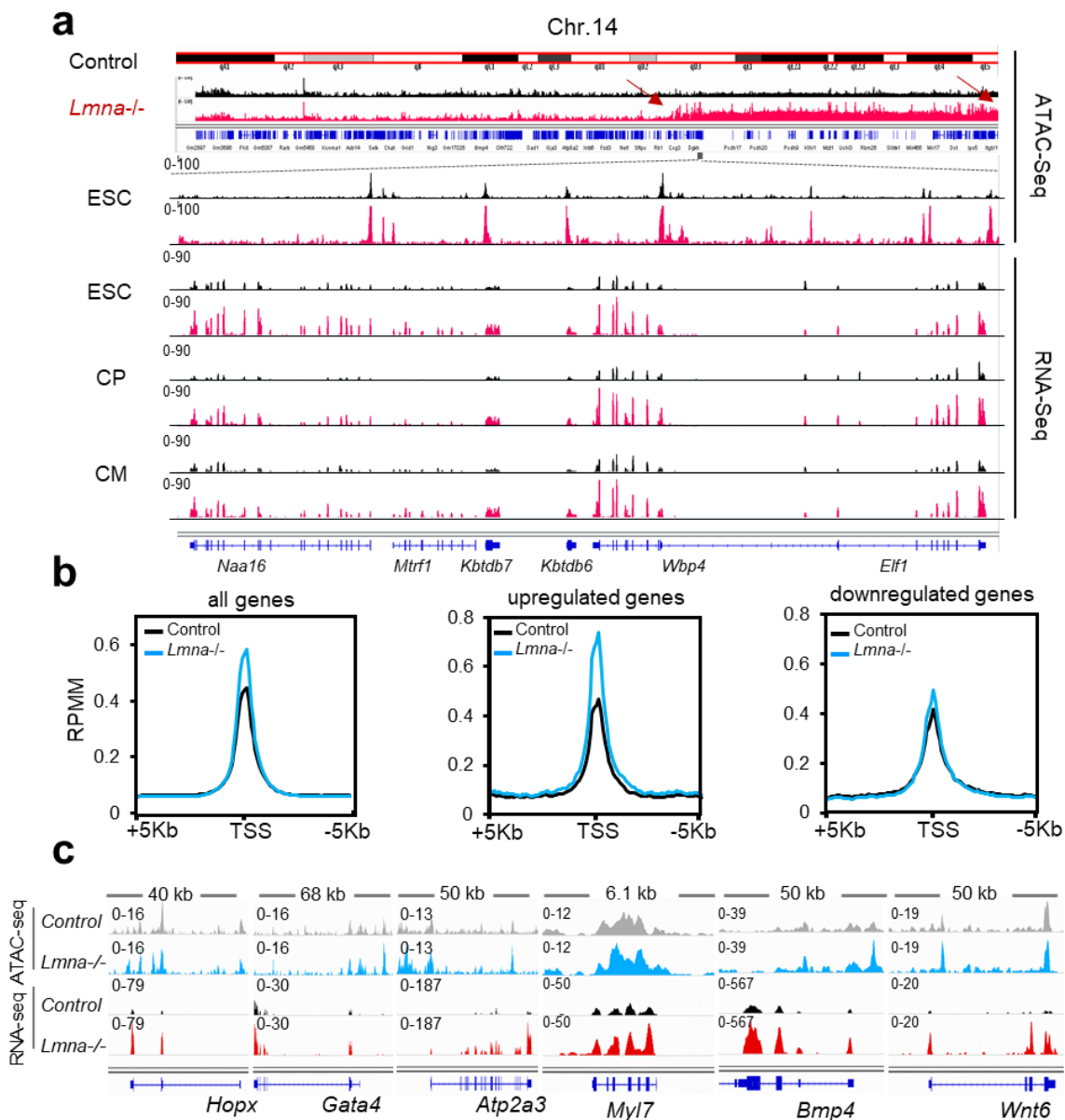


Figure 32. Increased chromatin accessibility in *Lmna*^{-/-} mESCs. **a** Genome tracks of ATAC-Seq reads in *Lmna*^{+/+} and *Lmna*^{-/-} ESCs and normalized RNA-Seq reads in control (black) and *Lmna*^{-/-} (red) ESCs, CPs and CMs at Chr. 14. The ATAC-Seq tracks show large-scale chromatin opening at Chr. 14 in *Lmna*^{-/-} ESC (red arrows), and the resulting transcriptional upregulation of genes located within this region in ESC, CPs and CMs. **b** Normalized ATAC-Seq signal intensity at the TSS \pm 5 kb of all genes (left) as well as genes upregulated (middle) and downregulated (right) upon lamin A loss of function in *Lmna*^{+/+} and *Lmna*^{-/-} ESCs (n=3 for both *Lmna*^{+/+} and *Lmna*^{-/-} ESCs). **c** Examples of genes showing increased chromatin accessibility and upregulation in *Lmna*^{-/-} ESCs. Genome tracks of merged ATAC-Seq and RNA-Seq reads of *Lmna*^{+/+} and *Lmna*^{-/-} ESCs are presented. ATAC-seq and data analysis were performed with the help of Linda Kessler.

3.3.4 Loss of *Lmna* primes cardiac genes for later activation

Cluster analysis revealed that a large set of genes that showed increased chromatin accessibility in ESCs were either upregulated in all stages of cardiac differentiation (Fig. 33a, cluster A) or specifically in ESCs, CPs or CMs (Fig. 33a, clusters B-G). Intersection of the ATAC-Seq and RNA-Seq analysis revealed that more than half of the genes upregulated upon lamin A/C loss in ESCs showed increased chromatin accessibility (Fig. 33a) and GO analysis of the overlapping genes indicated overrepresentation of GO terms linked to transcription, cell differentiation, outflow tract morphogenesis as well as Wnt signaling (Fig. 33b). Motif enrichment analysis within chromatin regions of genes upregulated upon lamin A/C LOF and characterized with more open chromatin identified binding motifs for Klf, Sox and Tead family members as well as *Gata4* binding motifs (Fig. 33c).

Interestingly, intersection of ATAC-Seq in ESCs with the RNA-Seq analysis from CPs and CMs, revealed a high overlap of genes that undergo chromatin opening as a result of lamin A/C loss in ESCs and genes that are upregulated only later during differentiation, i.e. in *Lmna*^{-/-} CPs and CMs (Fig. 33a). GO analysis of genes showing open chromatin conformation already at the ESC stage and upregulation in CPs and CMs revealed overrepresentation of GO terms linked to heart morphogenesis and cell fate commitment (Fig. 33d), supporting the notion that lamin A/C deficiency in ESCs primes cardiac specific genes for expression in later stages during development. Motif enrichment analysis within chromatin regions of genes upregulated upon lamin A/C LOF in CPs and CMs showing increase in chromatin accessibility (epigenetic priming) already in ESCs, identified binding motifs for Tead and Gata family members as well as *Meis1*, which regulates postnatal CM cell cycle arrest (Mahmoud, Kocabas et al. 2013) and *Foxo1*, shown to be activated and to contribute to the pathogenesis of cardiac laminopathies (Auguste, Gurha et al. 2018) (Fig. 33e). Genes, which were downregulated upon lamin A/C deficiency and showed decreased chromatin accessibility were linked to cell adhesion, cell migration and angiogenesis (Fig. 33f, 33g).

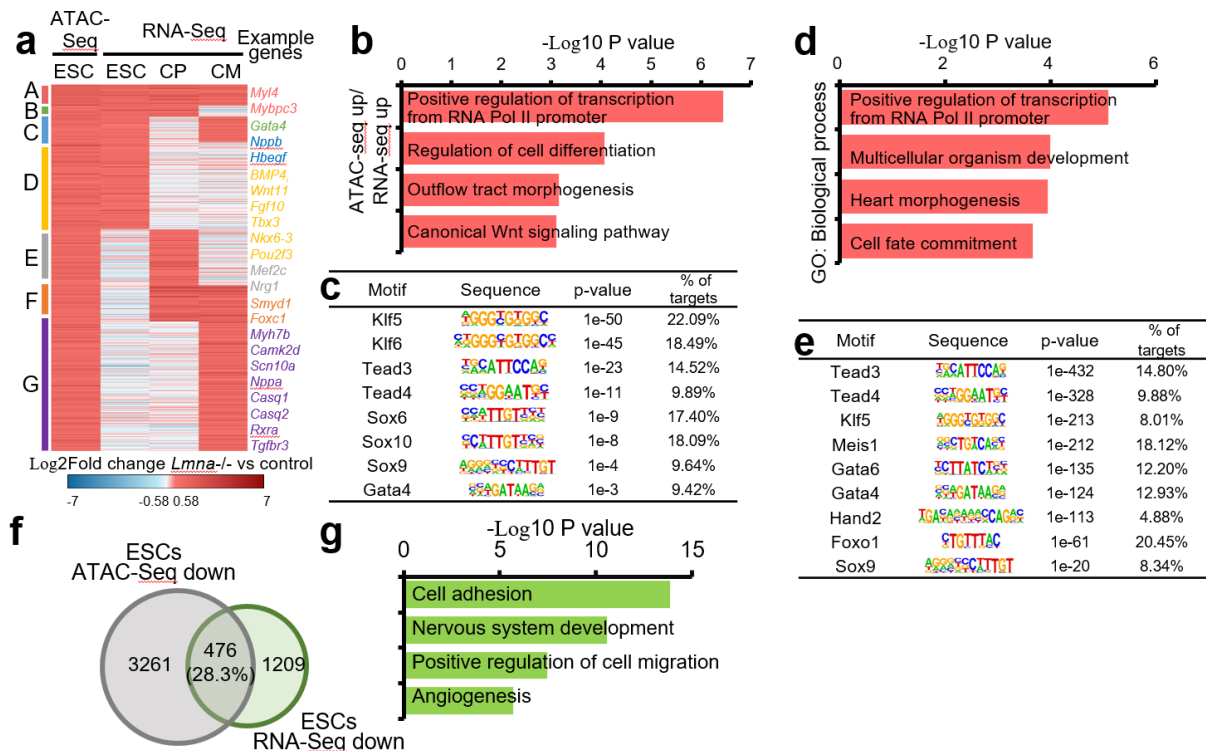


Figure 33. Loss of *Lmna* primes cardiac genes for later activation. **a** Hierarchical cluster analysis of genes showing increased chromatin accessibility in ESCs and upregulation either in *Lmna*^{-/-} ESCs, *Lmna*^{-/-} CPs or *Lmna*^{-/-} CMs. **b** GO analysis of the overlapped genes showing increased ATAC-Seq signal and upregulated upon lamin A loss of function in ESCs (Cluster A+B+C+D). Significance is presented as $-\text{Log}_{10}$ enrichment p values. **c** Enrichment of known TF motifs in ATAC-Seq peaks of genes showing increased chromatin accessibility and upregulation in *Lmna*^{-/-} ESCs. **d** GO analysis of the overlapped genes showing increased ATAC-Seq signal in *Lmna*^{-/-} ESC and significant upregulation in CPs and CMs (cluster A). **e** Consensus TF binding motifs in genes that are enriched in ATAC-Seq peaks in *Lmna*^{-/-} ESC and upregulated in both *Lmna*^{-/-} CPs and CMs. **f** Overlap of genes showing decreased ATAC-Seq signal and decreased expression in *Lmna*^{-/-} mESC. **g** GO terms of genes within the overlap shown in **f**. Significance is presented as $-\text{Log}_{10}$ enrichment p-values from pathway analysis using DAVID Bioinformatics Resources 6.8. Motif analysis analysis were performed with the help of Linda Kessler.

3.3.5 Lamin A rather than lamin C plays an important role in cardiac lineage restriction.

Recent studies suggest that lamin A and lamin C have distinct roles in LAD dynamics (Wong, Hoskins et al. 2021). To study which isoform is the cause for the observed phenotypes, I designed siRNA that specifically downregulate lamin A or lamin C. Western blot analysis of mESCs transfected with either control, lamin A or lamin C siRNA confirmed the specific and efficient downregulation of these isoforms (Fig. 34a). Importantly, only lamin A siRNA transfected cells showed dissociation of Ttn from nuclear periphery to nuclear interior (Fig. 34b, 34c). qPCR analysis on genes that were shown to be upregulated upon loss of lamin A/C revealed that depletion of lamin A but not lamin C resulted in upregulation of lamin A/C-target genes (Fig. 34d), suggesting the lamin A rather than lamin C plays an important role in cardiac lineage

restriction.

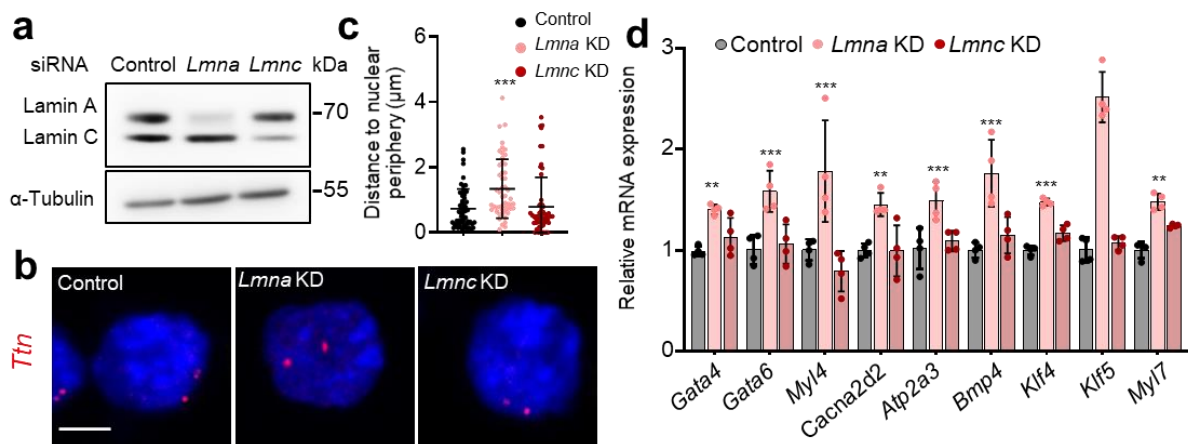


Figure 34. Lamin A rather than lamin C plays an important role in cardiac lineage restriction. **a** Western blot analysis of cells transfected with control siRNA, or siRNAs specifically targeting lamin A or lamin C. **b** Representative DNA FISH images of *Ttn* locus showing relocalization from the nuclear periphery into the nuclear interior upon lamin A but not upon lamin C depletion. Scale bars, 4 μ m. **c** Quantification of the distance of *Ttn* to nuclear periphery in individual nuclei of control, lamin A depleted or lamin C depleted mESCs (n=30-50). **d** Relative mRNA expression of genes upregulated upon lamin A/C loss of function in control, lamin A depleted or lamin C depleted mESCs (n=4). **c-d**: Data are represented as mean \pm SD; One-way ANOVA with Tukey correction comparisons was used; P-values are as follows: ***p < 0.001, **p < 0.01, *p < 0.05. Source data are provided as a Source Data file.

3.4 Cell-type specific role of lamin A/C in shaping chromatin accessibility

3.4.1 Increased chromatin accessibility in *Lmna*^{-/-} CMs

I next studied the specific role of lamin A/C on chromatin architecture in CMs. Consistent with my ESCs results, I observed an increase in chromatin accessibility at Chr. 14 as well as genes upregulated in *Lmna*^{-/-} CMs (Fig. 35a-35e), which belonged to GO terms related to heart morphogenesis, regulation of heart rate and contraction as well as calcium ion homeostasis, such as *Nkx2-5*, *Bmp10*, *Adrb1*, *Actc1*, *Ttn*, *Mybpc3*, *Myf7*, etc. (Fig. 35e). In contrast, genes which were downregulated upon lamin A/C-deficiency and showed decreased chromatin accessibility, were linked to cell differentiation and anterior/posterior patterning (Fig.35f-35g). Motif enrichment analysis within chromatin regions of genes upregulated upon lamin A/C LOF in CMs identified binding motifs for Mef2c, Isl1, Gata, Tead, Tbx family members and many other key cardiac TFs promoting CM differentiation as well as Meis1 and Foxo1 (Fig. 35d), consistent with the functional changes observed in lamin A/C-deficient CMs.

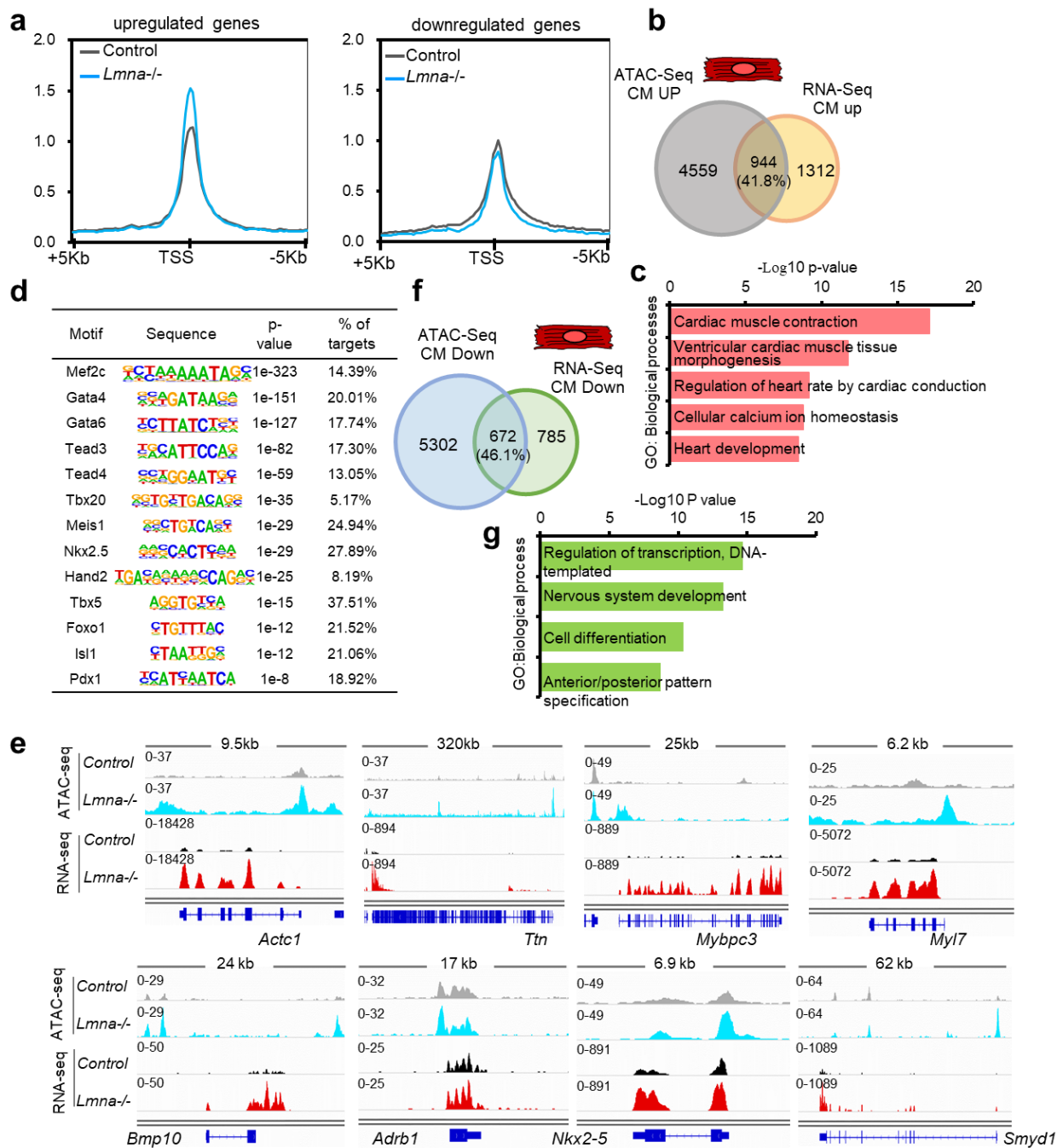


Figure 35. Increased chromatin accessibility in *Lmna*^{-/-} CMs. **a** Normalized ATAC-Seq signal intensity at TSS \pm 5 kb of upregulated (top) and downregulated (bottom) genes in *Lmna*^{+/+} (gray) and *Lmna*^{-/-} (blue) CMs. **b** Overlap of genes showing increased ATAC-Seq signal and upregulation in *Lmna*^{-/-} CMs. $n=3$; \log_2 fold change ≤ -0.58 , ≥ 0.58 ; p -value < 0.05 . **c** Representative GO terms within genes showing increased chromatin accessibility and expression in *Lmna*^{-/-} CMs. **d** Enrichment of known TF motifs in ATAC-Seq peaks of genes showing increased chromatin accessibility and upregulation in *Lmna*^{-/-} CMs. **e** Examples of genes showing increased chromatin accessibility and upregulation in *Lmna*^{-/-} CMs. Genome tracks of merged ATAC-Seq and RNA-Seq reads of *Lmna*^{+/+} and *Lmna*^{-/-} CMs are presented. **f** Overlap of genes showing decreased ATAC-Seq signal and decreased expression in *Lmna*^{-/-} CMs. **g** GO terms of genes within the overlap shown in **f**. Significance is presented as $-\log_{10}$ enrichment p -values from pathway analysis using DAVID Bioinformatics Resources 6.8. ATAC-seq and data analysis were performed with the help of Linda Kessler.

3.4.2 Up-regulated genes in *Lmna*^{-/-} CMs show a mESC and CM specific increased chromatin accessibility

I next compared the role of lamin A/C for chromatin organization in CMs to that in ESCs. Importantly, I found 55% overlap between genes that showed increased chromatin accessibility in both *Lmna*^{-/-} CMs and ESCs, whereas 45% showed more open chromatin only in CMs (Fig. 36a). Genes that showed increased chromatin accessibility only in *Lmna*^{-/-} ESCs but were upregulated in CMs belonged to GO terms linked to cell fate commitment, whereas 530 genes that showed chromatin opening in both *Lmna*^{-/-} ESCs and CMs were enriched in GO terms linked to cardiac muscle contraction and cellular calcium ion homeostasis (Fig. 36b, 36c). The 414 genes which showed specific chromatin opening upon lamin A/C loss only in CMs were enriched for GO terms associated with cardiac muscle contraction and sarcomere organization (Fig. 36b, 36c). Similarly, genes that showed decreased chromatin accessibility only in *Lmna*^{-/-} mESC and down regulated in CMs belonged to GO terms linked to cell cycle, chromosome segregation, whereas, genes showed decreased chromatin opening in both *Lmna*^{-/-} ESCs and CMs or only in CMs were enriched for GO terms associated with neuron development (Fig. 36d).

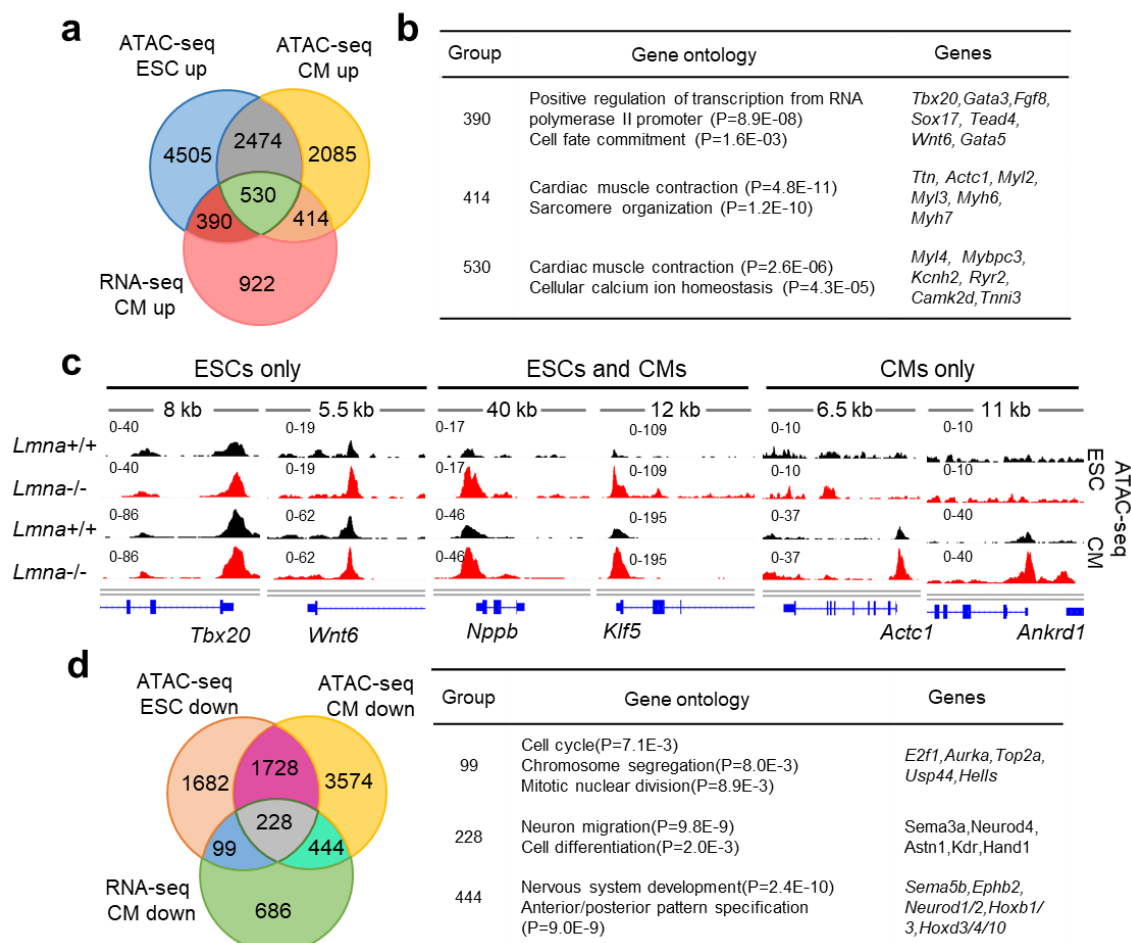


Figure 36. Up-regulated genes in *Lmna*^{-/-} CMs show a mESC and CMs specific in-cresed chromatin accessibility. **a** Overlap between genes upregulated in *Lmna*^{-/-} CMs and genes showing increased ATAC-Seq signal in

Lmna^{-/-} ESCs and CMs (left). **b** Enriched GO terms for the genes within the different overlaps are presented in a table in corresponding colors (right). **c** Examples of genes showing increased chromatin accessibility in *Lmna*^{-/-} ESCs and CMs as well as genes showing increased chromatin accessibility only in ESCs or CMs. Genome tracks of ATAC-Seq reads of *Lmna*^{+/+} and *Lmna*^{-/-} ESCs and CMs are presented. **d** Overlap between genes downregulated in *Lmna*^{-/-} CMs and genes showing decreased ATAC-Seq signal in *Lmna*^{-/-} ESCs and CMs (left). Enriched GO terms for the genes within the different overlaps are presented in a table in corresponding gene numbers (right).

3.4.3 LADs genes in *Lmna*^{-/-} mESCs show a mESC and CMs specific increased chromatin accessibility

I next studied the role of lamin A/C on genes within lamin A/C LADs in mESCs. Intersection of lamin A/C DamID data with ATAC-Seq data in ESCs and CMs revealed that genes within lamin A/C LADs that showed chromatin opening upon lamin A/C loss either in ESC stage or CM stage. Genes within lamin A/C LADs that showed chromatin opening specifically in ESCs were linked to cell aging and metabolism, whereas genes showing increased chromatin accessibility in both ESCs and CMs were linked to heart development and alternative cell fates (Fig. 37). Interestingly, among the genes showing specific chromatin opening in CMs were *Ttn* and *Actc1*, both found in lamin A/lamin B1 LADs which repositioned from the nuclear periphery to the nuclear interior in ESCs, suggesting that only gene repositioning from the nuclear lamina toward the interior is not sufficient to induce chromatin opening.

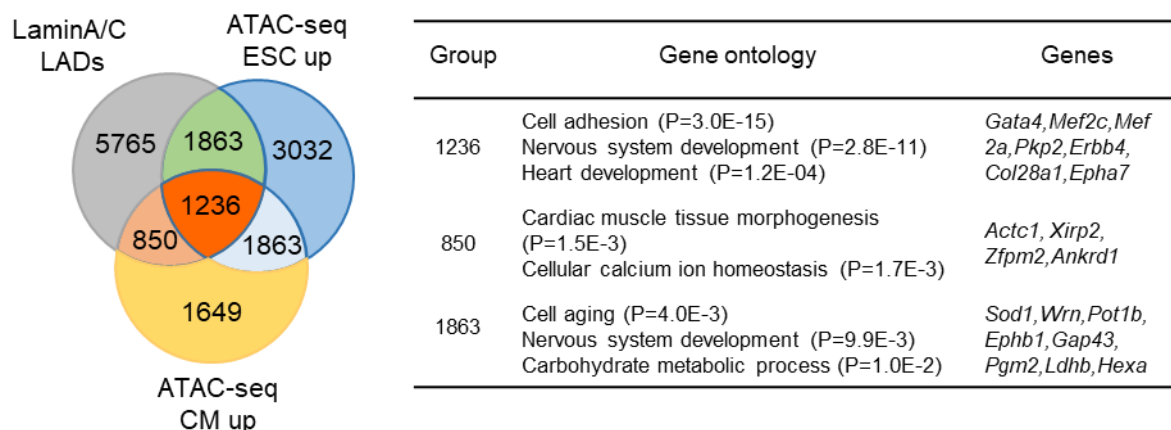


Figure 37. LADs genes in *Lmna*^{-/-} mESCs show a mESC and CMs specific increased chromatin accessibility. Overlap between genes within lamin A/C LADs and genes showing increased ATAC-Seq signal in *Lmna*^{-/-} ESCs and CMs (left). Enriched GO terms for the genes within the different overlaps are presented in a table in corresponding colors (right).

3.4.4 Lamin A/C rather than lamin B1 plays a dominant function of in cardiogenesis

I next compared the role of lamin A/C LADs with lamin B1 LADs on CM stage gene regulation upon lamin A/C loss. Intersection of lamin A/C DamID, lamin B1 DamID data in mESC with RNA-seq in CMs showed that 32% of the genes upregulated in CMs were within LADs, with 23% specifically within lamin A/C LADs and 8% within lamin A/C/B1 LADs, supporting a dominant function of lamin A/C in cardiogenesis (Fig. 38a). Further, I found that 26% of downregulated genes in *Lmna*^{-/-} CMs were in lamin A/C LADs whereas 14% in lamin A/C/B1 LADs in ESCs, supporting a direct role of lamin A/C in chromatin reorganization and transcriptional

activation particularly at genes related to cell cycle and anterior/posterior patterning (Fig. 38b). Taken together my data indicate that lamin A/C rather than lamin B1 plays a key role in transcriptional priming of genes involved in cardiac development, CM contraction and Ca²⁺ homeostasis in ESCs, whereas in CMs lamin A/C specifically regulates genes involved in cardiac contraction and sarcomere organization.

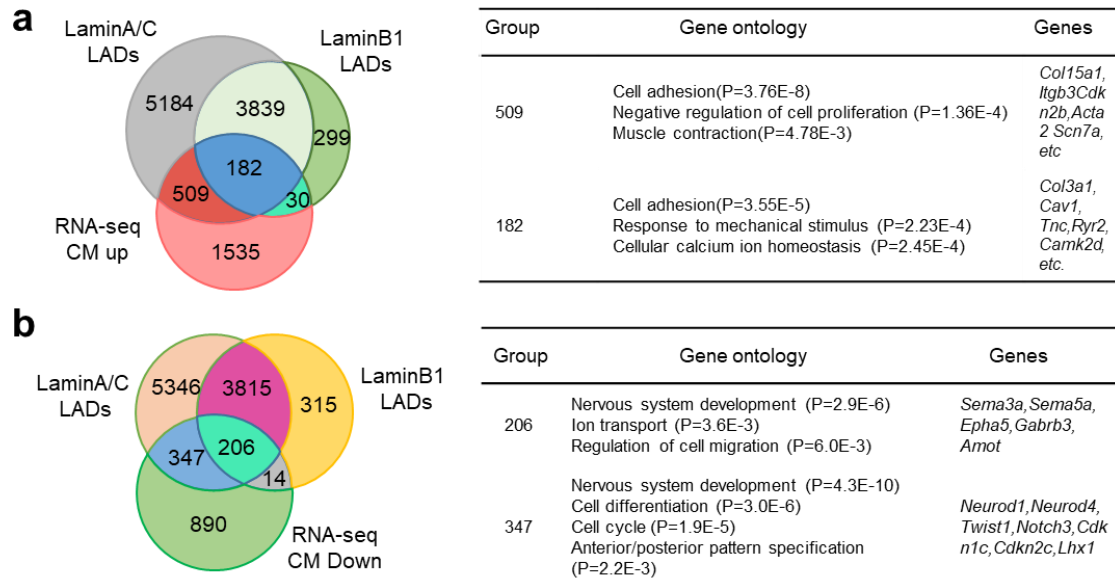


Figure 38. Lamin A/C rather than Lamin B1 plays a dominant function of in cardiogenesis. a-b Overlap between genes within lamin A/C and lamin B1 LADs and genes showing increased (a) and decreased (b) gene expression in *Lmna*^{-/-} CMs (left). Enriched GO terms for the genes within the different overlaps are presented in the table on the right. P-values are from pathway analysis using DAVID Bioinformatics Resources 6.8.

3.5 Lamin A/C is crucial for naïve pluripotency

3.5.1 Lamin A/C expression during mouse and human development

Since my results revealed an important function of lamin A/C in mESCs for cardiogenesis, I next studied lamin A/C expression in more detail. During mouse embryogenesis, *Lmna* mRNA levels were low in zygote and during cleavage, but were higher in the inner cell mass and mESCs and increased in CMs (Fig. 39a). Similarly, during human embryogenesis *LMNA* levels were higher in the inner cell mass and human-induced pluripotent stem cells (hiPSCs)-derived CMs (hiPSCs-CMs), however they were low in hiPSCs (Fig. 39b). To further confirm the expression of lamin A/C protein level in mouse mESCs and mESC-derived CMs as well as hiPSCs and hiPSCs-derived CMs, two different lamin A/C antibodies were used. Compared with mESC showing moderate lamin A/C protein expression, hiPSC showed undetectable lamin A/C protein levels. The committed mESC-CMs and hiPSC-CMs both showed high levels of lamin A/C protein expression (Fig. 39c).

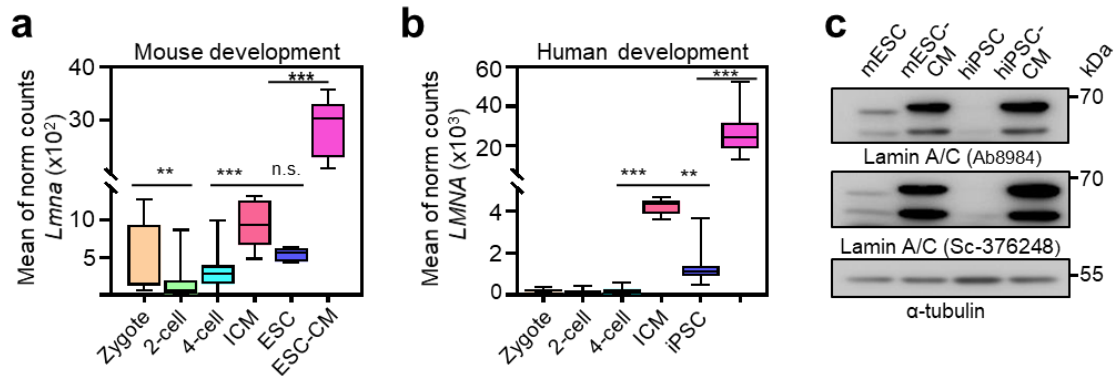


Figure 39. Lamin A/C expression during mouse and human development. **a** Boxplots showing the expression of *Lmna* in zygote, 2-, 4-cell stage, inner cell mass (ICM) ((Biase, Cao et al. 2014), GSE57249) as well as in mESCs and mESC-derived CMs (left panel). **b** Boxplots showing the expression of *LMNA* in human zygote, 2-, 4-cell stage, late blastocyst as well as in iPSC, and iPSC-derived CMs (Yan, Yang et al. 2013, Banovich, Li et al. 2018); GSE36552, GES101571 and GSE107654 (right panel). Values are mean of normalized counts. **c** Western blot analysis of lamin A/C in mouse mESCs and mESC-derived CMs as well as hiPSCs and hiPSCs-derived CMs using two different lamin A/C antibodies.

3.5.2 Lamin A/C is expressed in naïve mESCs and hiPSCs

Human iPSCs cultured in standard conditions represent a primed state (Shah, Lv et al. 2021), thus I next examined lamin A/C levels and function in naïve versus primed pluripotency. Interestingly, toggling of naïve mESCs to primed state by culturing naïve mESC in feeder free condition with DMEM/F12 medium supplemented with Activin A and bFGF leads to a complete loss of lamin A/C protein expression compared with naïve mESCs culturing in feeder condition with DMEM supplemented with 15% FCS and Lif (Fig. 40a), similarly to human iPSCs cultured in standard conditions. To further confirm lamin A/C is expressed in naïve state while absent in primed state, I converted primed hiPSC into naïve state by culturing primed hiPSC in 4i medium. Following an initial wave of widespread cell death, compacted and dome-shaped naïve colonies appeared about 6 to 8 days and were OCT4 positive (Fig. 40b, 40c). Immunofluorescence of lamin A/C showed that lamin A/C was highly expressed in naïve hiPSC suggesting a role of lamin A/C in naïve pluripotency (Fig. 40d).

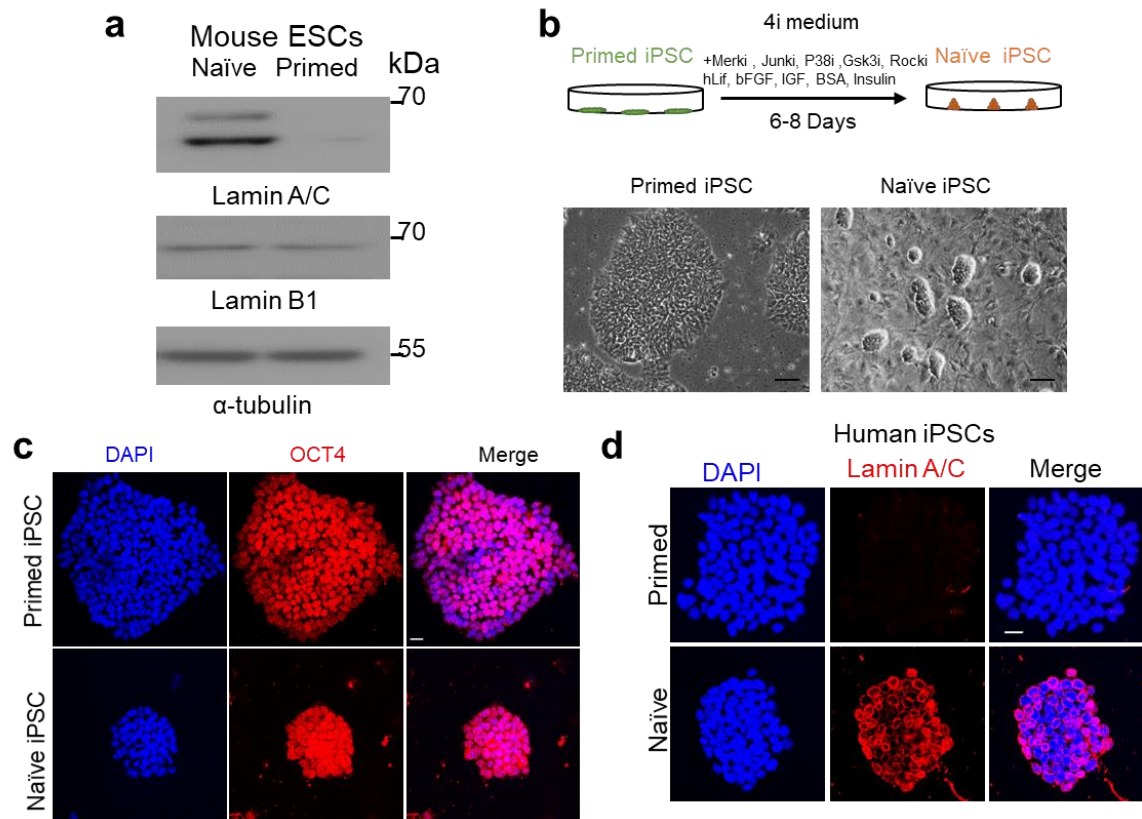


Figure 40. Lamin A/C expresses in naïve mESCs and hiPSCs. **a** Western blot analysis of lamin A/C in mESCs cultured in naïve (DMEM high glucose/feeder/lif) and primed state (DMEM/F12/KOSR/Activin A/bFGF/feeder free) conditions. **b** Schematic representation of the strategy used for conversion of primed human iPSCs into naïve hiPSCs (top panel) and representative phase contrast images showing colony morphology of hiPSC colonies cultured in standard conditions (primed state) or cultured in 4i medium (naïve state). Scale bars, 200µm. **c** Confocal images of immunostaining for OCT4 (red) and nucleus (DAPI, blue) in hiPSCs cultured in standard conditions or cultured in 4i medium on feeders. Scale bars, 20µm. **d** Confocal images of immunostaining for lamin A/C (red) and nucleus (DAPI, blue) in hiPSCs cultured in standard conditions (primed state) and cultured in 4i medium on feeders (naïve state), Scale bars, 20 µm.

3.5.3 Lamin A/C maintains naïve hiPSC pluripotency

To further study the role of lamin A/C on hiPSC pluripotency, I knockdown lamin A/C in both naïve iPSC and primed hiPSC. Lamin A/C-deficient human primed iPSCs failed to establish naïve pluripotency due to poor cell survival while silencing of lamin A/C in naïve iPSCs resulted in flatter colonies, suggesting an important role of lamin A/C in establishment and maintenance of naïve pluripotency (Fig. 41a-41c).

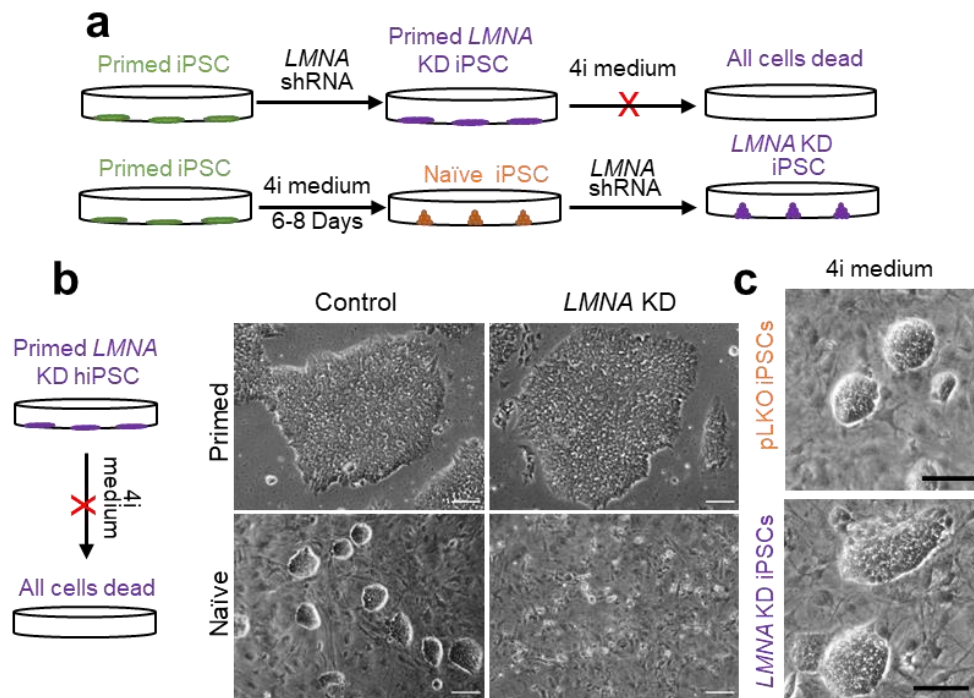


Figure 41. Lamin A/C maintains naïve hiPSC pluripotency. **a** Schematic representation of the two different strategies used to generate *LMNA*-deficient naïve hiPSCs. **b** Phase contrast images showing colony morphology of control and *LMNA* knockdown human iPSCs cultured in standard conditions (top panels) or cultured in 4i medium on feeders after stable knockdown of *LMNA*. Scale bars, 200 μ m. **c** Representative phase contrast images showing colony morphology of naïve human iPSC after *LMNA* knockdown. Scale bars, 200 μ m.

3.6 Distinct roles of lamin A/C in naïve PSC and CMs for cardiac laminopathies

3.6.1 Functional changes in cardiovascular cells following stage-specific loss of lamin A/C

I next investigated whether the functional changes in cardiovascular cells following loss of lamin A/C were due to its role in the suppression of cardiac gene expression program in naïve mESCs. Similar to ablation of *Lmna*, knockdown of lamin A/C in mESCs using shRNA led to precocious CM differentiation and significantly higher expression of key cardiac TFs, as well as CM marker genes (Fig. 42a). In contrast, depletion of lamin A/C in CPs, CMs led to a significant decrease of CM specific gene expression (Fig. 42b, 42c). Similarly, knockdown of lamin A/C in CMs isolated from neonatal mice showed significantly decreased expression of CM structural and contraction genes, suggesting its role in the suppression of cardiac gene expression program in naïve mESCs (Fig. 42d).

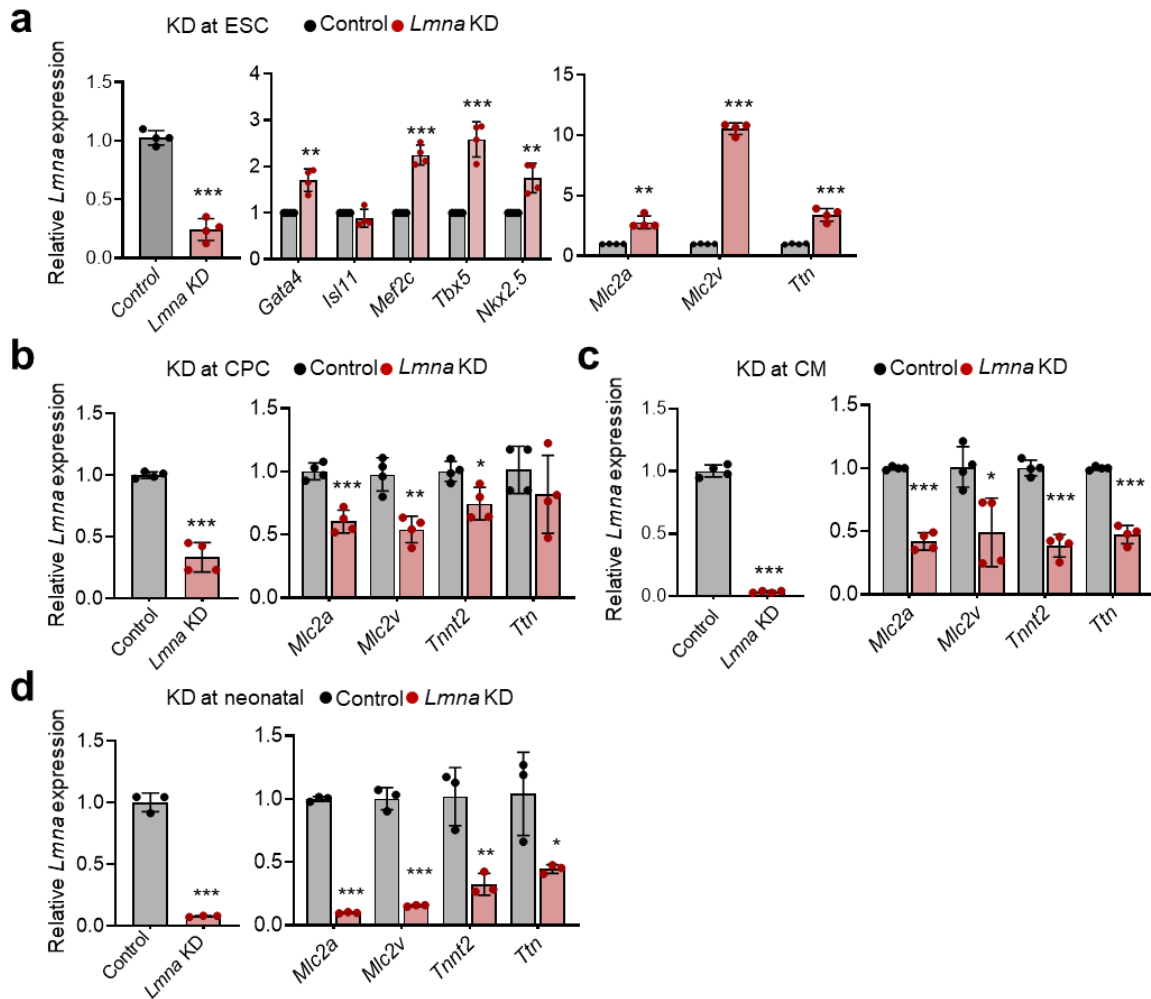


Figure 42. Functional changes in cardiovascular cells following stage-specific loss of lamin A/C. a-d Relative mRNA expression of *Lmna* and cardiomyocyte marker genes at day 10 of directed cardiac differentiation after shRNA mediated *Lmna* knockdown at different stages: mESC (a), CP (b) and CM stage (c), as well as in neonatal cardiomyocytes after shRNA mediated *Lmna* knockdown (d). Data are mean \pm SD, n = 4 for mESC, CP and CM stage KD, n=3 for neonatal CM KD, unpaired two-tailed Student's t-test was used.

3.6.2 RNA-seq analysis of CMs with CM-specific depletion of lamin A/C

To further analyze the expression changes of CMs with CM-specific depletion of lamin A/C, I performed RNA-sequencing of CMs with CM-specific depletion of lamin A/C. RNA-seq data analysis revealed upregulation of multilineage-specific TFs, mitogen-activated protein kinase (MAPK) as well as apoptosis-related molecules. Consistent with my qPCR analysis, many cardiac muscle contraction genes were downregulated, as well as genes involved in angiogenesis and cell migration (Fig. 43).

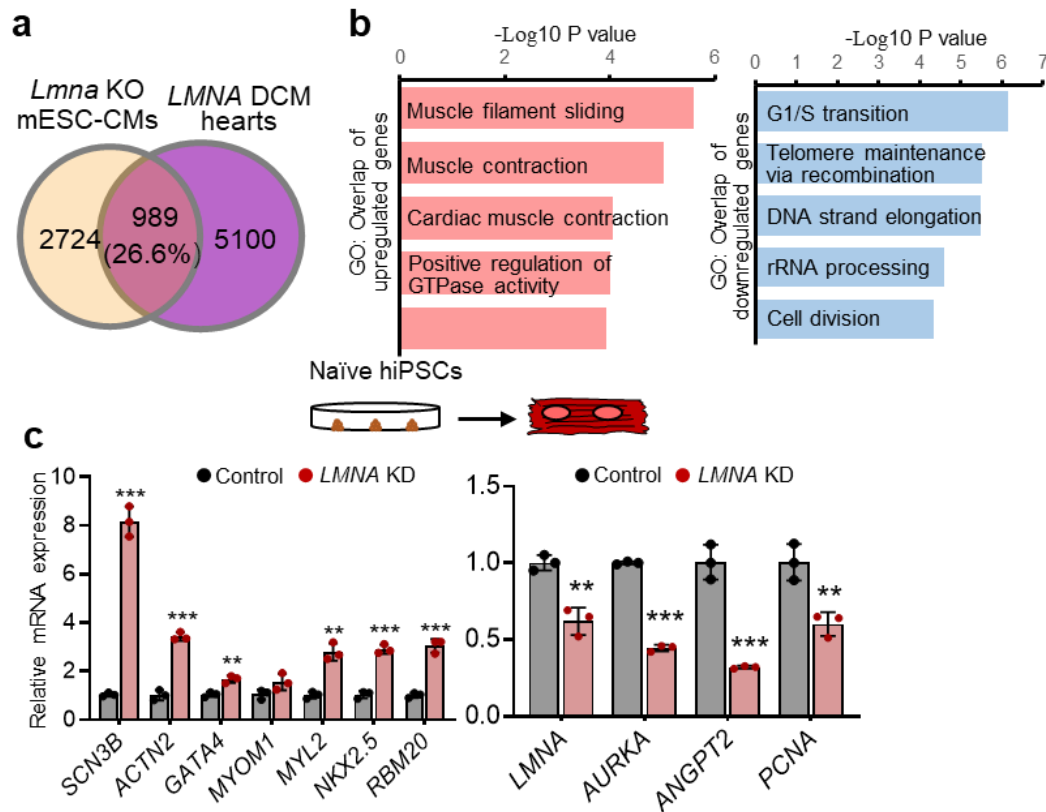


Figure 44. Comparison the transcriptome of *Lmna* KO mESC-CMs with the expression data from *LMNA*-associated DCM patients' heart. **a** Overlap of differentially expressed genes in DCM patients with pathogenic *LMNA* mutations (GSE120836 (Cheedipudi, Matkovich et al. 2019)) and *Lmna*^{-/-} mESCs-derived CMs. **b** GO analysis of common upregulated (red) and downregulated (blue) genes are presented in the middle and right panels. **c** Relative mRNA expression of genes upregulated in both DCM patients with pathogenic *LMNA* mutations and *Lmna*^{-/-} mESCs-derived CM in hiPSCs differentiated in cardiomyocytes after lamin A/C silencing in naïve hiPSCs. Data are mean ± SD, n = 3, unpaired two-tailed Student's t-test was used.

3.6.4 Comparison the transcriptome of *Lmna* KD CMs with the expression data from *LMNA*-associated DCM patients

Since I observed differences upon lamin A/C depletion in mESCs or specifically in CMs, I next compared the transcriptome of lamin A/C depletion specifically in CMs with the expression data from patients with *LMNA*-associated DCM. Interestingly, GO analysis revealed a different subset of overlapping genes (Fig. 45a, 45b), implying important distinct functions of lamin A/C in both mESCs and CMs for proper cardiogenesis and cardiac function. Genes upregulated in *Lmna* knockdown CMs and DCM patients were linked to intracellular signal transduction, JNK activity and ER stress (Fig. 45b), in stark contrast to depletion of lamin A/C in mESCs. In line with the transcriptomics analysis, genes involved in cell cycle were similarly downregulated (Fig. 45b). Both cardiac structural and contraction genes and genes involved in cell cycle were downregulated after silencing of lamin A/C in primed hiPSCs (Fig. 45c). Taken together, these results on the one hand suggest that lamin A/C function in naïve pluripotent stem cells contributes to the pathological phenotype resulting from lamin A/C depletion, and on the other hand imply important distinct functions of lamin A/C in both mESCs and CMs for proper cardiogenesis and cardiac function.

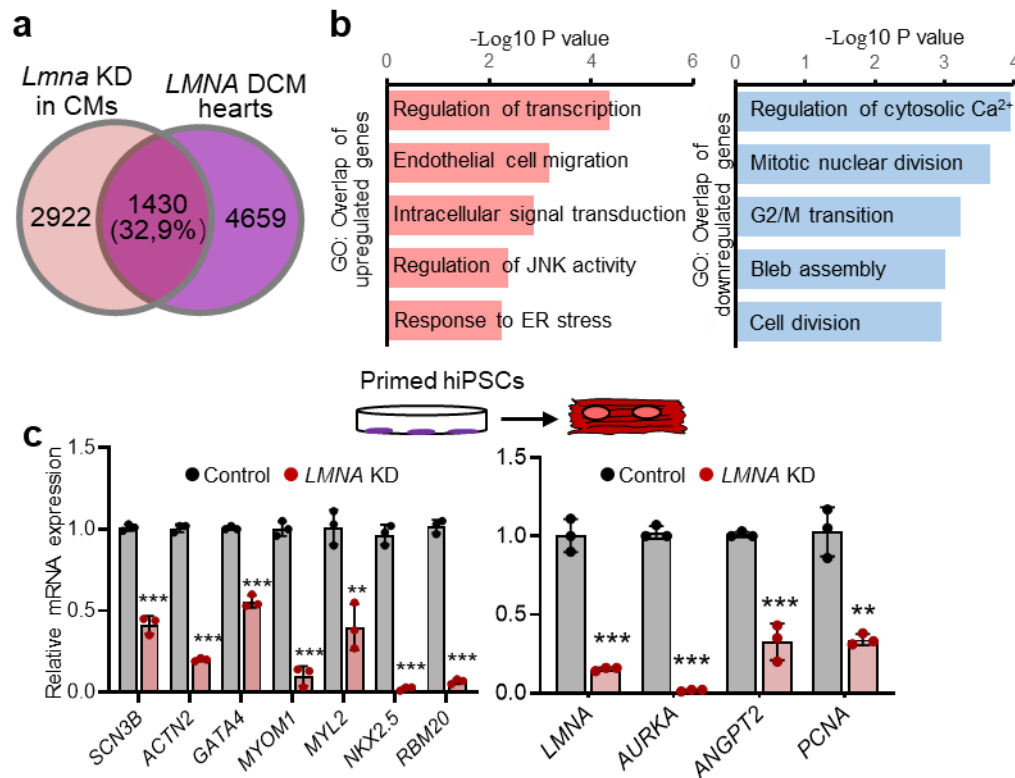


Figure 45. Comparison the transcriptome of *Lmna* KD CMs with the expression data from *LMNA*-associated DCM hearts. **a** Overlap of differentially expressed genes in DCM patients with pathogenic *LMNA* mutations (GSE120836 (Cheedipudi, Matkovich et al. 2019)) and mESCs-derived CMs after shRNA mediated *Lmna* knock-down at the CM stage. **b** GO analysis of common upregulated (red) and downregulated (blue) genes are presented in the middle and right panels. **c** Relative mRNA expression of genes upregulated in both DCM patients with pathogenic *LMNA* mutations and *Lmna*^{-/-} mESCs-derived CM in hiPSCs differentiated in cardiomyocytes after lamin A/C silencing in primed hiPSCs. Data are mean \pm SD, n = 3, unpaired two-tailed Student's t-test was used.

3.7 *Lmna* deficiency results in non-compaction cardiomyopathy

3.7.1 Ectopic cardiac gene activation *in vivo* upon *Lmna* ablation

Next, I sought to corroborate my *in vitro* cell culture-based findings *in vivo* using *Lmna*^{+/+} (control), *Lmna*^{+/-} and *Lmna*^{-/-} mice (Kim and Zheng 2013). Expression analysis revealed significant upregulation of CP and CM marker genes in dissected pharyngeal mesoderm and hearts of E8.5 embryos as well as E9.5 hearts upon *Lmna* ablation consistent with my *in vitro* cell culture-based studies (Fig. 46a, 46b).

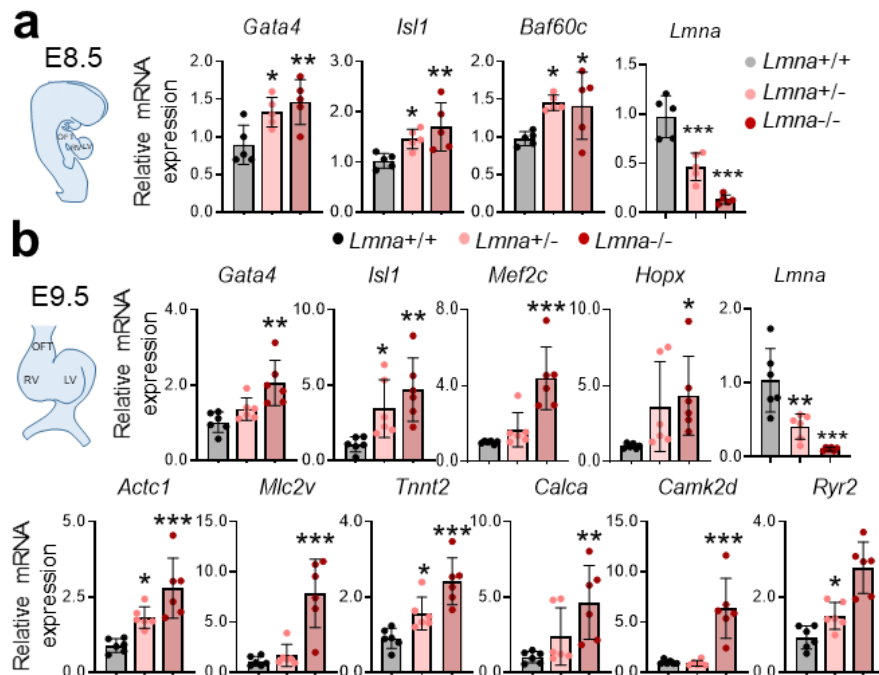


Figure 46. Ectopic cardiac gene activation in vivo upon *Lmna* ablation. a, b. qPCR analysis of dissected pharyngeal mesoderm/ hearts of E8.5 wild-type (n=5), *Lmna*^{+/-} (n=5) and *Lmna*^{-/-} (n=5) embryos (a) as well as dissected hearts of E9.5 wild-type (n=6), *Lmna*^{+/-} (n=6) and *Lmna*^{-/-} (n=6) embryos (b) for cardiac TFs and CM structural and contraction genes. Data are represented as mean \pm SD, One-way ANOVA comparisons were used.

3.7.2 Lamin A/C tethers CM specific genes to the nuclear periphery in non-CMs

Since I observed dissociation of CMs genes from nuclear periphery to nuclear interior in lamin A/C depleted mESCs. Next I examined the localization of cardiac genes in cardiomyocytes and non-CMs isolated from E14.5 embryos. FISH analysis showed that CMs specific genes were located in the nuclear interior of *Lmna*^{+/+} CMs and at the nuclear periphery in *Lmna*^{+/+} fibroblasts respectively suggesting dissociation of CMs gene from nuclear periphery is essential for CMs differentiation and heart development. Moreover, they were found in the nuclear interior in both CMs and fibroblasts isolated from E14.5 *Lmna*^{+/-} and *Lmna*^{-/-} embryos, supporting a role of lamin A/C in tethering CM specific genes to the nuclear periphery in non-CMs (Fig.47a, 47b).

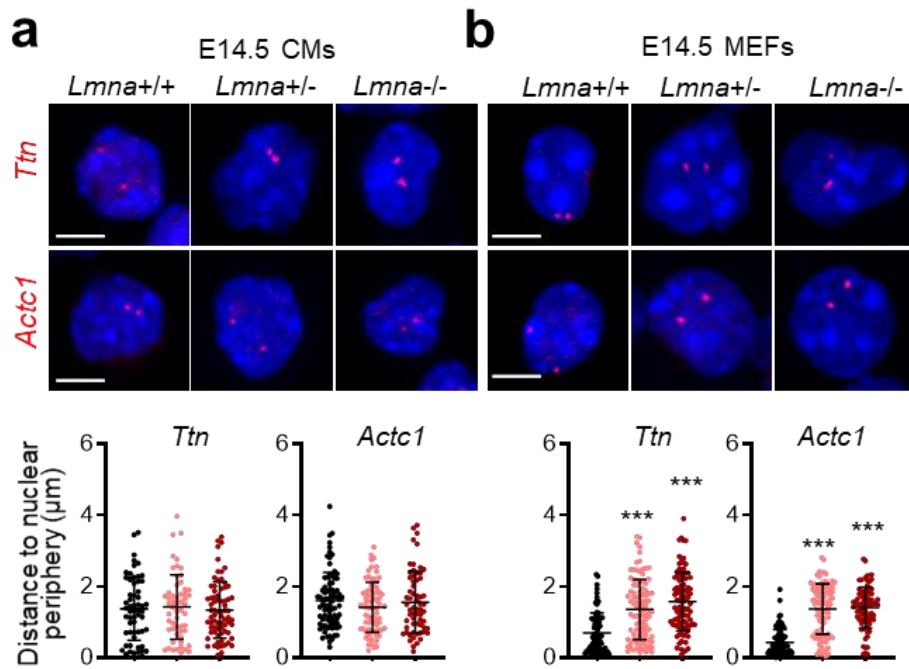


Figure 47. Lamin A/C tethers CM specific genes to the nuclear periphery in non-CMs. a, b Representative DNA FISH images of *Ttn* and *Actc1* gene loci in CMs (a, top) and fibroblasts (b, top) isolated from E14.5 embryos and quantification of the distance of these loci to the nuclear periphery (bottom). Data are represented as mean \pm SD, 30-50 cells were quantified, One-way ANOVA comparisons were used. Scale bars, 4 μ m.

3.7.3 Increased ejection fraction and fractional shortening in *Lmna*^{+/-} and *Lmna*^{-/-} right ventricle

Since I observed major changes in gene expression of cardiac TF and CM structural genes, I next performed transthoracic echocardiography to check whether there are functional and morphological changes in *Lmna* haploinsufficient and deficient mice. Echocardiography was performed with the help of Olga Lityagina. Functional analysis revealed significantly increased right ventricular ejection fraction and fractional shortening (RVEF and RVFS), an index of cardiac contractility, as well as lower RV systolic diameter in *Lmna*^{+/-} and *Lmna*^{-/-} embryos while the RV diastolic diameter was not different from the controls (Fig. 48a, 48b). In contrast, we did not observe differences in LV function (Fig. 48b).

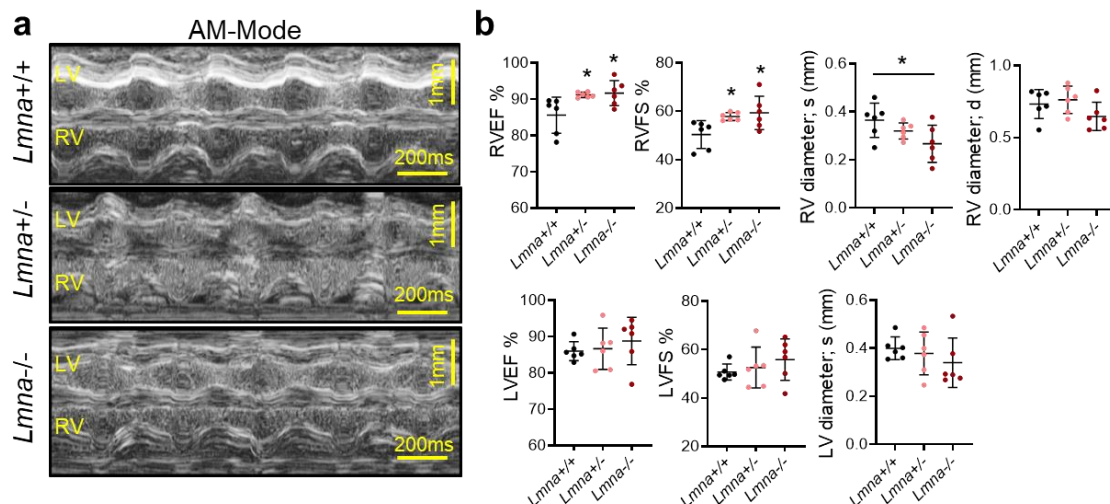
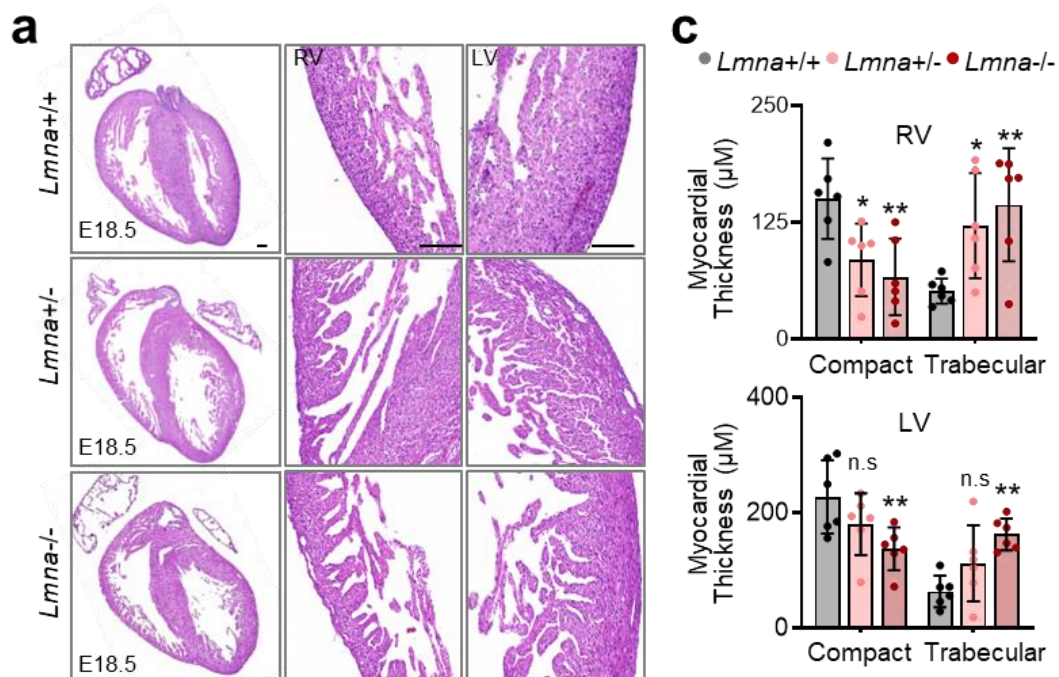


Figure 48. E16.5 heart function analysis by echocardiograms. **a** Representative AM-mode echocardiograms pictures of wild-type, *Lmna*^{+/-} and *Lmna*^{-/-} mice at E16.5. **b** Right and left ventricular ejection fraction (RVEF, LVEF), right and left ventricular fractional shortening (RVFS, LVFS), RV and LV systolic diameter as well as RV diastolic diameter assessed by echocardiography in wild-type, *Lmna*^{+/-} and *Lmna*^{-/-} embryos at E16.5. n=6 mice for each group. Data are represented as mean \pm SD, One-way ANOVA comparisons were used.

3.7.4 Non-compaction hearts in both *Lmna*^{+/-} and *Lmna*^{-/-} embryos

Mutations of *LMNA* have been associated several types of cardiomyopathies. Previously studies showed that *Lmna*^{-/-} mice develop dilated cardiomyopathy after birth, whether there is an embryonic heart defects in *Lmna*^{+/-} and *Lmna*^{-/-} mice is not known yet. To this end, I collected different stages of the embryonic heart of *Lmna*^{+/-} and *Lmna*^{-/-} mice and did H&E staining. Although I didn't observe a dilated heart phenotype during development, histological examination unveiled non-compaction of myocardium and excessive endocardium trabeculations in both *Lmna*^{+/-} and *Lmna*^{-/-} RV of the E18.5 embryos, while only *Lmna*^{-/-} embryos showed LV non-compaction (Fig. 49a, 49b), indicating the noncompaction cardiomyopathy in *Lmna*^{+/-} and *Lmna*^{-/-} embryos might be the earliest and primary phenotype. Endomucin staining for E18.5 hearts from wild-type, *Lmna*^{+/-} and *Lmna*^{-/-} embryos further confirmed the results from the histological analysis (Fig. 49c).



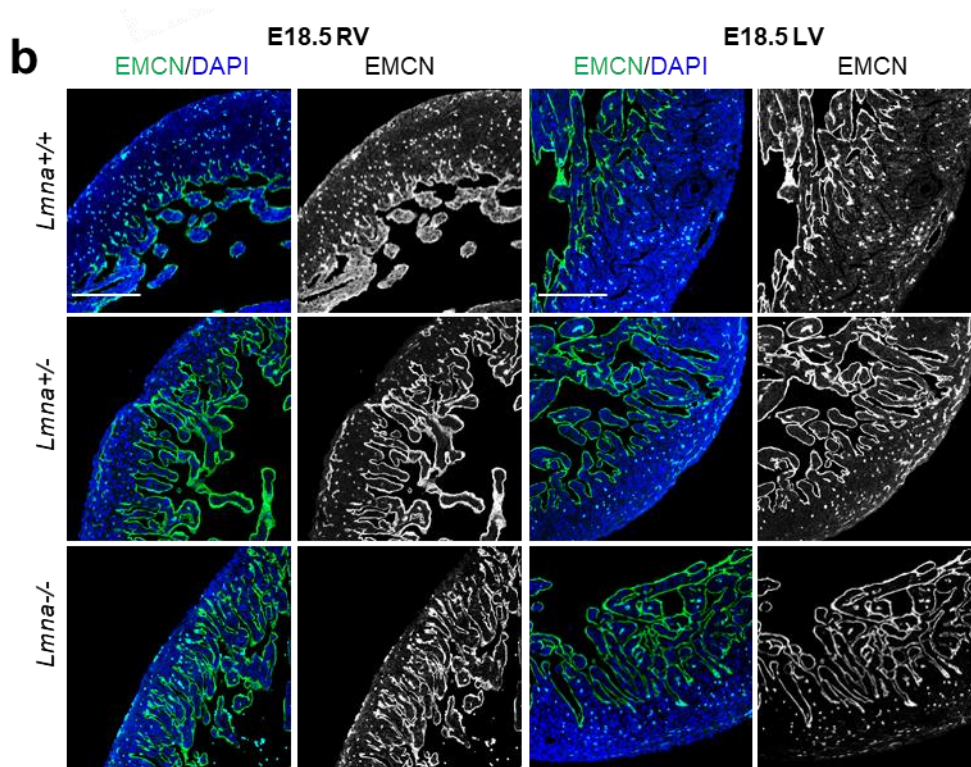


Figure 49. Non-compaction hearts in both *Lmna*^{+/-} and *Lmna*^{-/-} embryos. **a** H&E staining of representative heart sections from E18.5 wild-type, *Lmna*^{+/-} and *Lmna*^{-/-} embryos. Magnified images of indicated right ventricle (RV) and left ventricle (LV) regions are shown in the middle and right panel. **b** Endomucin staining of representative heart sections from wild-type, *Lmna*^{+/-} and *Lmna*^{-/-} embryos. **c** Quantification of RV and LV wall thickness (compact myocardium) and trabecular layer thickness from E18.5 wild-type (n=6), *Lmna*^{+/-} (n=6) and *Lmna*^{-/-} (n=6) hearts. Data are represented as mean \pm SD, One-way ANOVA comparisons were used.

3.7.5 Decreased CM proliferation in E18.5 *Lmna*^{+/-} and *Lmna*^{-/-} hearts

Insufficient cardiomyocytes proliferation and premature maturation in myocardium have been linked to ventricular non-compaction pathology (Kodo, Ong et al. 2016, Finsterer, Stoellberger et al. 2017). To test whether CM proliferation is effected in *Lmna* mutant hearts, I performed immunostaining for the mitotic marker phosphorylated-histone H3 (pH3) in combination with Troponin I, Indeed, I observed significant decrease in CM proliferation in E18.5 but not in E14.5 *Lmna*^{+/-} and *Lmna*^{-/-} hearts (Fig. 50a, 50b), suggesting the insufficient CM proliferation might contribute to the non-compaction phenotype in *Lmna*^{+/-} and *Lmna*^{-/-} heart.

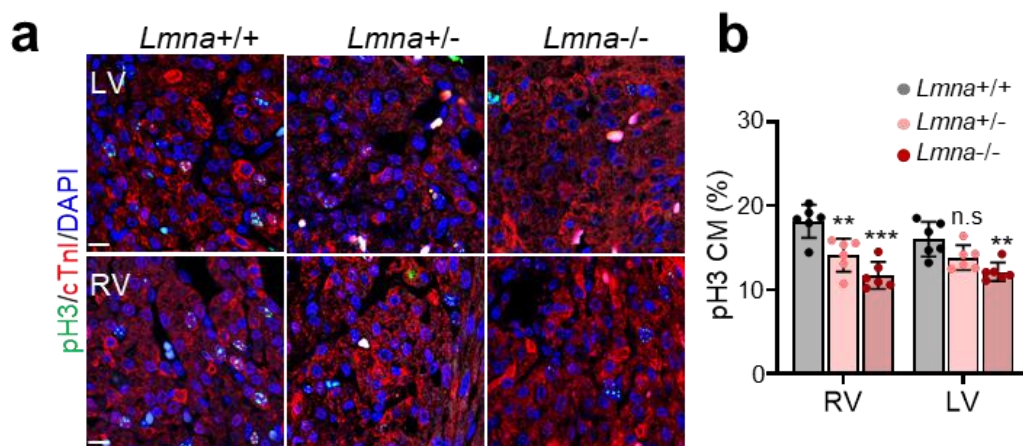


Figure 50. Decreased CM proliferation in E18.5 *Lmna*^{+/-} and *Lmna*^{-/-} hearts. Immunostaining of heart sections for the mitotic marker phospho-histone H3 (Ser10) (green), cardiac troponin I (cTnI, red) and nucleus (blue) (a) and quantification of the percentage of mitotic right and left ventricle (RV and LV) cardiomyocytes in wild-type (n=6), *Lmna*^{+/-} (n=6) and *Lmna*^{-/-} (n=6) mice at E18.5 (b). Data are represented as mean \pm SD, One-way ANOVA comparisons was used. Scale bars, 10 μ m.

3.7.6 Increased CMs binucleation in E18.5 *Lmna*^{+/-} and *Lmna*^{-/-} hearts

Embryonic cardiomyocytes are highly proliferative until birth. After birth there is a transition from mononucleated to the mature binucleated phenotype. Mononucleated cells are proliferative, whereas binucleated cells exit the cell cycle and no longer proliferate. Thus, I next checked whether there is an increase in CM binucleation upon *Lmna* LOF. Vybrant DyeCycle DNA dye has been used to assess DNA content and ploidy of nuclei, and separate mononucleated and binucleated CMs when combining with the concept behind doublet discrimination (Windmueller, Leach et al. 2020). FACS analysis of cells isolated from E18.5 hearts and stained with Vybrant DyeCycle DNA dye after removing endothelial cells revealed increased number of binucleated CMs in both *Lmna*^{+/-} and *Lmna*^{-/-} embryonic heart (Fig. 51a, 51c). Immunofluorescence staining of E18.5 CMs cultured for 12h after isolation with DAPI and Troponin I further confirmed precocious binucleation of *Lmna* mutant CMs (Fig. 51b, 51d), suggesting that precocious CM differentiation leads to premature binucleation and CM cell cycle withdrawal during fetal development.

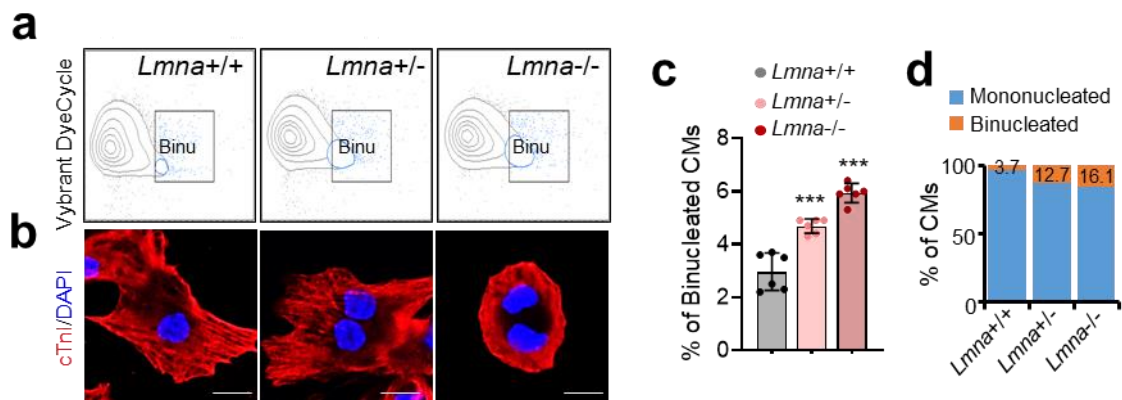


Figure 51. Increased CMs binucleation in E18.5 *Lmna*^{+/-} and *Lmna*^{-/-} hearts. a, c Representative FACS plots of cells isolated from E18.5 hearts and stained with Vybrant DyeCycle DNA dye (a) after removing endothelial cells, the % of binucleated CMs was determined (c). Data are represented as mean \pm SD, n=6 for each genotype, One-way ANOVA comparisons were used. b, d Immunofluorescence staining of E18.5 CMs cultured for 12h after isolation with cTnI (red) and DAPI (blue) (b) and quantification of binucleated CMs (d).

3.7.7 Decreased capillary density in E18.5 *Lmna*^{+/-} and *Lmna*^{-/-} hearts

Since I observed aberrant cardiovascular cell fate choices and decreased number of ECs upon *Lmna* loss in vitro. I next analyzed EC in heart sections by immunofluorescence staining with isolectin B4 (IB4, blood vessels, green) and wheat germ agglutinin (WGA, CMs, red). Consistent with the decreased number of ECs upon lamin A/C depletion observed in our in

in vitro system, I found significantly decreased capillary density in hearts from both *Lmna*^{+/-} and *Lmna*^{-/-} E18.5 embryos (Fig. 52a, 52b).

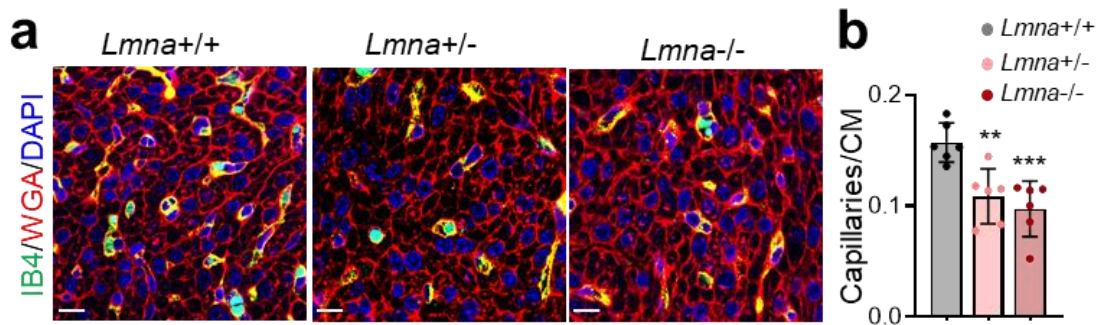
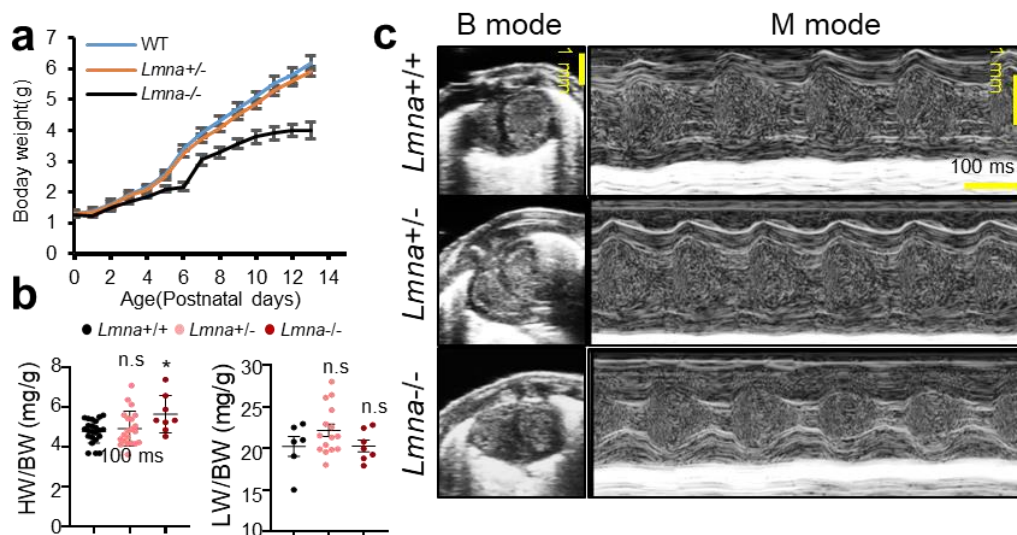


Figure 52. Decreased capillary density in E18.5 *Lmna*^{+/-} and *Lmna*^{-/-} hearts. **a** Immunofluorescence staining of E18.5 heart sections with isolectin B4 (IB4, blood vessels, green), wheat germ agglutinin (WGA, CMs, red) together with DAPI (blue) at E18.5. Scale bars, 10 μm. **b** Quantification of the capillaries/CM ratio in wild-type (n=6), *Lmna*^{+/-} (n=6) and *Lmna*^{-/-} (n=6) E18.5 embryos. Data are represented as mean ± SD, One-way ANOVA comparisons were used.

3.7.8 Echocardiographic analysis of P1 heart function

Since I observed a non-compaction with preserved ejection fraction phenotype during early heart development of *Lmna* mutant mice, I next checked the postnatal stage in which *Lmna* mice have been shown to develop DCM phenotype. At birth, *Lmna*^{+/-} and *Lmna*^{-/-} mice were indistinguishable from their control littermate mates, but a week later there was a clear difference in size and body weight of *Lmna*^{-/-} mice (Fig. 53a). *Lmna*^{+/-} and *Lmna*^{-/-} neonatal mice showed increased RVEF, while LVEF was increased only in *Lmna*^{-/-} mice (Fig. 53c, 53d), consistent with the more pronounced defects observed in the RV during embryogenesis. At P1 we observed significant right ventricular dilatation in *Lmna*^{+/-} and *Lmna*^{-/-} mice with no signs of pulmonary arterial hypertension (PAH) or pulmonary congestion (Fig. 53b, 53c). The left ventricular posterior wall thickness at end-diastole (LVPW:d) was also significantly increased in both *Lmna*^{+/-} and *Lmna*^{-/-} mice, whereas left ventricle (LV) ejection fraction (EF) and LV fractional shortening (FS) was significantly increased only in *Lmna*^{-/-} mice (Fig. 53d).



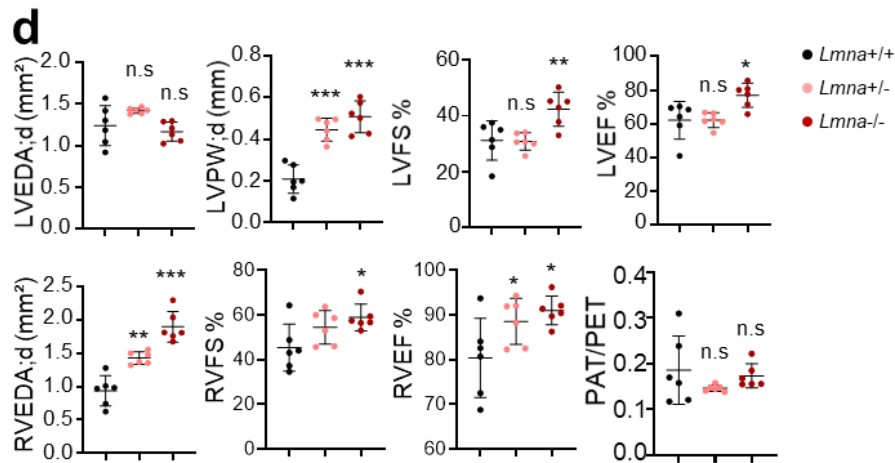
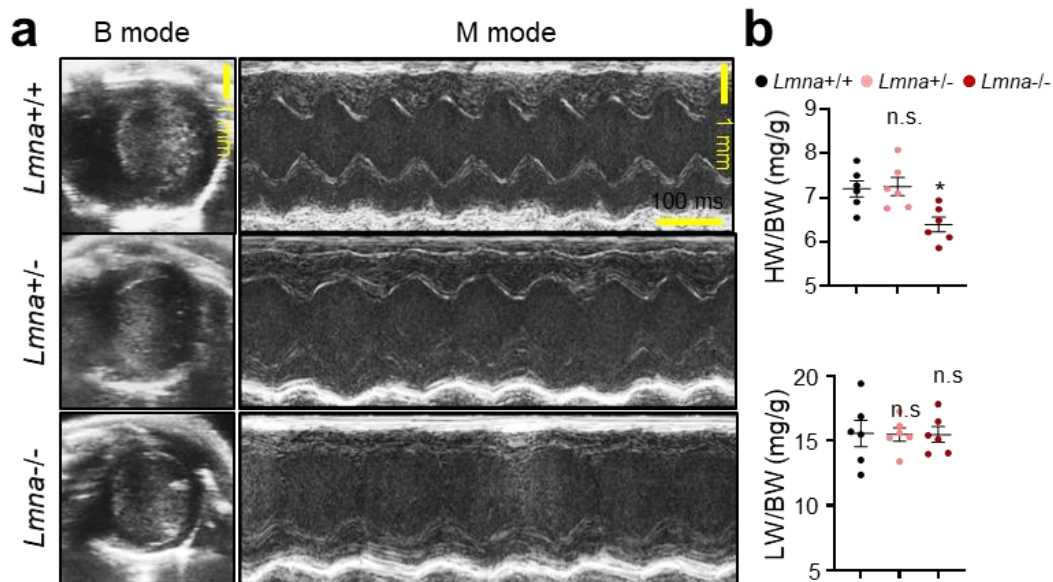


Figure 53. Echocardiographic analysis of P1 heart function. **a** Body weight at the indicated days after birth. n=6 mice for each group. **b** Quantification of the heart weight/body weight (HW/BW) in wild-type (n=23), *Lmna*^{+/-} (n=21) and *Lmna*^{-/-} (n=8) mice and lung weight/body weight (LW/BW) ratio of *Lmna*^{+/+} (n=6), *Lmna*^{+/-} (n=18) and *Lmna*^{-/-} (n=7) mice at P1. **c** Representative examples of B-mode and LV M-mode echocardiograms of wild-type, *Lmna*^{+/-} and *Lmna*^{-/-} mice at P1. Echocardiography was performed with the help of Felix A. Trogisch. **d** Left and right ventricular end-diastolic area (LVEDA;d and RVEDA;d), left ventricle posterior wall thickness (LVPW;d), left and right ventricular fractional shortening (RVFS and LVFS), ejection fraction (RVEF and LVEF) and pulmonary acceleration time/ pulmonary ejection time (PAT/PET) ratio assessed by echocardiography in wild-type (n=6), *Lmna*^{+/-} (n=6) and *Lmna*^{-/-} (n=6) mice at P1. Data are represented as mean \pm SD, One-way ANOVA comparisons were used.

3.7.9 Echocardiographic analysis of P14 heart function

In sharp contrast, two weeks after birth the HW/BW was strongly decreased in *Lmna*^{-/-} mice and LVEF, LVFS and LVPW:d were reduced, while left ventricular end-diastolic area (LVEDA) was increased (Fig. 54a-54c).



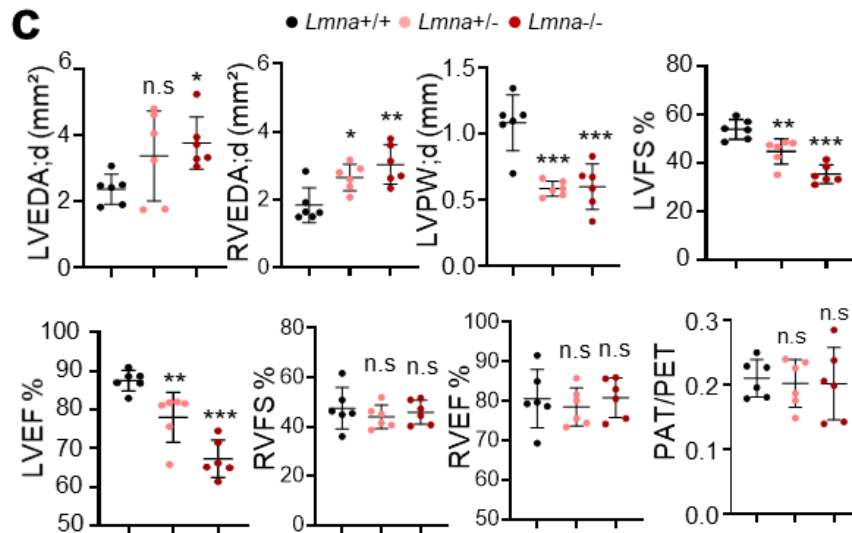


Figure 54. Echocardiographic analysis of P14 heart function. **a** Representative example of B-mode and LV M-mode echocardiograms of wild-type, *Lmna*^{+/-} and *Lmna*^{-/-} mice at P14. **b** Quantification of the heart weight/body weight (HW/BW) and lung weight/body weight (LW/BW) ratio of *Lmna*^{+/+} (n=6), *Lmna*^{+/-} (n=6) and *Lmna*^{-/-} (n=6) mice at P1. **c** Echocardiography was performed with the help of Felix A. Trogisch. Left and right ventricular end-diastolic area (LVEDA;d and RVEDA;d), left ventricle posterior wall thickness (LVPW;d), left and right ventricular fractional shortening (RVFS and LVFS), ejection fraction (RVEF and LVEF) and pulmonary acceleration time/ pulmonary ejection time (PAT/PET) ratio assessed by echocardiography in wild-type (n=6), *Lmna*^{+/-} (n=6) and *Lmna*^{-/-} (n=6) mice at P14. Data are represented as mean ± SD, One-way ANOVA comparisons were used.

3.7.10 Decreased capillary density in postnatal hearts

Similar to the embryonic hearts, I observed a decrease in capillary density in hearts from both *Lmna*^{+/-} and *Lmna*^{-/-} mice also at P1 (Fig. 55a). Furthermore, Immunofluorescence staining of heart sections for isolectin B4 (IB4, blood vessels), wheat germ ag-glutinin (WGA, CMs) revealed that lamin A/C-deficient CMs showed reduced size in cross sections (Fig. 55a). Similar differences were also observed at P4 and P14 (Fig. 55b, 55c).

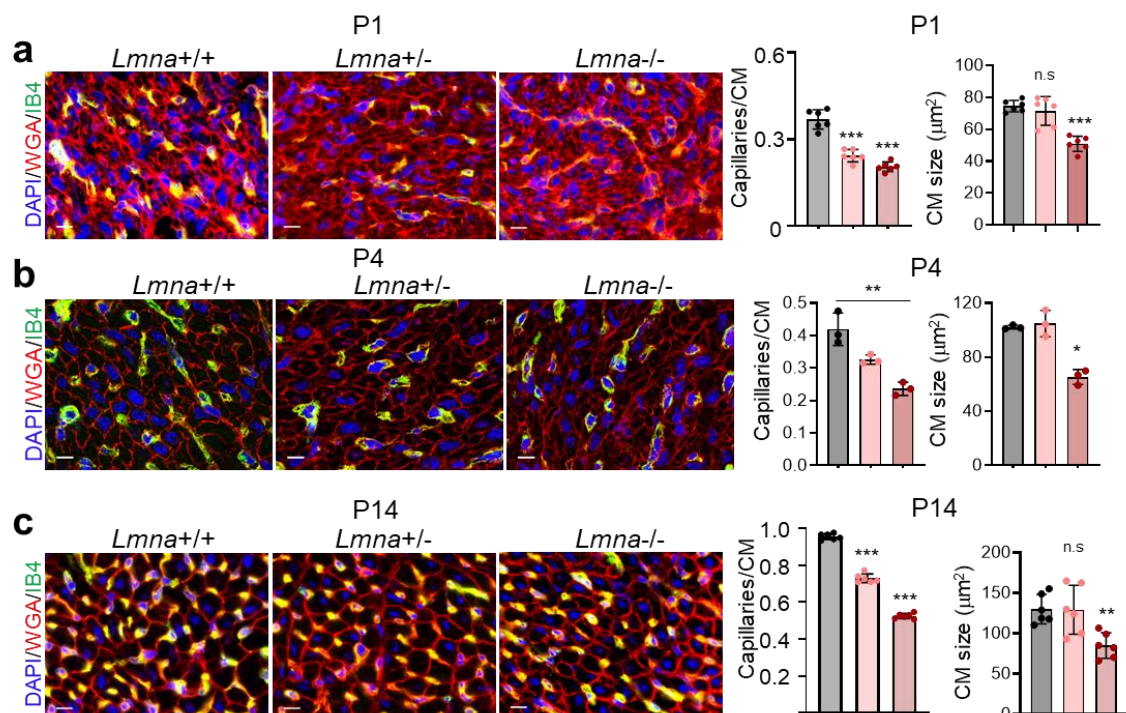
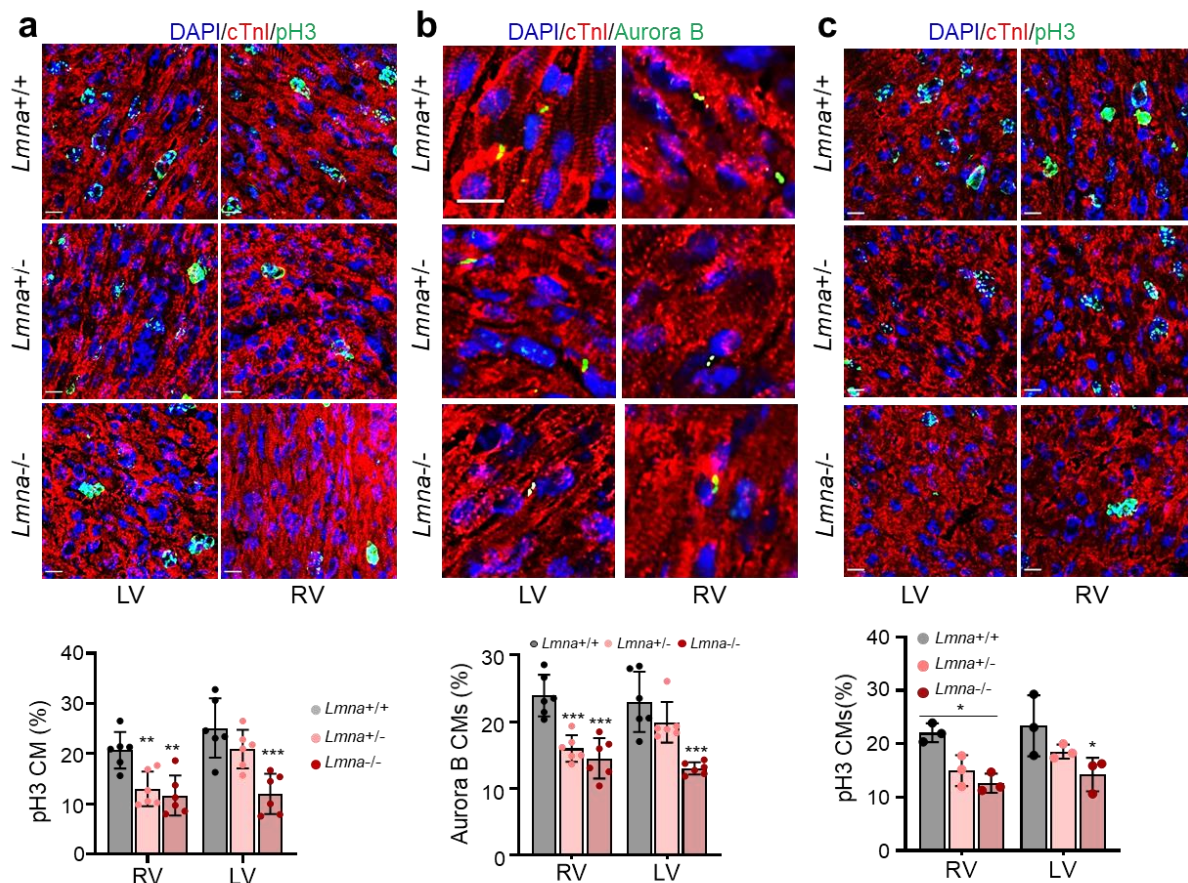


Figure 55. Decreased capillary density in postnatal hearts. **a** Immunofluorescence staining of heart sections for isolectin B4 (IB4, blood vessels), wheat germ agglutinin (WGA, CMs) together with DAPI at P1. Scale bars, 10 μ m. Quantification of the capillaries/CM ratio and the cardiomyocyte cross-sectional area in wild-type (n=6), *Lmna*^{+/-} (n=6) and *Lmna*^{-/-} (n=6) mice at P1. Data are represented as mean \pm SD, One-way ANOVA comparisons were used. **b** Immunofluorescence staining of heart sections for isolectin B4 (IB4, blood vessels), wheat germ agglutinin (WGA, CMs) together with DAPI at P4. Scale bars, 10 μ m. Quantification of the capillaries/CM ratio and the cardiomyocyte cross-sectional area in wild-type (n=3), *Lmna*^{+/-} (n=3) and *Lmna*^{-/-} (n=3) mice at P4. **c** Immunofluorescence staining of heart sections for isolectin B4 (IB4, blood vessels), wheat germ agglutinin (WGA, CMs) together with DAPI at P14. Scale bars, 10 μ m. Quantification of the capillaries/CM ratio and the cardiomyocyte cross-sectional area in wild-type (n=6), *Lmna*^{+/-} (n=6) and *Lmna*^{-/-} (n=6) mice at P14. Data are represented as mean \pm SD, One-way ANOVA comparisons were used.

3.7.11 Decreased CM proliferation in P1 and P4 *Lmna*^{+/-} and *Lmna*^{-/-} hearts

I next checked CMs proliferation in postnatal heart of *Lmna* mutant mice. Immunostaining for the mitotic marker phosphorylated-histone H3 (pH3) as well as the cytokinesis marker Aurora B in combination with Troponin I revealed significant decrease in CM proliferation at both P1 and P4 (Fig. 56a-56c), similar to the decreased CM proliferation observed in E18.5 embryonic hearts.



3.8 Premature binucleation, altered contractility and increased cell death of *Lmna*^{-/-} CMs

3.8.1 Precocious of *Lmna*^{+/-} and *Lmna*^{-/-} CMs binucleation

To study the effect of lamin A/C deficiency on CM function in more detail I utilized CMs isolated from P1 wild-type, *Lmna*^{+/-} and *Lmna*^{-/-} mice. A high percentage of *Lmna*^{+/-} and *Lmna*^{-/-} CMs were already binucleated at P1 similar to E18.5 hearts suggesting precocious CM binucleation in *Lmna*^{+/-} and *Lmna*^{-/-} CMs (Fig. 57a, 57c). Significant increased CMs binucleation was also observed in lamin A/C-deficient mESC-CMs (Fig. 57b, 57d).

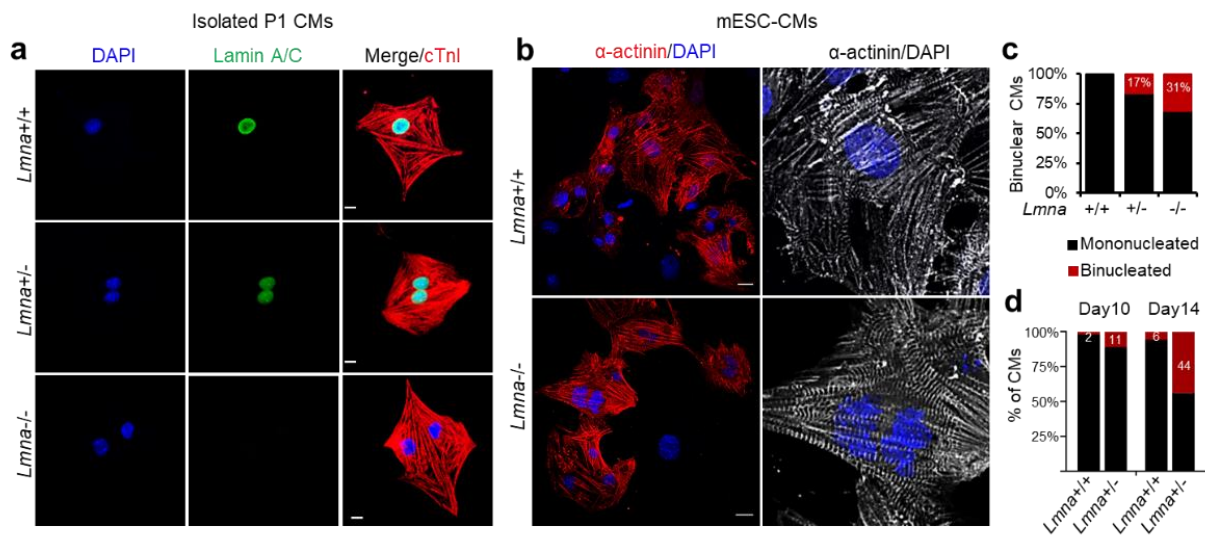


Figure 57. Precocious of *Lmna*^{+/-} and *Lmna*^{-/-} CMs binucleation. **a, c** Representative immunostaining of cardiomyocytes isolated from *Lmna*^{+/+} (n=6), *Lmna*^{+/-} (n=15) and *Lmna*^{-/-} (n=8) mice at P1 for lamin A/C (green), cardiac troponin I (red) and nucleus (DAPI, blue) (**a**) and quantification of binucleated CMs (**c**). **b, d** Immunofluorescent staining of FACS-sorted Nkx2-5+ CMs from d10 EBs for lamin A/C (green), cardiac troponin I (red) and DAPI (blue) and quantification of d10 and d14 binucleated CMs.

3.8.2 DNA damage in *Lmna*^{+/-} and *Lmna*^{-/-} CMs

Since lamin A/C protects the nucleus from DNA damage, I next analysed whether lamin A/C LOF results in increased DNA damage in CMs by immunostaining for the marker of DNA double-strand breaks (DSBs) γ H2AX. I observed a significantly higher percentage of γ -H2AX positive CMs isolated from *Lmna*^{+/-} and *Lmna*^{-/-} mice at P1 (Fig. 58a, 58d). Similar results were also observed in lamin A/C-deficient mESC-CMs (Fig. 58b, 58c) suggesting precocious CM binucleation and increased DNA damage-induced cell death in *Lmna*^{+/-} and *Lmna*^{-/-} CMs.

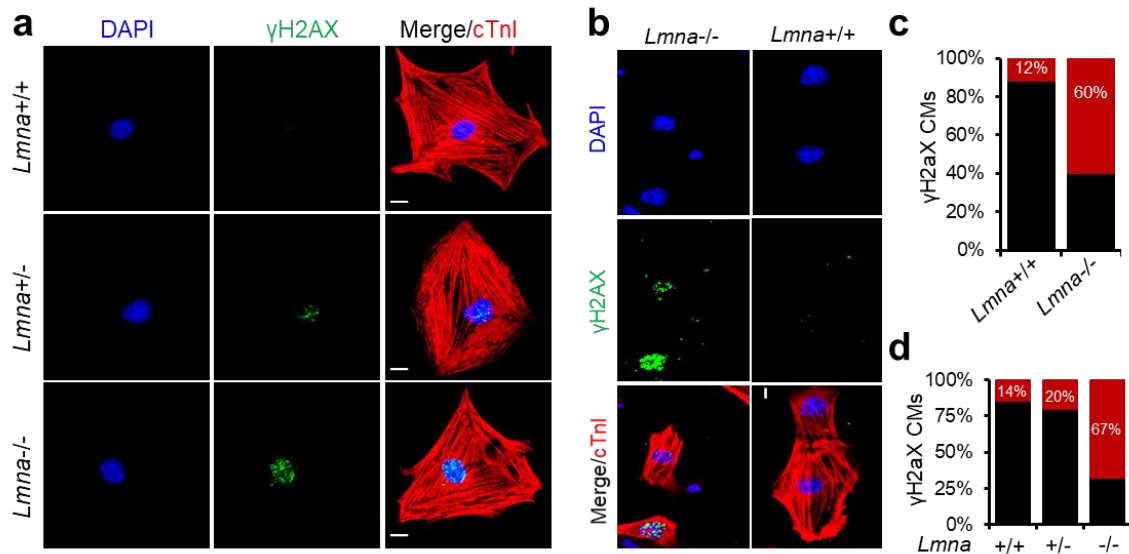


Figure 58. DNA damage in *Lmna*^{+/-} and *Lmna*^{-/-} CMs. **a, d** Representative immunofluorescence images of isolated cardiomyocytes from *Lmna*^{+/+} (n=6), *Lmna*^{+/-} (n=15) and *Lmna*^{-/-} (n=8) mice at P1 for the marker of DNA double-strand breaks (DSBs) γH2AX (green), cardiac troponin I (red) and nucleus (DAPI, blue) at P1 (**a**) and quantification of γH2AX positive CMs (**d**). **b, c** Immunostaining of FACS-sorted Nkx2-5+ cardiomyocytes from d10 EBs for γH2AX (green), cardiac troponin I (red) and DAPI (blue) (**b**) and quantification of γH2AX positive CMs (**c**).

3.8.3 Proarrhythmic beating in *Lmna*^{-/-} CMs

Since I observed many Ca²⁺ channels to be deregulated in *Lmna*^{-/-} CM, I analyzed the intracellular Ca²⁺-handling properties of wild-type, *Lmna*^{+/-} and *Lmna*^{-/-} CMs isolated from P1 mice. Although wild-type and most of *Lmna*^{+/-} CMs showed uniform Ca²⁺ transients, the peak height was significantly increased in *Lmna*^{+/-} CMs and the time to peak was shorter (Fig. 59a,59b), suggesting more rapid release of Ca²⁺ from sarcoplasmic reticulum stores, consistent with the increased levels of Ryr2. In contrast, 65% of *Lmna*^{-/-} CMs showed highly abnormal proarrhythmic Ca²⁺ transients (Fig. 59c). Similar functional alterations were observed in *Lmna*^{-/-} mESC-derived CMs, which showed arrhythmic contractions (Fig. 59d, 59e). Interestingly, 68% of lamin A/C depleted mouse neonatal CMs showed abnormal proarrhythmic Ca²⁺ transients, consistent with the role of lamin A/C in regulating chromatin conformation of genes involved in Ca²⁺ homeostasis in both mESCs and CMs (Fig. 59f-59h)

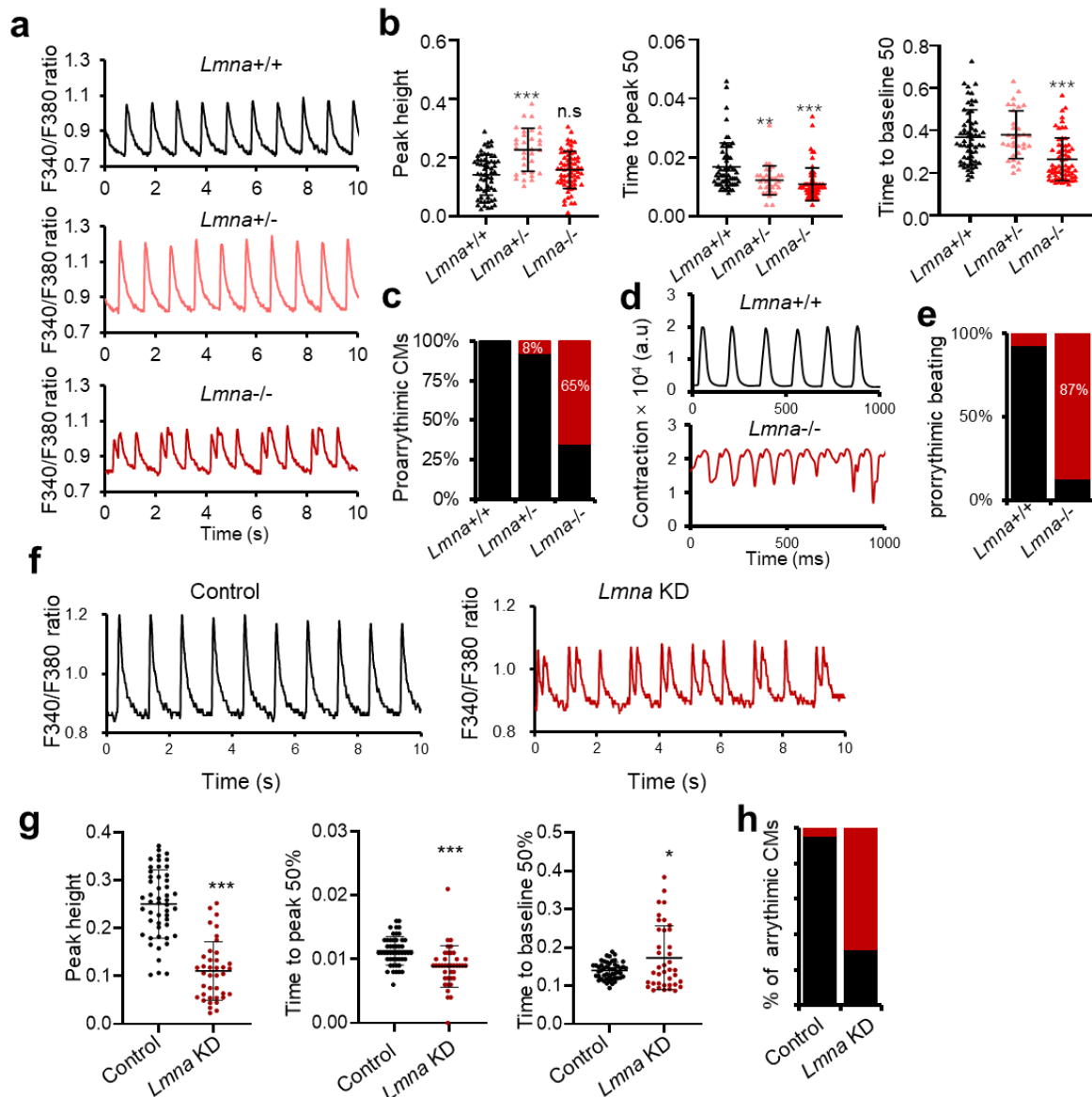


Figure 59. Proarrhythmic beating in *Lmna*^{-/-} CMs. **a** Representative Ca²⁺ transients traces recorded using fura-2-labeled P1 *Lmna*^{+/+}, *Lmna*^{+/-} and *Lmna*^{-/-} CMs. The ratio of the fura-2 AM signal excited at 340 nm and 380 nm (F340/F380) is shown. All traces were recorded for 20 s. **b** Peak height, time to peak 50% and time to baseline 50% of Ca²⁺ traces of *Lmna*^{+/+}, *Lmna*^{+/-} and *Lmna*^{-/-} CMs isolated from P1 mice. Data are represented as mean ± SD, n=35-60 cells from 3 independent CM isolations, one-way ANOVA comparisons were used. **c** Quantification of the percentage of CMs exhibiting pro-arrhythmic Ca²⁺ waves. **d, e** Plot of contraction amplitude and speed in spontaneously beating CMs at d10 extracted from image sequences using MUSCLEMOTION and quantification of proarrhythmic beating. **f** Representative Ca²⁺ transients traces of neonatal CMs after *Lmna* knockdown. The ratio of the fura-2 AM signal excited at 340 nm and 380 nm (F340/F380) is presented. All traces were recorded for 20 s. **g** Peak height, time to peak 50% and time to baseline 50% of Ca²⁺ traces of isolated neonatal cardiomyocytes after *Lmna* knockdown by shRNA. **h** Quantification of the percentage of CMs exhibiting proarrhythmic Ca²⁺ waves (red). 40-50 cells were quantified for each group.

3.8.4 Loss of *Lmna* leads to CMs specific cell death

Initially, the contraction amplitude of *Lmna*^{-/-} mESC-derived CMs was much higher than control CMs but decreased with time. Since I observed many dead cells in vitro CM cultures, I next analyzed cell death with Annexin V/7-AAD staining. FACS analysis revealed a dramatic increase of apoptotic and dead *Lmna*^{-/-} CMs in comparison to control CMs (Fig. 60a). The increased cell death was specific for lamin A/C-deficient CMs, because the non-CM population

lacking lamin A/C as well as lamin A/C-deficient mESCs did not show increased cell death (Fig. 60b). To test whether the mechanical forces on which CMs are constantly subjected are responsible for the increased cell death, I next stretched non-CM for 15 min at 15%. Intriguingly, mechanical stretch of *Lmna*^{+/+} and *Lmna*^{-/-} non-CMs resulted in dramatic increase of γ -H2AX in *Lmna*^{-/-} compared to control cells, suggesting that the increased cell death in *Lmna*^{-/-} CMs might be due to the inability of lamin A/C-deficient cells to respond adequately to mechanical stress (Fig. 60c). Directly after birth CMs are exposed to high oxygen levels resulting in cell cycle withdraw. To test whether *Lmna* deficient cells respond to oxidative stress, I treated mESC with H₂O₂ and allowed the cells to recover in fresh medium for 4h and 8h. I observed dramatic increase of γ -H2AX and defects in DNA damage repair in *Lmna*^{-/-} compared to control cells, suggesting that the premature cell cycle withdrawal and increased cell death in *Lmna*^{-/-} CMs might be also due to the inability of lamin A/C-deficient cells to respond adequately to oxidative stress during early postnatal life (Fig. 60d) (Puente, Kimura et al. 2014).

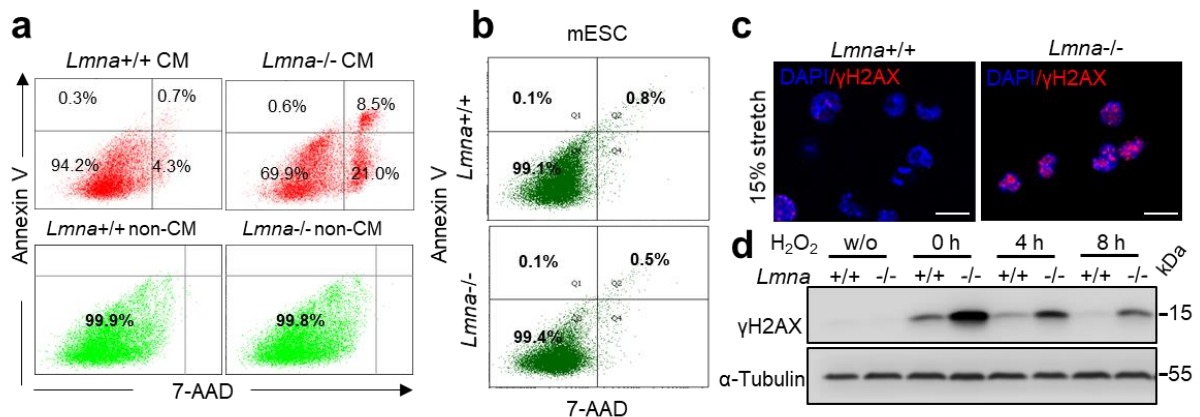


Figure 60. Loss of *Lmna* leads to CMs specific cell death. **a** Representative FACS analysis of CMs and non-CMs (n=3) in d10 EBs stained with Annexin V-APC and 7-AAD, showing an increase of early-stage apoptotic cells (Annexin V positive; 7-AAD negative), late-stage apoptotic cells (Annexin V positive; 7-AAD positive) and dead cells (7-AAD positive) in *Lmna*^{-/-} CMs. **b** Representative FACS analysis of mESCs stained with Annexin V-APC and 7-AAD. **c** Immunostaining for γ H2AX (red) and DAPI (blue) of *Lmna*^{+/+} and *Lmna*^{-/-} mESCs subjected to mechanical stretch (15% elongation). **d** Western blot analysis for γ H2AX of extracts from *Lmna*^{+/+} and *Lmna*^{-/-} mESCs either not treated (w/o) or treated with H₂O₂ (0h) and allowed to recover in fresh medium for 4h and 8h. Scale bars, 10 μ m.

3.9 *Gata4* activation upon *Lmna* loss leads to aberrant cardiac development

3.9.1 Transient knockdown of *Gata4* in *Lmna*^{-/-} mESC rescues *Lmna*^{-/-} phenotype

My results showed a significant upregulation of key cardiac TFs such as *Gata4* and significant enrichment of *Gata4* motifs at genes showing increase in chromatin accessibility upon lamin A/C loss. To investigate whether *Gata4* upregulation might be responsible for aberrant cardiovascular cell fate choices and precocious CM differentiation upon lamin A/C loss, I decreased *Gata4* levels by siRNA mediated *Gata4* silencing to transiently downregulate *Gata4* in mESCs shortly before differentiation (Fig. 61a, 61b). I observed pronounced rescue of the *Lmna*^{-/-} phenotype, i.e. a significant decrease of key cardiac TFs and reduced expression of CM marker genes as well as cardiomyocytes numbers (Fig. 61b-61d).

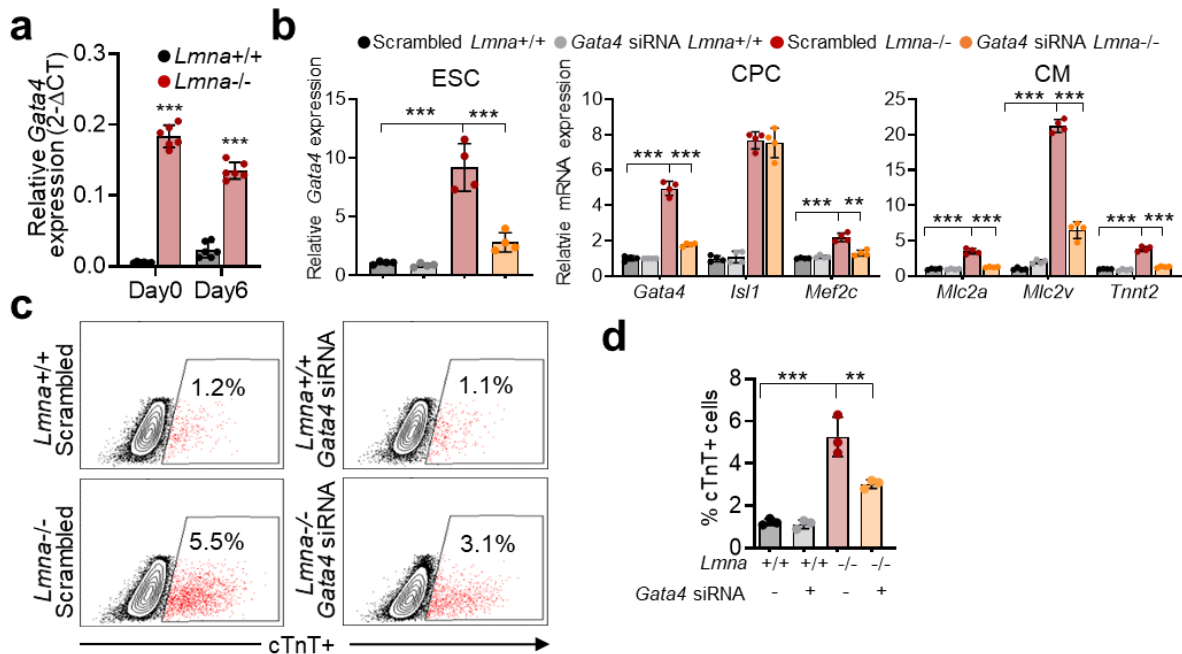


Figure 61. Rescue *Lmna*^{-/-} phenotype by transient knockdown of *Gata4* in *Lmna*^{-/-} mESC. **a** Relative *Gata4* mRNA expression in *Lmna*^{+/+} and *Lmna*^{-/-} ESCs and CPs (n=6). **b** Relative mRNA expression of *Gata4* in mESCs (left), cardiac progenitor marker genes in day 6 EBs (CP stage, middle), and cardiomyocyte marker genes in day 10 EBs (CM stage, right) after transient knockdown of *Gata4* by siRNA at the mESC stage. Data are represented as mean \pm SD, n=4, one-way ANOVA comparisons were used. **c** Representative FACS plots of cTnT⁺ CMs measured in day 10 EBs differentiated after transient knockdown of *Gata4* by siRNA in ESCs. **d** Percentage of cTnT⁺ CMs measured by flow cytometry at day 10 of differentiation after transient knockdown of *Gata4* by siRNA in mESCs. Data are represented as mean \pm SD, n=3, One-way ANOVA comparisons were used.

3.9.2 Rescue *Lmna*^{-/-} phenotype by stable knockdown of *Gata4* in *Lmna*^{-/-} mESC

To further confirm *Gata4* upregulation might be responsible for aberrant cardiovascular cell fate choices, I generated *Gata4* shRNA mediated stable knockdown mESC cell line by carefully titration to reduce *Gata4* expression back to control levels in CPs (Fig. 62). Similar to transient knockdown *Gata4* at mESC stage, stable knockdown *Gata4* during cardiomyocytes differentiation significantly rescued the precious cardiomyocytes differentiation upon *Lmna* loss (Fig. 62).

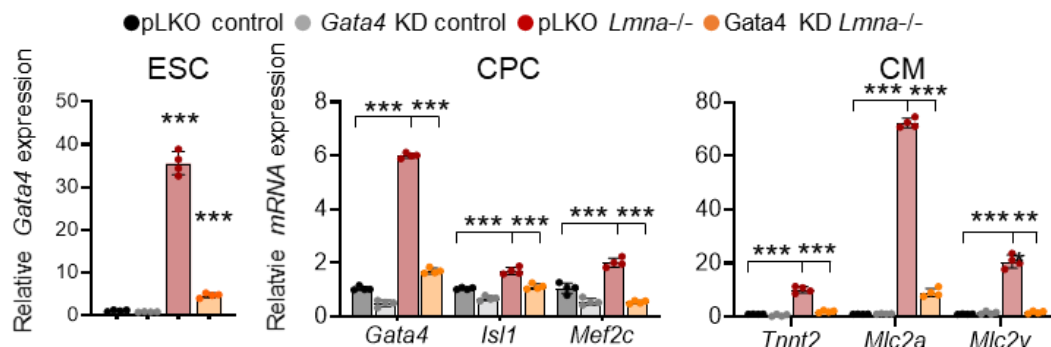


Figure 62. Rescue *Lmna*^{-/-} phenotype by stable knockdown of *Gata4* in *Lmna*^{-/-} mESC. Relative mRNA expression of *Gata4* in mESCs (left), cardiac progenitor marker genes in d6 EBs (CP stage, middle), and CM marker genes in day 10 EBs (CM stage, right) after stable knockdown of *Gata4* by shRNA in mESCs. Data are represented as mean \pm SD, n=4, one-way ANOVA comparisons were used.

3.9.3 Rescue *Lmna*^{-/-} phenotype by ablation of one *Gata4* allele in *Lmna*^{-/-} mESC

Lastly, I generated *Gata4*^{+/-}*Lmna*^{-/-} mESC cell line by ablation of one *Gata4* allele to reduce its expression (Fig. 63a). I detected a significant decrease of CM numbers and an increase of ECs in differentiating *Gata4*-depleted *Lmna*^{-/-} mESCs compared to *Lmna*^{-/-} mESCs (Fig. 63b-63d), demonstrating that decreasing *Gata4* levels rescues the aberrant cardiovascular choices and premature CM differentiation observed upon lamin A/C ablation. These data are consistent with a previous study showing that GATA4 promotes CM and represses the alternative endothelial/endocardial gene expression (Ang, Rivas et al. 2016).

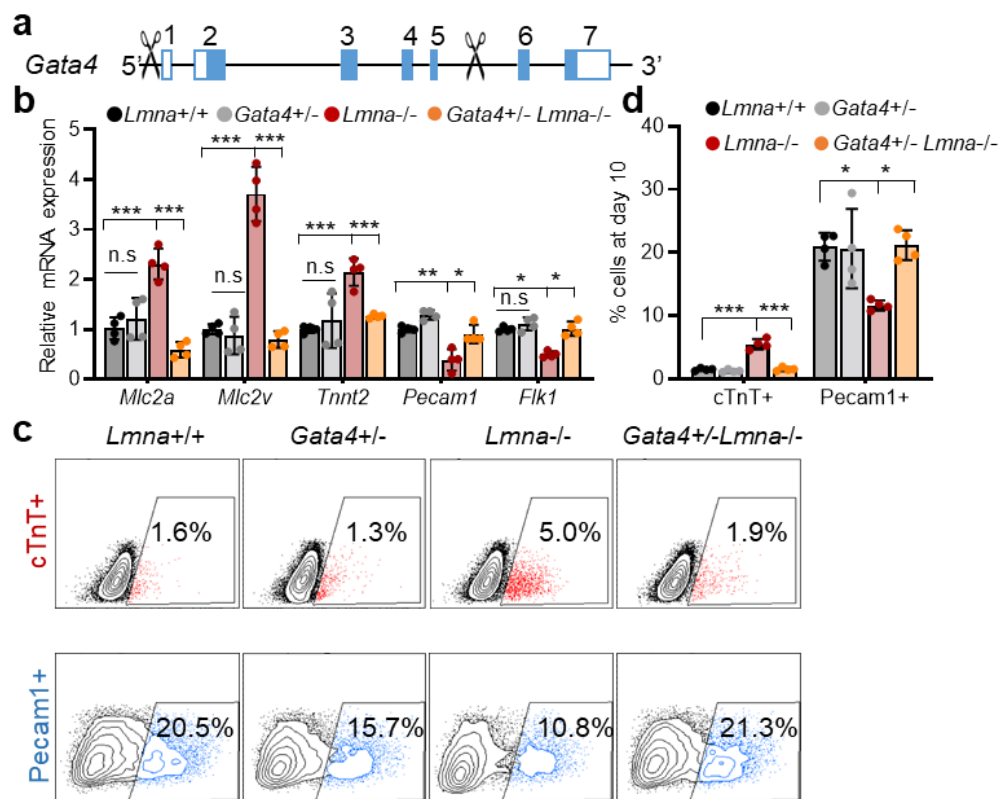


Figure 63. Rescue *Lmna*^{-/-} phenotype by ablation of one *Gata4* allele in *Lmna*^{-/-} mESC. **a** Schematic diagram of *Gata4*^{+/-} mESC generation by CRISPR/Cas9-mediated gene editing. **b** Relative mRNA expression of CM (*Mlc2a*, *Mlc2v*, and *Tnnt2*) and EC (*Pecam1* and *Flk1*) marker genes in day 10 EBs. Data are represented as mean ± SD, n=4, one-way ANOVA comparisons were used. **c** Percentage of cTnT⁺ CMs and Pecam1⁺ ECs measured by flow cytometry at day 10. Data are represented as mean ± SD, n=3, one-way ANOVA comparisons were used. **d** Representative FACS plots of cTnT⁺ CMs and Pecam1⁺ ECs in d10 EBs.

3.9.4 Ablation of one *Gata4* allele rescues *Lmna*^{+/-} and *Lmna*^{-/-} mice capillary density

I next corroborated my findings in vivo using CMV-Cre mediated germline *Gata4* ablation, to delete one functional *Gata4* allele in wild-type, *Lmna*^{+/-} and *Lmna*^{-/-} mice. Indeed, *Gata4*^{+/-}*Lmna*^{-/-} P1 mice had similar heart weight/body weight (HW/BW) to wild-type mice in contrast to *Gata4*^{+/+}*Lmna*^{-/-} P1 mice that showed significantly higher HW/BW (Fig. 64a). Moreover, I observed a pronounced rescue of the decreased capillary density in hearts from both *Gata4*^{+/-}*Lmna*^{+/-} and *Gata4*^{+/-}*Lmna*^{-/-} compared to *Lmna*^{+/-} and *Lmna*^{-/-} (Fig. 64b). In contrast, CMs

size in cross sections did not change (Fig. 64c), suggesting *Gata4* is responsible for the decreased EC number but not for decreased CM size in *Lmna* mutant mice.

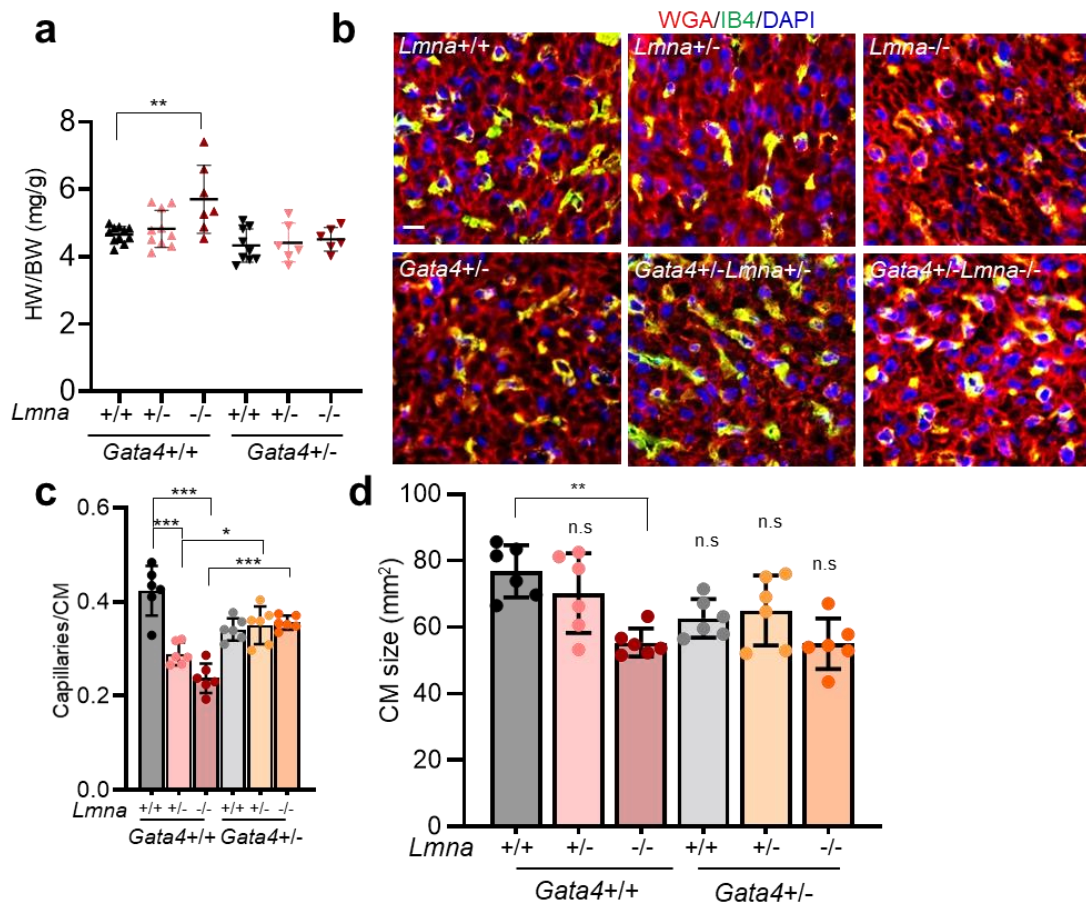


Figure 64. Ablation of one *Gata4* allele rescues *Lmna*^{+/-} and *Lmna*^{-/-} mice capillary density. **a** Heart weight to body weight ratio (HW/BW) of *Lmna*^{+/+} (n=11), *Lmna*^{+/-} (n=10), *Lmna*^{-/-} (n=7), *Gata4*^{+/-} (n=9), *Lmna*^{+/-}*Gata4*^{+/-} (n=6) and *Lmna*^{-/-}*Gata4*^{+/-} (n=6) mice at P1. **b** Immunofluorescence staining of heart sections for isolectin B4 (IB4, blood vessels), wheat germ agglutinin (WGA, CMs) together with DAPI at P1. Scale bars, 10 μ m. **c** Quantification of the capillaries/CM ratio. **d** Quantification of CM cross-sectional area in P1 mouse hearts with the indicated genotypes (n=6). Data are represented as mean \pm SD, n=6 mice for each group, one-way ANOVA comparisons were used.

3.9.5 Ablation of one *Gata4* allele rescues *Lmna*^{+/-} and *Lmna*^{-/-} CMs proliferation in vivo

Since the premature CM differentiation and binucleation resulted in CM cell cycle withdraw, I next studied whether deletion of one *Gata4* allele is sufficient to rescue the CM proliferation of *Lmna* mutant CMs and decrease CM binucleation. Indeed, I observed a rescue of the reduced CMs proliferation and precocious CMs binucleation in *Gata4*^{+/-}*Lmna*^{-/-} compared to *Lmna*^{-/-} mice (Fig. 65a-65c), supporting a key role of *Gata4* upregulation in cardiac laminopathies.

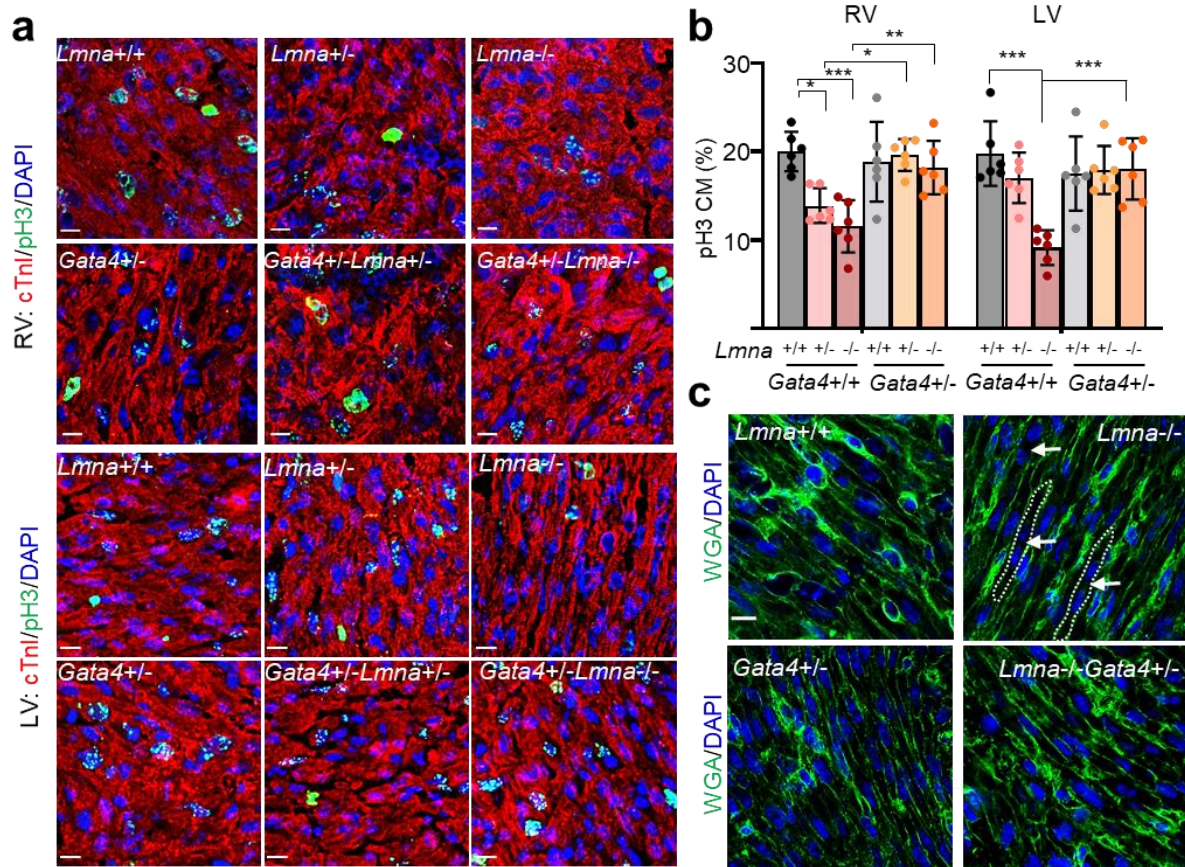


Figure 65. Ablation of one *Gata4* allele rescues *Lmna*^{+/-} and *Lmna*^{-/-} CMs proliferation in vivo. **a-b** Immunostaining of heart sections for the mitotic marker phospho-histone H3 (Ser10) (green), cardiac troponin I (red) and nucleus (DAPI, blue) at P1 (left) and quantification of the percentage of mitotic RV and LV cardiomyocytes at P1 (right). **c** Immunostaining of heart sections with wheat germ agglutinin (WGA, red) and DAPI (nucleus, blue). Binucleated cardiomyocytes are indicated with arrows. Scale bars, 10 μ m. Data are represented as mean \pm SD, n=6 mice for each group 4, one-way ANOVA comparisons were used. Scale bars, 10 μ m.

3.10 Working Model: key function of lamin A/C in naïve pluripotent stem cells for cardiac development and disease

Mutations of *LMNA* are associated with dilated cardiomyopathy and several pathogenic *LMNA* variants have also been identified linked with left ventricular non-compaction cardiomyopathy. Molecular mechanisms underlying the origin and development of the pathology are poorly understood. Here I show that lamin A/C plays a key role in chromatin organization in embryonic stem cells (ESCs), which safeguards naïve pluripotency and ensures proper cell fate choices during cardiogenesis. I report changes in chromatin compaction and localization of cardiac genes in *Lmna*^{-/-} ESCs resulting in precocious activation of a transcriptional program promoting cardiomyocyte versus endothelial cell fate. This is accompanied by premature cardiomyocyte differentiation, binucleation, cell cycle withdrawal and abnormal contractility. Importantly, I found early embryonic heart defects upon *Lmna* LOF, pointing to a primary and developmental origin of the non-compaction cardiomyopathy as a result of *Lmna* LOF. *Gata4* is activated by lamin A/C loss and *Gata4* silencing or haploinsufficiency rescues the aberrant cardiovascular cell fate choices induced by lamin A/C deficiency. In addition, I uncover divergent functions

of lamin A/C in naïve pluripotent stem cells and cardiomyocytes, which have distinct contributions to the transcriptional alterations of patients with *LMNA*-associated cardiomyopathy. I conclude that disruption of lamin A/C-dependent chromatin architecture in ESCs is a primary event in *LMNA* loss-of-function cardiomyopathy.

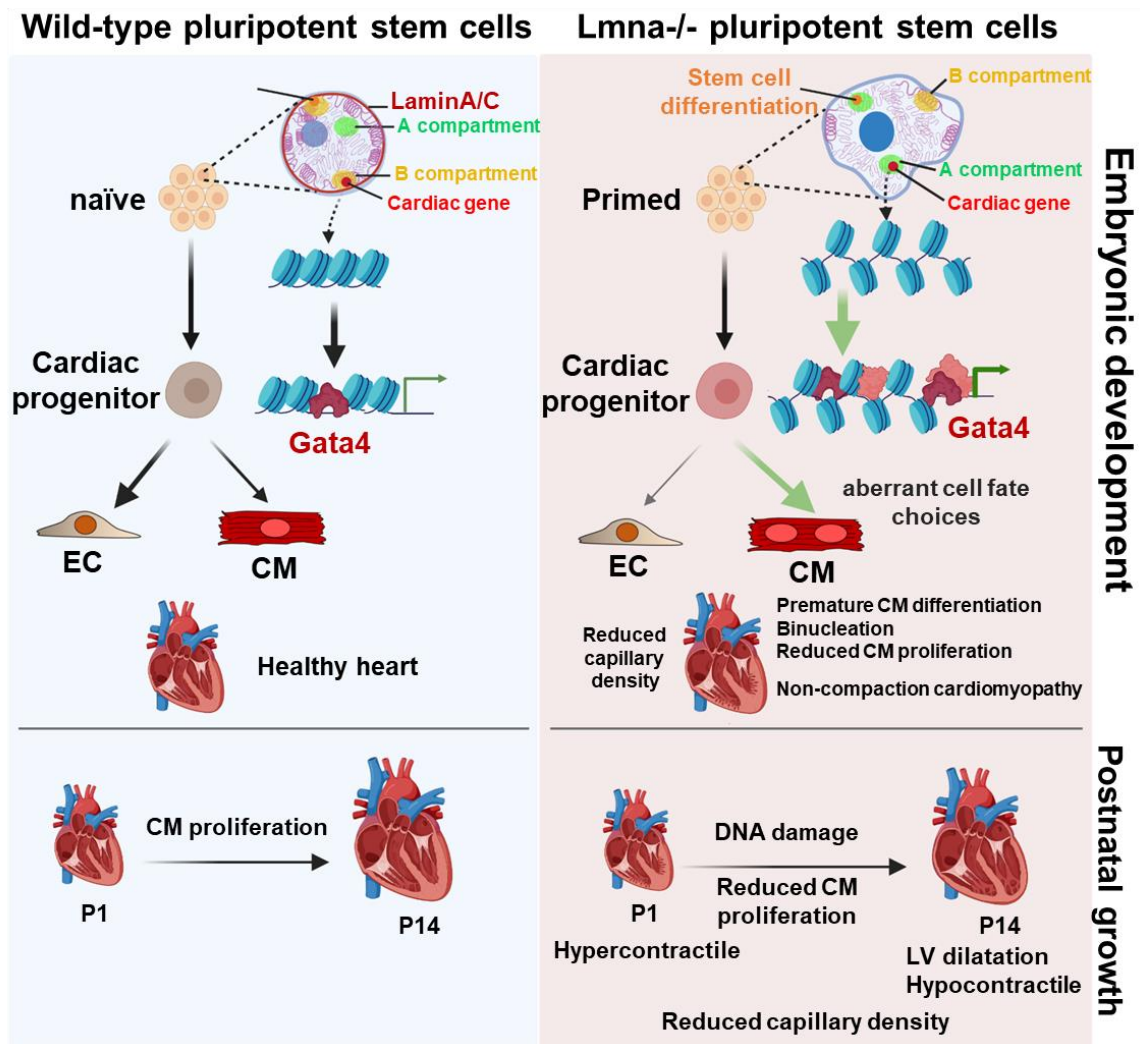


Figure 66. Key function of lamin A/C in naïve pluripotent stem cells for cardiac development and disease. In naïve pluripotent stem cells, lamin A/C tethers cardiac-specific genes and genes involved in stem cell differentiation to the repressive nuclear periphery. Lamin A/C loss leads to their dissociation from the nuclear lamina accompanied by major chromatin reorganization resulting in either ectopic expression in mESCs (e.g. *Gata4*, *Myf4*) or epigenetic priming for activation later in development. These changes lead to precocious activation of a gene expression program promoting cardiomyocyte versus endothelial cell fate, accompanied by premature cardiomyocyte differentiation, cell cycle withdrawal and abnormal contractility, which is dependent on *Gata4*.

4 DISCUSSION

4.1 LaminA/C plays a key role in alternative cardiovascular cell fate choices

Tight control of cell fate choices is crucial for normal development. Investigations have shown that nuclear lamina play a key role in gene repression and chromatin-nuclear lamina dynamics determine cellular identity by “locking” or “unlocking” genes at the nuclear periphery (Peric-Hupkes, Meuleman et al. 2010). Although most LADs seem to be conserved between cell types, a portion of chromatin nuclear lamina interactions only exist in certain cell types (Peric-Hupkes, Meuleman et al. 2010, Meuleman, Peric-Hupkes et al. 2013). For example, during mouse embryonic stem cell (ESC) differentiation into astrocytes (ACs), LADs which are specific to astrocytes are reorganized. This reorganization, on one hand, facilitates the detachment of the ACs genes from the ESCs LADs and involves ACs gene activation. On the other, a substantial number of genes are not immediately activated upon detachment from the nuclear lamina but rather become unlocked for activation at a later stage (Peric-Hupkes, Meuleman et al. 2010). During adipocytes differentiation, proadipogenic gene promoters are released from lamin A/C after differentiation into adipocytes, whereas many nonadipogenic, lineage-specific promoters retain lamin association (Lund, Oldenburg et al. 2013). In addition, release of lamin A/C from genes directly involved in glycolysis concurs with their transcriptional up-regulation after adipogenic induction, and with downstream elevations in H2BS112GlcNAc levels and O-GlcNAc cycling (Rønningen, Shah et al. 2015). Intriguingly, similar mechanism also occurs during cardiomyocytes differentiation. Hdac3 directly represses cardiac differentiation through tethering of cardiomyocyte genes to the nuclear lamina. Loss of Hdac3 in cardiac progenitor cells releases genomic regions from the nuclear periphery, leading to precocious cardiac gene expression and differentiation (Poleshko, Shah et al. 2017). Thus, dysregulated gene expression caused by genomic reorganization of LADs in cardiomyocytes has emerged as a plausible mechanism.

My work revealed that lamin A/C play a key role of in keeping CM lineage-specific genes in naïve pluripotent stem cells silent, thus preventing epigenetic priming and aberrant cardiovascular cell fate choices during development. Loss of lamin A/C promoted CM and repressed EC fate, as a result of activation of the key cardiac TF *Gata4* and precocious induction of a CM-specific gene expression program, as I demonstrated in my PhD thesis using a combination of in vitro and in vivo model systems (Wang, Elsherbiny et al. 2022, Wang and Dobrova 2023).

In contrast to lamin A/C deficiency, ESC lines harboring the *Lmna* p.H222P mutation, causing Emery-Dreifuss muscular dystrophy and cardiomyopathy (Arimura, Helbling-Leclerc et al. 2005), showed different differentiation behaviour (Guenantin, Jebeniani et al. 2021). Significantly decreased expression of cardiac mesoderm marker *Mesp1*, as well as cardiomyocytes

marker were observed in *Lmna* H222P/+ mESC lines (Guenantin, Jebeniani et al. 2021), suggesting that the molecular mechanisms resulting in heart disease as a result of distinct point mutation in the *Lmna* gene are different. Interestingly, patients harbouring distinct mutations in *LMNA* can develop a number of different tissue-specific syndromes collectively termed laminopathies, such as cardiomyopathy, muscular dystrophy, lipodystrophy syndromes, aging disorders and peripheral nerve disorders. How specific pathogenic *LMNA* mutations results in alternative fate choices and tissue-specific phenotypes would also be interesting for further study.

The nuclear lamina consists of two separate classes of lamins, A-type and B-type lamins. In contrast to lamin A/C deficiency or mutation, ablation of lamin B1 in mESCs did not largely affect CM differentiation, suggesting that lamin A/C rather than lamin B1 plays a key role in cardiac lineage restriction. Functionally, A-type and B-type lamins form distinct meshworks (Shimi, Pflieger et al. 2008) and while lamins B1 and B2 are localized at the periphery and associate mainly with transcriptionally inactive chromatin (Reddy, Zullo et al. 2008, Wen, Wu et al. 2009), lamins A and C are found at the nuclear periphery and in the nuclear interior and associate with both hetero- and euchromatin (Gesson, Rescheneder et al. 2016). However, the loss of A-type lamins results in alterations in B-type meshworks and vice versa, suggesting that their activity might be interconnected. In mESCs, 92% of lamin B1 LADs overlapped with lamin A LADs, whereas a large number of LADs were specific for lamin A/C. Located within LADs specifically associated with lamin A/C were genes for cardiac pioneer TFs, such as *Gata4*, *Gata6* and *Isl1* (Cirillo and Zaret 1999, Gao, Liang et al. 2019), which might explain why lamin A/C deficiency results in major defects in cardiovascular differentiation and function, whereas lamin B1 deletion does not show major effect.

4.2 3D chromatin reorganization upon *Lmna* loss

In the last years, several studies modeling *LMNA* cardiomyopathies in vitro using induced pluripotent stem cell (iPSCs)-derived CMs revealed that lamin A/C-mediated 3D chromatin architecture play an important role in cardiomyopathies. Using ATAC-seq, Lee et al. showed that K117fs mutant iPSC derived cardiomyocytes exhibit an increased open chromatin at gene promoters resided in lamin A/C LADs (Lee, Termglinchan et al. 2019). However, analysis of the 3D genome organization by Hi-C in R225x mutant CMs of another *LMNA* haploinsufficient model, which also showed contractile alterations (Bertero, Fields et al. 2019), did not detect pronounced changes in chromatin compartmentalization into open and closed states that could explain the altered transcriptional activity.

In my study, I performed both ATAC-seq and Hi-C and I observed a widespread increase in chromatin accessibility across the genome, as well as at genes upregulated upon lamin A/C

loss already in pluripotent stem cells. In contrast, there was little change in chromatin accessibility for downregulated genes. Intersection of the ATAC-Seq and RNA-Seq analysis revealed that more than half of the genes upregulated upon lamin A/C loss in ESCs showed increased chromatin accessibility. Moreover, Intersection of the ATAC-Seq with lamin A/C DamID shows 38.8% of the increased chromatin accessibility genes are within lamin A/C LADs. Moreover, 3D FISH experiments showed that the cardiac genes within lamin A/C LADs such as *Gata4*, *Isl1*, *Mef2C* and *Ttn*, relocalize from the repressive nuclear periphery to the active nuclear interior upon lamin A/C loss, suggesting loss of lamin A/C may affect the chromosome territories. Interestingly, I observed a shift of CM-specific genes from the nuclear periphery to the active nuclear interior for genes found specifically in lamin A LADs as well as for genes found in lamin A/B1 LADs, whereas *Kcnq1*, which is not found in LADs, was not affected, suggesting a role of lamin A/C in tethering cardiac genes to the repressive nuclear periphery in mESCs.

Consistent with 3D FISH results, Hi-C analysis revealed around 8% of the chromatin compartments switched from B to A and vice versa as a result of lamin A/C depletion. GO analysis of genes located in inactive B compartments that transitioned to active A compartments in *Lmna*^{-/-} mESCs were enriched for GO terms linked to calcium ion transmembrane transport, chromatin organization, muscle cell differentiation and relaxation of cardiac muscle, including genes such as *Myl4*, *Atp2a3*, *Ryr2*, *Camk2d*, etc.. Active chromatin compartments that transitioned to an inactive state were enriched for genes linked to protein phosphorylation, nervous system development, cell migration and adhesion. Chr. 14 showed the most changes with around 13% active to inactive or vice versa transitions, consistent with the large scale chromatin decompaction at this chromosome.

Further, I observed two modes of lamin A/C-mediated transcriptional control. First, lamin A/C keeps key genes involved in cell differentiation and cardiac morphogenesis silent, such as *Gata4* and *Gata6*, *Bmps*, *Fgf10*, *Wnts*, *Myl4*, etc. Upon lamin A/C depletion these genes are transcriptionally activated as a result of major changes in chromatin localization and organization. Second, lamin A/C restricts transcriptional permissiveness of chromatin at genes involved in cardiac morphogenesis and function, such as *Mef2c*, *Ryr2*, *Mybpc3*, *Lmod2*, *Neb1*, *Adrb2*, etc. Ablation of lamin A/C results in major changes of chromatin localization and structure at these genes resulting in chromatin opening, which, however, is not sufficient to elicit gene activation in ESCs. During cardiac differentiation these epigenetically primed genomic loci are easily accessible to cardiac TFs (e.g. *Gata4/6*, *Hand2*, *Meis1*, *Foxo1*, etc.), resulting in precocious activation of a gene expression program promoting CM versus EC fate, accompanied by premature CM maturation, binucleation, cell cycle withdrawal and abnormal contractility.

4.3 Role of pioneer transcription factors during cardiac development

In my study, I found lamin A/C depletion leads to significantly increased expression of pioneer cardiac transcription factors (TFs) both *in vitro* and *in vivo*. In line with the cell-culture-based phenotype, *Lmna*-deficient and haploinsufficient embryos showed increased expression of pioneer cardiac TFs such as *Gata4*, *Isl1* (Takeuchi and Bruneau 2009, Gao, Liang et al. 2019), during early cardiogenesis, increased expression of CM-specific structural and contraction genes, hypercontractility as well as precocious binucleation, decreased proliferation and non-compaction cardiomyopathy.

Gata4 represents a classical example of a pioneer factor, as it can efficiently bind to its target sequences on nucleosomal DNA (Cirillo and Zaret 1999). Overexpression of *Gata4*, *Tbx5* and the cardiac-specific component of the Brg1 chromatin complex Baf60c reprogrammed somatic into cardiac mesoderm (Takeuchi and Bruneau 2009), and combined expression of *Gata4*, *Tbx5* and *Mef2c* reprogrammed fibroblasts to a CM-like cell fate (Ieda, Fu et al. 2010). Furthermore, GATA4 has been shown to be a critical regulator of cardiac versus EC fate of cardiovascular progenitors (Ang, Rivas et al. 2016) and *Gata4* silencing rescued the aberrant cardiovascular cell fate and differentiation of *Lmna*^{-/-} mESCs both *in vitro* and *in vivo*, supporting a key role of *Gata4* upregulation for cardiac laminopathies. Interestingly, overexpression of *Gata4* in mESCs in serum containing medium promoted endoderm but not cardiac mesoderm fate, however overexpressing of any of the cardiac Gata factors expressed (*Gata4/5/6*) (Molkentin 2000) in serum-free conditions efficiently directed cardiac fate (Turbendian, Gordillo et al. 2013), suggesting that growth factor signaling might play an important role in controlling Gata TF functions in cardiogenesis. Thus, the activation of *Bmps*, *Fgf10* or *Wnts* in lamin A/C-deficient mESCs together with *Gata6* activation might contribute to the precocious activation of the cardiac gene program, which together with premature binding of Meis1 to chromatin can cause an early cell cycle withdrawal of lamin A/C-deficient CMs.

Interestingly, we observed more pronounced defects in the RV myocardium, which may be accounted by the different embryological origin of the RV compared to the LV myocardium (Meilhac and Buckingham 2018). The RV is formed by the second heart field (SHF) progenitor cells, marked by the expression of the pioneer TF *Isl1* (Cai, Liang et al. 2003, Gao, Liang et al. 2019), which is also found in lamin A LADs in ESCs and is significantly upregulated during early cardiogenesis upon lamin A/C loss. Interestingly, in contrast to the first heart field (FHF) progenitor cells, SHF precursors give rise to CMs and ECs (Moretti, Caron et al. 2006) and the crosstalk between these two distinct heart cell types is instrumental for proper cardiac development and myocardial compaction (Tian and Morrisey 2012), suggesting that abnormal cardiovascular cell fate choices and dysfunctional endothelium might play a role in *LMNA* LOF cardiomyopathy.

4.4 Cardiac defects in lamin A/C loss of function cardiomyopathy

In the past decade, large numbers of investigations have shown the phenotypes, molecular mechanisms and treatments for cardiomyopathies caused by different mutations. However, all these studies focus on the postnatal stage. Molecular mechanism underlying the origin and development of the pathology is largely unexplored yet. In this study, I showed *Lmna* loss results in non-compaction cardiomyopathy with preserved ejection fraction during embryonic development. Interestingly, another recent study also shows a developmental origin of *LMNA* associated cardiomyopathy. Guenantin et al. discovered that *Lmna* H222P/H222P embryonic hearts show hypertrabeculation, interventricular septum defect and enlarged atria during development, and decreased heart function at as early as E13.5 (Guenantin, Jebeniani et al. 2021). Moreover, *Lmna* H222P/H222P embryos also display higher rates of lethality compared with normal or heterozygous controls. Using *Lmna* H222P/+ mouse ESCs, the author shows that cardiac mesoderm marker *Mesp1* as well as *Snai1* and *Twist* which are involved in epithelial-to-mesenchymal transition of epiblast cells was decreased and cardiac mesoderm specification and cardiomyocytes differentiation were impaired (Guenantin, Jebeniani et al. 2021). This is in stark contrast to *Lmna*^{+/-} and *Lmna*^{-/-} mESCs, which showed premature CM differentiation. Since Lamin A/C was expressed in mESC cells and dramatically decreased with the exit from pluripotency and absent in mesoderm. There is a possibility that the mesoderm defects during *Lmna* H222P/+ mESC differentiation are due to LADs reorganization and the unable activation of these genes in mESC. Furthermore, ascertaining whether other *LMNA* mutations have an impaired heart development and act through the same pathways will be a critical next step.

During embryonic stage and at birth, *Lmna*-null mice showed increased ejection fraction and fractional shortening. Two weeks after birth heart function was significantly decreased in *Lmna*-deficient and haploinsufficient mice and the left ventricle was dilated, consistent with the clinical phenotype. The sharp contrast to the observations directly after birth is most likely due to the increased cell death specifically in lamin A/C-deficient CMs and to the decreased CM proliferation in the immediate postnatal window (P1-P7), which may be connected to the epigenetic priming at *Meis1* and *Foxo1* binding sites. *Meis1* regulates postnatal CM cell cycle arrest (Mahmoud, Kocabas et al. 2013) whereas *FoxO* proteins are key regulators of apoptosis (van der Horst and Burgering 2007) and were shown to be activated and to contribute to the pathogenesis of cardiac laminopathies (Auguste, Gurha et al. 2018). In addition, the premature cell cycle arrest and elevated cell death could be due to the inability of *Lmna*^{-/-} CMs to respond adequately to oxidative and mechanical stress. Indeed, mechanosensing by the nuclear lamina have been shown to protect against nuclear rupture, DNA damage, and cell-cycle withdrawal, while the oxygen-rich postnatal environment was proposed to induce cell-cycle arrest through the DNA damage response pathway (Puente, Kimura et al. 2014, Cho, Vashisth et al. 2019).

Interestingly, we observed increased DNA damage and cell death in *Lmna*^{-/-} non-CMs subjected to stretch and oxidative stress, suggesting that activation of the DNA damage pathway might contribute to the premature cell cycle arrest and increased cell death upon lamin A/C LOF. Importantly, during embryogenesis the RV and the LV eject blood at a high pressure into the systemic circulation as blood shunts through the ductus arteriosus and foramen ovale, while after birth the pulmonary circulation is a low-pressure circuit. Thus, the differences observed in RV and LV function during embryogenesis and after birth might be due to the important function of lamin A/C in mechanosensing and response.

4.5 Endothelial cell dysfunction in lamin A/C LOF cardiomyopathy

The crosstalk between endothelial cells and cardiomyocytes is crucial for cardiac development and postnatal heart function. Two main subtype of endothelial cells exist in mammalian heart: endocardial cells and coronary endothelial cells. During heart development cardiac progenitors from the mesodermal primitive streak differentiate into a cardiac crescent, then form a linear heart tube. The heart tube consists of an outer myocardial layer and an inner endocardial layer, and these two layers are separated by an acellular extracellular matrix (ECM) layer called the cardiac jelly (Harvey 2002). Endocardial cells are one of the earliest endothelial populations acquired in development and are identified by expression of *Nfatc1*, *Npr3* and *Cyt11* (de La Pompa, Timmerman et al. 1998, Misfeldt, Boyle et al. 2009). Whereas, endothelial cells of coronary vessels arise later in development and form coronary vessels in the myocardium, providing oxygen and nutrients to parenchymal cells and removing waste products (Lavine and Ornitz 2009). Markers expressed by coronary endothelial cells include *Apln*, *Fabp4* and *CD36*. Moreover, both capillary and endocardial ECs are in close proximity to CMs and provide multiple autocrine and paracrine signals controlling CMs proliferation (Rhee, Paik et al. 2021), maturation (Rhee, Paik et al. 2021), contraction, hypertrophy (Accornero, Van Berlo et al. 2011, Kivelä, Hemanthakumar et al. 2019) and metabolism (Wan and Rodrigues 2016).

Although numerous of studies have shown cardiomyocytes dysfunction in *LMNA* associated cardiomyopathies, the role of endothelium in these diseases, especially during early development, remains largely unexplored. A recent study have suggested that vascular dysfunction mediated through *KLF2* may contribute to the pathogenesis of *LMNA*-related DCM (Sayed, Liu et al. 2020). In my PhD work, I showed *Lmna*^{-/-} and *Lmna*^{+/-} mice not only exhibit a reduced capillary density but also an excessive trabeculations during early heart development. The abnormal function of endocardial or development of the coronary endothelium and improper crosstalk between endocardium and myocardium have been shown linked with left ventricular non-compaction cardiomyopathy phenotype (Rhee, Chung et al. 2018, Rhee, Paik et al. 2021). Thus it would be interesting to address whether endocardial/coronary EC dysfunction contributes to *LMNA* associated noncompaction cardiomyopathy. Moreover, it has been shown that

endocardium contribute to most of coronary vessels (Wu, Zhang et al. 2012), and abnormal endocardial to coronary endothelial transformation leads to pathophysiological process of congenital and postnatal heart diseases involving cardiac morphogenesis, valve disorders, coronary malformations, and cardiomyopathy. Hence, it would also be possible that the reduced capillary density in *Lmna* knockout mice is due to the defects of the endocardial transformation. Moreover, endocardium also gives rise to mesenchymal cells that subsequently expand, migrate along ventricular walls, and contribute to pericytes, SMCs, fibroblasts, intramyocardial adipocytes as well as hematopoietic cells (Zhang, Lui et al. 2018). Defects or abnormal of endocardium lineage differentiation would also affect other cell types and lead to heart disease. Thus, exploring the role of endothelium in *LMNA* associated cardiomyopathies has just begun.

4.6 Distinct role of lamin A/C in pluripotent stem cells and committed CMs

Importantly, I observed different epigenetic and transcriptional alterations upon lamin A/C depletion in naïve pluripotent stem cells or specifically in CMs. Both of these contributed to the transcriptional changes detected in patients with *LMNA*-associated DCM mutations, suggesting distinct functions of lamin A/C-dependent chromatin architecture in committed versus uncommitted cells for cardiac development and disease. Motif enrichment analysis within chromatin regions of genes upregulated upon lamin A/C LOF and characterized with more open chromatin in mESC vs CMs identified common and cell type specific binding motifs, consistent with the functional changes observed in lamin A/C-deficient mESC or CMs. Identifying the factors that mediate such distinct chromatin organization in mESC and CM will be an interesting line of research in the future. It has been long thought that while B-type lamins are expressed throughout development, A-type lamins are expressed only highly after commitment of cells to a particular differentiation pathway. However, my data clearly demonstrate that lamin A/C is not only expressed in naïve pluripotent stem cells but also plays essential role in naïve pluripotency maintenance and establishment and in preventing precocious CM differentiation. Interestingly, lamin A/C protein levels dramatically decreased with the exit from pluripotency and were only high again in CMs, suggesting that lack of lamin A/C provides a window of opportunity for stem cells to acquire specific fate.

Another study using an iPSC model harboring the T10I mutation in *LMNA* suggested a role of the nuclear lamina in safeguarding cellular identity for committed cells (Shah, Lv et al. 2021). In T10I iPSC-CMs, the peripheral heterochromatin enriched for non-myocyte lineage genes was disrupted, resulting in the activation of alternative cell fate genes. Upregulation of non-cardiac genes was also observed in iPSC-CMs carrying the R225X mutation in lamin A/C. Importantly, *CACNA1A*, encoding a neuronal P/Q-type calcium channel, was upregulated, and pharmacological inhibition partially rescued the altered electrophysiological properties of R225X iPSC-CMs (Bertero, Fields et al. 2019). In this context, it is important to note that in

contrast to mouse/human blastocysts and naïve mouse mESCs, hiPSCs cultured in standard conditions represent a primed state and do not express detectable levels of lamin A/C protein (Wang, Elsherbiny et al. 2022). Since lamin A/C plays an important role in chromatin organization in naïve pluripotent stem cells, which is essential for normal cardiogenesis, some important aspects of lamin A/C function cannot be modeled using hiPSCs and requires studies using naïve hiPSCs carrying *LMNA* mutations. Overall, my study showed a distinct role of lamin A/C in pluripotent stem cells and differentiated cells.

5 SUMMARY

In my PhD work, I studied how chromatin tethering to the nuclear lamina controls cardiovascular cell fate choices, development and function. I found that ablation of lamin A/C rather than lamin B1 in mouse embryonic stem cells (mESCs) results in precocious activation of a transcriptional program promoting cardiomyocyte versus endothelial cell fate. This was accompanied by premature cardiomyocyte differentiation, cell cycle withdrawal and abnormal contractility. I next corroborated my findings *in vivo* using *Lmna*^{+/+} (control), *Lmna*^{+/-} and *Lmna*^{-/-} mice. Expression analysis revealed significant upregulation of cardiac progenitor and cardiomyocyte marker genes in dissected pharyngeal mesoderm and hearts of E8.5 embryos as well as E9.5 hearts upon *Lmna* ablation consistent with my *in vitro* cell culture-based studies. Histological examination unveiled non-compaction cardiomyopathy in both *Lmna*^{+/-} and *Lmna*^{-/-} embryos. Further, I also found precocious CM differentiation and premature binucleation coupled to CM cell cycle withdrawal during fetal heart development.

Using a combination of RNA-seq, ATAC-seq, Hi-C and 3D FISH, I next studied the effect of lamin A/C loss on the three-dimensional (3D) chromatin organization and gene expression. ATAC-seq revealed a widespread increase in chromatin accessibility across the genome, as well as at genes upregulated upon lamin A/C loss already in pluripotent stem cells. Moreover, Hi-C and 3D FISH experiments showed that around 8% of chromatin compartments switched from active A to inactive B compartments and vice versa as a result of lamin A/C depletion and were highly associated with lamina-associated domains (LADs). Cardiac genes within lamin A/C LADs such as *Gata4*, *Isl1*, *Mef2c* and *Ttn* relocalized from the repressive nuclear periphery to the active nuclear interior upon lamin A/C loss of function. Importantly, *Gata4* was activated by lamin A/C loss and *Gata4* silencing or haploinsufficiency rescued the aberrant cardiovascular cell fate choices induced by lamin A/C deficiency.

In addition, I uncovered divergent functions of lamin A/C in naïve pluripotent stem cells and cardiomyocytes, which have distinct contributions to the transcriptional alterations of patients with LMNA-associated cardiomyopathy. In naïve pluripotent stem cells, lamin A/C keeps cell differentiation and cardiac morphogenesis genes silent, such as *Gata4/6*, *Bmps*, *Ryr2*, *Wnts*, *Myl4*, etc. Upon lamin A/C LOF, these genes are ectopically expressed in mESCs or later stage. Whereas, in CMs lamin A/C specifically regulates genes involved in cardiac contraction and sarcomere organization.

In summary, my results showed that epigenetic alterations in ESCs play a crucial role in LMNA-related cardiomyopathies and disruption of lamin A/C-dependent chromatin architecture in ESCs is a primary event in LMNA loss-of-function cardiomyopathy.

Still, an important question remains: how do different and specific LMNA mutations result in phenotypic diversity? Environmental factors, such as diet, exercise, and stress, as well as age,

sex, and other comorbidities, might also contribute to the phenotypic variability in patients with pathogenic LMNA mutations. Identifying cell-type-specific interacting partners for nuclear lamins and the effect of lamin mutations on these interactions would also be important in understanding the wide-ranging clinical phenotypes and may pinpoint druggable protein–protein interfaces for therapeutic applications. Given the important role of lamin A/C in heart development and CM differentiation, developmental changes in asymptomatic-at-birth LMNA patients might result in late changes in heart structure and function, warranting further investigation.

6 REFERENCES

- Accornero, F., J. H. Van Berlo, M. J. Benard, J. N. Lorenz, P. Carmeliet and J. D. Molkentin (2011). "Placental growth factor regulates cardiac adaptation and hypertrophy through a paracrine mechanism." *Circulation research* **109**(3): 272-280.
- Alcalá-Vida, R., M. Garcia-Forn, C. Castany-Pladevall, J. Creus-Muncunill, Y. Ito, E. Blanco, A. Golbano, K. Crespí-Vázquez, A. Parry and G. Slater (2021). "Neuron type-specific increase in lamin B1 contributes to nuclear dysfunction in Huntington's disease." *EMBO molecular medicine* **13**(2): e12105.
- Amendola, M. and B. van Steensel (2015). "Nuclear lamins are not required for lamina-associated domain organization in mouse embryonic stem cells." *EMBO Rep* **16**(5): 610-617.
- Andres, V. and J. M. Gonzalez (2009). "Role of A-type lamins in signaling, transcription, and chromatin organization." *J Cell Biol* **187**(7): 945-957.
- Ang, Y.-S., R. N. Rivas, A. J. Ribeiro, R. Srivas, J. Rivera, N. R. Stone, K. Pratt, T. M. Mohamed, J.-D. Fu and C. I. Spencer (2016). "Disease model of GATA4 mutation reveals transcription factor cooperativity in human cardiogenesis." *Cell* **167**(7): 1734-1749. e1722.
- Arimura, T., A. Helbling-Leclerc, C. Massart, S. Varnous, F. Niel, E. Lacene, Y. Fromes, M. Toussaint, A.-M. Mura and D. I. Keller (2005). "Mouse model carrying H222P-Lmna mutation develops muscular dystrophy and dilated cardiomyopathy similar to human striated muscle laminopathies." *Human molecular genetics* **14**(1): 155-169.
- Auguste, G., P. Gurha, R. Lombardi, C. Coarfa, J. T. Willerson and A. J. Marian (2018). "Suppression of Activated FOXO Transcription Factors in the Heart Prolongs Survival in a Mouse Model of Laminopathies." *Circ Res* **122**(5): 678-692.
- Auguste, G., L. Rouhi, S. J. Matkovich, C. Coarfa and A. J. Marian (2020). "BET bromodomain inhibition attenuates cardiac phenotype in myocyte-specific Lamin A/C-deficient mice." *The Journal of clinical investigation* **130**(9).
- Austin, K. M., M. A. Trembley, S. F. Chandler, S. P. Sanders, J. E. Saffitz, D. J. Abrams and W. T. Pu (2019). "Molecular mechanisms of arrhythmogenic cardiomyopathy." *Nature Reviews Cardiology* **16**(9): 519-537.
- Awad, M. M., D. Dalal, E. Cho, N. Amat-Alarcon, C. James, C. Tichnell, A. Tucker, S. D. Russell, D. A. Bluemke and H. C. Dietz (2006). "DSG2 mutations contribute to arrhythmogenic right ventricular dysplasia/cardiomyopathy." *The American Journal of Human Genetics* **79**(1): 136-142.
- Awad, M. M., D. Dalal, C. Tichnell, C. James, A. Tucker, T. Abraham, P. J. Spevak, H. Calkins and D. P. Judge (2006). "Recessive arrhythmogenic right ventricular dysplasia due to novel cryptic splice mutation in PKP2." *Human mutation* **27**(11): 1157-1157.
- Babicki, S., D. Arndt, A. Marcu, Y. Liang, J. R. Grant, A. Maciejewski and D. S. Wishart (2016). "Heatmapper: web-enabled heat mapping for all." *Nucleic Acids Res* **44**(W1): W147-153.
- Baldini, A., F. Fulcoli and E. Illingworth (2017). "Tbx1: transcriptional and developmental functions." *Current topics in developmental biology* **122**: 223-243.
- Banovich, N. E., Y. I. Li, A. Raj, M. C. Ward, P. Greenside, D. Calderon, P. Y. Tung, J. E. Burnett, M. Myrthil, S. M. Thomas, C. K. Burrows, I. G. Romero, B. J. Pavlovic, A. Kundaje, J. K. Pritchard and Y. Gilad (2018). "Impact of regulatory variation across human iPSCs and differentiated cells." *Genome Res* **28**(1): 122-131.
- Barascu, A., C. Le Chalony, G. Pennarun, D. Genet, N. Imam, B. Lopez and P. Bertrand (2012). "Oxidative stress induces an ATM-independent senescence pathway through p38 MAPK-mediated lamin B1 accumulation." *The EMBO journal* **31**(5): 1080-1094.
- Barnes, R. M., B. A. Firulli, S. J. Conway, J. W. Vincentz and A. B. Firulli (2010). "Analysis of the Hand1 cell lineage reveals novel contributions to cardiovascular, neural crest, extra-embryonic, and lateral mesoderm derivatives." *Developmental Dynamics* **239**(11): 3086-3097.
- Barnett, D. W., E. K. Garrison, A. R. Quinlan, M. P. Stromberg and G. T. Marth (2011). "BamTools: a C++ API and toolkit for analyzing and managing BAM files." *Bioinformatics* **27**(12): 1691-1692.

- Bartman, T. and J. Hove (2005). "Mechanics and function in heart morphogenesis." Developmental dynamics: an official publication of the American Association of Anatomists **233**(2): 373-381.
- Bedrosian, T. A., J. Houtman, J. S. Eguiguren, S. Ghassemzadeh, N. Rund, N. M. Novaresi, L. Hu, S. L. Parylak, A. M. Denli and L. Randolph-Moore (2021). "Lamin B1 decline underlies age-related loss of adult hippocampal neurogenesis." The EMBO journal **40**(3): e105819.
- Beffagna, G., G. Occhi, A. Nava, L. Vitiello, A. Ditadi, C. Basso, B. Bauce, G. Carraro, G. Thiene and J. A. Towbin (2005). "Regulatory mutations in transforming growth factor- β 3 gene cause arrhythmogenic right ventricular cardiomyopathy type 1." Cardiovascular research **65**(2): 366-373.
- Berman, B. P., D. J. Weisenberger, J. F. Aman, T. Hinoue, Z. Ramjan, Y. Liu, H. Noushmehr, C. P. Lange, C. M. van Dijk and R. A. Tollenaar (2012). "Regions of focal DNA hypermethylation and long-range hypomethylation in colorectal cancer coincide with nuclear lamina-associated domains." Nature genetics **44**(1): 40.
- Bernasconi, P., N. Carboni, G. Ricci, G. Siciliano and G. Lattanzi (2018). "Elevated TGF β 2 serum levels in Emery-Dreifuss Muscular Dystrophy: Implications for myocyte and tenocyte differentiation and fibrogenic processes." Nucleus **9**(1): 1.
- Bertero, A., P. A. Fields, V. Ramani, G. Bonora, G. G. Yardimci, H. Reinecke, L. Pabon, W. S. Noble, J. Shendure and C. E. Murry (2019). "Dynamics of genome reorganization during human cardiogenesis reveal an RBM20-dependent splicing factory." Nature communications **10**(1): 1-19.
- Bertero, A., P. A. Fields, A. S. Smith, A. Leonard, K. Beussman, N. J. Sniadecki, D.-H. Kim, H.-F. Tse, L. Pabon and J. Shendure (2019). "Chromatin compartment dynamics in a haploinsufficient model of cardiac laminopathy." Journal of Cell Biology **218**(9): 2919-2944.
- Bertrand, A. T., L. Renou, A. Papadopoulos, M. Beuvin, E. Lacène, C. Massart, C. Ottolenghi, V. Decostre, S. Maron, S. Schlossarek, M.-E. Cattin, L. Carrier, M. Malissen, T. Arimura and G. Bonne (2012). "DelK32-lamin A/C has abnormal location and induces incomplete tissue maturation and severe metabolic defects leading to premature death." Human molecular genetics **21**(5): 1037-1048.
- Bhattacharyya, S., V. Chandra, P. Vijayanand and F. Ay (2019). "Identification of significant chromatin contacts from HiChIP data by FitHiChIP." Nat Commun **10**(1): 4221.
- Bian, Q., N. Khanna, J. Alvikas and A. S. Belmont (2013). " β -Globin cis-elements determine differential nuclear targeting through epigenetic modifications." Journal of Cell Biology **203**(5): 767-783.
- Bianchi, A., C. Mozzetta, G. Pegoli, F. Lucini, S. Valsoni, V. Rosti, C. Petrini, A. Cortesi, F. Gregoretti and L. Antonelli (2020). "Dysfunctional polycomb transcriptional repression contributes to Lamin A/C dependent muscular dystrophy." The Journal of Clinical Investigation.
- Biase, F. H., X. Cao and S. Zhong (2014). "Cell fate inclination within 2-cell and 4-cell mouse embryos revealed by single-cell RNA sequencing." Genome Res **24**(11): 1787-1796.
- Bickmore, W. A. and B. van Steensel (2013). "Genome architecture: domain organization of interphase chromosomes." Cell **152**(6): 1270-1284.
- Bidault, G., M. Garcia, M.-C. Vantyghem, P.-H. Ducluzeau, R. Morichon, K. Thiyagarajah, S. Moritz, J. Capeau, C. Vigouroux and V. Bérézziat (2013). "Lipodystrophy-linked LMNA p. R482W mutation induces clinical early atherosclerosis and in vitro endothelial dysfunction." Arteriosclerosis, Thrombosis, and Vascular Biology **33**(9): 2162-2171.
- Bin Imtiaz, M. K., B. N. Jaeger, S. Bottes, R. A. Machado, M. Vidmar, D. L. Moore and S. Jessberger (2021). "Declining lamin B1 expression mediates age-dependent decreases of hippocampal stem cell activity." Cell Stem Cell **28**(5): 967-977. e968.
- Bione, S., E. Maestrini, S. Rivella, M. Mancini, S. Regis, G. Romeo and D. Toniolo (1994). "Identification of a novel X-linked gene responsible for Emery-Dreifuss muscular dystrophy." Nature genetics **8**(4): 323-327.
- Blighe K, R. S., Lewis M (2020). "EnhancedVolcano: Publication-ready volcano plots with enhanced colouring and labeling." <https://github.com/kevinblighe/EnhancedVolcano>.
- Bloom, S. and P. Cancilla (1969). "Conformational changes in myocardial nuclei of rats." Circulation research **24**(2): 189-196.

- Bloom, S., V. G. Lockard and M. Bloom (1996). "Intermediate filament-mediated stretch-induced changes in chromatin: a hypothesis for growth initiation in cardiac myocytes." Journal of molecular and cellular cardiology **28**(10): 2123-2127.
- Bolger, A. M., M. Lohse and B. Usadel (2014). "Trimmomatic: a flexible trimmer for Illumina sequence data." Bioinformatics **30**(15): 2114-2120.
- Bonev, B., N. M. Cohen, Q. Szabo, L. Fritsch, G. L. Papadopoulos, Y. Lubling, X. Xu, X. Lv, J.-P. Hugnot and A. Tanay (2017). "Multiscale 3D genome rewiring during mouse neural development." Cell **171**(3): 557-572. e524.
- Bonne, G., M. R. D. Barletta, S. Varnous, H.-M. Bécane, E.-H. Hammouda, L. Merlini, F. Muntoni, C. R. Greenberg, F. Gary and J.-A. Urtizberea (1999). "Mutations in the gene encoding lamin A/C cause autosomal dominant Emery-Dreifuss muscular dystrophy." Nature genetics **21**(3): 285-288.
- Bonne, G., E. Mercuri, A. Muchir, A. Urtizberea, H. M. Bécane, D. Recan, L. Merlini, M. Wehnert, R. Boor, U. Reuner, M. Vorgerd, E. M. Wicklein, B. Eymard, D. Duboc, I. Penisson-Besnier, J. M. Cuisset, X. Ferrer, I. Desguerre, D. Lacombe, K. Bushby, C. Pollitt, D. Toniolo, M. Fardeau, K. Schwartz and F. Muntoni (2000). "Clinical and molecular genetic spectrum of autosomal dominant Emery-Dreifuss muscular dystrophy due to mutations of the lamin A/C gene." Ann Neurol **48**(2): 170-180.
- Brayson, D. and C. M. Shanahan (2017). "Current insights into LMNA cardiomyopathies: Existing models and missing LINC's." Nucleus **8**(1): 17-33.
- Brodehl, A., R. A. Ferrier, S. J. Hamilton, S. C. Greenway, M.-A. Brundler, W. Yu, W. T. Gibson, M. L. McKinnon, B. C. McGillivray, N. Alvarez, M. Giuffre, J. A. Schwartzentruber and B. Gerull (2016). "Mutations in FLNC are Associated with Familial Restrictive Cardiomyopathy." Human Mutation **37**.
- Brodehl, A. and B. Gerull (2022). "Genetic Insights into Primary Restrictive Cardiomyopathy." **11**(8).
- Brodehl, A., S. A. Pour Hakimi, C. Stanasiuk, S. Ratnavadivel, D. Hendig, A. Gaertner, B. Gerull, J. Gummert, L. Paluszkiwicz and H. Milting (2019). "Restrictive cardiomyopathy is caused by a novel homozygous desmin (DES) mutation p. Y122H leading to a severe filament assembly defect." Genes **10**(11): 918.
- Bronshtein, I., E. Kepten, I. Kanter, S. Berezin, M. Lindner, A. B. Redwood, S. Mai, S. Gonzalo, R. Foisner and Y. Shav-Tal (2015). "Loss of lamin A function increases chromatin dynamics in the nuclear interior." Nature communications **6**(1): 1-9.
- Bu, L., X. Jiang, S. Martin-Puig, L. Caron, S. Zhu, Y. Shao, D. J. Roberts, P. L. Huang, I. J. Domian and K. R. Chien (2009). "Human ISL1 heart progenitors generate diverse multipotent cardiovascular cell lineages." Nature **460**(7251): 113-117.
- Buckingham, M., S. Meilhac and S. Zaffran (2005). "Building the mammalian heart from two sources of myocardial cells." Nature Reviews Genetics **6**(11): 826-835.
- Burke, B. and C. L. Stewart (2013). "The nuclear lamins: flexibility in function." Nature reviews Molecular cell biology **14**(1): 13-24.
- Burke, B. and C. L. Stewart (2013). "The nuclear lamins: flexibility in function." Nat Rev Mol Cell Biol **14**(1): 13-24.
- Burton, P., M. Yacoub and P. Barton (1999). "Cyclin-dependent kinase inhibitor expression in human heart failure. A comparison with fetal development." European heart journal **20**(8): 604-611.
- Buxboim, A., J. Swift, J. Irianto, K. R. Spinler, P. D. P. Dingal, A. Athirasala, Y.-R. C. Kao, S. Cho, T. Harada and J.-W. Shin (2014). "Matrix elasticity regulates lamin-A, C phosphorylation and turnover with feedback to actomyosin." Current Biology **24**(16): 1909-1917.
- Cai, C.-L., X. Liang, Y. Shi, P.-H. Chu, S. L. Pfaff, J. Chen and S. Evans (2003). "Isl1 identifies a cardiac progenitor population that proliferates prior to differentiation and contributes a majority of cells to the heart." Developmental cell **5**(6): 877-889.
- Cai, Z.-J., Y.-K. Lee, Y.-M. Lau, J. C.-Y. Ho, W.-H. Lai, N. L.-Y. Wong, D. Huang, J.-j. Hai, K.-M. Ng and H.-F. Tse (2020). "Expression of Lmna-R225X nonsense mutation results in dilated cardiomyopathy and conduction disorders (DCM-CD) in mice: Impact of exercise training." International Journal of Cardiology **298**: 85-92.

- Cao, H. and R. A. Hegele (2000). "Nuclear lamin A/C R482Q mutation in Canadian kindreds with Dunnigan-type familial partial lipodystrophy." Human molecular genetics **9**(1): 109-112.
- Cao, H. and R. A. Hegele (2003). "LMNA is mutated in Hutchinson-Gilford progeria (MIM 176670) but not in Wiedemann-Rautenstrauch progeroid syndrome (MIM 264090)." Journal of human genetics **48**(5): 271-274.
- Capanni, C., E. Mattioli, M. Columbaro, E. Lucarelli, V. K. Parnaik, G. Novelli, M. Wehnert, V. Cenni, N. M. Maraldi and S. Squarzoni (2005). "Altered pre-lamin A processing is a common mechanism leading to lipodystrophy." Human molecular genetics **14**(11): 1489-1502.
- Caron, M., M. Auclair, B. Donadille, V. Bereziat, B. Guerci, M. Laville, H. Narbonne, C. Bodemer, O. Lascols and J. Capeau (2007). "Human lipodystrophies linked to mutations in A-type lamins and to HIV protease inhibitor therapy are both associated with prelamin A accumulation, oxidative stress and premature cellular senescence." Cell Death & Differentiation **14**(10): 1759-1767.
- Cattin, M. E., A. T. Bertrand, S. Schlossarek, M. C. Le Bihan, S. Skov Jensen, C. Neuber, C. Crocini, S. Maron, J. Lainé, N. Mougénot, S. Varnous, Y. Fromes, A. Hansen, T. Eschenhagen, V. Decostre, L. Carrier and G. Bonne (2013). "Heterozygous Lmna^{delK32} mice develop dilated cardiomyopathy through a combined pathomechanism of haploinsufficiency and peptide toxicity." Hum Mol Genet **22**(15): 3152-3164.
- Cattin, M. E., A. Ferry, A. Vignaud, N. Mougénot, A. Jacquet, K. Wahbi, A. T. Bertrand and G. Bonne (2016). "Mutation in lamin A/C sensitizes the myocardium to exercise-induced mechanical stress but has no effect on skeletal muscles in mouse." Neuromuscul Disord **26**(8): 490-499.
- Cattin, M. E., A. Muchir and G. Bonne (2013). "'State-of-the-heart' of cardiac laminopathies." Curr Opin Cardiol **28**(3): 297-304.
- Caux, F., E. Duboscq, O. Lascols, B. Buendia, O. Chazouilleres, A. Cohen, J.-C. Courvalin, L. Laroche, J. Capeau and C. Vigouroux (2003). "A new clinical condition linked to a novel mutation in lamins A and C with generalized lipoatrophy, insulin-resistant diabetes, disseminated leukomelanodermic papules, liver steatosis, and cardiomyopathy." The Journal of Clinical Endocrinology & Metabolism **88**(3): 1006-1013.
- Cesarini, E., C. Mozzetta, F. Marullo, F. Gregoretti, A. Gargiulo, M. Columbaro, A. Cortesi, L. Antonelli, S. Di Pelino and S. Squarzoni (2015). "Lamin A/C sustains PcG protein architecture, maintaining transcriptional repression at target genes." Journal of Cell Biology **211**(3): 533-551.
- Chai, R. J., H. Werner, P. Y. Li, Y. L. Lee, K. T. Nyein, I. Solovei, T. D. A. Luu, B. Sharma, R. Navasankari, M. Maric, L. Y. E. Sim, Y. J. Loh, E. Aliwarga, J. W. L. Cheong, A. Chojnowski, M. I. Autio, Y. Haiyang, K. K. Boon Tan, C. T. Keng, S. L. Ng, W. L. Chew, M. Ferenczi, B. Burke, R. S. Y. Foo and C. L. Stewart (2021). "Disrupting the LINC complex by AAV mediated gene transduction prevents progression of Lamin induced cardiomyopathy." Nat Commun **12**(1): 4722.
- Charniot, J. C., C. Pascal, C. Bouchier, P. Sébillon, J. Salama, L. Duboscq-Bidot, M. Peuchmaurd, M. Desnos, J. Y. Artigou and M. Komajda (2003). "Functional consequences of an LMNA mutation associated with a new cardiac and non-cardiac phenotype." Human mutation **21**(5): 473-481.
- Chatzifrangkeskou, M., C. Le Dour, W. Wu, J. P. Morrow, L. C. Joseph, M. Beuvin, F. Sera, S. Homma, N. Vignier, N. Mougénot, G. Bonne, K. E. Lipson, H. J. Worman and A. Muchir (2016). "ERK1/2 directly acts on CTGF/CCN2 expression to mediate myocardial fibrosis in cardiomyopathy caused by mutations in the lamin A/C gene." Human Molecular Genetics **25**(11): 2220-2233.
- Chatzifrangkeskou, M., D. Yadin, T. Marais, S. Chardonnet, M. Cohen-Tannoudji, N. Mougénot, A. Schmitt, S. Crasto, E. Di Pasquale and C. Macquart (2018). "Cofilin-1 phosphorylation catalyzed by ERK1/2 alters cardiac actin dynamics in dilated cardiomyopathy caused by lamin A/C gene mutation." Human Molecular Genetics **27**(17): 3060-3078.
- Cheedipudi, S. M., S. J. Matkovich, C. Coarfa, X. Hu, M. J. Robertson, M. Sweet, M. Taylor, L. Mestroni, J. Cleveland and J. T. Willerson (2019). "Genomic reorganization of lamin-associated domains in cardiac myocytes is associated with differential gene expression and DNA methylation in human dilated cardiomyopathy." Circulation research **124**(8): 1198-1213.

- Chen, L., L. Lee, B. A. Kudlow, H. G. Dos Santos, O. Sletvold, Y. Shafeghati, E. G. Botha, A. Garg, N. B. Hanson and G. M. Martin (2003). "LMNA mutations in atypical Werner's syndrome." The Lancet **362**(9382): 440-445.
- Chen, N. Y., Y. Yang, T. A. Weston, J. N. Belling, P. Heizer, Y. Tu, P. Kim, L. Edillo, S. J. Jonas and P. S. Weiss (2019). "An absence of lamin B1 in migrating neurons causes nuclear membrane ruptures and cell death." Proceedings of the National Academy of Sciences **116**(51): 25870-25879.
- Chen, S. N., R. Lombardi, J. Karmouch, J. Y. Tsai, G. Czernuszewicz, M. R. G. Taylor, L. Mestroni, C. Coarfa, P. Gurha and A. J. Marian (2019). "DNA Damage Response/TP53 Pathway Is Activated and Contributes to the Pathogenesis of Dilated Cardiomyopathy Associated With LMNA (Lamin A/C) Mutations." Circ Res **124**(6): 856-873.
- Cho, S., M. Vashisth, A. Abbas, S. Majkut, K. Vogel, Y. Xia, I. L. Ivanovska, J. Irianto, M. Tewari and K. Zhu (2019). "Mechanosensing by the lamina protects against nuclear rupture, DNA damage, and cell-cycle arrest." Developmental cell **49**(6): 920-935. e925.
- Choy, M.-K., B. M. Javierre, S. G. Williams, S. L. Baross, Y. Liu, S. W. Wingett, A. Akbarov, C. Wallace, P. Freire-Pritchett and P. J. Rugg-Gunn (2018). "Promoter interactome of human embryonic stem cell-derived cardiomyocytes connects GWAS regions to cardiac gene networks." Nature communications **9**(1): 1-10.
- Cirillo, L. A. and K. S. Zaret (1999). "An early developmental transcription factor complex that is more stable on nucleosome core particles than on free DNA." Molecular cell **4**(6): 961-969.
- Coffinier, C., S. Y. Chang, C. Nobumori, Y. Tu, E. A. Farber, J. I. Toth, L. G. Fong and S. G. Young (2010). "Abnormal development of the cerebral cortex and cerebellum in the setting of lamin B2 deficiency." Proceedings of the National Academy of Sciences **107**(11): 5076-5081.
- Coffinier, C., H. J. Jung, Z. Li, C. Nobumori, U. J. Yun, E. A. Farber, B. S. Davies, M. M. Weinstein, S. H. Yang and J. Lammerding (2010). "Direct Synthesis of Lamin A, Bypassing Prelamin A Processing, Causes Misshapen Nuclei in Fibroblasts but No Detectable Pathology in Mice*." Journal of Biological Chemistry **285**.
- Constantinescu, D., H. L. Gray, P. J. Sammak, G. P. Schatten and A. B. Csoka (2006). "Lamin A/C expression is a marker of mouse and human embryonic stem cell differentiation." Stem cells **24**(1): 177-185.
- Corces, M. R., A. E. Trevino, E. G. Hamilton, P. G. Greenside, N. A. Sinnott-Armstrong, S. Vesuna, A. T. Satpathy, A. J. Rubin, K. S. Montine, B. Wu, A. Kathiria, S. W. Cho, M. R. Mumbach, A. C. Carter, M. Kasowski, L. A. Orloff, V. I. Risca, A. Kundaje, P. A. Khavari, T. J. Montine, W. J. Greenleaf and H. Y. Chang (2017). "An improved ATAC-seq protocol reduces background and enables interrogation of frozen tissues." Nat Methods **14**(10): 959-962.
- Corrado, D., C. Basso, G. Thiene, W. J. McKenna, M. J. Davies, F. Fontaliran, A. Nava, F. Silvestri, C. Blomstrom-Lundqvist and E. K. Wlodarska (1997). "Spectrum of clinicopathologic manifestations of arrhythmogenic right ventricular cardiomyopathy/dysplasia: a multicenter study." Journal of the American College of Cardiology **30**(6): 1512-1520.
- Corrado, D. and G. Thiene (2006). "Arrhythmogenic right ventricular cardiomyopathy/dysplasia: clinical impact of molecular genetic studies." Circulation **113**(13): 1634-1637.
- Cremer, T., K. Küpper, S. Dietzel and S. Fakan (2004). "Higher order chromatin architecture in the cell nucleus: on the way from structure to function." Biology of the Cell **96**(8): 555-567.
- Dan, L., H. Lian, X. Zhang, H. Shao, H. Lan, C. Qin, L. Zhang and G. S. Wu (2010). "LMNA E82K Mutation Activates FAS and Mitochondrial Pathways of Apoptosis in Heart Tissue Specific Transgenic Mice." Plos One **5**(12): e15167.
- David, R., C. Brenner, J. Stieber, F. Schwarz, S. Brunner, M. Vollmer, E. Mentele, J. Müller-Höcker, S. Kitajima and H. Lickert (2008). "MesP1 drives vertebrate cardiovascular differentiation through Dkk-1-mediated blockade of Wnt-signalling." Nature cell biology **10**(3): 338-345.
- de La Pompa, J. L., L. A. Timmerman, H. Takimoto, H. Yoshida, A. J. Elia, E. Samper, J. Potter, A. Wakeham, L. Marengere and B. L. Langille (1998). "Role of the NF-ATc transcription factor in morphogenesis of cardiac valves and septum." Nature **392**(6672): 182-186.
- Delgado-Olguín, P., Y. Huang, X. Li, D. Christodoulou, C. E. Seidman, J. Seidman, A. Tarakhovskiy and B. G. Bruneau (2012). "Epigenetic repression of cardiac progenitor gene expression by Ezh2 is required for postnatal cardiac homeostasis." Nature genetics **44**(3): 343.

- Dittmer, T. A. and T. Misteli (2011). "The lamin protein family." Genome Biol **12**(5): 222.
- Dixon, J. R., I. Jung, S. Selvaraj, Y. Shen, J. E. Antosiewicz-Bourget, A. Y. Lee, Z. Ye, A. Kim, N. Rajagopal and W. Xie (2015). "Chromatin architecture reorganization during stem cell differentiation." Nature **518**(7539): 331.
- Dixon, J. R., S. Selvaraj, F. Yue, A. Kim, Y. Li, Y. Shen, M. Hu, J. S. Liu and B. Ren (2012). "Topological domains in mammalian genomes identified by analysis of chromatin interactions." Nature **485**(7398): 376-380.
- Dobin, A., C. A. Davis, F. Schlesinger, J. Drenkow, C. Zaleski, S. Jha, P. Batut, M. Chaisson and T. R. Gingeras (2013). "STAR: ultrafast universal RNA-seq aligner." Bioinformatics **29**(1): 15-21.
- Dobrova, G. and T. Braun (2012). When silence is broken: polycomb group proteins in heart development, Am Heart Assoc. **110**: 372-374.
- Doetschman, T. and M. Azhar (2012). "Cardiac-specific inducible and conditional gene targeting in mice." Circulation research **110**(11): 1498-1512.
- Earle, A. J., T. J. Kirby, G. R. Fedorchak, P. Isermann, J. Patel, S. Iruvanti, S. A. Moore, G. Bonne, L. L. Wallrath and J. Lammerding (2020). "Mutant lamins cause nuclear envelope rupture and DNA damage in skeletal muscle cells." Nature materials **19**(4): 464-473.
- Epstein, J. A., H. Aghajanian and M. K. Singh (2015). "Semaphorin signaling in cardiovascular development." Cell metabolism **21**(2): 163-173.
- Evans, S. M., D. Yelon, F. L. Conlon and M. L. Kirby (2010). "Myocardial lineage development." Circulation research **107**(12): 1428-1444.
- Ewels, P., M. Magnusson, S. Lundin and M. Kaller (2016). "MultiQC: summarize analysis results for multiple tools and samples in a single report." Bioinformatics **32**(19): 3047-3048.
- Fatkin, D., C. MacRae, T. Sasaki, M. R. Wolff, M. Porcu, M. Frenneaux, J. Atherton, H. J. Vidaillet Jr, S. Spudich and U. De Girolami (1999). "Missense mutations in the rod domain of the lamin A/C gene as causes of dilated cardiomyopathy and conduction-system disease." New England Journal of Medicine **341**(23): 1715-1724.
- Finlan, L. E., D. Sproul, I. Thomson, S. Boyle, E. Kerr, P. Perry, B. Ylstra, J. R. Chubb and W. A. Bickmore (2008). "Recruitment to the nuclear periphery can alter expression of genes in human cells." PLoS genetics **4**(3): e1000039.
- Finsterer, J., C. Stoellberger and J. A. Towbin (2017). "Left ventricular noncompaction cardiomyopathy: cardiac, neuromuscular, and genetic factors." Nature Reviews Cardiology **14**(4): 224-237.
- Fisher, D. Z., N. Chaudhary and G. Blobel (1986). "cDNA sequencing of nuclear lamins A and C reveals primary and secondary structural homology to intermediate filament proteins." Proceedings of the National Academy of Sciences **83**(17): 6450-6454.
- Fong, L. G., J. K. Ng, J. Lammerding, T. A. Vickers and S. G. Young (2006). "Prelamin A and lamin A appear to be dispensable in the nuclear lamina." Journal of Clinical Investigation **116**(3): 743-752.
- Fraser, J., C. Ferrai, A. M. Chiariello, M. Schueler, T. Rito, G. Laudanno, M. Barbieri, B. L. Moore, D. C. Kraemer and S. Aitken (2015). "Hierarchical folding and reorganization of chromosomes are linked to transcriptional changes in cellular differentiation." Molecular systems biology **11**(12).
- Freund, A., R.-M. Laberge, M. Demaria and J. Campisi (2012). "Lamin B1 loss is a senescence-associated biomarker." Molecular biology of the cell **23**(11): 2066-2075.
- Fujii, S., A. Hirota and K. Kamino (1981). "Optical indications of pace-maker potential and rhythm generation in early embryonic chick heart." The Journal of physiology **312**(1): 253-263.
- Funkhouser, C. M., R. Sknepnek, T. Shimi, A. E. Goldman, R. D. Goldman and M. Olvera de la Cruz (2013). "Mechanical model of blebbing in nuclear lamin meshworks." Proceedings of the National Academy of Sciences **110**(9): 3248-3253.
- Gafni, O., L. Weinberger, A. A. Mansour, Y. S. Manor, E. Chomsky, D. Ben-Yosef, Y. Kalma, S. Viukov, I. Maza and A. Zviran (2013). "Derivation of novel human ground state naive pluripotent stem cells." Nature **504**(7479): 282-286.
- Galata, Z., I. Kloukina, I. Kostavasili, A. Varela, C. H. Davos, M. Makridakis, G. Bonne and Y. Capetanaki (2018). "Amelioration of desmin network defects by α B-crystallin overexpression

- confers cardioprotection in a mouse model of dilated cardiomyopathy caused by LMNA gene mutation." Journal of Molecular and Cellular Cardiology **125**: 73-86.
- Gao, R., X. Liang, S. Cheedipudi, J. Cordero, X. Jiang, Q. Zhang, L. Caputo, S. Günther, C. Kuenne and Y. Ren (2019). "Pioneering function of Isl1 in the epigenetic control of cardiomyocyte cell fate." Cell research **29**(6): 486-501.
- Garg, A., R. A. Speckman and A. M. Bowcock (2002). "Multisystem dystrophy syndrome due to novel missense mutations in the amino-terminal head and alpha-helical rod domains of the lamin A/C gene." The American journal of medicine **112**(7): 549-555.
- Gaspar, J. M. (2018). "Improved peak-calling with MACS2." bioRxiv: 496521.
- Gati, S., R. Rajani, G. S. Carr-White and J. B. Chambers (2014). "Adult left ventricular noncompaction: reappraisal of current diagnostic imaging modalities." JACC: Cardiovascular Imaging **7**(12): 1266-1275.
- Gerbino, A., C. Forleo, S. Milano, F. Piccapane, G. Procino, M. Pepe, M. Piccolo, P. Guida, N. Resta and S. Favale (2021). "Pro-inflammatory cytokines as emerging molecular determinants in cardiomyopathies." Journal of Cellular and Molecular Medicine **25**(23): 10902-10915.
- Gerull, B., S. Klaassen and A. Brodehl (2020). "The Genetic Landscape of Cardiomyopathies."
- Gesson, K., P. Rescheneder, M. P. Skoruppa, A. von Haeseler, T. Dechat and R. Foisner (2016). "A-type lamins bind both hetero- and euchromatin, the latter being regulated by lamina-associated polypeptide 2 alpha." Genome research **26**(4): 462-473.
- Gibcus, J. H. and J. Dekker (2013). "The hierarchy of the 3D genome." Molecular cell **49**(5): 773-782.
- Gonzalez-Suarez, I., A. B. Redwood, S. M. Perkins, B. Vermolen, D. Lichtensztejin, D. A. Grotzky, L. Morgado-Palacin, E. J. Gapud, B. P. Sleckman and T. Sullivan (2009). "Novel roles for A-type lamins in telomere biology and the DNA damage response pathway." The EMBO journal **28**(16): 2414-2427.
- Greenway, S. C., G. J. Wilson, J. Wilson, K. George and P. F. Kantor (2012). "Sudden death in an infant with angina, restrictive cardiomyopathy, and coronary artery bridging: an unusual phenotype for a β -myosin heavy chain (MYH7) sarcomeric protein mutation." Circulation: Heart Failure **5**(6): e92-e93.
- Grego-Bessa, J., L. Luna-Zurita, G. del Monte, V. Bolós, P. Melgar, A. Arandilla, A. N. Garratt, H. Zang, Y.-s. Mukoyama and H. Chen (2007). "Notch signaling is essential for ventricular chamber development." Developmental cell **12**(3): 415-429.
- Gruenbaum, Y. and R. Foisner (2015). "Lamins: nuclear intermediate filament proteins with fundamental functions in nuclear mechanics and genome regulation." Annual review of biochemistry **84**: 131-164.
- Guelen, L., L. Pagie, E. Brasset, W. Meuleman, M. B. Faza, W. Talhout, B. H. Eussen, A. de Klein, L. Wessels and W. de Laat (2008). "Domain organization of human chromosomes revealed by mapping of nuclear lamina interactions." Nature **453**(7197): 948-951.
- Guenantin, A.-C., I. Jebeniani, J. Leschik, E. Watrin, G. Bonne, N. Vignier and M. Puceat (2021). "Targeting the histone demethylase LSD1 prevents cardiomyopathy in a mouse model of laminopathy." The Journal of clinical investigation **131**(1).
- Guo, Y., Y. Kim, T. Shimi, R. D. Goldman and Y. Zheng (2014). "Concentration-dependent lamin assembly and its roles in the localization of other nuclear proteins." Molecular biology of the cell **25**(8): 1287-1297.
- Gupta, P., Z. T. Bilinska, N. Sylvius, E. Boudreau, J. P. Veinot, S. Labib, P. M. Bolongo, A. Hamza, T. Jackson and R. Ploski (2010). "Genetic and ultrastructural studies in dilated cardiomyopathy patients: a large deletion in the lamin A/C gene is associated with cardiomyocyte nuclear envelope disruption." Basic research in cardiology **105**(3): 365-377.
- Hahn, C. and M. A. Schwartz (2009). "Mechanotransduction in vascular physiology and atherogenesis." Nature reviews Molecular cell biology **10**(1): 53-62.
- Hamczyk, M. R., R. Villa-Bellosta, P. Gonzalo, M. J. Andrés-Manzano, P. Nogales, J. F. Bentzon, C. López-Otín and V. Andrés (2018). "Vascular smooth muscle-specific progerin expression accelerates atherosclerosis and death in a mouse model of Hutchinson-Gilford progeria syndrome." Circulation **138**(3): 266-282.
- Harvey, R. P. (2002). "Patterning the vertebrate heart." Nature Reviews Genetics **3**(7): 544-556.

- Haugaa, K. H., N. E. Hasselberg and T. Edvardsen (2015). "Mechanical dispersion by strain echocardiography: a predictor of ventricular arrhythmias in subjects with lamin A/C mutations." *JACC: Cardiovascular Imaging* **8**(1): 104-106.
- He, A., Q. Ma, J. Cao, A. Von Gise, P. Zhou, H. Xie, B. Zhang, M. Hsing, D. C. Christodoulou and P. Cahan (2012). "Polycomb repressive complex 2 regulates normal development of the mouse heart." *Circulation research* **110**(3): 406-415.
- Heinz, S., C. Benner, N. Spann, E. Bertolino, Y. C. Lin, P. Laslo, J. X. Cheng, C. Murre, H. Singh and C. K. Glass (2010). "Simple combinations of lineage-determining transcription factors prime cis-regulatory elements required for macrophage and B cell identities." *Mol Cell* **38**(4): 576-589.
- Hermida-Prieto, M., L. Monserrat, A. Castro-Beiras, R. Laredo, R. Soler, J. Peteiro, E. Rodríguez, B. Bouzas, N. Álvarez and J. Muñiz (2004). "Familial dilated cardiomyopathy and isolated left ventricular noncompaction associated with lamin A/C gene mutations." *The American journal of cardiology* **94**(1): 50-54.
- Ho, C. Y., D. E. Jaalouk, M. K. Vartiainen and J. Lammerding (2013). "Lamin A/C and emerin regulate MKL1–SRF activity by modulating actin dynamics." *Nature* **497**(7450): 507-511.
- Hodgkinson, K., S. Connors, N. Merner, A. Haywood, T. L. Young, W. McKenna, B. Gallagher, F. Curtis, A. Bassett and P. Parfrey (2013). "The natural history of a genetic subtype of arrhythmogenic right ventricular cardiomyopathy caused by a p. S358L mutation in TMEM43." *Clinical genetics* **83**(4): 321-331.
- Höger, T. H., K. Zatloukal, I. Waizenegger and G. Krohne (1990). "Characterization of a second highly conserved B-type lamin present in cells previously thought to contain only a single B-type lamin." *Chromosoma* **99**(6): 379-390.
- Hogers, B., M. DeRuiter, A. Baasten, A. Gittenberger-de Groot and R. Poelmann (1995). "Intracardiac blood flow patterns related to the yolk sac circulation of the chick embryo." *Circulation research* **76**(5): 871-877.
- Hogers, B., M. C. DeRuiter, A. C. Gittenberger-de Groot and R. E. Poelmann (1999). "Extraembryonic venous obstructions lead to cardiovascular malformations and can be embryolethal." *Cardiovascular Research* **41**(1): 87-99.
- Hsiao, E. C., Y. Yoshinaga, T. D. Nguyen, S. L. Musone, J. E. Kim, P. Swinton, I. Espineda, C. Manalac, P. J. deJong and B. R. Conklin (2008). "Marking embryonic stem cells with a 2A self-cleaving peptide: a NKX2-5 emerald GFP BAC reporter." *PLoS One* **3**(7): e2532.
- Huang da, W., B. T. Sherman and R. A. Lempicki (2009). "Systematic and integrative analysis of large gene lists using DAVID bioinformatics resources." *Nat Protoc* **4**(1): 44-57.
- Hussain, I., N. Patni, M. Ueda, E. Sorkina, C. M. Valerio, E. Cochran, R. J. Brown, J. Peeden, Y. Tikhonovich and A. Tiulpakov (2018). "A novel generalized lipodystrophy-associated progeroid syndrome due to recurrent heterozygous LMNA p. T10I mutation." *The Journal of Clinical Endocrinology & Metabolism* **103**(3): 1005-1014.
- Ieda, M., J. D. Fu, P. Delgado-Olguin, V. Vedantham, Y. Hayashi, B. G. Bruneau and D. Srivastava (2010). "Direct reprogramming of fibroblasts into functional cardiomyocytes by defined factors." *Cell* **142**(3): 375-386.
- Jahed, Z. and M. R. Mofrad (2019). "The nucleus feels the force, LINCed in or not!" *Curr Opin Cell Biol* **58**: 114-119.
- Jakobs, P. M., E. L. Hanson, K. A. Crispell, W. Toy, H. Keegan, K. Schilling, T. B. Icenogle, M. Litt and R. E. Hershberger (2001). "Novel lamin A/C mutations in two families with dilated cardiomyopathy and conduction system disease." *Journal of cardiac failure* **7**(3): 249-256.
- Jia, Y., J. S.-L. Vong, A. Asafova, B. K. Garvalov, L. Caputo, J. Cordero, A. Singh, T. Boettger, S. Günther and L. Fink (2019). "Lamin B1 loss promotes lung cancer development and metastasis by epigenetic derepression of RET." *Journal of Experimental Medicine* **216**(6): 1377-1395.
- Joshi-Mukherjee, R., W. Coombs, H. Musa, E. Oxford, S. Taffet and M. Delmar (2008). "Characterization of the molecular phenotype of two arrhythmogenic right ventricular cardiomyopathy (ARVC)-related plakophilin-2 (PKP2) mutations." *Heart Rhythm* **5**(12): 1715-1723.
- Kaski, J. P., P. Syrris, M. Burch, M.-T. Tome-Esteban, M. Fenton, M. Christiansen, P. S. Andersen, N. Sebire, M. Ashworth and J. E. Deanfield (2008). "Idiopathic restrictive

- cardiomyopathy in children is caused by mutations in cardiac sarcomere protein genes." Heart **94**(11): 1478-1484.
- Kato, K., N. Takahashi, Y. Fujii, A. Umehara, S. Nishiuchi, T. Makiyama, S. Ohno and M. Horie (2016). "LMNA cardiomyopathy detected in Japanese arrhythmogenic right ventricular cardiomyopathy cohort." Journal of Cardiology **68**(4): 346-351.
- Kattman, S. J., T. L. Huber and G. M. Keller (2006). "Multipotent flk-1+ cardiovascular progenitor cells give rise to the cardiomyocyte, endothelial, and vascular smooth muscle lineages." Developmental cell **11**(5): 723-732.
- Kattman, S. J., A. D. Witty, M. Gagliardi, N. C. Dubois, M. Niapour, A. Hotta, J. Ellis and G. Keller (2011). "Stage-specific optimization of activin/nodal and BMP signaling promotes cardiac differentiation of mouse and human pluripotent stem cell lines." Cell stem cell **8**(2): 228-240.
- Kim, Y., A. A. Sharov, K. McDole, M. Cheng, H. Hao, C.-M. Fan, N. Gaiano, M. S. Ko and Y. Zheng (2011). "Mouse B-type lamins are required for proper organogenesis but not by embryonic stem cells." Science **334**(6063): 1706-1710.
- Kim, Y., X. Zheng and Y. Zheng (2013). "Proliferation and differentiation of mouse embryonic stem cells lacking all lamins." Cell Res **23**(12): 1420-1423.
- Kim, Y. and Y. Zheng (2013). "Generation and characterization of a conditional deletion allele for Lmna in mice." Biochem Biophys Res Commun **440**(1): 8-13.
- Kind, J., L. Pagie, S. S. de Vries, L. Nahidiazar, S. S. Dey, M. Bienko, Y. Zhan, B. Lajoie, C. A. de Graaf and M. Amendola (2015). "Genome-wide maps of nuclear lamina interactions in single human cells." Cell **163**(1): 134-147.
- Kind, J., L. Pagie, H. Ortazokoyun, S. Boyle, S. S. De Vries, H. Janssen, M. Amendola, L. D. Nolen, W. A. Bickmore and B. van Steensel (2013). "Single-cell dynamics of genome-nuclear lamina interactions." Cell **153**(1): 178-192.
- Kind, J. and B. van Steensel (2014). "Stochastic genome-nuclear lamina interactions: modulating roles of Lamin A and BAF." Nucleus **5**(2): 124-130.
- Kitajima, S., A. Takagi, T. Inoue and Y. Saga (2000). "MesP1 and MesP2 are essential for the development of cardiac mesoderm." Development **127**(15): 3215-3226.
- Kivelä, R., K. A. Hemanthakumar, K. Vaparanta, M. Robciuc, Y. Izumiya, H. Kidoya, N. Takakura, X. Peng, D. B. Sawyer and K. Elenius (2019). "Endothelial cells regulate physiological cardiomyocyte growth via VEGFR2-mediated paracrine signaling." Circulation **139**(22): 2570-2584.
- Kodo, K., S.-G. Ong, F. Jahanbani, V. Termglinchan, K. Hirono, K. InanlooRahatloo, A. D. Ebert, P. Shukla, O. J. Abilez and J. M. Churko (2016). "iPSC-derived cardiomyocytes reveal abnormal TGF- β signalling in left ventricular non-compaction cardiomyopathy." Nature cell biology **18**(10): 1031-1042.
- Kolb, T., K. Maaß, M. Hergt, U. Aebi and H. Herrmann (2011). "Lamin A and lamin C form homodimers and coexist in higher complex forms both in the nucleoplasmic fraction and in the lamina of cultured human cells." Nucleus **2**(5): 425-433.
- Kostareva, A., A. Gudkova, G. Sjöberg, S. Mörner, E. Semernin, A. Krutikov, E. Shlyakhto and T. Sejersen (2009). "Deletion in TNNI3 gene is associated with restrictive cardiomyopathy." International Journal of Cardiology **131**(3): 410-412.
- Kubben, N., J. W. Voncken, G. Konings, M. van Weeghel, M. M. van den Hoogenhof, M. Gijbels, A. van Erk, K. Schoonderwoerd, B. van den Bosch, V. Dahlmans, C. Calis, S. M. Houten, T. Misteli and Y. M. Pinto (2011). "Post-natal myogenic and adipogenic developmental defects and metabolic impairment upon loss of A-type lamins." Nucleus **2**(3): 195-207.
- Kulikova, O., A. Brodehl, A. Kiseleva, R. Myasnikov, A. Meshkov, C. Stanasiuk, A. Gartner, M. Divashuk, E. Sotnikova, S. Koretskiy, M. Kharlap, V. Kozlova, E. Mershina, P. Pilus, V. Sinitsyn, H. Milting, S. Boytsov and O. Drapkina (2021). "The Desmin (DES) Mutation p.A337P Is Associated with Left-Ventricular Non-Compaction Cardiomyopathy." Genes (Basel) **12**(1).
- Kumar, S., S. H. Baldinger, E. Gandjbakhch, P. Maury, J.-M. Sellal, A. F. Androulakis, X. Waintraub, P. Charron, A. Rollin and P. Richard (2016). "Long-term arrhythmic and nonarrhythmic outcomes of lamin A/C mutation carriers." Journal of the American college of cardiology **68**(21): 2299-2307.

- Kumaran, R. I. and D. L. Spector (2008). "A genetic locus targeted to the nuclear periphery in living cells maintains its transcriptional competence." The Journal of cell biology **180**(1): 51-65.
- Kuo, C. T., E. E. Morrisey, R. Anandappa, K. Sigrist, M. M. Lu, M. S. Parmacek, C. Soudais and J. M. Leiden (1997). "GATA4 transcription factor is required for ventral morphogenesis and heart tube formation." Genes & development **11**(8): 1048-1060.
- Lammerding, J., L. G. Fong, J. Y. Ji, K. Reue, C. L. Stewart, S. G. Young and R. T. Lee (2006). "Lamins A and C but not lamin B1 regulate nuclear mechanics." Journal of Biological Chemistry **281**(35): 25768-25780.
- Lammerding, J., J. Hsiao, P. C. Schulze, S. Kozlov, C. L. Stewart and R. T. Lee (2005). "Abnormal nuclear shape and impaired mechanotransduction in emerin-deficient cells." The Journal of cell biology **170**(5): 781-791.
- Lammerding, J., P. C. Schulze, T. Takahashi, S. Kozlov, T. Sullivan, R. D. Kamm, C. L. Stewart and R. T. Lee (2004). "Lamin A/C deficiency causes defective nuclear mechanics and mechanotransduction." The Journal of clinical investigation **113**(3): 370-378.
- Langmead, B. and S. L. Salzberg (2012). "Fast gapped-read alignment with Bowtie 2." Nat Methods **9**(4): 357-359.
- Lavine, K. J. and D. M. Ornitz (2009). "Shared circuitry: developmental signaling cascades regulate both embryonic and adult coronary vasculature." Circulation research **104**(2): 159-169.
- Lawrence, M., R. Gentleman and V. Carey (2009). "rtracklayer: an R package for interfacing with genome browsers." Bioinformatics **25**(14): 1841-1842.
- Lee, J., V. Termglinchan, S. Diecke, I. Itzhaki, C. K. Lam, P. Garg, E. Lau, M. Greenhaw, T. Seeger and H. Wu (2019). "Activation of PDGF pathway links LMNA mutation to dilated cardiomyopathy." Nature **572**(7769): 335-340.
- Lee, Y. K., Y. Jiang, X. R. Ran, Y. M. Lau, K. M. Ng, W. H. Lai, C. W. Siu and H. F. Tse (2016). "Recent advances in animal and human pluripotent stem cell modeling of cardiac laminopathy." Stem Cell Res Ther **7**(1): 139.
- Lee, Y. K., Y. M. Lau, Z. J. Cai, W. H. Lai, L. Y. Wong, H. F. Tse, K. M. Ng and C. W. Siu (2017). "Modeling treatment response for lamin A/C related dilated cardiomyopathy in human induced pluripotent stem cells." Journal of the American Heart Association **6**(8): e005677.
- Leemans, C., M. C. van der Zwalm, L. Brueckner, F. Comoglio, T. van Schaik, L. Pagie, J. van Arensbergen and B. van Steensel (2019). "Promoter-intrinsic and local chromatin features determine gene repression in LADs." Cell **177**(4): 852-864. e814.
- Lemke, S. B. and F. Schnorrer (2017). "Mechanical forces during muscle development." Mechanisms of development **144**: 92-101.
- Li, H., B. Handsaker, A. Wysoker, T. Fennell, J. Ruan, N. Homer, G. Marth, G. Abecasis, R. Durbin and S. Genome Project Data Processing (2009). "The Sequence Alignment/Map format and SAMtools." Bioinformatics (Oxford, England) **25**(16): 2078-2079.
- Liang, J. J., K. Goodsell, M. Grogan and M. J. Ackerman (2016). "LMNA-mediated arrhythmogenic right ventricular cardiomyopathy and charcot-marie-tooth type 2B1: A patient-discovered unifying diagnosis." Journal of cardiovascular electrophysiology **27**(7): 868-871.
- Lieberman-Aiden, E., N. L. Van Berkum, L. Williams, M. Imakaev, T. Ragoczy, A. Telling, I. Amit, B. R. Lajoie, P. J. Sabo and M. O. Dorschner (2009). "Comprehensive mapping of long-range interactions reveals folding principles of the human genome." science **326**(5950): 289-293.
- Lin, E. W., G. F. Brady, R. Kwan, A. I. Nesvizhskii and M. B. Omary (2020). "Genotype-phenotype analysis of LMNA-related diseases predicts phenotype-selective alterations in lamin phosphorylation." FASEB J **34**(7): 9051-9073.
- Lin, F. and H. J. Worman (1995). "Structural organization of the human gene (LMNB1) encoding nuclear lamin B1." Genomics **27**(2): 230-236.
- Lindsley, R. C., J. G. Gill, T. L. Murphy, E. M. Langer, M. Cai, M. Mashayekhi, W. Wang, N. Niwa, J. M. Nerbonne and M. Kyba (2008). "Mesp1 coordinately regulates cardiovascular fate restriction and epithelial-mesenchymal transition in differentiating ESCs." Cell stem cell **3**(1): 55-68.
- Lityagina, O. and G. Dobrova (2021). "The LINC Between Mechanical Forces and Chromatin." Front Physiol **12**: 710809.

- Liu, B., J. Wang, K. M. Chan, W. M. Tjia, W. Deng, X. Guan, J.-d. Huang, K. M. Li, P. Y. Chau and D. J. Chen (2005). "Genomic instability in laminopathy-based premature aging." Nature medicine **11**(7): 780-785.
- Liu, Z., H. Shan, J. Huang, N. Li, C. Hou and J. Pu (2016). "A novel lamin A/C gene missense mutation (445 V> E) in immunoglobulin-like fold associated with left ventricular non-compaction." Europace **18**(4): 617-622.
- Lombardi, R., S. N. Chen, A. Ruggiero, P. Gurha, G. Z. Czernuszewicz, J. T. Willerson and A. J. Marian (2016). "Cardiac fibro-adipocyte progenitors express desmosome proteins and preferentially differentiate to adipocytes upon deletion of the desmoplakin gene." Circulation research **119**(1): 41-54.
- Lombardi, R., J. Dong, G. Rodriguez, A. Bell, T. K. Leung, R. J. Schwartz, J. T. Willerson, R. Brugada and A. J. Marian (2009). "Genetic fate mapping identifies second heart field progenitor cells as a source of adipocytes in arrhythmogenic right ventricular cardiomyopathy." Circ Res **104**(9): 1076-1084.
- Love, M. I., W. Huber and S. Anders (2014). "Moderated estimation of fold change and dispersion for RNA-seq data with DESeq2." Genome Biol **15**(12): 550.
- Luis, N. M., L. Morey, L. Di Croce and S. A. Benitah (2012). "Polycomb in stem cells: PRC1 branches out." Cell stem cell **11**(1): 16-21.
- Lund, E., A. R. Oldenburg, E. Delbarre, C. T. Freberg, I. Duband-Goulet, R. Eskeland, B. Buendia and P. Collas (2013). "Lamin A/C-promoter interactions specify chromatin state-dependent transcription outcomes." Genome research **23**(10): 1580-1589.
- Lund, E. G., I. Duband-Goulet, A. Oldenburg, B. Buendia and P. Collas (2015). "Distinct features of lamin A-interacting chromatin domains mapped by ChIP-sequencing from sonicated or micrococcal nuclease-digested chromatin." Nucleus **6**(1): 30-39.
- MacGrogan, D., J. Münch and J. L. de la Pompa (2018). "Notch and interacting signalling pathways in cardiac development, disease, and regeneration." Nature Reviews Cardiology **15**(11): 685-704.
- MacLeod, H. M., M. R. Culley, J. M. Huber and E. M. McNally (2003). "Lamin A/C truncation in dilated cardiomyopathy with conduction disease." BMC Medical Genetics **4**(1): 1-7.
- Maggi, L., M. Mavroidis, S. Psarras, Y. Capetanaki and G. Lattanzi (2021). "Skeletal and cardiac muscle disorders caused by mutations in genes encoding intermediate filament proteins." International Journal of Molecular Sciences **22**(8): 4256.
- Mahmoud, A. I., F. Kocabas, S. A. Muralidhar, W. Kimura, A. S. Koura, S. Thet, E. R. Porrello and H. A. Sadek (2013). "Meis1 regulates postnatal cardiomyocyte cell cycle arrest." Nature **497**(7448): 249-253.
- Majkut, S., P. D. P. Dingal and D. E. Discher (2014). "Stress sensitivity and mechanotransduction during heart development." Current Biology **24**(10): R495-R501.
- Manilal, S., N. T. Man, C. Sewry and G. Morris (1996). "The Emery-Dreifuss muscular dystrophy protein, emerin, is a nuclear membrane protein." Human molecular genetics **5**(6): 801-808.
- Marcus, F. I., W. J. McKenna, D. Sherrill, C. Basso, B. Bauce, D. A. Bluemke, H. Calkins, D. Corrado, M. G. Cox and J. P. Daubert (2010). "Diagnosis of arrhythmogenic right ventricular cardiomyopathy/dysplasia: proposed modification of the task force criteria." Circulation **121**(13): 1533-1541.
- Margueron, R. and D. Reinberg (2011). "The Polycomb complex PRC2 and its mark in life." Nature **469**(7330): 343-349.
- Markandeya, Y. S., T. Tsubouchi, T. A. Hacker, M. R. Wolff, L. Belardinelli and R. C. Balijepalli (2016). "Inhibition of late sodium current attenuates ionic arrhythmia mechanism in ventricular myocytes expressing LaminA-N195K mutation." Heart Rhythm **13**(11): 2228-2236.
- Maron, B. J., J. A. Towbin, G. Thiene, C. Antzelevitch, D. Corrado, D. Arnett, A. J. Moss, C. E. Seidman and J. B. Young (2006). "Contemporary definitions and classification of the cardiomyopathies: an American Heart Association scientific statement from the council on clinical cardiology, heart failure and transplantation committee; quality of care and outcomes research and functional genomics and translational biology interdisciplinary working groups; and council on epidemiology and prevention." Circulation **113**(14): 1807-1816.

- Marsman, R. F., A. Bardai, A. V. Postma, J. C. Res, T. T. Koopmann, L. Beekman, A. C. van der Wal, Y. M. Pinto, R. H. Lekanne Deprez and A. A. Wilde (2011). "A complex double deletion in LMNA underlies progressive cardiac conduction disease, atrial arrhythmias, and sudden death." Circulation: Cardiovascular Genetics **4**(3): 280-287.
- Marullo, F., E. Cesarini, L. Antonelli, F. Gregoretti, G. Oliva and C. Lanzuolo (2016). "Nucleoplasmic Lamin A/C and Polycomb group of proteins: An evolutionarily conserved interplay." Nucleus **7**(2): 103-111.
- Matthes, S. A., S. Taffet and M. Delmar (2011). "Plakophilin-2 and the migration, differentiation and transformation of cells derived from the epicardium of neonatal rat hearts." Cell communication & adhesion **18**(4): 73-84.
- Maynard, S., G. Keijzers, M. Akbari, M. B. Ezra, A. Hall, M. Morevati, M. Scheibye-Knudsen, S. Gonzalo, J. Bartek and V. A. Bohr (2019). "Lamin A/C promotes DNA base excision repair." Nucleic acids research **47**(22): 11709-11728.
- McKeon, F. D., M. W. Kirschner and D. Caput (1986). "Homologies in both primary and secondary structure between nuclear envelope and intermediate filament proteins." Nature **319**(6053): 463-468.
- McNally, E. M. and L. Mestroni (2017). "Dilated Cardiomyopathy: Genetic Determinants and Mechanisms." Circ Res **121**(7): 731-748.
- Meilhac, S. M. and M. E. Buckingham (2018). "The deployment of cell lineages that form the mammalian heart." Nature Reviews Cardiology **15**(11): 705-724.
- Meilhac, S. M., M. Esner, R. G. Kelly, J.-F. Nicolas and M. E. Buckingham (2004). "The clonal origin of myocardial cells in different regions of the embryonic mouse heart." Developmental cell **6**(5): 685-698.
- Meinke, P., E. Mattioli, F. Haque, S. Antoku, M. Columbaro, K. R. Straatman, H. J. Worman, G. G. Gundersen, G. Lattanzi and M. Wehnert (2014). "Muscular dystrophy-associated SUN1 and SUN2 variants disrupt nuclear-cytoskeletal connections and myonuclear organization." PLoS genetics **10**(9): e1004605.
- Méjat, A. (2010). "LINC complexes in health and disease." Nucleus **1**(1): 40-52.
- Merner, N. D., K. A. Hodgkinson, A. F. Haywood, S. Connors, V. M. French, J.-D. Drenckhahn, C. Kupprion, K. Ramadanova, L. Thierfelder and W. McKenna (2008). "Arrhythmogenic right ventricular cardiomyopathy type 5 is a fully penetrant, lethal arrhythmic disorder caused by a missense mutation in the TMEM43 gene." The American Journal of Human Genetics **82**(4): 809-821.
- Meuleman, W., D. Peric-Hupkes, J. Kind, J.-B. Beaudry, L. Pagie, M. Kellis, M. Reinders, L. Wessels and B. Van Steensel (2013). "Constitutive nuclear lamina–genome interactions are highly conserved and associated with A/T-rich sequence." Genome research **23**(2): 270-280.
- Mewborn, S. K., M. J. Puckelwartz, F. Abuisneineh, J. P. Fahrenbach, Y. Zhang, H. MacLeod, L. Dellefave, P. Pytel, S. Selig and C. M. Labno (2010). "Altered chromosomal positioning, compaction, and gene expression with a lamin A/C gene mutation." PloS one **5**(12): e14342.
- Misfeldt, A. M., S. C. Boyle, K. L. Tompkins, V. L. Bautch, P. A. Labosky and H. S. Baldwin (2009). "Endocardial cells are a distinct endothelial lineage derived from Flk1+ multipotent cardiovascular progenitors." Developmental biology **333**(1): 78-89.
- Mogensen, J. and E. Arbustini (2009). "Restrictive cardiomyopathy." Current Opinion in Cardiology **24**(3): 214-220.
- Molkentin, J. D. (2000). "The zinc finger-containing transcription factors GATA-4, -5, and -6. Ubiquitously expressed regulators of tissue-specific gene expression." J Biol Chem **275**(50): 38949-38952.
- Molkentin, J. D., Q. Lin, S. A. Duncan and E. N. Olson (1997). "Requirement of the transcription factor GATA4 for heart tube formation and ventral morphogenesis." Genes & development **11**(8): 1061-1072.
- Montefiori, L. E., D. R. Sobreira, N. J. Sakabe, I. Aneas, A. C. Joslin, G. T. Hansen, G. Bozek, I. P. Moskowitz, E. M. McNally and M. A. Nóbrega (2018). "A promoter interaction map for cardiovascular disease genetics." Elife **7**: e35788.
- Moretti, A., L. Caron, A. Nakano, J. T. Lam, A. Bernshausen, Y. Chen, Y. Qyang, L. Bu, M. Sasaki and S. Martin-Puig (2006). "Multipotent embryonic isl1+ progenitor cells lead to cardiac, smooth muscle, and endothelial cell diversification." Cell **127**(6): 1151-1165.

- Morey, L., A. Santanach, E. Blanco, L. Aloia, E. P. Nora, B. G. Bruneau and L. Di Croce (2015). "Polycomb regulates mesoderm cell fate-specification in embryonic stem cells through activation and repression mechanisms." Cell stem cell **17**(3): 300-315.
- Mory, P. B., F. Crispim, T. Kasamatsu, M. A. Gabbay, S. A. Dib and R. S. Moisés (2008). "Atypical generalized lipodystrophy and severe insulin resistance due to a heterozygous LMNA p. T10I mutation." Arquivos Brasileiros de Endocrinologia & Metabologia **52**: 1252-1256.
- Mounkes, L. C., S. Kozlov, L. Hernandez, T. Sullivan and C. L. Stewart (2003). "A progeroid syndrome in mice is caused by defects in A-type lamins." Nature **423**(6937): 298-301.
- Mounkes, L. C., S. V. Kozlov, J. N. Rottman and C. L. Stewart (2005). "Expression of an LMNA-N195K variant of A-type lamins results in cardiac conduction defects and death in mice." Human Molecular Genetics **14**(15): 2167-2180.
- Mozzetta, C. and F. S. Tedesco (2019). "Challenging the "chromatin hypothesis" of cardiac laminopathies with LMNA mutant iPS cells." The Journal of Cell Biology **218**(9): 2826.
- Muchir, A., G. Bonne, A. J. van der Kooi, M. van Meegen, F. Baas, P. A. Bolhuis, M. de Visser and K. Schwartz (2000). "Identification of mutations in the gene encoding lamins A/C in autosomal dominant limb girdle muscular dystrophy with atrioventricular conduction disturbances (LGMD1B)." Human molecular genetics **9**(9): 1453-1459.
- Muchir, A., P. Pavlidis, V. Decostre, A. J. Herron, T. Arimura, G. Bonne and H. J. Worman (2007). "Activation of MAPK pathways links LMNA mutations to cardiomyopathy in Emery-Dreifuss muscular dystrophy." The Journal of clinical investigation **117**(5): 1282-1293.
- Muchtar, E., L. A. Blauwet and M. A. Gertz (2017). "Restrictive cardiomyopathy: genetics, pathogenesis, clinical manifestations, diagnosis, and therapy." Circulation research **121**(7): 819-837.
- Naetar, N., B. Korbei, S. Kozlov, M. A. Kerenyi, D. Dorner, R. Kral, I. Gotic, P. Fuchs, T. V. Cohen and R. Bittner (2008). "Loss of nucleoplasmic LAP2 α -lamin A complexes causes erythroid and epidermal progenitor hyperproliferation." Nature cell biology **10**(11): 1341-1348.
- Niessen, K. and A. Karsan (2008). "Notch signaling in cardiac development." Circulation research **102**(10): 1169-1181.
- Nihoyannopoulos, P. and D. Dawson (2009). "Restrictive cardiomyopathies." European Journal of Echocardiography **10**(8): iii23-iii33.
- Nikolova, V., C. Leimena, A. C. McMahon, A. C. Tan, S. Chandar, D. Jogia, S. H. Kesteven, J. Michalicek, R. Otway and F. Verheyen (2004). "Defects in nuclear structure and function promote dilated cardiomyopathy in lamin A/C-deficient mice." Journal of Clinical Investigation **113**(3): 357-369.
- Nishiuchi, S., T. Makiyama, T. Aiba, K. Nakajima, S. Hirose, H. Kohjitani, Y. Yamamoto, T. Harita, M. Hayano and Y. Wuriyanghai (2017). "Gene-based risk stratification for cardiac disorders in LMNA mutation carriers." Circulation: cardiovascular genetics **10**(6): e001603.
- Nmezi, B., J. Xu, R. Fu, T. J. Armiger, G. Rodriguez-Bey, J. S. Powell, H. Ma, M. Sullivan, Y. Tu and N. Y. Chen (2019). "Concentric organization of A-and B-type lamins predicts their distinct roles in the spatial organization and stability of the nuclear lamina." Proceedings of the National Academy of Sciences **116**(10): 4307-4315.
- Nora, E. P., B. R. Lajoie, E. G. Schulz, L. Giorgetti, I. Okamoto, N. Servant, T. Piolot, N. L. van Berkum, J. Meisig and J. Sedat (2012). "Spatial partitioning of the regulatory landscape of the X-inactivation centre." Nature **485**(7398): 381-385.
- O'Donnell, A. and K. E. Yutzey (2020). "Mechanisms of heart valve development and disease." Development **147**(13): dev183020.
- Oldenburg, A., N. Briand, A. L. Sørensen, I. Cahyani, A. Shah, J. Ø. Moskaug and P. Collas (2017). "A lipodystrophy-causing lamin A mutant alters conformation and epigenetic regulation of the anti-adipogenic MIR335 locus." Journal of Cell Biology **216**(9): 2731-2743.
- Osorio, F. G., C. L. Navarro, J. Cadianos, I. López-Mejía and C. López-Otín (2011). "Splicing-Directed Therapy in a New Mouse Model of Human Accelerated Aging." Science translational medicine **3**(106): 106ra107.
- Ostlund, C., J. Ellenberg, E. Hallberg, J. Lippincott-Schwartz and H. J. Worman (1999). "Intracellular trafficking of emerin, the Emery-Dreifuss muscular dystrophy protein." Journal of Cell Science **112**(11): 1709-1719.

- Pagliara, S., K. Franze, C. R. McClain, G. W. Wylde, C. L. Fisher, R. J. Franklin, A. J. Kabla, U. F. Keyser and K. J. Chalut (2014). "Auxetic nuclei in embryonic stem cells exiting pluripotency." *Nature materials* **13**(6): 638-644.
- Paller, M. S., C. M. Martin and M. E. Pierpont (2018). "Restrictive cardiomyopathy: an unusual phenotype of a lamin A variant." *5*(4): 724-726.
- Palstra, R.-J., B. Tolhuis, E. Splinter, R. Nijmeijer, F. Grosveld and W. de Laat (2003). "The β -globin nuclear compartment in development and erythroid differentiation." *Nature genetics* **35**(2): 190-194.
- Parameswaran, M. and P. P. Tam (1995). "Regionalisation of cell fate and morphogenetic movement of the mesoderm during mouse gastrulation." *Developmental genetics* **17**(1): 16-28.
- Parent, J. J., J. A. Towbin and J. L. Jefferies (2015). "Left ventricular noncompaction in a family with lamin A/C gene mutation." *Texas Heart Institute Journal* **42**(1): 73.
- Patni, N., X. Li, B. Adams-Huet, C. Vasandani, R. A. Gomez-Diaz and A. Garg (2019). "Regional body fat changes and metabolic complications in children with Dunnigan lipodystrophy-causing LMNA variants." *The Journal of Clinical Endocrinology & Metabolism* **104**(4): 1099-1108.
- Peled, Y., M. Gramlich, G. Yoskovitz, M. S. Feinberg, A. Afek, S. Polak-Charcon, E. Pras, B. A. Sela, E. Konen, O. Weissbrod, D. Geiger, P. M. Gordon, L. Thierfelder, D. Freimark, B. Gerull and M. Arad (2014). "Titin mutation in familial restrictive cardiomyopathy." *Int J Cardiol* **171**(1): 24-30.
- Pennarun, G., J. Picotto, L. Etourneaud, A.-R. Redavid, A. Certain, L. R. Gauthier, P. Fontanilla-Ramirez, D. Busso, C. Chabance-Okumura and B. Thézé (2021). "Increase in lamin B1 promotes telomere instability by disrupting the shelterin complex in human cells." *Nucleic acids research* **49**(17): 9886-9905.
- Peric-Hupkes, D., W. Meuleman, L. Pagie, S. W. Bruggeman, I. Solovei, W. Brugman, S. Gräf, P. Flicek, R. M. Kerkhoven and M. van Lohuizen (2010). "Molecular maps of the reorganization of genome-nuclear lamina interactions during differentiation." *Molecular cell* **38**(4): 603-613.
- Perrot, A., S. Hussein, V. Ruppert, H. H. Schmidt, M. S. Wehnert, N. T. Duong, M. G. Posch, A. Panek, R. Dietz and I. Kindermann (2009). "Identification of mutational hot spots in LMNA encoding lamin A/C in patients with familial dilated cardiomyopathy." *Basic research in cardiology* **104**(1): 90-99.
- Peter, M., G. Kitten, C. Lehner, K. Vorburger, S. Bailer, G. Maridor and E. Nigg (1989). "Cloning and sequencing of cDNA clones encoding chicken lamins A and B1 and comparison of the primary structures of vertebrate A- and B-type lamins." *Journal of molecular biology* **208**(3): 393-404.
- Poleshko, A., P. P. Shah, M. Gupta, A. Babu, M. P. Morley, L. J. Manderfield, J. L. Ifkovits, D. Calderon, H. Aghajanian and J. E. Sierra-Pagán (2017). "Genome-nuclear lamina interactions regulate cardiac stem cell lineage restriction." *Cell* **171**(3): 573-587. e514.
- Politz, J. C. R., D. Scalzo and M. Groudine (2016). "The redundancy of the mammalian heterochromatic compartment." *Current opinion in genetics & development* **37**: 1-8.
- Probst, S., E. Oechslin, P. Schuler, M. Greutmann, P. Boyé, W. Knirsch, F. Berger, L. Thierfelder, R. Jenni and S. Klaassen (2011). "Sarcomere gene mutations in isolated left ventricular noncompaction cardiomyopathy do not predict clinical phenotype." *Circulation: Cardiovascular Genetics* **4**(4): 367-374.
- Puente, B. N., W. Kimura, S. A. Muralidhar, J. Moon, J. F. Amatruda, K. L. Phelps, D. Grinsfelder, B. A. Rothermel, R. Chen, J. A. Garcia, C. X. Santos, S. Thet, E. Mori, M. T. Kinter, P. M. Rindler, S. Zacchigna, S. Mukherjee, D. J. Chen, A. I. Mahmoud, M. Giacca, P. S. Rabinovitch, A. Aroumougame, A. M. Shah, L. I. Szweda and H. A. Sadek (2014). "The oxygen-rich postnatal environment induces cardiomyocyte cell-cycle arrest through DNA damage response." *Cell* **157**(3): 565-579.
- Quarta, G., P. Syrris, M. Ashworth, S. Jenkins, K. Zuborne Alapi, J. Morgan, A. Muir, A. Pantazis, W. J. McKenna and P. M. Elliott (2012). "Mutations in the Lamin A/C gene mimic arrhythmogenic right ventricular cardiomyopathy." *European heart journal* **33**(9): 1128-1136.
- Quijada, P., M. A. Trembley and E. M. Small (2020). "The role of the epicardium during heart development and repair." *Circulation research* **126**(3): 377-394.

- Quinlan, A. R. and I. M. Hall (2010). "BEDTools: a flexible suite of utilities for comparing genomic features." *Bioinformatics* **26**(6): 841-842.
- Ragni, C. V., N. Diguët, J.-F. Le Garrec, M. Novotova, T. P. Resende, S. Pop, N. Charon, L. Guillemot, L. Kitasato and C. Badouel (2017). "Amotl1 mediates sequestration of the Hippo effector Yap1 downstream of Fat4 to restrict heart growth." *Nature communications* **8**(1): 14582.
- Ragoczy, T., A. Telling, D. Scalzo, C. Kooperberg and M. Groudine (2014). "Functional redundancy in the nuclear compartmentalization of the late-replicating genome." *Nucleus* **5**(6): 626-635.
- Raharjo, W. H., P. Enarson, T. Sullivan, C. L. Stewart and B. Burke (2001). "Nuclear envelope defects associated with LMNA mutations cause dilated cardiomyopathy and Emery-Dreifuss muscular dystrophy." *Journal of cell science* **114**(24): 4447-4457.
- Ramirez, F., V. Bhardwaj, L. Arrigoni, K. C. Lam, B. A. Gruning, J. Villaveces, B. Habermann, A. Akhtar and T. Manke (2018). "High-resolution TADs reveal DNA sequences underlying genome organization in flies." *Nat Commun* **9**(1): 189.
- Ramírez, F., F. Dündar, S. Diehl, B. A. Gruning and T. Manke (2014). "deepTools: a flexible platform for exploring deep-sequencing data." *Nucleic acids research* **42**(W1): W187-W191.
- Ramirez, F., D. P. Ryan, B. Gruning, V. Bhardwaj, F. Kilpert, A. S. Richter, S. Heyne, F. Dündar and T. Manke (2016). "deepTools2: a next generation web server for deep-sequencing data analysis." *Nucleic Acids Res* **44**(W1): W160-165.
- Rana, M. S., M. Théveniau-Ruissy, C. De Bono, K. Mesbah, A. Francou, M. Rammah, J. N. Domínguez, M. Roux, B. Laforest and R. H. Anderson (2014). "Tbx1 coordinates addition of posterior second heart field progenitor cells to the arterial and venous poles of the heart." *Circulation research* **115**(9): 790-799.
- Rankin, J., M. Auer-Grumbach, W. Bagg, K. Colclough, N. T. Duong, J. Fenton-May, A. Hattersley, J. Hudson, P. Jardine and D. Josifova (2008). "Extreme phenotypic diversity and nonpenetrance in families with the LMNA gene mutation R644C." *American journal of medical genetics Part A* **146**(12): 1530-1542.
- Rao, S. S., M. H. Huntley, N. C. Durand, E. K. Stamenova, I. D. Bochkov, J. T. Robinson, A. L. Sanborn, I. Machol, A. D. Omer and E. S. Lander (2014). "A 3D map of the human genome at kilobase resolution reveals principles of chromatin looping." *Cell* **159**(7): 1665-1680.
- Reddy, K., J. Zullo, E. Bertolino and H. Singh (2008). "Transcriptional repression mediated by repositioning of genes to the nuclear lamina." *Nature* **452**(7184): 243-247.
- Rhee, S., J. I. Chung, D. A. King, G. D'amato, D. T. Paik, A. Duan, A. Chang, D. Nagelberg, B. Sharma and Y. Jeong (2018). "Endothelial deletion of Ino80 disrupts coronary angiogenesis and causes congenital heart disease." *Nature communications* **9**(1): 1-16.
- Rhee, S., D. T. Paik, J. Y. Yang, D. Nagelberg, I. Williams, L. Tian, R. Roth, M. Chandy, J. Ban and N. Belbachir (2021). "Endocardial/endothelial angiocrines regulate cardiomyocyte development and maturation and induce features of ventricular non-compaction." *European Heart Journal* **42**(41): 4264-4276.
- Robson, M. I., I. Jose, R. Czapiewski, A. Sivakumar, A. R. Kerr and E. C. Schirmer (2017). "Constrained release of lamina-associated enhancers and genes from the nuclear envelope during T-cell activation facilitates their association in chromosome compartments." *Genome research* **27**(7): 1126-1138.
- Roncarati, R., C. V. Anselmi, P. Krawitz, G. Lattanzi, Y. Von Kodolitsch, A. Perrot, E. Di Pasquale, L. Papa, P. Portararo and M. Columbaro (2013). "Doubly heterozygous LMNA and TTN mutations revealed by exome sequencing in a severe form of dilated cardiomyopathy." *European journal of human genetics* **21**(10): 1105-1111.
- Roncarati, R., C. Viviani Anselmi, P. Krawitz, G. Lattanzi, Y. von Kodolitsch, A. Perrot, E. di Pasquale, L. Papa, P. Portararo, M. Columbaro, A. Forni, G. Faggian, G. Condorelli and P. N. Robinson (2013). "Doubly heterozygous LMNA and TTN mutations revealed by exome sequencing in a severe form of dilated cardiomyopathy." *European Journal of Human Genetics* **21**(10): 1105-1111.
- Rønningen, T., A. Shah, A. R. Oldenburg, K. Vekterud, E. Delbarre, J. Ø. Moskaug and P. Collas (2015). "Prepatterning of differentiation-driven nuclear lamin A/C-associated chromatin domains by GlcNAcylated histone H2B." *Genome research* **25**(12): 1825-1835.

- Ross-Innes, C. S., R. Stark, A. E. Teschendorff, K. A. Holmes, H. R. Ali, M. J. Dunning, G. D. Brown, O. Gojis, I. O. Ellis, A. R. Green, S. Ali, S. F. Chin, C. Palmieri, C. Caldas and J. S. Carroll (2012). "Differential oestrogen receptor binding is associated with clinical outcome in breast cancer." *Nature* **481**(7381): 389-U177.
- Rothballer, A., T. U. Schwartz and U. Kutay (2013). "LINCing complex functions at the nuclear envelope: what the molecular architecture of the LINC complex can reveal about its function." *Nucleus* **4**(1): 29-36.
- Rubin, A. J., B. C. Barajas, M. Furlan-Magaril, V. Lopez-Pajares, M. R. Mumbach, I. Howard, D. S. Kim, L. D. Boxer, J. Cairns and M. Spivakov (2017). "Lineage-specific dynamic and pre-established enhancer-promoter contacts cooperate in terminal differentiation." *Nature genetics* **49**(10): 1522.
- Saga, Y., N. Hata, S. Kobayashi, T. Magnuson, M. F. Seldin and M. M. Taketo (1996). "MesP1: a novel basic helix-loop-helix protein expressed in the nascent mesodermal cells during mouse gastrulation." *Development* **122**(9): 2769-2778.
- Saga, Y., S. Miyagawa-Tomita, A. Takagi, S. Kitajima, J. Miyazaki and T. Inoue (1999). "MesP1 is expressed in the heart precursor cells and required for the formation of a single heart tube." *Development* **126**(15): 3437-3447.
- Sagelius, H., Y. Rosengarten, M. Hanif, M. R. Erdos, B. Rozell, F. S. Collins and M. Eriksson (2008). "Targeted transgenic expression of the mutation causing Hutchinson-Gilford progeria syndrome leads to proliferative and degenerative epidermal disease." *J Cell Sci* **121**(Pt 7): 969-978.
- Sahinoz, M., S. Khairi, A. Cuttitta, G. F. Brady, A. Rupani, R. Meral, M. K. Tayeh, P. Thomas, M. Riebschleger and S. Camelo-Piragua (2018). "Potential association of LMNA-associated generalized lipodystrophy with juvenile dermatomyositis." *Clinical diabetes and endocrinology* **4**(1): 1-6.
- Sala, L., B. J. van Meer, L. G. J. Tertoolen, J. Bakkers, M. Bellin, R. P. Davis, C. Denning, M. A. E. Dieben, T. Eschenhagen, E. Giacomelli, C. Grandela, A. Hansen, E. R. Holman, M. R. M. Jongbloed, S. M. Kamel, C. D. Koopman, Q. Lachaud, I. Mannhardt, M. P. H. Mol, D. Mosqueira, V. V. Orlova, R. Passier, M. C. Ribeiro, U. Saleem, G. L. Smith, F. L. Burton and C. L. Mummery (2018). "MUSCLEMOTION: A Versatile Open Software Tool to Quantify Cardiomyocyte and Cardiac Muscle Contraction In Vitro and In Vivo." *Circ Res* **122**(3): e5-e16.
- Salvarani, N., S. Crasto, M. Miragoli, A. Bertero, M. Paulis, P. Kunderfranco, S. Serio, A. Forni, C. Lucarelli and M. Dal Ferro (2019). "The K219T-Lamin mutation induces conduction defects through epigenetic inhibition of SCN5A in human cardiac laminopathy." *Nature communications* **10**(1): 1-16.
- Sayed, N., C. Liu, M. Ameen, F. Himmati, J. Z. Zhang, S. Khanamiri, J. R. Moonen, A. Wnorowski, L. Cheng, J. W. Rhee, S. Gaddam, K. C. Wang, K. Sallam, J. H. Boyd, Y. J. Woo, M. Rabinovitch and J. C. Wu (2020). "Clinical trial in a dish using iPSCs shows lovastatin improves endothelial dysfunction and cellular cross-talk in LMNA cardiomyopathy." *Sci Transl Med* **12**(554).
- Schirmer, E. C. and L. Gerace (2004). "The stability of the nuclear lamina polymer changes with the composition of lamin subtypes according to their individual binding strengths." *Journal of Biological Chemistry* **279**(41): 42811-42817.
- Schreiber, K. H. and B. K. Kennedy (2013). "When lamins go bad: nuclear structure and disease." *Cell* **152**(6): 1365-1375.
- Schuettengruber, B., D. Chourrout, M. Vervoort, B. Leblanc and G. Cavalli (2007). "Genome regulation by polycomb and trithorax proteins." *Cell* **128**(4): 735-745.
- Sebillon, P., C. Bouchier, L. Bidot, G. Bonne, K. Ahamed, P. Charron, V. Drouin-Garraud, A. Millaire, G. Desrumeaux and A. Benaiche (2003). "Expanding the phenotype of LMNA mutations in dilated cardiomyopathy and functional consequences of these mutations." *Journal of Medical Genetics* **40**(8): 560-567.
- Sedaghat-Hamedani, F., J. Haas, F. Zhu, C. Geier, E. Kayvanpour, M. Liss, A. Lai, K. Frese, R. Pribe-Wolferts and A. Amr (2017). "Clinical genetics and outcome of left ventricular non-compaction cardiomyopathy." *European heart journal* **38**(46): 3449-3460.
- Sedmera, D., T. Pexieder, V. Rychterova, N. Hu and E. B. Clark (1999). "Remodeling of chick embryonic ventricular myoarchitecture under experimentally changed loading conditions." *The*

- Anatomical Record: An Official Publication of the American Association of Anatomists **254**(2): 238-252.
- Sedmera, D., T. Pexieder, M. Vuillemin, R. P. Thompson and R. H. Anderson (2000). "Developmental patterning of the myocardium." The Anatomical Record: An Official Publication of the American Association of Anatomists **258**(4): 319-337.
- Servant, N., N. Varoquaux, B. R. Lajoie, E. Viara, C.-J. Chen, J.-P. Vert, E. Heard, J. Dekker and E. Barillot (2015). "HiC-Pro: an optimized and flexible pipeline for Hi-C data processing." Genome Biology **16**(1): 259.
- Shackleton, S., D. J. Lloyd, S. N. Jackson, R. Evans, M. F. Niermeijer, B. M. Singh, H. Schmidt, G. Brabant, S. Kumar and P. N. Durrington (2000). "LMNA, encoding lamin A/C, is mutated in partial lipodystrophy." Nature genetics **24**(2): 153-156.
- Shah, P. P., W. Lv, J. H. Rhoades, A. Poleshko, D. Abbey, M. A. Caporizzo, R. Linares-Saldana, J. G. Heffler, N. Sayed and D. Thomas (2021). "Pathogenic LMNA variants disrupt cardiac lamina-chromatin interactions and de-repress alternative fate genes." Cell Stem Cell **28**(5): 938-954. e939.
- Shen, L., N. Shao, X. Liu and E. Nestler (2014). "ngs.plot: Quick mining and visualization of next-generation sequencing data by integrating genomic databases." BMC Genomics **15**: 284.
- Shimi, T., V. Butin-Israeli, S. A. Adam, R. B. Hamanaka, A. E. Goldman, C. A. Lucas, D. K. Shumaker, S. T. Kosak, N. S. Chandel and R. D. Goldman (2011). "The role of nuclear lamin B1 in cell proliferation and senescence." Genes & development **25**(24): 2579-2593.
- Shimi, T., M. Kittisopikul, J. Tran, A. E. Goldman, S. A. Adam, Y. Zheng, K. Jaqaman and R. D. Goldman (2015). "Structural organization of nuclear lamins A, C, B1, and B2 revealed by superresolution microscopy." Molecular biology of the cell **26**(22): 4075-4086.
- Shimi, T., K. Pflughaar, S.-i. Kojima, C.-G. Pack, I. Solovei, A. E. Goldman, S. A. Adam, D. K. Shumaker, M. Kinjo and T. Cremer (2008). "The A-and B-type nuclear lamin networks: microdomains involved in chromatin organization and transcription." Genes & development **22**(24): 3409-3421.
- Siersbæk, R., J. G. S. Madsen, B. M. Javierre, R. Nielsen, E. K. Bagge, J. Cairns, S. W. Wingett, S. Traynor, M. Spivakov and P. Fraser (2017). "Dynamic rewiring of promoter-anchored chromatin loops during adipocyte differentiation." Molecular cell **66**(3): 420-435. e425.
- Siu, C.-W., Y.-K. Lee, J. C.-Y. Ho, W.-H. Lai, Y.-C. Chan, K.-M. Ng, L.-Y. Wong, K.-W. Au, Y.-M. Lau and J. Zhang (2012). "Modeling of lamin A/C mutation premature cardiac aging using patient-specific induced pluripotent stem cells." Aging (Albany NY) **4**(11): 803.
- Sommariva, E., S. Brambilla, C. Carbuicchio, E. Gambini, V. Meraviglia, A. Dello Russo, F. Farina, M. Casella, V. Catto and G. Pontone (2016). "Cardiac mesenchymal stromal cells are a source of adipocytes in arrhythmogenic cardiomyopathy." European heart journal **37**(23): 1835-1846.
- Sosa, B. A., A. Rothballer, U. Kutay and T. U. Schwartz (2012). "LINC complexes form by binding of three KASH peptides to domain interfaces of trimeric SUN proteins." Cell **149**(5): 1035-1047.
- Sperber, H., J. Mathieu, Y. Wang, A. Ferreccio, J. Hesson, Z. Xu, K. A. Fischer, A. Devi, D. Detraux and H. Gu (2015). "The metabolome regulates the epigenetic landscape during naive-to-primed human embryonic stem cell transition." Nature cell biology **17**(12): 1523-1535.
- Stark, R. and G. Brown DiffBind: differential binding analysis of ChIP-Seq peak data. Bioconductor (2011).
- Steensel, B. v. and S. Henikoff (2000). "Identification of in vivo DNA targets of chromatin proteins using tethered dam methyltransferase." Nature biotechnology **18**(4): 424-428.
- Stewart, C. and B. Burke (1987). "Teratocarcinoma stem cells and early mouse embryos contain only a single major lamin polypeptide closely resembling lamin B." Cell **51**(3): 383-392.
- Stroud, M. J., I. Banerjee, J. Veevers and J. Chen (2014). "Linker of nucleoskeleton and cytoskeleton complex proteins in cardiac structure, function, and disease." Circ Res **114**(3): 538-548.
- Subramanyam, L., V. Simha and A. Garg (2010). "Overlapping syndrome with familial partial lipodystrophy, Dunnigan variety and cardiomyopathy due to amino-terminal heterozygous missense lamin A/C mutations." Clinical genetics **78**(1): 66-73.

- Swift, J., I. L. Ivanovska, A. Buxboim, T. Harada, P. D. P. Dingal, J. Pinter, J. D. Pajerowski, K. R. Spinler, J.-W. Shin and M. Tewari (2013). "Nuclear lamin-A scales with tissue stiffness and enhances matrix-directed differentiation." *Science* **341**(6149): 1240104.
- Taimen, P., K. Pflieger, T. Shimi, D. Möller, K. Ben-Harush, M. R. Erdos, S. A. Adam, H. Herrmann, O. Medalia and F. S. Collins (2009). "A progeria mutation reveals functions for lamin A in nuclear assembly, architecture, and chromosome organization." *Proceedings of the National Academy of Sciences* **106**(49): 20788-20793.
- Tajik, A., Y. Zhang, F. Wei, J. Sun, Q. Jia, W. Zhou, R. Singh, N. Khanna, A. S. Belmont and N. Wang (2016). "Transcription upregulation via force-induced direct stretching of chromatin." *Nature materials* **15**(12): 1287-1296.
- Takeuchi, J. K. and B. G. Bruneau (2009). "Directed transdifferentiation of mouse mesoderm to heart tissue by defined factors." *Nature* **459**(7247): 708-711.
- Tam, P., M. Parameswaran, S. J. Kinder and R. P. Weinberger (1997). "The allocation of epiblast cells to the embryonic heart and other mesodermal lineages: the role of ingression and tissue movement during gastrulation." *Development* **124**(9): 1631-1642.
- Tapley, E. C. and D. A. Starr (2013). "Connecting the nucleus to the cytoskeleton by SUN–KASH bridges across the nuclear envelope." *Current opinion in cell biology* **25**(1): 57-62.
- Taylor, M., S. Graw, G. Sinagra, C. Barnes, D. Slavov, F. Brun, B. Pinamonti, E. E. Salcedo, W. Sauer and S. Pyxaras (2011). "Genetic variation in titin in arrhythmogenic right ventricular cardiomyopathy–overlap syndromes." *Circulation* **124**(8): 876-885.
- Tian, Y. and E. E. Morrisey (2012). "Importance of myocyte-nonmyocyte interactions in cardiac development and disease." *Circ Res* **110**(7): 1023-1034.
- Timmerman, L. A., J. Grego-Bessa, A. Raya, E. Bertrán, J. M. Pérez-Pomares, J. Díez, S. Aranda, S. Palomo, F. McCormick and J. C. Izpisua-Belmonte (2004). "Notch promotes epithelial-mesenchymal transition during cardiac development and oncogenic transformation." *Genes & development* **18**(1): 99-115.
- Tiso, N., D. A. Stephan, A. Nava, A. Bagattin, J. M. Devaney, F. Stanchi, G. Larderet, B. Brahmabhatt, K. Brown and B. Bauce (2001). "Identification of mutations in the cardiac ryanodine receptor gene in families affected with arrhythmogenic right ventricular cardiomyopathy type 2 (ARVD2)." *Human molecular genetics* **10**(3): 189-194.
- Tools, P. (2015). By Broad Institute.
- Towbin, J. A., A. Lorts and J. L. Jefferies (2015). "Left ventricular non-compaction cardiomyopathy." *The Lancet* **386**(9995): 813-825.
- Turbendian, H. K., M. Gordillo, S. Y. Tsai, J. Lu, G. Kang, T. C. Liu, A. Tang, S. Liu, G. I. Fishman and T. Evans (2013). "GATA factors efficiently direct cardiac fate from embryonic stem cells." *Development* **140**(8): 1639-1644.
- Turgay, Y., M. Eibauer, A. E. Goldman, T. Shimi, M. Khayat, K. Ben-Harush, A. Dubrovsky-Gaup, K. T. Sapra, R. D. Goldman and O. Medalia (2017). "The molecular architecture of lamins in somatic cells." *Nature* **543**(7644): 261-264.
- Umbarkar, P., S. Tousif and A. P. Singh (2022). "Fibroblast GSK-3 α Promotes Fibrosis via RAF-MEK-ERK Pathway in the Injured Heart." **131**(7): 620-636.
- van der Horst, A. and B. M. Burgering (2007). "Stressing the role of FoxO proteins in lifespan and disease." *Nat Rev Mol Cell Biol* **8**(6): 440-450.
- Van der Kooi, A., G. Bonne, B. Eymard, D. Duboc, B. Talim, M. Van der Valk, P. Reiss, P. Richard, L. Demay and L. Merlini (2002). "Lamin A/C mutations with lipodystrophy, cardiac abnormalities, and muscular dystrophy." *Neurology* **59**(4): 620-623.
- van Engelen, B. G., A. Muchir, C. J. Hutchison, A. J. van der Kooi, G. Bonne and M. Lammens (2005). "The lethal phenotype of a homozygous nonsense mutation in the lamin A/C gene." *Neurology* **64**(2): 374-376.
- van Koningsbruggen, S., M. Gierliński, P. Schofield, D. Martin, G. J. Barton, Y. Ariyurek, J. T. den Dunnen and A. I. Lamond (2010). "High-resolution whole-genome sequencing reveals that specific chromatin domains from most human chromosomes associate with nucleoli." *Molecular biology of the cell* **21**(21): 3735-3748.
- Van Rijsingen, I. A., E. Arbustini, P. M. Elliott, J. Mogensen, J. F. Hermans-van Ast, A. J. Van Der Kooi, J. P. Van Tintelen, M. P. Van Den Berg, A. Pilotto and M. Pasotti (2012). "Risk factors

- for malignant ventricular arrhythmias in lamin A/C mutation carriers: a European cohort study." Journal of the American College of Cardiology **59**(5): 493-500.
- Van Steensel, B. and A. S. Belmont (2017). "Lamina-associated domains: links with chromosome architecture, heterochromatin, and gene repression." Cell **169**(5): 780-791.
- van Steensel, B., J. Delrow and S. Henikoff (2001). "Chromatin profiling using targeted DNA adenine methyltransferase." Nature genetics **27**(3): 304-308.
- Varga, R., M. Eriksson, M. R. Erdos, M. Olive, I. Harten, F. Kolodgie, B. C. Capell, J. Cheng, D. Faddah and S. Perkins (2006). "Progressive vascular smooth muscle cell defects in a mouse model of Hutchinson–Gilford progeria syndrome." Proceedings of the National Academy of Sciences **103**(9): 3250-3255.
- Vergnes, L., M. Péterfy, M. O. Bergo, S. G. Young and K. Reue (2004). "Lamin B1 is required for mouse development and nuclear integrity." Proceedings of the National Academy of Sciences **101**(28): 10428-10433.
- Vincent, S. D. and M. E. Buckingham (2010). "How to make a heart: the origin and regulation of cardiac progenitor cells." Current topics in developmental biology **90**: 1-41.
- Vincenzo, M., M. Michelangelo, S. Costanza, T. Francesca, C. Lucia, A. Greta, R. Anna, B. Fulvia, C. M. Adelaide and L. Giovanna (2022). "A Single mtDNA Deletion in Association with a LMNA Gene New Frameshift Variant: A Case Report." Journal of Neuromuscular Diseases(Preprint): 1-6.
- Vining, K. H. and D. J. Mooney (2017). "Mechanical forces direct stem cell behaviour in development and regeneration." Nature Reviews Molecular Cell Biology **18**(12): 728.
- Volpi, E. V., E. Chevret, T. Jones, R. Vatcheva, J. Williamson, S. Beck, R. D. Campbell, M. Goldsworthy, S. H. Powis and J. Ragoussis (2000). "Large-scale chromatin organization of the major histocompatibility complex and other regions of human chromosome 6 and its response to interferon in interphase nuclei." J Cell Sci **113**(9): 1565-1576.
- Vorburger, K., C. Lehner, G. Kitten, H. Eppenberger and E. Nigg (1989). "A second higher vertebrate B-type lamin: cDNA sequence determination and in vitro processing of chicken lamin B2." Journal of molecular biology **208**(3): 405-415.
- Wada, E., M. Kato, K. Yamashita, H. Kokuba and Y. K. Hayashi (2019). "Deficiency of emerin contributes differently to the pathogenesis of skeletal and cardiac muscles in LmnaH222P/H222P mutant mice." PLoS ONE **14**(8): e0221512-.
- Wada, E., M. Kato, K. Yamashita, H. Kokuba, W.-C. Liang, G. Bonne and Y. K. Hayashi (2019). "Deficiency of emerin contributes differently to the pathogenesis of skeletal and cardiac muscles in LmnaH222P/H222P mutant mice." Plos one **14**(8): e0221512.
- Walling, B. L. and P. M. Murphy (2021). "Protean regulation of leukocyte function by nuclear lamins." Trends in Immunology **42**(4): 323-335.
- Wan, A. and B. Rodrigues (2016). "Endothelial cell–cardiomyocyte crosstalk in diabetic cardiomyopathy." Cardiovascular research **111**(3): 172-183.
- Wang, Y. and G. Dobрева (2023). "Epigenetics in LMNA-Related Cardiomyopathy." Cells **12**(5): 783.
- Wang, Y., A. Elsherbiny, L. Kessler, J. Cordero, H. Shi, H. Serke, O. Lityagina, F. A. Trogisch, M. M. Mohammadi and I. El-Battrawy (2022). "Lamin A/C-dependent chromatin architecture safeguards naïve pluripotency to prevent aberrant cardiovascular cell fate and function." Nature Communications **13**(1): 1-24.
- Wang, Y., Y. Fang, P. Lu, B. Wu and B. Zhou (2021). "NOTCH signaling in aortic valve development and calcific aortic valve disease." Frontiers in Cardiovascular Medicine **8**: 682298.
- Wang, Y., A. J. Herron and H. J. Worman (2006). "Pathology and nuclear abnormalities in hearts of transgenic mice expressing M371K lamin A encoded by an LMNA mutation causing Emery-Dreifuss muscular dystrophy." Hum Mol Genet **15**(16): 2479-2489.
- Wang, Y., A. A. Panteleyev, D. M. Owens, K. Djabali, C. L. Stewart and H. J. Worman (2008). "Epidermal expression of the truncated prelamin A causing Hutchinson–Gilford progeria syndrome: effects on keratinocytes, hair and skin." Hum Mol Genet **17**(15): 2357-2369.
- Ward, M. and T. Iskratsch (2019). "Mix and (mis-) match—The mechanosensing machinery in the changing environment of the developing, healthy adult and diseased heart." Biochimica et Biophysica Acta (BBA)-Molecular Cell Research.

- Watanabe, Y., S. Miyagawa-Tomita, S. D. Vincent, R. G. Kelly, A. M. Moon and M. E. Buckingham (2010). "Role of mesodermal FGF8 and FGF10 overlaps in the development of the arterial pole of the heart and pharyngeal arch arteries." Circulation research **106**(3): 495-503.
- Wen, B., H. Wu, Y. Shinkai, R. A. Irizarry and A. P. Feinberg (2009). "Large histone H3 lysine 9 dimethylated chromatin blocks distinguish differentiated from embryonic stem cells." Nature genetics **41**(2): 246-250.
- West, G., J. Gullmets, L. Virtanen, S.-P. Li, A. Keinänen, T. Shimi, M. Mauermann, T. Heliö, M. Kaartinen and L. Ollila (2016). "Deleterious assembly of the lamin A/C mutant p. S143P causes ER stress in familial dilated cardiomyopathy." Journal of cell science **129**(14): 2732-2743.
- West, G., M. Turunen, A. Aalto, L. Virtanen, S.-P. Li, T. Heliö, A. Meinander and P. Taimen (2022). "A heterozygous p. S143P mutation in LMNA associates with proteasome dysfunction and enhanced autophagy-mediated degradation of mutant lamins A and C." Frontiers in Cell and Developmental Biology.
- Wiens, D. J., T. K. Mann, D. E. Feddersen, W. K. Rathmell and B. H. Franck (1992). "Early heart development in the chick embryo: effects of isotretinoin on cell proliferation, α -actin synthesis, and development of contractions." Differentiation **51**(2): 105-112.
- Wijchers, P. J., G. Geeven, M. Eyres, A. J. Bergsma, M. Janssen, M. Versteegen, Y. Zhu, Y. Schell, C. Vermeulen and E. De Wit (2015). "Characterization and dynamics of pericentromere-associated domains in mice." Genome research **25**(7): 958-969.
- Windmueller, R., J. P. Leach, A. Babu, S. Zhou, M. P. Morley, A. Wakabayashi, N. B. Petrenko, P. Viatour and E. E. Morrissey (2020). "Direct Comparison of Mononucleated and Binucleated Cardiomyocytes Reveals Molecular Mechanisms Underlying Distinct Proliferative Competencies." Cell Rep **30**(9): 3105-3116 e3104.
- Wolf, C. M., L. Wang, R. Alcalai, A. Pizard, P. G. Burgon, F. Ahmad, M. Sherwood, D. M. Branco, H. Wakimoto and G. I. Fishman (2008). "Lamin A/C haploinsufficiency causes dilated cardiomyopathy and apoptosis-triggered cardiac conduction system disease." Journal of Molecular & Cellular Cardiology **44**(2): 293-303.
- Wong, X., V. E. Hoskins, A. J. Melendez-Perez, J. C. Harr, M. Gordon and K. L. Reddy (2021). "Lamin C is required to establish genome organization after mitosis." Genome biology **22**(1): 1-27.
- Wood, A. M., J. M. R. Danielsen, C. A. Lucas, E. L. Rice, D. Scalzo, T. Shimi, R. D. Goldman, E. D. Smith, M. M. Le Beau and S. T. Kosak (2014). "TRF2 and lamin A/C interact to facilitate the functional organization of chromosome ends." Nature communications **5**(1): 1-9.
- Worman, H. J. and J.-C. Courvalin (2004). "How do mutations in lamins A and C cause disease?" The Journal of clinical investigation **113**(3): 349-351.
- Wu, B., Z. Zhang, W. Lui, X. Chen, Y. Wang, A. A. Chamberlain, R. A. Moreno-Rodriguez, R. R. Markwald, B. P. O'Rourke and D. J. Sharp (2012). "Endocardial cells form the coronary arteries by angiogenesis through myocardial-endocardial VEGF signaling." Cell **151**(5): 1083-1096.
- Wu, W., A. Muchir, J. Shan, G. Bonne and H. J. Worman (2011). "Mitogen-activated protein kinase inhibitors improve heart function and prevent fibrosis in cardiomyopathy caused by mutation in lamin A/C gene." Circulation **123**(1): 53-61.
- Wu, W., J. Shan, G. Bonne, H. J. Worman and A. Muchir (2010). "Pharmacological inhibition of c-Jun N-terminal kinase signaling prevents cardiomyopathy caused by mutation in LMNA gene." Biochimica et Biophysica Acta (BBA)-Molecular Basis of Disease **1802**(7): 632-638.
- Yaffe, E. and A. Tanay (2011). "Probabilistic modeling of Hi-C contact maps eliminates systematic biases to characterize global chromosomal architecture." Nature genetics **43**(11): 1059.
- Yan, L., M. Yang, H. Guo, L. Yang, J. Wu, R. Li, P. Liu, Y. Lian, X. Zheng, J. Yan, J. Huang, M. Li, X. Wu, L. Wen, K. Lao, R. Li, J. Qiao and F. Tang (2013). "Single-cell RNA-Seq profiling of human preimplantation embryos and embryonic stem cells." Nat Struct Mol Biol **20**(9): 1131-1139.

- Yang, J., M. A. Argenziano, M. Burgos Angulo, A. Bertalovitz, M. N. Beidokhti and T. V. McDonald (2021). "Phenotypic Variability in iPSC-Induced Cardiomyocytes and Cardiac Fibroblasts Carrying Diverse LMNA Mutations." Frontiers in physiology: 2162.
- Yang, L., J. Sun, Z. Chen, L. Liu, Y. Sun, J. Lin, X. Hu, M. Zhao, Y. Ma and D. Lu (2022). "The LMNA p. R541C mutation causes dilated cardiomyopathy in human and mice." International Journal of Cardiology **363**: 149-158.
- Yang, S. H., D. A. Andres, H. P. Spielmann, S. G. Young and L. G. Fong (2008). "Progerin elicits disease phenotypes of progeria in mice whether or not it is farnesylated." J Clin Invest **118**(10): 3291-3300.
- Yang, S. H., S. Y. Chang, S. Ren, Y. Wang, D. A. Andres, H. P. Spielmann, L. G. Fong and S. G. Young (2011). "Absence of progeria-like disease phenotypes in knock-in mice expressing a non-farnesylated version of progerin." Hum Mol Genet **20**(3): 436-444.
- Yang, S. H., M. Meta, X. Qiao, D. Frost, J. Bauch, C. Coffinier, S. Majumdar, M. O. Bergo, S. G. Young and L. G. Fong (2006). "A farnesyltransferase inhibitor improves disease phenotypes in mice with a Hutchinson-Gilford progeria syndrome mutation." J Clin Invest **116**(8): 2115-2121.
- Yang, Z., N. E. Bowles, S. E. Scherer, M. D. Taylor, D. L. Kearney, S. Ge, V. V. Nadvoretzkiy, G. DeFreitas, B. Carabello and L. I. Brandon (2006). "Desmosomal dysfunction due to mutations in desmoplakin causes arrhythmogenic right ventricular dysplasia/cardiomyopathy." Circulation research **99**(6): 646-655.
- Yu, G., L. G. Wang and Q. Y. He (2015). "ChIPseeker: an R/Bioconductor package for ChIP peak annotation, comparison and visualization." Bioinformatics **31**(14): 2382-2383.
- Yu, H.-C., C. R. Coughlin, E. A. Geiger, B. J. Salvador, E. R. Elias, J. L. Cavanaugh, K. C. Chatfield, S. D. Miyamoto and T. H. Shaikh (2016). "Discovery of a potentially deleterious variant in TMEM87B in a patient with a hemizygous 2q13 microdeletion suggests a recessive condition characterized by congenital heart disease and restrictive cardiomyopathy." Cold Spring Harbor Molecular Case Studies **2**.
- Zhang, H., K. O. Lui and B. Zhou (2018). "Endocardial Cell Plasticity in Cardiac Development, Diseases and Regeneration." Circ Res **122**(5): 774-789.
- Zhang, H., W. Pu, G. Li, X. Huang, L. He, X. Tian, Q. Liu, L. Zhang, S. M. Wu and H. M. Sucov (2016). "Endocardium minimally contributes to coronary endothelium in the embryonic ventricular free walls." Circulation research **118**(12): 1880-1893.
- Zhang, W., H. Chen, X. Qu, C. P. Chang and W. Shou (2013). Molecular mechanism of ventricular trabeculation/compaction and the pathogenesis of the left ventricular noncompaction cardiomyopathy (LVNC). American Journal of Medical Genetics Part C: Seminars in Medical Genetics, Wiley Online Library.
- Zhang, Y., T. Li, S. Preissl, J. Grinstein, E. Farah, E. Destici, A. Y. Lee, S. Chee, Y. Qiu and K. Ma (2019). "3D chromatin architecture remodeling during human cardiomyocyte differentiation reveals A role of HERV-H in demarcating chromatin domains." bioRxiv: 485961.
- Zheng, X., J. Hu, S. Yue, L. Kristiani, M. Kim, M. Sauria, J. Taylor, Y. Kim and Y. Zheng (2018). "Lamins organize the global three-dimensional genome from the nuclear periphery." Molecular cell **71**(5): 802-815. e807.
- Zhou, X., B. Maricque, M. Xie, D. Li, V. Sundaram, E. A. Martin, B. C. Koebbe, C. Nielsen, M. Hirst, P. Farnham, R. M. Kuhn, J. Zhu, I. Smirnov, W. J. Kent, D. Haussler, P. A. Madden, J. F. Costello and T. Wang (2011). "The Human Epigenome Browser at Washington University." Nat Methods **8**(12): 989-990.

7 CURRICULUM VITAE

Contact

Name: Yinuo Wang

Birthday: 23/01/1990

Email: Yinuo.Wang@medma.uni-heidelberg.de

Address: Ludolf-Krehl-Str. 7-11 Haus B, Ebene 4, Raum B 2.31, 68167 Mannheim, Germany



Education

- 2017-Present Heidelberg University Mannheim Medical Faculty, PhD
- 2012-2015 Peking University Health Science Center, Master degree
- 2008-2012 Henan University, College of Pharmacy, Bachelor degree

Publications

- Wang Y, Elsherbiny A, Kessler L, et al. Lamin A/C-dependent chromatin architecture safeguards naïve pluripotency to prevent aberrant cardiovascular cell fate and function[J]. *Nature Communications*, 2022, 13(1): 1-24.
- Wang, Yinuo, and Gergana Dobрева. "Epigenetics in LMNA-Related Cardiomyopathy." *Cells* 12.5 (2023): 783.
- Linda Kessler, Rui Gao, Nalan Tetik-Elsherbiny, Olga Lityagina, Azhar Zhailauova, Yonggang Ren, Felix A. Trogisch, Julio Cordero, Yanliang Dou, Yinuo Wang, ... & Dobрева, G. (2022). *Rnf20 shapes the endothelial control of heart morphogenesis and function*. *bioRxiv*, 2022-09.
- Zhao X S, Wang Y N, Lv M, et al. miR-153-3p, a new bio-target, is involved in the pathogenesis of acute graft-versus-host disease via inhibition of indoleamine- 2,3-dioxygenase[J]. *Oncotarget*, 2016, 7(30): 4 8321-48334. (Co-fist author).
- Wang Y, Zhao X, Ye X, et al. Plasma microRNA-586 is a new biomarker for acute graft-versus-host disease[J]. *Annals of hematology*, 2015, 94(9): 1505-1514.
- Wang Y N, Yu L, Zhao X S, et al. Establishment of plasma microRNA detection method by using taqman probe based quantitative reverse transcription PCR[J]. *Cellular and molecular biology (Noisy-le-Grand, France)*, 2014, 61(3): 51-56.
- 王奕诺, 万峻, 赵晓甦. 吡啶胺2,3-双加氧酶在移植物抗宿主病中的作用研究进展[J]. *中华内科杂志*, 2015, 54(11).
- 万峻, 王奕诺, 张伟, 等. 一种血浆游离miRNAs绝对定量的方法:, CN105039512A[P]. 2015

8 ACKNOWLEDGEMENT

I would like to express my sincere appreciation to everyone who has offered their support during my doctoral research in Germany.

First of all, I would like to acknowledge and give my sincerely grateful to my supervisor Prof. Dr. Gergana Dobрева who made this work possible. She is an outstanding scientist in cardiovascular field. She gave me the chance to pursue my research dream and she guides me throughout all the stages of my PhD. She supports me, encourages me, and leads me from “naïve” to “mature”. Without her I would not have been able to complete this research. She is not only talented but also hard working, which makes me regard her as an example to follow. Importantly we know each other and share common values on science. And she will lead me to start my new science career.

I also extend my gratitude to my labmates, institute members, and collaborating groups who have contributed to this project. I want to thank Adel Elsherbiny for the Hi-C experiment, Linda Kessler for the assistance with ATAC-seq, Dr. Julio Cordero for bioinformatics support and sequencing analysis, Haojie Shi for working with me on revision, Felix A. Trogisch and Olga Lityagina for echocardiography, and Ibrahim El-Battrawy, Mengying Huang, and Xuehui Fan for providing hiPSC. I appreciate everyone else who has assisted me in any way, and I am thankful for their contributions to this research.

Furthermore, I am deeply grateful to my family members, particularly my parents and wife, for their unwavering support and encouragement throughout my doctoral research journey. Their encouragement and well wishes have been a constant source of motivation, and I am grateful for their presence in my life.

Once again, I extend my heartfelt thanks to everyone who has supported me during this research journey. Your contributions have been instrumental in helping me achieve my goals and complete this project successfully.

Thank you all.